Cranfield University

Raed Al-Asadi

BSc, MSc in Agricultural Machinery

Combined sensor of dielectric constant and visible and near infrared spectroscopy to measure soil compaction using artificial neural networks

School of Applied Sciences

Doctorate of Philosophy

PhD Thesis

Academic Year: 2010 - 2014

Supervisor: Dr Abdul Mounem Mouazen

Co-Supervisor: Dr Tim Brewer

May 2014

Cranfield University

School of Applied Sciences

Doctorate of Philosophy

PhD Thesis

Academic Year 2010 – 2014

Raed Al-Asadi

Combined sensor of dielectric constant and visible and near infrared spectroscopy to measure soil compaction using artificial neural networks

Supervisor: Dr Abdul Mounem Mouazen

Co-Supervisor: Dr Tim Brewer

May 2014

This thesis is submitted in partial fulfilment of the requirements for the degree of Doctor of Philosophy

Abstract

Soil compaction is a widely spread problem in agricultural soils that has negative agronomic and environmental impacts. The former may lead to poor crop growth and yield, whereas the latter may lead to poor hydraulic properties of soils, and high risk to flooding, soil erosion and degradation. Therefore, the elimination of soil compaction must be done on regular bases. One of the main parameters to quantify soil compaction is soil bulk density (BD). Mapping of within field variation in soil BD will be a main requirement for within field management of soil compaction. The aim of this research was to develop a new approach for the measurement of soil BD as an indicator of soil compaction. The research relies on the fusion of data from visible and near infrared spectroscopy (vis-NIRS), to measure soil gravimetric moisture content (ω), with frequency domain reflectometry (FDR) data to measure soil volumetric moisture content (θv). The values of the estimated ω and θv, for the same undisturbed soil samples were collected from selected locations, textures, soil moisture contents and land use systems to derive soil BD.

A total of 1013 samples were collected from 32 sites in the England and Wales. Two calibration techniques for vis-NIRS were evaluated, namely, partial least squares regression (PLSR) and artificial neural networks (ANN). ThetaProbe calibration was performed using the general formula (GF), soil specific calibration (SSC), the output voltage (OV) and artificial neural networks (ANN). ANN analyses for both ω and θv properties were based either on a single input variable or multiple input variables (data fusion). Effects of texture, moisture content, and land use on the prediction accuracy on ω, θv and BD were evaluated to arrive at the best experimental conditions for the measurement of BD with the proposed new system. A prototype was developed and tested under laboratory conditions and implemented *in-situ* for mapping of ω, θv and BD. When using the entire dataset (general data set), results proved that high measurement accuracy can be obtained for ω and θv with PLSR and the best performing traditional calibration method of the ThetaProbe with R^2 values of 0.91 and 0.97, and root mean square error of prediction (RMSEp) of 0.027 g g^{-1}

and 0.019 cm^3 cm^{-3}, respectively. However, the ANN – data fusion method resulted in improved accuracy (R^2 = 0.98 and RMSEp = 0.014 g g^{-1} and 0.015 cm^3 cm^{-3}, respectively). This data fusion approach gave the best accuracy for BD assessment when only vis-NIRS spectra and ThetaProbe V were used as an input data (R^2 = 0.81 and RMSEp = 0.095 g cm^{-3}). The moisture level (L) impact on BD prediction revealed that the accuracy improved with soil moisture increasing, with RMSEp values of 0.081, 0.068 and 0.061 g cm^{-3}, for average ω of 0.11, 0.20 and 0.28 g g^{-1}, respectively. The influence of soil texture was discussed in relation with the clay content in %. It was found that clay positively affected vis-NIRS accuracy for ω measurement and no obvious impact on the dielectric sensor readings was observed, hence, no clear influence of the soil textures on the accuracy of BD prediction. But, RMSEp values of BD assessment ranged from 0.046 to 0.115 g cm^{-3}. The land use effect of BD prediction showed measurement of grassland soils are more accurate compared to arable land soils, with RMSEp values of 0.083 and 0.097 g cm^{-3}, respectively. The prototype measuring system showed moderate accuracy during the laboratory test and encouraging precision of measuring soil BD in the field test, with RMSEp of 0.077 and 0.104 g cm-3 of measurement for arable land and grassland soils, respectively. Further development of the prototype measuring system expected to improve prediction accuracy of soil BD. It can be concluded that BD can be measured accurately by combining the vis-NIRS and FDR techniques based on an ANN-data fusion approach.

Keywords: Bulk density, vis-NIR Spectroscopy, FDR, Artificial neural networks, multi-sensor.

DEDICATION

To my father

ABDULZAHRA Al-ASADI

For his endless encouraging and supporting during my study.

This thesis is dedicated also to all my family members, who never stop believing in me.

ACKNOWLEDGEMENTS

I would like to thank my supervisor Dr Abdul Mounem Mouazen who believed in me and opened to me this precious research opportunity, during the research time Abdul always offered me the right advices to improve my research skills, helping me on both scientific and personal life aspects. Abdul decisions were objective show deep knowledge of the research subject. I also gratefully acknowledge my co-supervisor Dr Tim Brewer who added high value to the research through his wise and helpful contributions. Tim was very patient with me in learning new techniques and methods of research. Without my supervisors deep knowledge and patience it would be impossible for me to carryout and finish this study.

I like to thank Douglas Bomford Trust and EPSRC for their financial support, all staff in the Environmental Science and Technology Department for their kind helps and supports during the field work and laboratory analysis, special thanks to Dr Kim Blackburn for his kind advices during the process of design the dielectric senor of the prototype, and many thanks to Bob Walker for his guiding and advice during the field measurements.

I also would like to thank my colleagues: Zaka Quraishi, Boyan Kuang Reuben Okparanma, and Graham Halcro for their collaboration during the study.

I would like to thank all my family members for their patience and understanding for me been away from them and for their encouragements.

Table of contents

Table of figures

List of the Tables

List of appendixes

LIST OF ABBREVIATIONS

Artificial neural networks.....ANN

Bulk density..... BD

Broyden–Fletcher–Goldfarb–Shanno algorithm..... BFGS

Clay content.....CC

Coefficients.....a_1 and a_0

Dielectric constant.....K

Dielectric constant for a dry soil sample.....K_0

Dielectric constant for a wet soil sample.....K_1

Exponential function.....Exp

Equation……..Eqn

Frequency domain reflectometry.....FDR

General formula for ThetaProbe calibration.....GF

Gravimetric moisture conten.....ω

Hyperbolic tangent function.....Tanh

Logarithmic function.....Log

Manufacturer calibration of ThetaProbe.....M

Measured volumetric moisture content by oven drying.....θvt

Organic matter content.....OM

Output voltage calibration of ThetaProbe.....OV

Output voltage of ThetaProbe.....V

Partial least squares regression.....PLSR

Particle size distribution.....PSD

Ploy vinyl chloride.....PVC

Ratio of prediction deviation.....RPD

Root mean square error.....RMSE

Root mean square error of prediction.....RMSEp

Sand.....S

Silt.....SL

Specific soil calibration of ThetaProbe.....SSC

Standard deviation.....SD

ThetaProbe digital moisture metre type.....HH2

Time Domain Reflectometry.....TDR

United States Department of Agriculture.....USDA

Visible and near infrared spectroscopy.....Vis-NIRS

Volumetric moisture content.....θv

Chapter 1

Thesis Structure

This thesis concerns the development of soil compaction sensors, using innovative approach of combining dielectric and vis-NIRS sensors for in-situ applications, which was established earlier by the Al-Asadi and Mouazen (2014) publication. In this thesis further easements of soil BD provided, under different affecting factors, namely, modelling approach, soil moisture level, soil texture and land use. The aim was to explore the potential of using this measuring system at minimum prediction error, develop specific calibration models for level of the presumed affecting factors, by choosing the optimum soil status to conduct the field measurements and the right calibration model would increase considerably the measuring system accuracy.

The thesis will be divided into the six chapters (Figure 1-1) as following:

- Chapter 1 is the introduction, where a general introduction of soil compaction problem and a glance of the measuring techniques, the research gap and the aim and specific objectives of the research are also been addressed in the first chapter.
- Chapter 2 provide literature review with expanding of the negative impacts and suggested ways to minimise soil compaction, and a historical development of the measuring systems of soil compaction were reviewed.
- Chapter 3 shows the materials and methods adopted to conduct this research.
- Chapter 4 shows the detailed results of the different calibration techniques performance and prediction accuracy under wide range of studying parameters.
- Chapter 5 addresses scientific discussions of each result obtained in the results chapter.

- Finally, chapter 6 concerns of showing the extracted conclusions of the whole research topics and the suggested future work. The list of publications to date is also added.

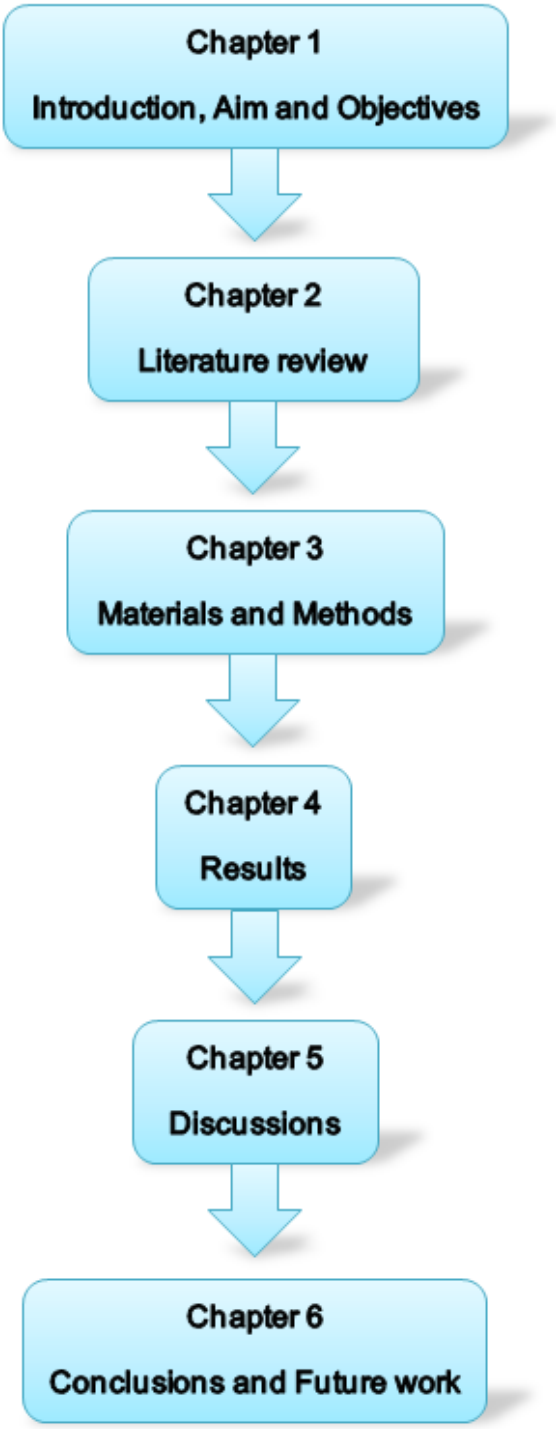

Figure 1-1 Thesis structure, showing the 6 different chapters.

1. Introduction

1.1. Background

It's hard to imagine agriculture today without the use of modern agricultural machinery. Farmers began by using animals to power their machinery, but with the invention of the steam engine and later the internal combustion engine, agricultural machinery has entered a new era of mass production and reliability. The increase in world population has put enormous pressure on agriculture to produce sufficient agricultural products to feed the world; however, this couldn't be achieved without mechanised agriculture.

Soil is a natural, dynamic, porous medium consisting of air, water and solid materials in various ratios. The solid materials of the soil are mainly minerals (clay, silt and sand) mixed with organic material, which acts as cement agent forming soil aggregates and structure. The porous nature of agriculture soil makes it the ideal environment for plant roots to develop, distribute and absorb minerals and nutrients needed for the plant growth. For optimum plant growth, the soil content by volume is 50% solids (45% mineral and 5% organic), and 50% voids of which half is filled by water and half by gas. Maintaining a good balance between these two major phases was always the key success for plant growth and yield

Man used soil for agriculture since the ancient times. Our ancestors have not reported the problem of soil compaction. When farmers noticed the need to looseness their soils to restore a good crop yield by overcoming the foot pass of the soil top layer, animals have been used to till lands after been cultivated. It was the time when the fossil fuels become available and affordable and significant mass increase of agriculture machinery, leading to unbearable mechanical force on soil structure. The increase in mass of agricultural machinery has led to recognising soil compaction as a major problem affecting crop growth and yield.

Soil compaction is the rearrangement of soil aggregates and/or particles in such a way that the voids and pores mainly between aggregates and particles

become smaller. Soil compaction can have a number of negative effects on soil quality and crop production including damage to the soil structure (Wolkowski and Lowery, 2008), deterioration of the soils' physical and hydraulic properties (Strudley et al., 2008; Lipiec et al., 2009), which reduces the ability of a soil to hold water and air that are necessary for plant root growth and function, leading to a decline in the ability of crops to take up nutrients and water efficiently (Rosolem et al., 2001; Chen and Weil, 2011). The net effect is a decrease in crop yield. Soil compaction is associated with increase in bulk density (BD) and penetration resistance (PR), while significant reduction of porosity and pore space may be expected (Hakansson, 1990). Therefore, soil compaction also affects the hydraulic properties of the soil. This includes decrease in infiltration rate, which typically leads to surface run off. This enhances soil erosion particularly in areas with intensive rainfall (Franzen et al., 1994). The increase of flood risk is expected, particularly in areas with steep slopes that experience intensive rainfall (Presbitero et al., 2005). The increase of soil resistance to penetration affects not only plant growth but also leads to increase energy requirement for tillage. Therefore, the occurrence of soil compaction should be avoided, which is a better strategy than to remediate the problem by a proper management of tillage, which is energy demanding and expensive. Managing the traffic of agricultural machinery by means of controlled traffic farming systems is another strategy, which is increasingly adopted (Lamers et al., 1986; Chamen and Audsley, 1993; Wang et al., 2005).

There are several factors that influence the occurrence of soil compaction. Many researchers agree that the fundamental cause of soil compaction lies with the use of heavy agriculture machinery (Frey et al., 2009; Tóth et al., 2008). Compaction by agricultural machinery is one of the effects that human activity has had on soils during the last 150 years. Livestock trampling is a significant cause of compaction, especially in the surface horizon of finer textured soils, but effects are confined to the upper 15 cm of the profile (Willatt and Pullar 1983; Kelly 1985). Livestock impact on grasslands during the wet soil conditions reported to be among those factors causing compression stresses, which lead to soil compaction (Vrindts et al., 2005; Hamza and Anderson, 2005). Other

factors causing soil compaction are the repeated use of same tillage tools at the same depth and extreme weather conditions (Mouazen and Ramon, 2006; Quraishi, 2013).

Canarache and Van den Akker. (2003) stated that “European soils are more threatened than ever in history”. However, susceptibility of soil to compaction is associated with soil physical conditions including, soil type, moisture content and organic matter content (OM) (Quraishi, 2013). Soils with low OM could be compacted easier as compared with higher OM content soils. In fact, OM acts like a cement agent bonding soil aggregates together strongly. Clayey soils are highly compactable (Table 1-1), especially when exposed to external load and associated with high moisture content, this is due to the presence of water around clay particles, which acts as a lubricant, thus making it easier for the soil fractions to slide against each other. Although, sandy soils do not form aggregates, they can also be compacted when they are subjected to heavy machinery during field operations. Soil water content during traffic and cultivation determines the severity and extent of soil compaction. Soil water acts as a lubricant, permitting soil aggregates and individual particles to move in response to pressure from the transit of animals, vehicles and tillage equipment. This leads to the loss of air spaces and the closer packing of soil particles. Thus, compaction risk is greater in moist soils (FAO, 2003).

Table 1-1 Evaluation of soil susceptibility to compaction according to soil texture (after Wolkowski and Lowery, 2008).

Desorption	Evaluation
No mineral texture (Peat soils, rocks, etc.)	Low
Coarse (clay < 18 % and sand >65 %)	Low
Medium (18 % < clay < 35 % and sand > 15 %, or clay <18 % and 15 % < sand <65 %)	Medium
Medium fine (clay <35 % and sand <15 %)	Medium/High*
Fine (35 % < clay < 60 %)	High
Very fine (clay > 60 %)	High

*Final evaluation can be affected by percentages of organic matter and sand.

To prevent and/or reduce soil compaction several procedures can be followed, for example:

- Reducing the axle load of agriculture machinery (Duiker, 2004; Nevens and Reheul, 2003).
- Controlled Traffic Farming, Chamen, (2011) stated the advantages of a traffic control system to prevent soil compaction and how it benefitted crop productivity. Figure 1-2 shows the percentage reduction in yield of different crops in comparison to controlled traffic farming.

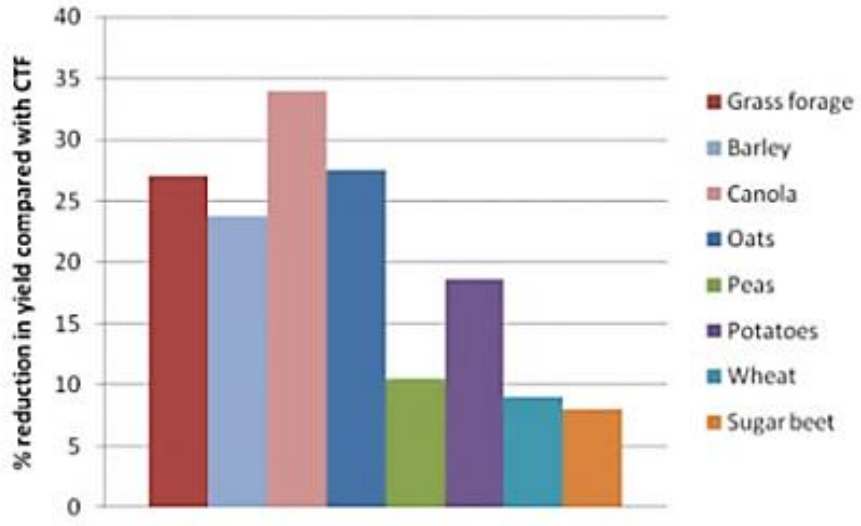

Figure 1-2 Reduction in yield (%) of combinable crops compared with controlled traffic farming. (after, Chamen, 2011).

- Use of a combination of fibrous and tap rooted crops in a rotation to penetrate soils, by developing deep root channels and to add organic matter to the soil (Hamza and Anderson, 2005).
- Avoid tillage during wet soil conditions (Alakukku et al., 2003)
- Reduce tire inflation pressure when large mass agricultural machines have to be used (Ansorge and Godwin, 2007)
- Use track tires instead of wheel tyres, particularly in heavy soils to increase the contact area, hence reduce contact pressure (Keller and Arvidsson, 2004),

- Use of dual tyres to increase the contact area and reduce the contact pressure(Servad et al. 2005: Botta et al., 2006),
- Carry out several operations in one pass (Mitchel et al., 2004),
- Use 4-wheall drive tractors (Botta et al., 2012),
- Early identification of increasing soil BD for field management of soil compaction, as BD is one of the main indicators of soil compaction.

Understanding therefore how and to what extent soil compaction may be eliminated seems of vital importance to the future wellbeing of agricultural systems. Land management is the key factor for this target, where a quantitative and realistic measuring system of soil compaction is one of the successful tools that can be used to generate maps of compacted areas, to enable the identification of management actions that could be deployed to solve the problem. Due to the complex nature of agricultural soils, it has been difficult to characterise soil compaction rapidly, easily and cost effectively (Aragón et al., 2000; Horn et al., 2000; Mouazen et al., 2003), which has hindered the study of soil compaction and its consequent remediation (Quraishi and Mouazen, 2013a).

One of the main parameters to quantify soil compaction is BD. It is widely used for assessing soil compaction (Grossman, 1981; Bardy, 1984; Singh et al., 1992). The most common, traditional method for BD measurement is the core sampling method (e.g. Kopecki ring), which is laborious, time consuming, expensive and difficult to conduct particularly under dry soil conditions (Quraishi and Mouazen, 2013b). However, although BD might be considered as an indicator of soil compaction, it does not necessarily indicate changes in soil function, for example, air and water movement (Quraishi and Mouazen, 2013a). Other parameters such as saturated hydraulic conductivity and infiltration rate are more closely related to soil compaction (Fleige and Horn, 2000). However, in comparison with the latter parameters, assessment of BD with a portable measurement system is possible (Quraishi and Mouazen, 2013a; Al-Asadi and Mouazen, 2014) and enables faster, easier, and more cost effective data acquisition, which is particularly useful for precision agriculture applications.

For simplicity reasons, researchers have considered soil strength as an indicator for soil compaction. It is attributed to the fact that PR is the easiest parameter to be measured under off-line or on-line measurement conditions (Adamchuk et al., 2004; Andrade-Sánchez et al., 2008; Hemmat et al., 2009). But, soil strength is a dynamic property that changes with time and also spatially within a field due to the influences of climate, soil management and plant growth (Cantero-Martínez et al., 2003). Mouazen and Ramon (2006) explained that PR is simultaneously affected by moisture content, texture, BD and OM. It also changes due to the external load of agricultural machinery, animal traction and tillage tools (Mouazen et al., 2002, Quraishi and Mouazen, 2013a). This dynamic nature makes the utilisation of soil strength for the characterisation of within field variability of soil compaction to be of limited value. This has stimulated the development of soil compaction sensors that measure causal parameters, while providing cost effective and high resolution data about soil compaction. For example, Mouazen and Ramon (2006) reported an innovative approach for on-line measurement of soil compaction indicated as BD, as a function of PR, moisture content, clay content (CC) and OM. Similar approach was developed for a portable system for the measurement of soil BD (Quraishi and Mouazen, 2013b). The need for multiple-soil parameters to be measured simultaneously necessitates the need for a multi-sensor and data fusion approach to arrive at a measurement system that enables a meaningful estimation of this complex and important parameter in soil.

Multiple sensors and data fusion have been introduced as a new concept in proximal soil sensing (Kuang et al., 2012). Data fusion is an important tool that may improve the performance of a detecting system by integrating data from a range of sensors (Mahmood et al., 2009). Despite the fact that this is a new concept, several studies have reported on non-mobile (Hummel et al., 2004; Quraishi and Mouazen, 2013b) and mobile systems (Glancey et al., 1989; Mouazen et al., 2003; Adamchuk et al., 2004; Mouazen et al., 2005; Mouazen and Ramon, 2006; Naderi-Boldaji et al., 2011b; Quraishi and Mouazen, 2013a) for the measurement of soil compaction. Many researchers have shown that the cone penetrometer accuracy is affected by the soil properties (Tekeste et al.,

2005; Sun et al., 2011; Quraishi and Mouazen, 2013b). To eliminate the moisture content effect on the cone penetrometer measurement accuracy of soil resistance, Vaz et al. (2001) combined time domain reflectometry (TDR) with a cone penetrometer to measure soil resistance simultaneously with soil moisture. Results showed that TDR reading improved soil resistance accuracy by considering the influence of soil moisture content. Their combined penetrometer-TDR probe consisted of a paired wire coiled around the penetrometer cone (Figure 1-3).

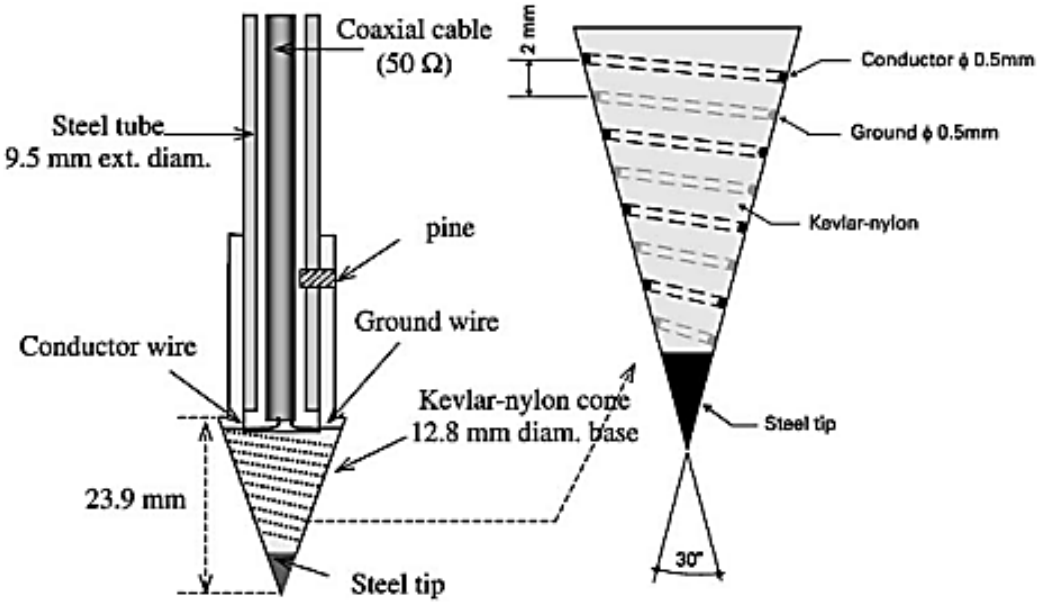

Figure 1-3 Schematic drawing of the combined cone penetrometer and a time domain reflectometry (TDR) sensors (after, Vaz et al., 2001).

Mouazen et al. (2003) successfully developed an on-line combined mapping system of soil compaction, based on a multi-sensor system of a single beam load cell and a wheel gauge to measure draught and the working depth of a subsoiler, respectively, and a visible and near infrared spectrophotometer to measure soil moisture content. They used a numerical–statistical modelling scheme to fuse the input data on subsoiler draught, depth and moisture content, and calculate BD as the system output. Naderi-Boldaji et al. (2013) developed a three-parameter model for on-line BD estimation, as a function of PR,

volumetric water content (θv) and CC, measured by a triple sensor consisting of a horizontal penetrometer, a dielectric sensor and a gamma-ray sensor, respectively. Results were not encouraging. Quraishi and Mouazen (2013a) expand the calibration of the Quraishi and Mouazen (2013b) reported a data fusion approach of BD assessment, based on the fusion of data on gravimetric moisture content (ω), OM and CC, measured with a visible and near infrared (vis-NIR) spectrophotometer and penetration resistance measured with a penetrometer. They concluded that improvement of soil BD prediction was achievable by considering the influence of ω, OM and CC. However, a large number of variables e.g. ω, OM, CC and penetration resistance is required as input for the artificial neural networks (ANN) analysis to predict BD. The accumulated error of vis-NIR measurement of ω, OM and CC would sum up to a considerable error of BD assessment. Therefore, a simpler approach is needed that is based on a fusion of fewer input variables (e.g. ω and θv), where error in BD assessment is small (Table 1-2).

Table 1-2 Comparison results of soil bulk density (BD) estimation, using data fusion techniques including multiple linear regression (MLR), Matlab artificial neural networks (ANN) and Statistica ANN, as a function of various input sets (after, Quraishi and Mouazen, 2013b).

Model	MLR (R^2)		RMSE	Matlab (R^2)			RMSE	Statistica (R^2)			RMSE
	C	*V*		*C*	*V*	*T*		*C*	*V*	*T*	
PR	0.04	0.03	0.19	0.04	0.02	0.02	0.20	0.06	0.14	0.01	0.18
PR, MC	0.12	0.15	0.17	0.44	0.33	0.49	0.14	0.61	0.59	0.42	0.15
PR, OM	0.25	0.26	0.16	0.29	0.26	0.48	0.14	0.53	0.60	0.41	0.15
PR, CC	0.37	0.38	0.15	0.49	0.35	0.58	0.14	0.61	0.69	0.69	0.12
PR, MC, OM	0.25	0.26	0.16	0.51	0.38	0.68	0.11	0.62	0.52	0.53	0.14
PR, MC, CC	0.41	0.41	0.14	0.21	0.19	0.42	0.34	0.61	0.74	0.71	0.11
PR, OM, CC	0.37	0.38	0.15	0.55	0.36	0.60	0.13	0.71	0.70	0.68	0.12
PR, MC, OM, CC	0.51	0.49	0.13	0.72	0.55	0.74	0.10	0.76	0.79	0.81	0.11

PR is penetration resistance (MPa), MC is moisture content (kg kg^{-1}) OM is organic matter content (kg kg^{-1}), CC is clay content (kg kg^{-1}) and RMSE is root mean square error (Mg m^{-3}), *C* is calibration, V is leave-one-out cross-validation and *T* is test sets for the calibration methods.

1.2. Research aim and objectives

- **Research gaps**

The aforementioned portable and on-line systems for the measurement of BD provide indirect estimation as a function of PR, draught and/or bearing capacity. None of them measure BD directly or estimate BD based on a physical model for BD estimation. The only portable system developed recently by Quraishi and Mouazen (2013c) is based on a large number of input variables e.g. PR, moisture content, CC and OM. This is the reason why there is a need for a simple, portable measuring system that provides a practical application for mapping of soil compaction.

- **Assumption**

The assumption of this thesis is that by combining a vis-NIRS to measure ω and a dielectric constant sensor to measure θv, BD can be derived using an existing model.

- **Research aim**

The overall aim of the thesis is to explore and evaluate the potential of a multi-sensor and data fusion approach consisting of dielectric constant and vis-NIRS techniques for non-invasive, laboratory and *in-situ* measurements of soil BD to indicate soil compaction of selected soil textures and different agricultural practices. This new concept relies on simultaneous measurement of ω and θv, with a vis-NIR spectrophotometer and a frequency domain reflectometry (FDR) sensor, respectively. Afterword, the measured ω and θv values at a point are the only input parameter needed to calculate BD according to the fact that soil water content can be expressed in different ways, for example, relatively to the mass of the soil solid particles, or to the total soil volume, the various indexes are defined as follow:

- Mass Wetness ω is the relative mass of the soil water to the dry soil particles after 24 h of oven drying at 105 °C (Figure 1-4).

$$\omega = \frac{M_w}{M_s} \qquad 1\text{-}1$$

Where ω is soil's gravimetric moisture content (g g^{-1}), M_w is mass of soil water (g) and M_s is mass of soil solid particles (g).

- Volume wetness (θv): volumetric water content of the soil is commonly computed as a ratio between the volume of soil's water to the total volume of the soil (Figure 1-4).

$$\theta_v = \frac{V_w}{V_t} \qquad 1\text{-}2$$

Where θ_v is soil's volumetric moisture content (cm^3 cm^{-3}), V_w is the volume of soil water (cm^3) and V_t is the total volume of the soil sample (cm^3).

On the other hand, soil BD can be defined as the ratio of the solid particles mass to the total soil volume.

$$BD = \frac{M_s}{V_t} = \frac{M_s}{(V_a + V_w + V_s)} \qquad 1\text{-}3$$

Where BD is soil bulk density (g cm^{-3}), M_s is mass of soil solid particles (g), V_t is the total volume of the soil sample (cm^3) and V_a , V_w and V_s are volumes of the soil air, water and solid particles, respectively (cm^3).

From Equ. 1-3, V_t can be written as follows:

$$V_t = \frac{M_s}{BD} \qquad 1\text{-}4$$

Water density (ρ_w) is the mass of the volume unit, which is computed as follows:

$$\rho_w = \frac{M_w}{V_w} \qquad 1\text{-}5$$

And

$$V_w = \frac{M_w}{\rho_w} \qquad 1\text{-}6$$

By substituting Eqn. 1-4 and 1-6 in Eqn. 1-2, we obtain

$$\theta_v = \frac{V_w}{V_t} = \frac{M_w/\rho_w}{M_s/BD} = \frac{M_w}{\rho_w} * \frac{BD}{M_s} \qquad 1\text{-}7$$

And by substituting Eqn. 1-1 in Eqn. 1-7, the following equation can be derived

$$\theta_v = \omega * \left[\frac{BD}{\rho_w}\right] \qquad 1\text{-}8$$

Assuming that ρw = 1 g cm^{-3}, the previous equation can be written as follows (Hill, 1998):

$$BD = \frac{\theta v}{\omega} \qquad 1\text{-}9$$

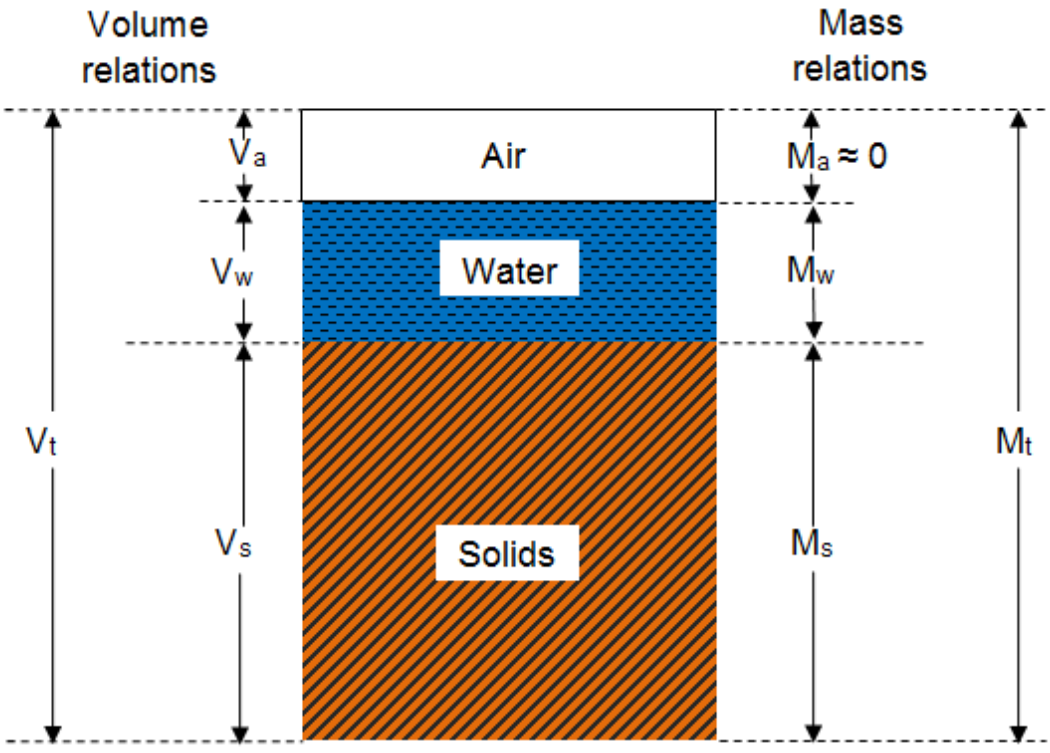

Figure 1-4 Schematic diagram of soil three phases

The ultimate aim of this work is to achieve a portable prototype system for BD assessment.

- **The research objectives:**
  - To develop, under laboratory and field conditions, calibration functions for the dielectric probe for the measurement of θv of selected soil textures in UK soils under different tillage systems and land use.
  - To develop, under laboratory and field conditions, a general calibration model of vis-NIRS for the measurement of ω of the selected soil textures in UK soils under different tillage systems and land use.
  - To determine, under field conditions, soil BD based on measured θv and ω obtained with the dielectric and vis-NIRS sensors, respectively. For verification of the system performance, values will be compared with the corresponding values obtained by the traditional oven drying method.
  - To evaluate the best soil and operational conditions, at which the best measurement accuracy of θv, ω and BD can be obtained. These include soil moisture content, texture classes, and land use (e.g. arable land vs grassland).
  - To evaluate the best data fusion modelling techniques and calibration methods for vis-NIRS and FDR sensors, which may results in the highest measurement accuracy of the parameters under consideration.
  - To develop and test a prototype portable measurement system of BD. The system will be validated for the accuracy of measurement of θv, ω and BD in three selected arable and grassland fields in one commercial farm in UK.
  - To map the spatial variation in soil compaction of the selected three fields in the UK.

Chapter 2

2. Literature review

This literature review provides a discussion about the linkage between soil compaction and modern agriculture, focusing on methods of measuring soil compaction *in-situ*. In order to eliminate the diverse effects of soil compaction several solutions are reviewed and land management is identified as a key factor and the most effective one among them. However, the need of an objective, cost effective and portable measuring system of soil compaction is needed to achieve this goal. A new combined measuring system has been introduced, which consists of a vis-NIR spectrophotometer and a dielectric probe.

The overarching focus however is on the vis-NIR spectroscopy and its dielectric properties that enable it to measure soil moisture contents. The aim is to bring together and draw conclusions from research to understand the impacts of laboratory and field measurements under different soil and crop conditions. Soil compaction sensors and their development is therefore a major backdrop to this review.

2.1. Introduction

Intensification of crop and animal farming is widespread globally, involving shorter crop rotations and the use of heavier machines, increasing the risk of soil compaction (Hamza and Anderson, 2005).

Soil compaction can be defined as packing the solid components of soil into a smaller volume. The negative effects of this on soil can include:

- damage to the soil structure,
- increased soil bulk density (BD),
- increased soil penetration resistance (PR),
- decreased porosity and pore space,
- decreased infiltration rate and hydraulic properties,

- increased soil susceptibility for flooding and erosion,
- restricted air and water movement into and through the soil.

Farming systems have, to a certain extent, developed efficiently to meet the high pressures that accompany intensive agriculture, but the inevitable consequences of mechanized farming systems have caused the deterioration of many healthy soils to the extent that crop yields have decreased (Chamen, 2011). Newell-Price et al. (2012) have identified the importance of soil compaction in grasslands, where it may have severe impacts on the agriculture and environment in England and Wales. They concluded after a study of 300 grassland fields that there is a need to improve our understanding of soil compaction in grasslands and to identify and evaluate mitigation methods that could have the potential to remediate soil compaction. Their survey results indicate that around 10% of grassland soils are in poor condition, around 60% in moderate condition and around 30% only in good condition.

2.1.1. Causes of soil compaction:

- **Initial soil conditions**

Field traffic at the wrong moisture content increases the potential for soil compaction. This is due to the fact that soil moisture content is the dominant property affecting soil strength (Hamza and Anderson, 2005). Soil water acts as a lubricant, making it easier for soil fractions to slide against each other. As the soil strength decreases, the same axle load of field machinery compacts a soil more when it is wet than when it is dry (Figure 2-1) (e.g. Arvidsson, 2001). Tarawally et al. (2006) concluded that the level of compaction caused by machinery trafficking on cultivated fields was highly influenced by the soil-water status and such trafficking could have an impact on soil hydraulic processes. They reported the highest levels of soil compaction were found under soil water states corresponding to field operations undertaken at field saturation and field capacity.

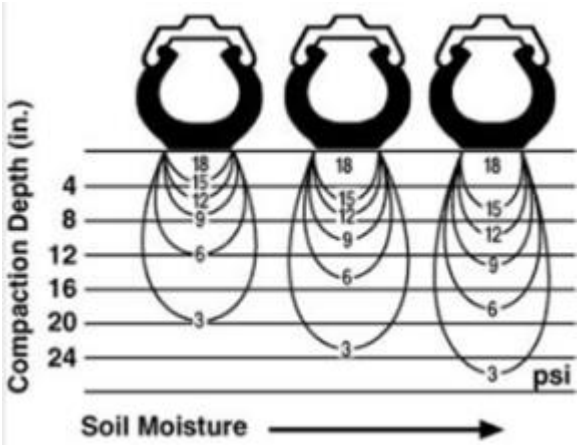

Figure 2-1 Depth of soil compaction as soil moisture content increases (after, Soehne, 1958).

Soil compaction can be exaggerated by the lack of organic matter this has been recognized worldwide (Défossez et al. 2014; Hamza and Anderson, 2005). Soil organic matter acts as a cementing agent, strengthening soil structure, making soil more resistant to failure (Thomas et al., 1996). This is the reason why soils with high organic matter are more resistive to compaction occurrence. Fine textured soils (with a higher percentage of silt and clay) naturally have more total porosity than soils with a coarse texture. For that, finer texture soils often can be more compact (Daum, 2014).

- **Farm machinery size**

The majority of the soil compaction under intensive agriculture is derived from external loads on the soil from farm machinery. Tractor mass has, for example, increased over the past 70 years from less than 3 tons to approximately 20 tons per machine to meet the high power requirements of field operations (Blue-Jet, 2014). This has the potential to cause significant damage to the structure of the tilled soil and subsoil, thus reducing crop production and increasing environmental risk (Defossez and Richard, 2002). The higher axle load increase the depth of soil structure damage in the soil profile (Figure 2-2) (Soehne, 1958; DeJong-Hughes et al., 2001).

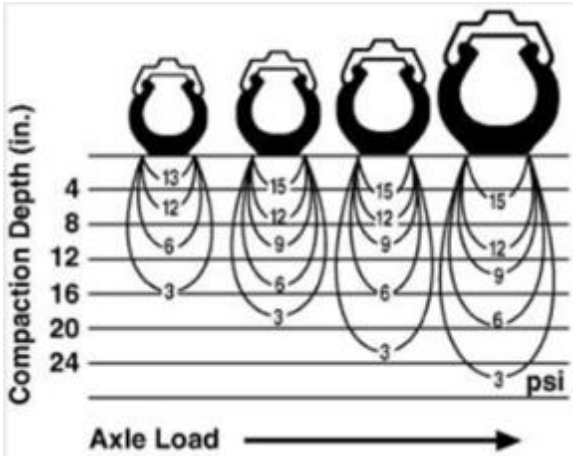

Figure 2-2 Depth of soil compaction as axle load increases (after, Soehne, 1958).

Wolkowski and Lowery (2008) stated heavy agriculture machinery is main factor of causing soil compaction, for example, modern loaded combine harvesters and manure tankers weigh 20 to 30 (t). They reported machinery weighting more than 10 (t) can raise the possibility of subsoil compaction to a depth that cannot be removed by conventional tillage (Figure 2-3).

Figure 2-3 Shows modern agriculture machinery damages of soil (after, Wolkowski and Lowery, 2008).

- **Tillage tools**

Soil tillage implements can stimulate soil compaction just below the depth of tillage, especially when soils are wet, when choosing the same depth and equipment (plough, disk, or chisel plough) of tillage for long periods of time that it will lead inevitably to hardpan formation. Hardpans lead to decrease soil permeability rates, restricting roots access to moisture and nutrients above the hardpan only (Figure 2-4). Raper et al. (2005) found that conventional tillage systems were considerably decreasing the hardpan depth from soil surface comparing to no-till treatment. They conducted their measurements in field has Silty soil texture in the South-eastern USA.

Figure 2-4 Roots of a cotton plant stunted and diverted sideways by a very compact subsurface layer (after Shaxson and Barber, 2003).

Tolon-Becerra et al. (2011) linked soil compaction caused by three tillage systems, namely, direct sowing (no tillage), chisel plough and mouldboard plough on maize (*Zea mays* L.) with seeding emergence and yield. They found that the yields of three growing seasons were directly related to mass of the maize roots system, which was clearly affected by soil compaction caused by the three different tillage systems, although, seeding emerging of direct sowing was faster than the other tillage systems tested, but similar results were achieved 18 days after sowing. Abu-Hamdeh (2003) studied the influence of tillage systems (e.g. on-tillage, chisel ploughing and mouldboard ploughing), axle loads (6 and 16 t) and tire inflation pressures (120 and 350 kPa) on okra (*Abelmoschus esculentus* L.) root system distribution and soil BD and PR, on a loamy soil texture in Irbid, Jordan. He reported that the effect the experiment treatments could be sensed down to 48 cm depth. Author also stated that the greatest effect was observed with the 16 (t) axle load, 350 (kPa) tire inflation pressure and no-tillage treatments, while the lowest effect was with 6 (t) axle load, and chisel ploughed treatments.

- **Multiple field passes:**

Literature demonstrated that the degree of compaction is affected by the number of machine passes over the same soil (Horn et al., 2001). Experimental reports have shown that all soil parameters were affected negatively after machinery first passage, but high frequency trafficking of light machinery could cause as much soil damage as one pass from heavy machinery (Schäffer et al. 2007). This explains that the majority of compaction is built after the first three passes (Canillas and Salokhe, 2002).

Patel and Mani (2011) evaluated soil compaction by different passes of tractor with varying loads on a Sandy loam soil texture. They compared the influence of 4.40, 6.40 and 8.40 (kN) normal loads and 1, 6, 11 and 16 number of passes on soil compaction level caused. They reported that soil BD and PR in 0-15 cm depth zone continuously increased up to the 16 passes of the tractor, and with higher rates of higher loads. The higher loads and larger number of passes caused more damage to the soil, but most of this damage was in the soil layer

from 0 to 30 cm. Taghavifar and Mardani (2014) investigated a compensation of three factors on soil compaction, including: wheel load (1, 2 and 3 kN), velocity (0.5, 0.75 and 1 m s^{-1}) and multiple wheel passages (1, 2 and 3 passages) on clay loam soil texture at a soil bin (Figure 2-5). They concluded that increasing the wheel load and the number of passes both have increased soil compaction, while the increase of the wheel velocity had an adverse effect.

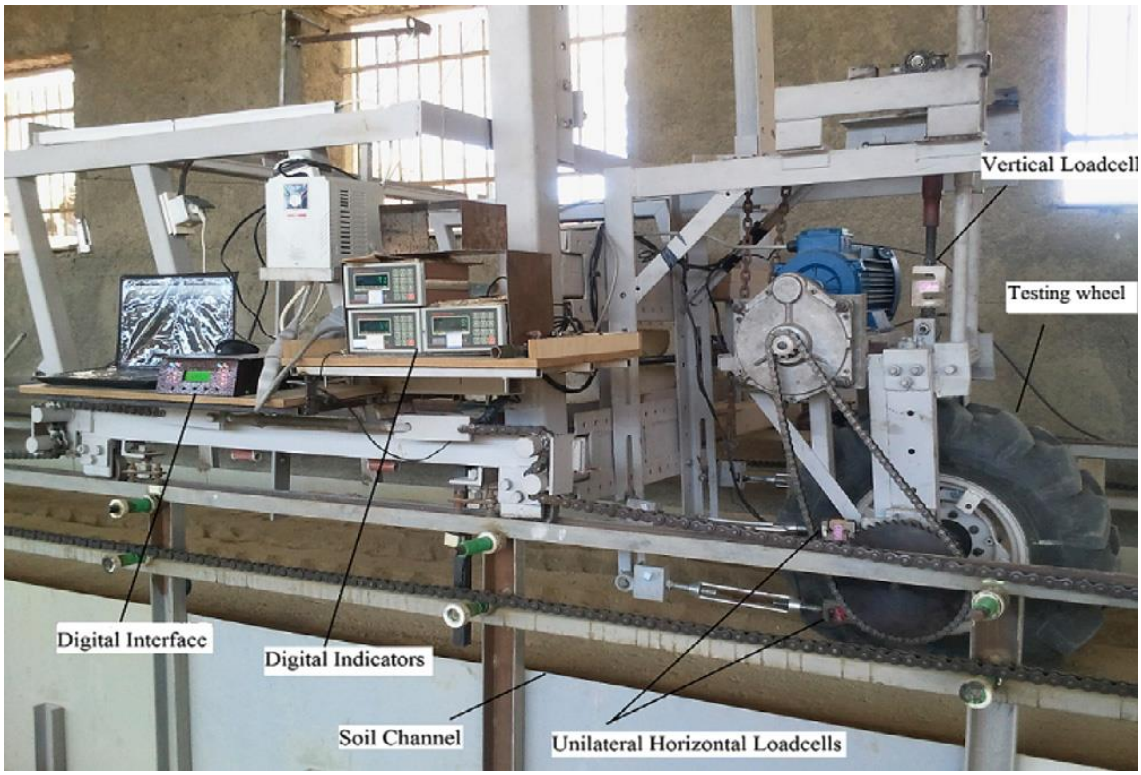

Figure 2-5 Single wheel testing system of soil compaction in a soil bin. (after, Taghavifar and Mardani, 2014).

Nevens and Reheul (2003) attempted to quantify the negative impacts of soil compaction on the maize (*Zea mays* L.) yields, on a sandy loam soil in Belgium, with traditional soil tillage, artificially compacted and subsoiled treatments. The artificial compaction treatment produced by multiple passages of a tractor increased the soil PR to more than 1.5 MPa for the soil depth from 0 to 35 cm. They also observed maize plants were smaller and flowering was delayed when growing in compacted soils, and the yield loss was 13.2 % compared to the

traditional tillage treated plots. However, the subsoiled plots didn't show significant effect on maize crop.

- **Contact area and tyres inflation pressure**

The contact area between soil and tyres or tracks is an important factor affecting the degree and depth of soil compaction occurrence. Increasing the contact area distributes the downward force coming from the weight of the tractor over a larger area, reducing the contact pressure, hence, the damage to the soil. The contact area can be increased by, for example, using double or triple traction wheels, using track of half-track tyres or by decreasing tyres inflation pressure. The average ground contact pressure (wheel load divided by contact area between tyres and soil surface) estimates the average value of the vertical load in the contact area (Alakukku, 1999). To eliminate soil compaction, recommendations have been given for maximum values of average ground contact pressure and inflation pressure 50 cm depth.

For example, Spoor et al. (2003) recommend a maximum ground contact stress of 65 kPa (tyre inflation pressure 40 kPa), while for hard soils (not particularly vulnerable to compaction) they recommended maximum to be a 200 kPa (160 kPa). Technical solutions to reduce ground contact stress (e.g. number of wheels, tyres construction, tyres cross-section, tyres diameter, tracks) and tyres inflation pressure are discussed by Chamen et al. (2003) and Ansorge and Godwin (2007). Rodríguez et al. (2012) evaluated four tire types effects on contact pressures with three inflation pressures (207, 276 and 345 kPa) and six loads on a tire (10, 20, 30, 40, 50 and 60 kN). They measured the vertical stress under the tires with sensors placed at 10, 30, 50 and 70 cm depth. Tire types A and B (Figure 2-6) produced lower contact pressure (Figure 2-7) and they concluded that type of tire is one of the factors affecting the magnitude of the stress propagated through the soil and cause compaction.

Figure 2-6 Four different tire types used in a test of causing vertical stress (after, Rodríguez et al. 2012).

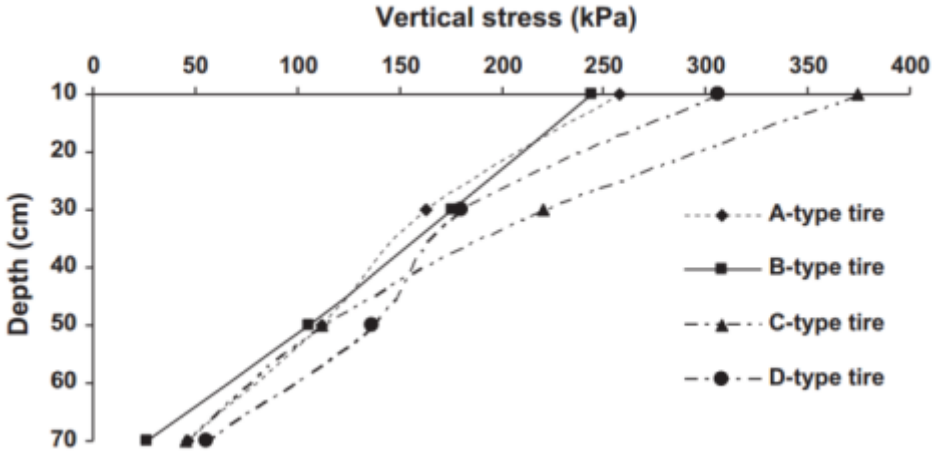

Figure 2-7 Vertical stress under four types of tires (after, Rodríguez et al. 2012).

- **Livestock interaction**

Hoof pressure from grazing animals can have a considerable negative influence on soil properties and consequently cause an unfavourable environment for plant growth, particularly when associated with wet soil conditions. The impact depth of trampling leading to soil compaction changes depending on animal weight and soil moisture content, for example, it could be within the range from 5 to 20 cm (Ferrero and Lipiec, 2000). Terashima et al. (1999) concluded that

grazing animals could damage soil properties up to 20 cm depth, but the greatest compression occurred in the top 5 cm. Lemus (2011) stated soil types with higher CC (medium to heavy textures) are more liable to hoof compaction comparing to sandier soils (light textures).

- **Weather conditions and natural causes**

Soil deformation may occurs from natural causes, frequent floods, heavy rains and snow accumulating on the soil surface can create high weight and thus induce compaction. The effect of rainfall or irrigation drops energy can also cause considerable damage of soil structure, causing soil small fractions to form a thin layer of mud at the soil surface drying into a hard surface soil crust, which can reduce infiltration rate, oxygen diffusion and limit the emergence of germinating crops (Stiegler, 2014) (Figure 2-8).

Figure 2-8 A thin surface crust caused by raindrop impact on a bare soil of poor structure (after, Shaxson and Barber, 2003).

2.1.2. Negative effects of soil compaction

Zhang et al. (2006) evaluated the effects of three levels of compaction on the hydraulic properties of silt loam soils. Three levels of soil compaction were compared by increasing soil BD by 0%, 10% and 20%. They found that increasing soil BD by 20% significantly changed the water retention curves for both saturated and unsaturated hydraulic conductivity. However, increasing the BD by 10% also affected the hydraulic properties of the soil but not significantly. Soil compaction caused by farm traffic or tillage systems affects nutrient transformations and uptake due to the changes in soil hydraulic properties, aeration, and diffusive properties, as well as by its effect on root growth and distribution. The effect on each of these properties depends on the soil water regime. In most cases, nutrient uptake is reduced by soil compaction (Lipiec and Stępniewski, 1995).

Soane and van Ouwerkerk (1995) have linked soil compaction to the unfavourable effects of increased agricultural productivity on the environment. The scientific literature provides evidence that soil compaction contributes to adverse effects such as soil structure deterioration (Horn et al., 1995), declines in crop yield (Radford et al., 2001), increased risk of runoff and soil erosion (Fullen, 1985), heightened potential surface water contamination by organic waste and agrochemicals (Lipiec et al., 2003), and increased production costs due to the inefficient use of nutrients and power requirements for tillage (Soane et al., 1982).The effect of soil compaction on crop yields varies considerably according to soil texture and location (Hester and Harrison, 2012), cation exchange capacity, pH, soil organic matter content and crop characteristics (Lal, 2006).

In addition to the negative effects on soil and related environmental consequences, soil compaction can also affect crop growth and yield (Arvidsson and Håkansson, 2014; Alakukku and Elonen, 1995; Siczek and Lipiec. 2011). Arvidsson and Håkansson (1996) reported significant yield loss as a result of soil compaction and associated with poor conditions for crop growth. Arvidsson and Håkansson (2014) found that moderate compaction led barley crop yield

only to increase significantly ($P < 0.05$), compared with zero trafficking and previously loosened soil. The greatest yield losses associated with soil compaction were observed for horse bean, peas, potato and sugar beet (Table 2-1).

Table 2-1 Yield loss (%) with three passes track-by-track by a tractor weight of 3900 (kg) with inflation pressure of 195 and 155 (kPa) for the front and rear tyres, respectively, as compared with no traffic (after, Arvidsson and Håkansson 2014).

Crop	Yield loss (%)
Spring wheat	0.3
Barley	-0.4
Spring oilseed rape	3.6
Oats	8.7
Sugar beet	9.4
Potato	9.9
Peas	11.3
Horse bean	21.7
Winter rye	0.6
Winter wheat	3.0
Winter oilseed rape	8.8

2.1.3. Methods to measure soil compaction:

Soil compaction can be indicated as soil BD, infiltration rate, porosity, PR, and others. Methods can be divided into laboratory and field measurements. Lal and Shukla (2004) classified assessment methods of soil compaction to direct and indirect methods. Figure (2-9) shows a flow chart of soil compaction measurement methods.

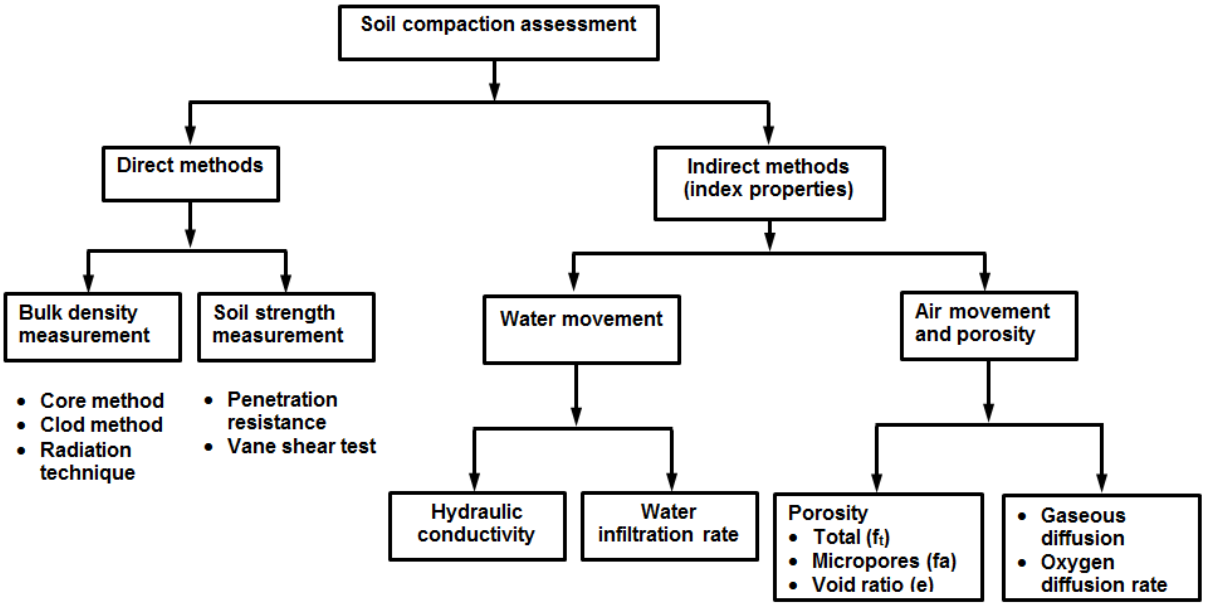

Figure 2-9 Soil compaction measuring methods (after, Lal and Shukla, 2004).

As in this study the aim is to develop a field measurement system, the review will consider field methods (*in-situ)* only. *In-situ* methods can be divided into direct or indirect methods as follows:

- **Direct methods**:

1. BD assessments: Traditionally, one of the most common parameter to indicate soil compaction is soil BD. There are several ways to measure soil BD. The basic principle is by core sampling (e.g. Kopecki ring). Measurement is conducted in the field by inserting a cylinder of known volume into the soil to collect an undisturbed soil sample, weighting the wet core sample, and weighting the dry core sample after oven drying for 24 h at 104 °C. Soil BD can be calculated by the following formula:

$$\mathrm{BD} = \frac{\mathrm{WW}-\mathrm{DW}}{\mathrm{V}} \qquad 2\text{-}1$$

Where: BD is soil bulk density (g cm^{-3}), WW and DW is wet and dry weight (g) of the core sample, respectively and V is the core volume (cm^{-3}).

2. Penetration Resistance (PR): Soil compaction usually measured by PR, which is a measure of soil strength or a resistance to a deformation and it is frequently referred to as cone index. The cone penetrometer is the common

type of many types of penetrometers, which is an instrument in a shape of cylindrical rod ended with a cone-shaped tip purposed to penetrate the soil easily, and the measuring of PR by a bearing or a strain gauge at the other end. A soil penetrometer is an instrument used for estimating soil PR, whether it is a vertical (Motavalli et al., 2003) or a horizontal penetrometer (Hemmat et al., 2009). The amount of force required to penetrate the soil body is related to the soil compaction level and depends upon the penetrometer dimensions. However, PR is not only affected by BD, but simultaneously also influenced soil texture, OM, and moisture content, which make PR limited for estimating soil compaction.

3. Shear vane: It is a tool primarily used to determined soil shear strength of the cohesive soils with strength generally up to 200 kPa. This method is not applicable to fractional soils (e.g. Sandy or Sandy loam soils) or soils contaminated with gravels. The shear vane measures the soil resistance to shear failure. The vane consists of four rectangular blades in a cruciform at the end of a steel rod. The test works by pushing the vane into the soil and applying rotating torque until the soil fails. The shear strength can then be calculated by analysing the failure torque the applied torque to the rod. Soil cohesion and friction coefficient can be calculated based on Mohr Coulomb criteria of soil failure, based on a plot of maximum shear stress measured versus displacement (Schnaid, 2009).
4. Gamma-ray: Photons from a gamma source are absorbed or scattered at the time of interaction with the electrons of soil atoms, such that the number of photons incident on the detector at a given time is related to BD of the soil sample (Smith and Mullins, 2000).

- **Indirect methods including**: In addition to soil BD, soil compaction can also be expressed in terms of infiltration rate, total porosity and void ratio. In all cases total soil compaction is accompanied by soil volume decrease primarily on the soil air account, which either compressed of expelled out of the soil. Neither soil solid particles nor liquids are evidently compressible. However, soil solids could be rearranged or deformed under a compactive stress Lal

and Shukla (2004). Following are examples of indirect methods of measuring soil compaction:

1. Infiltration rate: Infiltration is the process, by which arriving water at the soil surface enters the soil, with its rate considerably reduced by compaction due to the deterioration of soil structure. Infiltration rate provides good sign of soil compaction (Haynes, 2010). Abu-Hamdeh (2004) found Infiltration rate decreased with increasing the axle load of different tillage regimes. At the same axle load, he reported infiltration rate was higher in the chisel-ploughed plots in comparison to the disk-ploughed or mouldboard-ploughed plots. There are many factors affecting the infiltration rate including soil structure, moisture content, surface condition, soil and water temperatures and if is tested by the double ring kit, the head of the applied water, diameter and depth of embedment of rings, also, would influence the infiltration rate measurements (ASTM).
2. Porosity: Porosity is usually expressed as a percentage of the empty spaces to total volume. There are many methods can be used to estimate soil total porosity, for example, directly by calculate the total volume of the sample pores, using water saturation method (pore volume = total volume of water − volume of water left after saturation), and optically, using a microscope to determine the of soil solids verses the area of the pores (Lal and Shukla, 2004; Carter, and Gregorich, 2007). Compaction causes a decreasing in total porosity (Douglas and McKyes, 1978; Schäffer et al. 2007). This decreasing not only may occur with a changes of pore morphology (Arvidsson and Håkansson, 1996), but also the pore size distribution may be changed (Richard et al., 2001), as macropores and micropores are not equally affected by compaction (Horn et al. 1995). So far, soil compaction was often assessed using total porosity, although total porosity value does not allow identifying the class of pores affected or the structural damages that occurred (Boivin et al. 2006)

Among the above discussed parameters to indicate soil compaction, soil BD might be the best indicator, although, it does not necessarily reflect soil functioning (e.g. air and water movement) (Quraishi and Mouazen, 2013b).

Other parameters e.g. saturated hydraulic conductivity and infiltration rate are more closely related to soil compaction (Fleige and Horn, 2000), compared to soil BD. The measurement of the soil hydraulic properties in the field is tedious and time consuming methods, the same drawbacks of measuring soil BD with the core sampling method. However, in comparison with the measurement of soil hydraulic parameters, the assessment of soil BD with a portable measuring system is possible (Quraishi and Mouazen, 2013b) and is faster, easier and more cost effective, which is particularly useful for precision agriculture applications and environmental risk assessment.

2.2. Spectroscopy

2.2.1. Background

Spectroscopy is basically an experimental science, which is concerned with the absorption, emission or scattering of electromagnetic radiation by atoms or molecules (Hollas, 2004). Electromagnetic radiation is the technical term for light, not just the human eye sensitive or visible light, but any light from radio frequencies to gamma rays. As the name suggests, light of all kinds is radiated through conjoined electric and magnetic fields (Tranter et al., 2000).

The absorption, emission and scattering phenomenas of light contain important spectra information about the structure and composition of matter. Spectroscopy is a powerful and sensitive tool used increasingly for chemical and physical analysis, as well as a method of probing electronic and nuclear structure and chemical bonding. The key to interpreting this spectral information is the knowledge that certain atomic and molecular processes involve only certain energy ranges. Figure 2-10 shows the regions of the electromagnetic spectrum and the associated energy transitions that occur in atomic and molecular processes (Thompson and Staley, 2014).

There are many types of spectroscopy for example:

- Electron spectroscopy
- Fourier transform spectroscopy
- Mass spectrometry

- Raman spectroscopy
- Optical spectroscopy

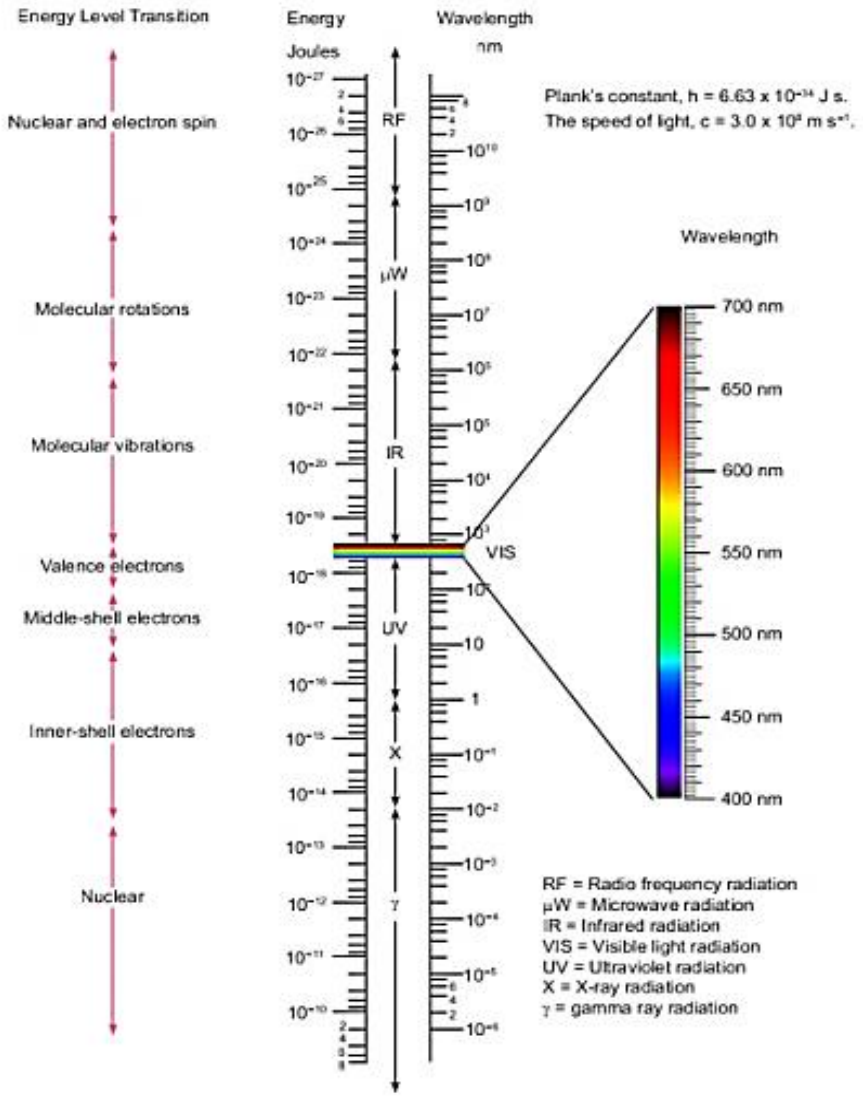

Figure 2-10 Electromagnetic radian regions and the associated energy transitions that occur in atomic and molecular processes (after, Thompson and Staley, 2014).

It is impossible to construct one single spectral device capable of covering whole optical range and providing information about the different processes of absorption, emission and scattering of light. This is particularly because of the technical limited operational ranges of light sources, detectors and other optical

components. Consequently, optical spectrophotometers can be classified according to their operating wavelength ranges as follow:

- Ultra Violet-visible (UV-VIS) (175-750 nm).
- Near-Infrared (NIR) (750-2500 nm).
- Mid-Infrared (MIR) (2.5-25 μm).
- Far-Infrared (FIR) (25-1000 μm).

Some spectrophotometers manufacturers are capable of covering neighbouring spectral regions, for instance, Vis-NIR, MIR-FIR or NIR-MIR spectrophotometers are now commercially available (e.g from Bruker Optics GmbH, Ettlingen).

Gauglitz and Vo-Dinh (2003) stated that comparing to the rest optical spectroscopic techniques, NIR showed the greatest variety of instrumentation principles, and the market for commercially available instruments is undergoing continuous change and growth. They showed that NIR spectroscopy has a vast variety of applications in many fields, for example, agriculture, food processing, medical and pharmaceutical, polymer and plastics industrials, environmental measurements, and remote sensing.

Visible and Near-infrared spectrometers differ considerably with respect to cost, size and portability, time needed for the measurement and environmental conditions for on-line applications in industry. According to their measurement techniques, NIR spectrophotometers fall into the following categories (Gauglitz and Vo-Dinh, 2003):

- Fourier-Transform spectrophotometers
- Scanning-Grating spectrophotometers
- Diode array spectrophotometers (fixed-grating spectrometers)
- Filter spectrophotometers
- Light-emitting diode (LED) spectrophotometers
- Acousto-optical tuneable filter (AOTF) spectrophotometers

Burns and Circzak (2008) expressed that the NIR spectroscopy is widely used in agriculture applications for determining the quality of grain products, oilseeds, coffee, tea, spices, fruits, vegetables, sugarcane, fats, and dairy products e.g. eggs, meat and milk. They explained the advantages of NIR spectroscopy as it meet the criteria of being accurate, reliable, rapid, non-destructive, and inexpensive. The accomplishment of sustainable agricultural and environmental management requests a better understanding and precise information of the soil at increasingly finer scales. Traditional soil sampling and laboratory analyses cannot efficiently supply this important information because they are slow and expensive for spatial scales (Viscarra Rossel and McBratney, 1998).

2.2.2. Visible and near infrared spectroscopy (Vis-NIRS) implementation in soil science

Visible and near infrared spectroscopy refers to the electromagnetic spectrum range, that starts from 400 nm to 700 nm for visible light and from 700 to 2500 nm for the near infrared range. When near infrared radiation interacts with a soil sample, it is the overtones and combinations of fundamental vibrations of chemical bonds in the mid infrared that are detected (Miller, 2001). Generally, the NIR region is characterised by broad, superimposed and weak vibrational modes giving soil NIR spectra few and broad absorption features (Figure 2-11b). In the visible region electronic excitations are the main processes as the energy of the radiation is high.

Some dominant soil components and absorption peaks in the MIR range are indicated in Figure 2-11A for quartz (Q) as sand, organic compounds (OC), calcite (Ca), kaolinite (K), smectite (S), and (OH) features of free water and lattice minerals. Due to the broad and overlapping bands vis-NIR spectra are visually not very resolving and are difficult to interpret (Figure 2-11B). Nevertheless, this region does contain useful information on organic and inorganic materials in the soil. Absorptions in the visible region (400–780 nm) are primarily associated with minerals that contain iron (e.g. haematite, goethite) (e.g. Sherman and Waite, 1985). Soil organic matter can also have broad absorptions in the visible rang, which are dominated by the darkness of

humic acid. Absorptions in the NIR (780-2500 nm) result from the overtones of OH, SO_4 and CO_3 groups as well as combinations of fundamental features of H_2O and CO_2 (*e.g.* Clark, 1999). Clay minerals can show absorption in NIR-region due to metal-OH bend plus O-H stretch combination (Viscarra Rossel et al., 2006). Water has a strong influence on vis-NIR spectra of soils. The dominating absorption bands of water at 1450 and 1950 nm are characteristic for soil spectra (Figure 2-11B), but there are also weaker bands all over the vis-NIR range (Mouazen et al., 2006). In addition to soil water, soil texture and colour all affect the spectral features of the vis-NIR soil spectra, hence the prediction performance of soil properties (Mouazen et al., 2005a; Mouazen et al., 2006b; Mouazen et al., 2007).

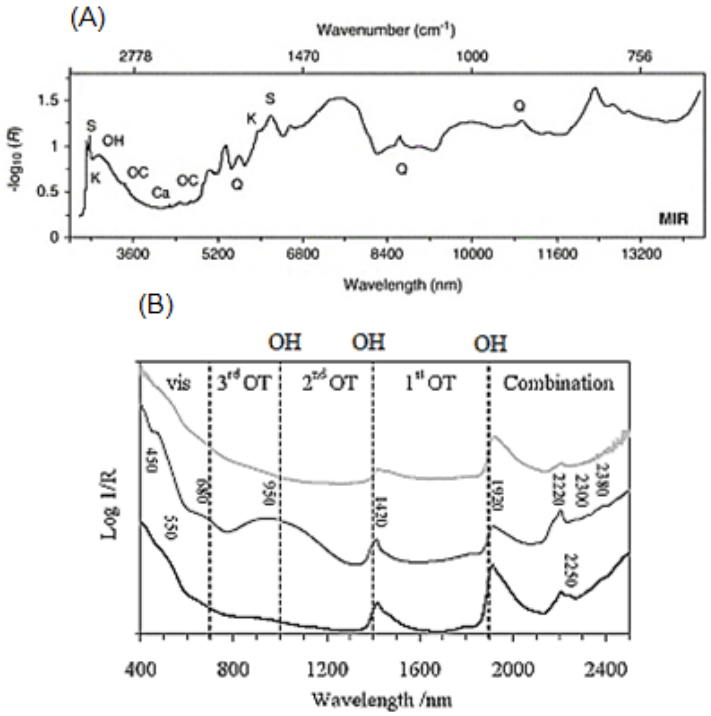

Figure 2-11 Soil diffuse reflectance spectra (A) the MIR 2500–25000 nm (4000–400 cm-1) showing approximately where the fingerprints for quartz (Q) as sand, organic compounds (OC), calcite (Ca), kaolinite (K), smectite (S), and (OH), and (B) the vis-NIR 400–2500 nm (25,000–4000 cm-1) showing approximately the combination, first, second and third overtone (OT) vibrations occur as well as the vis range with red (680 nm), green (550 nm) and blue (450 nm) bands (after Stenberg et al., 2010).

2.2.3. Vis-NIRS analyses of soil properties

Vis-NIRS has become increasingly used for rapid analyses of soil chemical, physical and biological properties that can be useful for different applications. The early stages of the instrumentation of the light detector were with a single wavelength transmitter and receiver to measure the influence of a single soil element on spectra data (e.g. soil OM) (Shonk et al., 1991). With vis-NIRS detectors development and increased commercially availability, they are used widely across the world to determine most soil properties, such as soil moisture content (Qurishi and Mouazen, 2013b), soil organic matter (Li et al., 2012), CC (Viscarra Rossel et al. 2009), total nitrogen, phosphorous, pH, magnesium, calcium, cation exchange capacity and potassium under laboratory (Pietrzykowski and Chodak, 2014; Ben-Dor & Banin, 1995; Chang et al., 2001; Mouazen et al., 2010) and field soil conditions (Mouazen et al., 2006; Waiser et al., 2007; Marín-González et al., 2013). Less success was reported for the measurement of mineral nitrogen (Stenberg et al., 2010; Kuang et al., 2012). Soil properties were divided from accuracy of measurement point of view into two categories, namely spectrally active and in-active categories (Stenberg et al., 2010. Soil organic carbon (Nocita et al. 2014), organic matter, CC and moisture content sit under the first category, and have direct spectral response in the NIR range. This is the reason why these properties can be measured with high accuracy (Kuang et al., 2012). The remaining soil properties have no direct spectral response in the NIR range, but measurement can be successful through co-variation through other soil properties having direct spectral response (Stenberg et al., 2010).

Researchers attempted to use different calibration algorithms, among which partial least squares regression (PLSR) is the most popular, for its simplicity and availability of user friendly Unscrambler software. Studies concluded that non-linear methods such as artificial neural networks or support vector machine result in a better predicting performance as compared to the linear PLSR (Mouazen et al., 2010; Viscarra Rossel and Berhens, 2010). Christy et al. (2003) presented a soil mapping system, which implementing NIR

spectrophotometer with the range 900–1700 nm to measure a number of soil properties in a single field in central Iowa. They used principal component regression analysis as a calibration technique, giving the following results for the estimation soil moisture, total carbon, total nitrogen, and pH with R^2 values of 0.82, 0.87, 0.86, and 0.72, respectively, and RMSEp values of 2.996, 0.453, 0.029 and 0.464, respectively. Lee et al (2009) used the ASD FieldSpec Pro FR spectrophotometer (Analytical Spectral Devices, Boulder, Colorado, USA) to estimate soil physical and chemical properties and determine the significant wavelength ranges or bands for selected soil elements. They obtained mixed estimation accuracies for soil elements with R^2 values of 0.80, 0.72, 0.78, 0.80, 0.87 and 0.24 and RPD values of 2.24, 1.88, 2.11, 2.22, 2.73 and 1.15 for clay, silt, sand, Ca, organic carbon and K, respectively. They concluded that reducing the spectra wavelength between 1770 to 2500 nm wouldn't affect estimation accuracy when compared with the full wavelength range spectrum of the spectrophotometer (350 – 2500 nm). Mouazen et al. (2007) arrived at a similar conclusion but for a spectral range of 350-177 nm as compared with 350 – 2500 nm. Yang et al. (2011) found total nitrogen could be predicted more accurately than total carbon with R^2>0.90 and RPD>3.3, using spectra data only from the visible range (400-700 nm). However, the prediction of total carbon needed almost the full range of the ASDi spectrophotometer with range 350 – 2500 nm wavelength.

Morgan et al. (2009) used vis-NIR spectra to predict soil organic and inorganic carbon using the PLSR calibration technique. They reported that *in-situ* spectroscopy can measure organic and inorganic carbon with lower accuracy compared to the grounded and dried samples in the laboratory. Similar results were reported by other researchers (e.g. Chang et al., 2001; Tekin et al., 2012). However, Stenberg (2010) found a contrast results, so that accuracy of soil properties measurement were higher when wet (fresh) samples are used as compared to dry samples. The diverse and contradict results reported by different research group around the world necessitate the need for further research to come to robust conclusions on the capability and limitations of the vis-NIR spectroscopy application for soil analyses.

2.2.4. Vis-NIRS analysis of soil moisture

vis-NIRS has been shown to provide an alternative measuring method to predict ω under laboratory non-mobile measurement conditions (Mouazen et al., 2006; Quraishi, 2013) and on-line mobile conditions (Mouazen et al., 2005; Kuang and Mouazen, 2012). These successful applications were attributed to the strong influence of the O-H bond on vis-NIR spectra of soils (Kuang et al., 2012; Stenberg et al., 2010). Viscarra Rossel and McBratney (1998) reported on the typical reflectance spectrum measured for 60 prepared soil samples showing evidence of the strong absorption bands of O-H bonds in soil water at around 1450, 1950 and 2500 nm. Similarly, Bowers and Hanks (1965) stated that reflectance wavelength magnitudes are noticeable at several different soil moisture levels and they concluded that the absorption bands are highly affected by water and specifically represent the overtones of the fundamental frequencies at which water molecules vibrate (Figure 2-12).

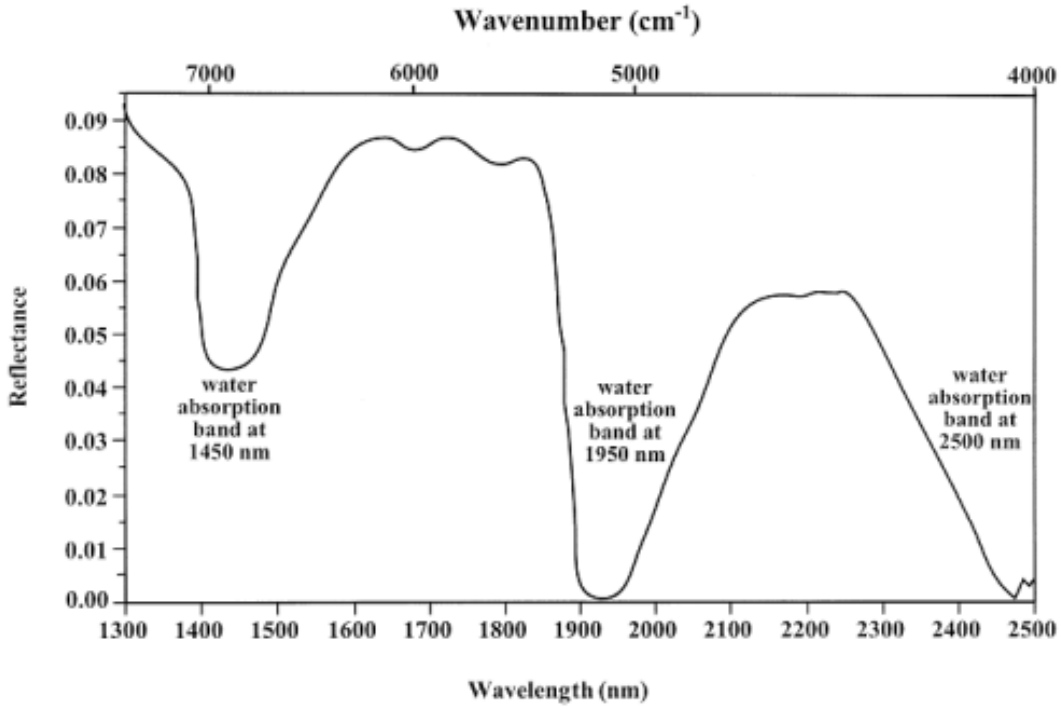

Figure 2-12 The representative NIR reflectance spectrum of soil samples, showing the three water absorption bands at 1450, 1950 and 2500 nm (after Viscarra Rossel and McBratney, 1998).

Mouazen et al. (2005a) during laboratory studies of soil, measured diffuse reflected vis-NIR spectra characteristics at various moisture content levels. Significant variations in the curves shape and reflectance percentages corresponding to soil moisture levels were reported (Figure 2-13). They concluded that increasing soil moisture content will result in a darker soil surface which will consequently decrease the reflected light.

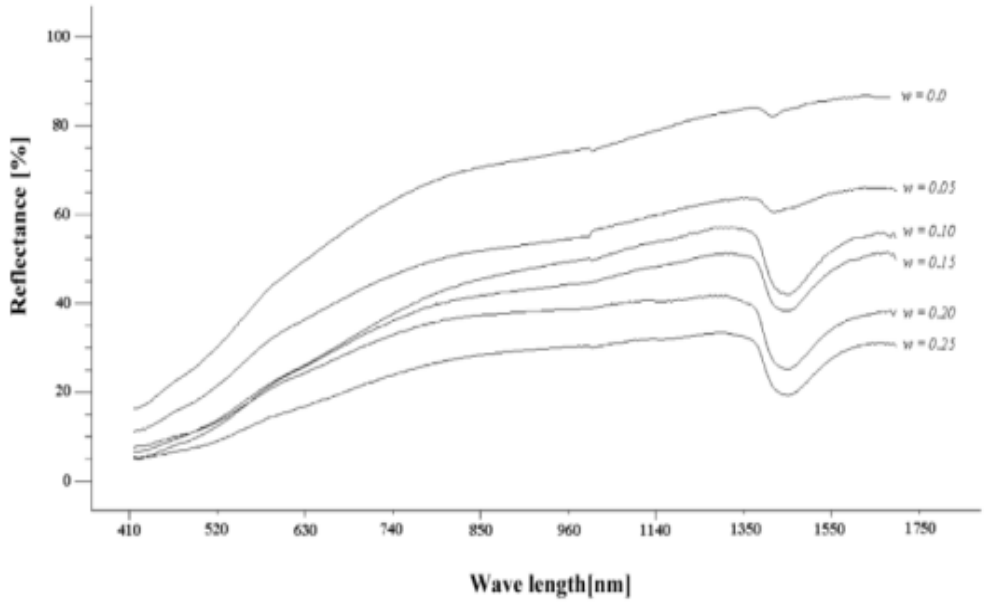

Figure 2-13 Effect of soil moisture content on the reflectance spectra (after Mouazen et al., 2005b).

Al-Asadi and Mouazen (2014) found that the ANN calibration technique more accurately predicted soil moisture content using the ASDi vis-NIR spectrophotometer (350 – 2500 nm), as compared to the PLSR calibration method. They tested both calibration methods using a wide range of soil texture, moisture levels and land use. However, they reported that soil moisture content could be estimated even better at field scale with a specific calibration model in comparison with multi-field measurement. Similar conclusion was reported by Mouazen et al. (2006b).

2.3. Dielectric sensors implementation in soil science

Materials in nature can be divided into conductors and insulators due to their response to an applied electric field. A conductor is a type of material, which permits the flow of electric charges in one or more directions, like copper, aluminum, iron, etc. On the other hand, dielectric materials or insulators won't allow electric charges to pass through them, but instead, they only slightly shift from their average equilibrium positions causing dielectric polarization. From an electromagnetic standpoint, soil is classified as a dielectric material. A wet soil medium has three dielectric components consisting of: the solid matrix, a gaseous stage, and the liquid water stage. The liquid water can also be subdivided further into free water and bound water, which is due to the restriction in its mobility by adsorption on solid particle surfaces (Hallikainen et al., 1985). Under dry conditions (or the pure soil minerals) the dielectric constant of the soil is between 3 and 5 (Gaskin and Miller, 1996).

Dielectric sensors have been widely used for determining soil water content. They attempt to distinguish the relationship between the dielectric constant of the soil-water-air matrix and θv (Figure 2-14). This is particularly due to the dielectric constant of the free water having a high permanent electric dipole moment, resulting in a substantially high value (~ 80) unlike both soil (~5 for pure soil minerals) and air (~1) (Topp et al. 1980; Gaskin and Miller, 1996; Robinson et al., 1999), and thus dominates the dielectric constant of the soil-water-air matrix (Schmutz, 2007). In other words, the overall dielectric constant of the soil as a matrix is greatly influenced by the water content in the soil (Robinson et al., 2003).

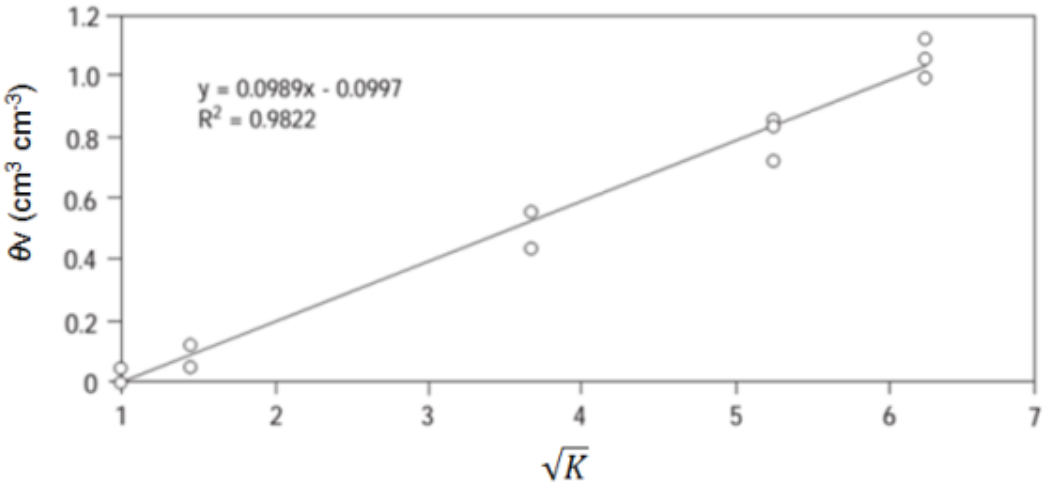

Figure 2-14 Relationship between the square root of the soil dielectric constant ($\sqrt{K}$) (dimensionless) and volumetric water content (θv) (m^3 m^{-3}) (after, Gaskin and Miler 1996).

Dielectric constant based soil moisture sensors take several forms as follows:

- Time Domain Reflectometry (TDR).
- Frequency Domain Reflectometry (FDR) which can be also subdivided into capacitance and impedance sensing probes.

- **Time Domain Reflectometry (TDR)**

Time domain reflectometry is used to test electrical cable continuity. Its principle relies on transmitting a fast rise-time electromagnetic signal (in the form of a step-wave) through the conductor and measuring the velocity of the transmitted signal through the conductor. If the conductor has uniform impedance and is properly terminated, the whole propagated signal will be received at the far-end termination and no reflected signal will be received by the TDR. If the conductor impedance has any discontinuities, a reflectance signal will be sent back towards the TDR. However, increasing the conductor impedance will generate a reflection that reinforces the original signal, whereas any decrease in the

conductor impedance will produce a reflection that opposes the original signal (Behari, J. 2005; O'Connor and Dowding, 1999).

The time (*t*) of the TDR pulse propagating one return trip in a transmission and receiving through line of length *L* (m), is expressed by:

$$t = \frac{2L\sqrt{\varepsilon_a}}{C} \qquad 2\text{-}2$$

Where *t* is the round trip propagation time (s), *C* is the speed of light in the free space (3 x 10^8 m s^{-1}) and ε_a is the apparent permittivity of the medium (Moret-Fernández et al., 2012; Robinson et al., 2003).

Topp et al (1980) first used the TDR measuring system (Figure 2-15) to predict θv. They collected worldwide mineral soil samples with different textures and moistures, and measured the samples using a range between 20 MHz and 1 GHz. They derived an empirical relation with an error of ±0.01 for estimating θv from *K* for mineral soils. The relation can be written as follows:

$$\theta\mathrm{v} = -0.053 + 0.0292K - 0.00055K^2 + 0.0000043K^3 \qquad 2\text{-}3$$

Where: θv is soil volumetric moisture content and *K* is the dielectric constant of the soil, the dielectric constant does not have units or dimensions because it expresses the ratio of permittivity of a substance to that of free space or a vacuum.

Ponizovsky et al., (1999) studied how different soil textures affect TDR calibration. They tested sandy, loamy sand, sandy clay, silt loam and clay soil textures, finding that the performance of the TDR calibration models was significantly influenced by the soil texture.

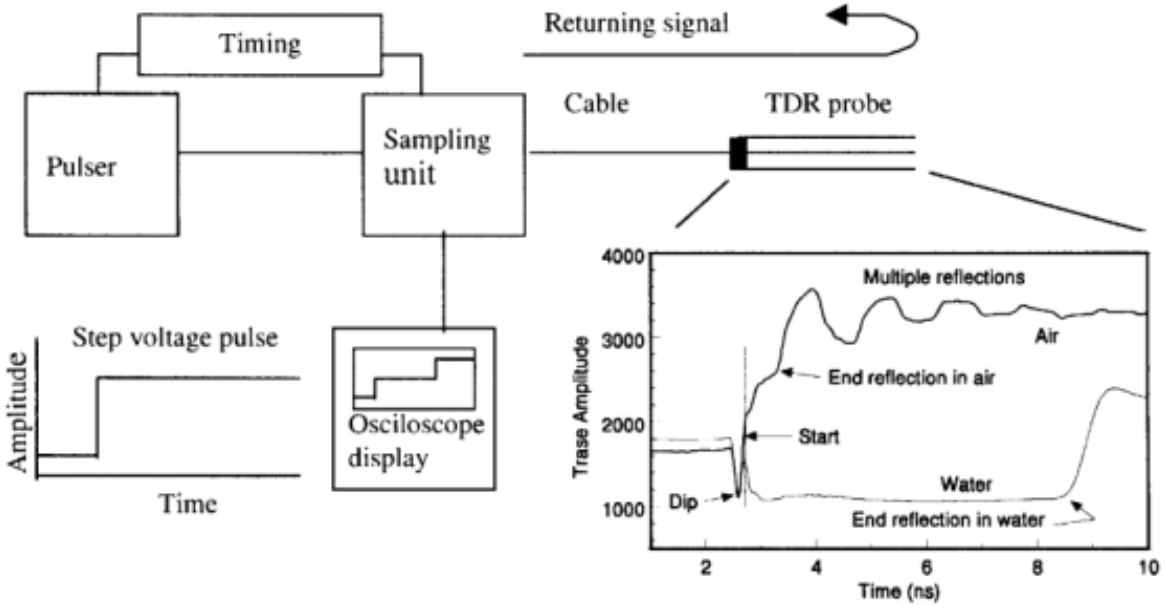

Figure 2-15 A schematic diagram of the TDR main components and a chart of two wave propagations through air and water (Robinson et al., 2003).

- **Frequency Domain Reflectometry (FDR)**

The complex nature of the TDR technique led to soil dielectric constant measurement based on FDR becoming popular method for the measurement of soil θv during the last few decades (Topp et al., 1980; Miller and Gaskin, 1996; Robinson et al., 1999). FDR in comparison is cheaper to manufacture, less complicated, and has a faster reading response. However, because of the complex electrical field around the probe, the sensor needs to be calibrated for different soil types (Kaleita et al., 2005). Some commercial sensors have been able to remove the soil type effect of the sensitivity by using a high operating frequency (Delta-T Devices Ltd., 1999). Gaskin and Miller (1996) used a FDR sensor with a 100 MHz operating frequency to measure soil θv, which is the soil impedance sensitivity corresponding to the variation of soil θv. This sensor was commercialized under the name of ThetaProbe (Delta-T Devices, Cambridge, UK) (Figure 2-16). The ThetaProbe (Delta-T Devices Ltd., 1999) was reported to be capable of measuring soil θv with ±0.01 m^3 m^{-3} accuracy after a single calibration using two readings of wet and dry soil samples for the soil type

specific calibration, although, ±0.05 m^3 m^{-3} accuracy can be achieved when generalised calibration by the manufacturer is applied (Foley and Harris, 2007; Jones et al., 2002; Walker et al., 2004).

Figure 2-16 ThetaProbe soil moisture sensor. The four stainless steel electrodes are 6 (cm) in length and 3 (mm) in diameter (after, Kaleita et al., 2005).

Using a ThetaProbe, Gaskin and Miller (1996) provided a third order polynomial relationship between the standing wave signal, which converted to a voltage output reading (V), and the soil dielectric constant, written as follows:

$$\sqrt{K} = 1.07 - 6.4V - 6.4V^2 + 4.7V^3 \qquad 2\text{-}4$$

Where: $\sqrt{K}$ is the square root of the soil dielectric constant (dimensionless) and V is the output voltage of ThetaProbe (mV).

Soil texture strongly affects the accuracy of the FDR sensors for the measurement of θv. Cosh et al. (2005) tested the ThetaProbe accuracy using different calibration models for Clayey, Loamy and Sandy soil textures and they compared soil texture calibration models with the generalised calibration by the manufacturer and with the Topp and Reynold (1998) calibration formulas. Figure 2-17 shows the effect of the different calibration models on the predicted function between θv and soil dielectric constant. They concluded that soil texture has considerable influence on the calibration of the ThetaProbe.

Ponizovsky et al. (1999) also reported the performance of dielectric-based sensors is affected by soil texture.

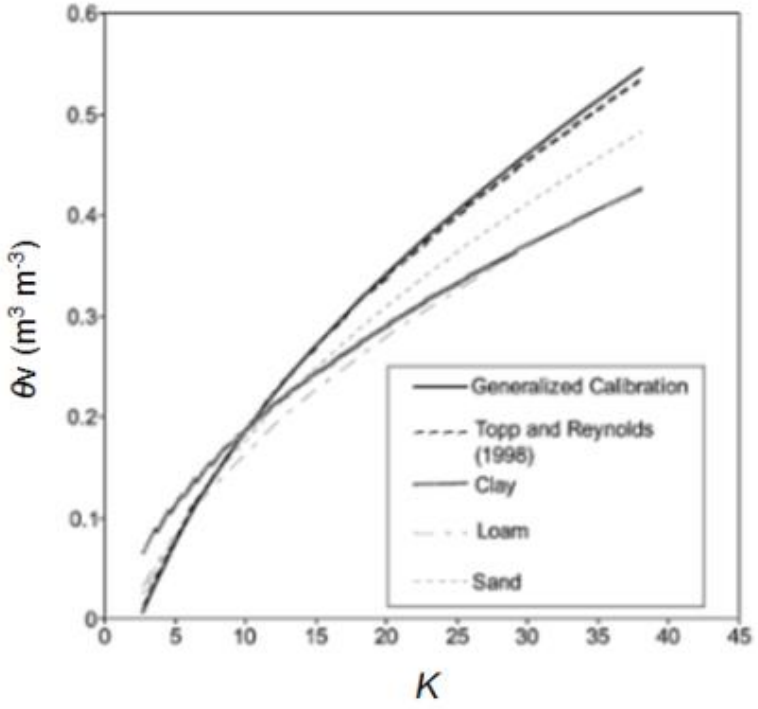

Figure 2-17 Plot of volumetric soil moisture content (θv) as a function of dielectric constant (K) for various calibration models of ThetaProbe (after, Cosh et al. 2005).

Rowlandson et al. (2013) established calibration models for a number of soil textures and different land use using dielectric-based soil moisture sensor. The results show the best estimation accuracy was obtained with loamy fine sand and the accuracy declined with increasing clay fraction (Table 2-2). They calculated the two calibration parameters (A and B) for each individual soil texture to be used in a general calibration relation written as follows:

$$\theta \mathrm{v} = \mathrm{A}\sqrt{K} + \mathrm{B} \qquad 2\text{-}5$$

Where θv is soil volumetric moisture content (m^3 m^{-3}) and $\sqrt{K}$ is the square root of soil dielectric constant.

Since salinity affects the output of FDR sensors, many researchers have studied the effect of soil salinity on the dielectric measurement accuracy. It has been pointed out that soil conductance could be avoided and the measurement accuracy could be significantly improved by using a higher frequency of 30 MHz (Sun et al., 2006). Singh et al. (1992) identified a strong polarization effect due to soil electrical conductivity around 15.86 MHz frequency and they reported that this effect is relatively low at 47.45 MHz frequency. Gaskin and Miller (1996) and Sun et al. (2006) have chosen a 100 MHz operating frequency for soil dielectric sensors in order to minimize the influence of soil salt content on soil moisture content prediction. Robinson et al (1999) reported that the ThetaProbe overestimated soil dielectric constant for sandy and sandy loam soils by approximately 1.5 when compared with TDR estimation results. They suggested that the reason for this was because of the high soil BD around the electrodes.

Table 2-2 Accuracy of the ThetaProbe calibration for different soil textures, land use, number of soil samples (n) and the individual calibration parameters A and B for the general calibration relation (after, Rowlandson et al., 2013).

Soil texture	Land cover	A	B	R^2	RMSE (m^3 m^{-3})	Bias (m^3 m^{-3})	SN
Loamy fine sand	Grassland	0.1054	-0.1505	0.97	0.0121	0.0012	10
Clay	Wheat	0.0975	-0.1489	0.88	0.0491	0.0024	11
Loam	Soybeans	0.0967	-0.1518	0.73	0.0391	0.0015	17
Loamy very fine sand	Canola	0.0762	-0.0829	0.84	0.0241	<0.001	13
Silty loam	Soybeans	0.0898	-0.0952	0.56	0.0398	0.0016	16
Silty clay loam	Wheat	0.077	-0.039	0.84	0.0356	0.0013	12
Fine sandy loam	Corn	0.1153	-0.1905	0.83	0.0337	0.0011	13
Clay loam	Canola	0.0936	-0.1073	0.80	0.04	0.0016	11
				Average	0.034		

RMSE is root mean square error; SN is sample number.

2.4. Multi-sensors and data fusion approaches in soil science

Since agricultural soil is naturally complex material that exhibit spatial and in depth heterogeneity. Quantitative estimation of one or more soil properties cannot be made successfully with one sensing technology. Peers working on the development of soil sensors realised this fact, for which they proposed solutions based on multi-sensor and data fusion approaches. A comprehensive literature review discussed these in more details (Kuang et al., 2012). However, these sensing systems can be categorised into on-line (mobile) and *in-situ* (non-mobile) systems. The following section will discuss the major sensors reported in the open literature.

2.4.1. Historical developing of the on-line multi-sensors

On-line sensors collect data in real time. They are either drawn by a tractor or a quad bike. Many researchers and manufacturers have attempted to develop on-line multi-sensors for measuring soil mechanical, physical and chemical soil properties (Adamchuk et al., 2004). The first on-line measuring system was developed in 1991, when Shonk et al. (1991) presented a measuring system of soil organic matter, which was basically a transmitting and receiving unit using a single wavelength (660 nm) of light. The system was fitted on a tractor, which travelled at a speed of 4.8-6.5 km/h and measured soil organic matter at 7.5-10 cm depth. The system prediction accuracies were various depending on soil organic matter percentage; R^2 values of 0.89 and 0.95 with <1% and >6% of soil organic matter, respectively, were reported.

There are several types of sensors that measure 'indirectly' soil compaction depending on the soil property to be measured. Hemmat and Adamchuk (2008) classified soil compaction sensors into three families, namely, water content sensors, soil strength sensors, fluid permeability sensors and their combinations (Figure 5-3). Mosaddeghi et al. (2007) stated that we should not only rely on the strain-related properties as the dependent variable for the assessment of soil compaction, whereas different soil properties can also be considered as a sign of compaction.

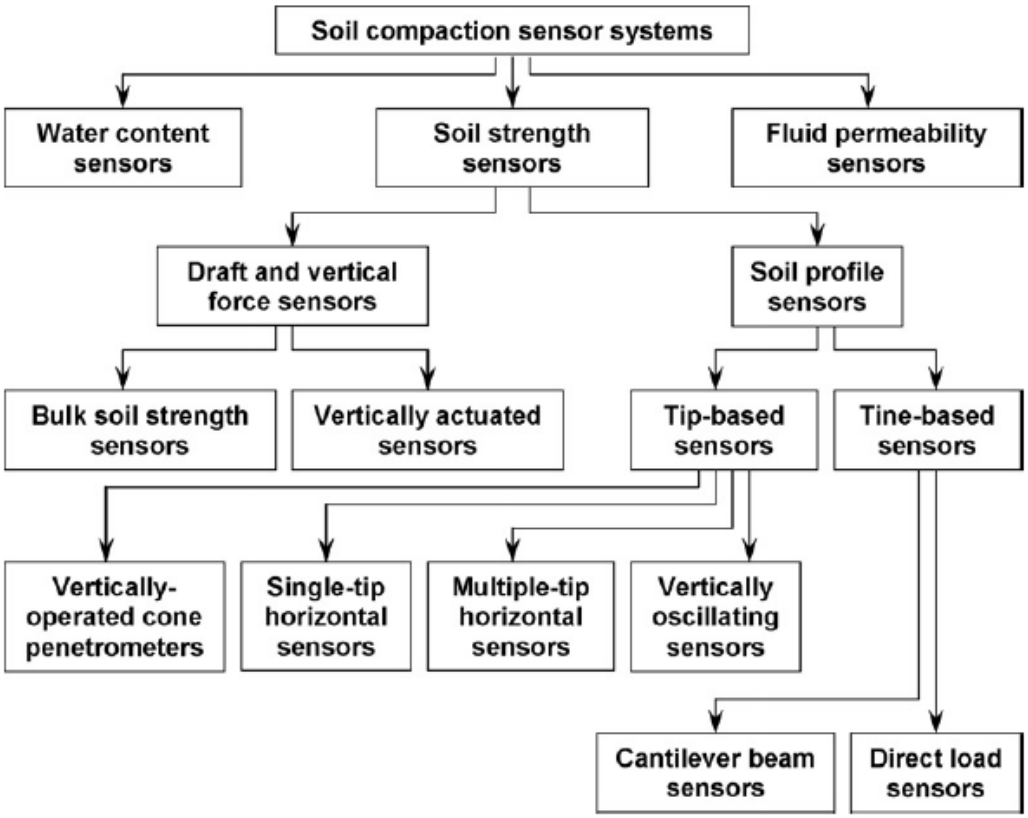

Figure 2-18 Classification of soil compaction sensor systems (after, Hemmat and Adamchuk, 2008).

Stombaugh (2014) has developed an on-line air permeability sensor to assess soil compaction, which consists of a subsoil plough with a vertical plate containing two outlet holes on each side (Figure 2-19). The system is sensitive to the air flow changes due to various soil BD. Author reported low accuracy of measurement due to the difficulty of separating the effect of soil compaction from soil texture interaction.

Figure 2-19 On-line air permeability measuring system to estimate soil compaction (A) and the subsoiler with the outlet holes plate attached (B) (after, Stombaugh, 2014).

Adamchuk et al (2008) used a sensor array consisting of optical reflectance and dielectric (capacity-based) sensors, in addition to a vertical cutting blade attached to a platform of three sets of load cells (Figure 2-20), which were deployed to measure OM and moisture content of the soil, respectively. The whole dataset collected by the system was used to predict spatial variability of soil mechanical resistance. They reported a marginal correlation between soil mechanical resistance obtained from the mapping system and soil PR measured using a standard vertical penetrometer (R^2 = 0.32).

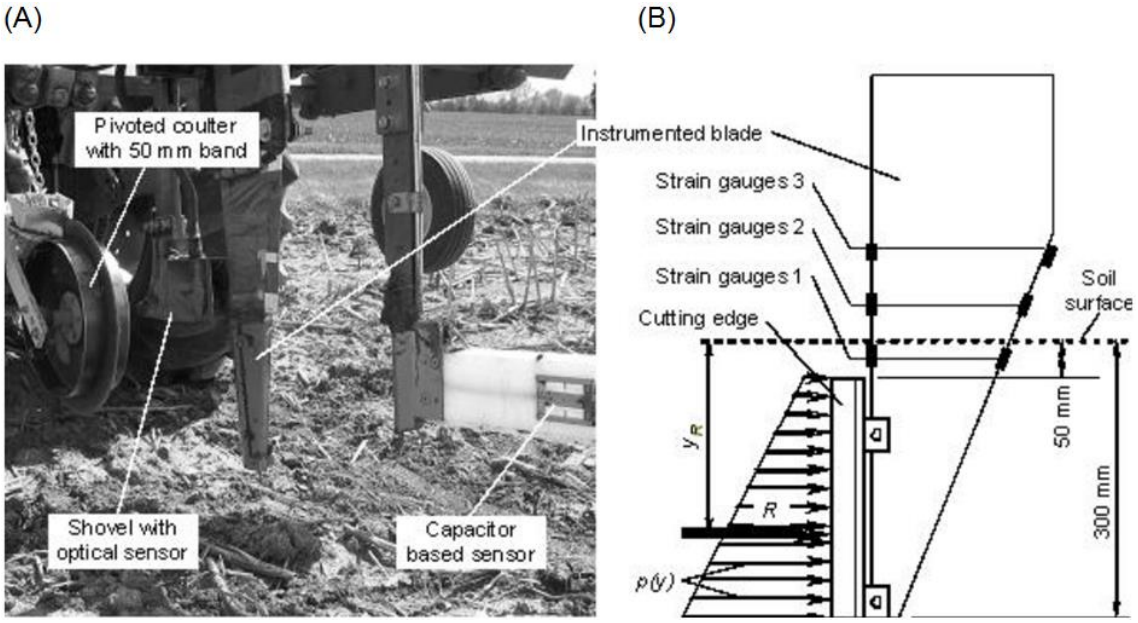

Figure 2-20 On-line soil mapping system (A) and free-body diagram of the system and the vertical cutting blade (after, Adamchuk et al, 2008).

Mouazen et al. (2005) developed a multi-sensor platform for the measurement of soil moisture content and BD (Mouazen and Ramon, 2006). The platform consisted of a draught sensor, a depth sensor and a vis-NIRS probe, attached to the back of a cutting tool (e.g. subsoiler). This platform was later used for the measurement of soil pH, phosphorous, moisture content and organic carbon (Mouazen et al. 2007), achieving good results, plotted in Table 2-3. The vis-NIR measurement was based on a vis-NIR spectrometer developed by Zeiss Company (Zeiss Corona 45 visnir fibre, Germany), which consisted of two detectors including a Silicon-diode-array detector for the visible and short infrared wavelength region (306.5–1135.5 nm) and an InGaAs diode-array detector for the NIR region (944.5–1710.9 nm). A light source of a tungsten-halogen bulb with a 20 W power was used to illuminate the soil surface through two fibre optic cables for illumination and reflectance with a 45° angle between them formed in a lens holder (Figure 2-21).

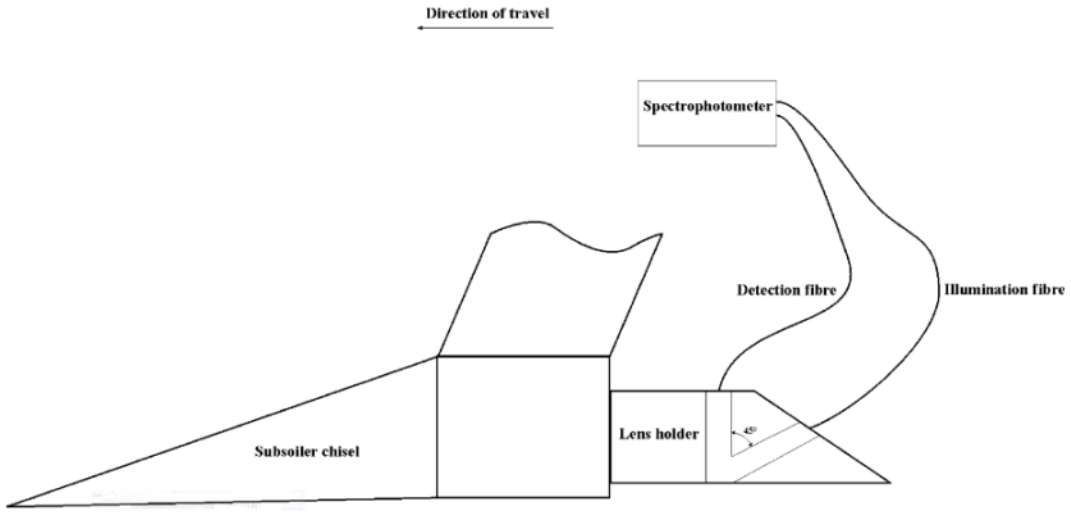

Figure 2-21 Schematic diagram of the lens holder attached to subsoiler chisel for the on-line measuring system (after, Mouazen et al., 2007).

Table 2-3 Results of soil properties prediction using Zeiss Corona 45 vis-NIR spectrometer and deploying PLSR with leave-one-cross-validation calibration methods (after, Mouazen et al, 2007).

Property	R^2	Slope	Intercept	RMSEp	RPD
C-org	0.74	0.77	0.381	0.480	1.97
C-tot	0.73	0.75	0.355	0.268	1.92
MC	0.89	0.89	0.015	0.024	3.00
pH	0.71	0.74	1.830	0.215	2.14
P-avl	0.69	0.74	1.963	1.345	1.80
P-ext	0.73	0.75	9.696	11.523	1.94

RMSEp is the root mean square error of prediction; RPD is the residual prediction deviation = standard deviation (SD) divided by RMSEp; C-org is organic carbon; C-tot is total carbon; P-ext is extractable phosphorous; P-avl is available phosphorous; MC is moisture content.

Sun et al (2006) designed and tested an on-line measuring system of soil moisture and PR using a horizontal combined probe (Figure 2-22), which is a cone penetrometer and a FDR capacitance type sensor. The other measuring system components were: cone blade with 40 (cm) in length and 5 (cm) in width, load cell and data acquisition electronic board (PCL-818, SPECTRE) using Delphi 6.0 software. The capacitance probe showed high accuracy of (θv)

prediction at silt loam soil texture with R^2 = 0.99 compared to the oven-drying method. However, a weak (R^2 = 0.51) estimation of soil BD was reported.

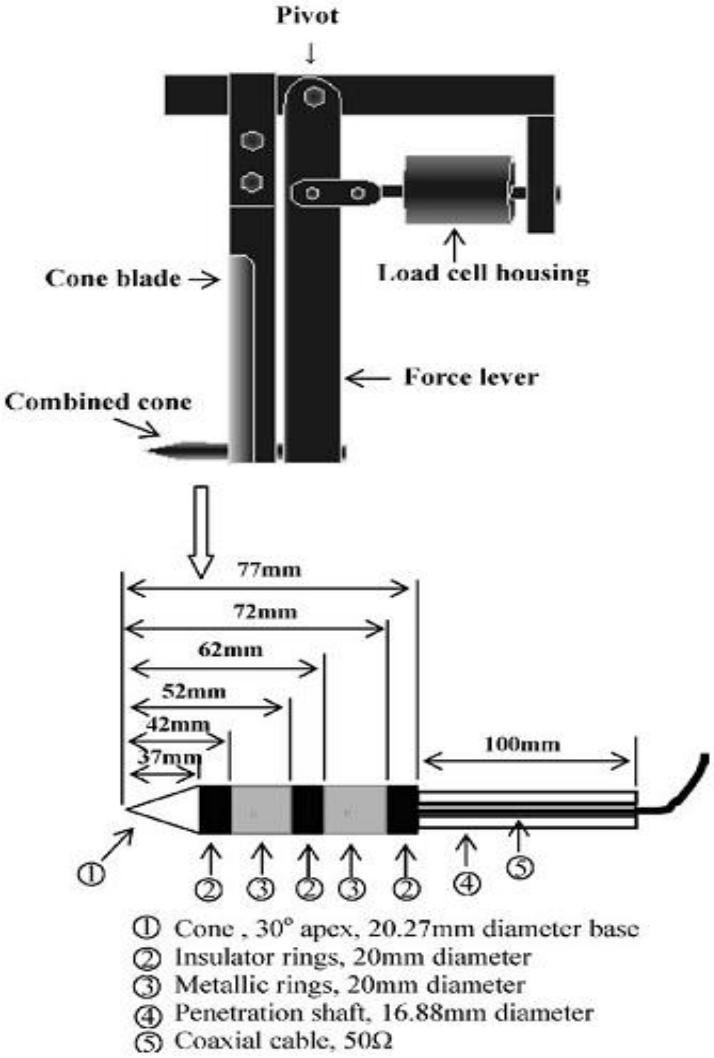

Figure 2-22 An on-line horizontal combined penetrometer for measurement of volumetric moisture content (θv) and penetration resistance (PR) (after, Sun et al. 2006).

Christy (2008) developed a soil mapping system using a vis-NIR spectrometer with the wavelength range of 900 to1700 nm built into a shank (Figure 2-23). This was commercialized and is available currently for research use by Veris Technologies, USA. It consisted of a sapphire window mounted on the bottom of the shank, a tungsten halogen bulb used to illuminate the soil, a fiber optic to

direct reflected light and InGaAs photodiode-array spectrophotometer manufactured by Control Development Inc., South Bend, IN, USA. Labview software (National Instruments, Austin, TX, USA) was used for data acquisition and all subsequent data processing.

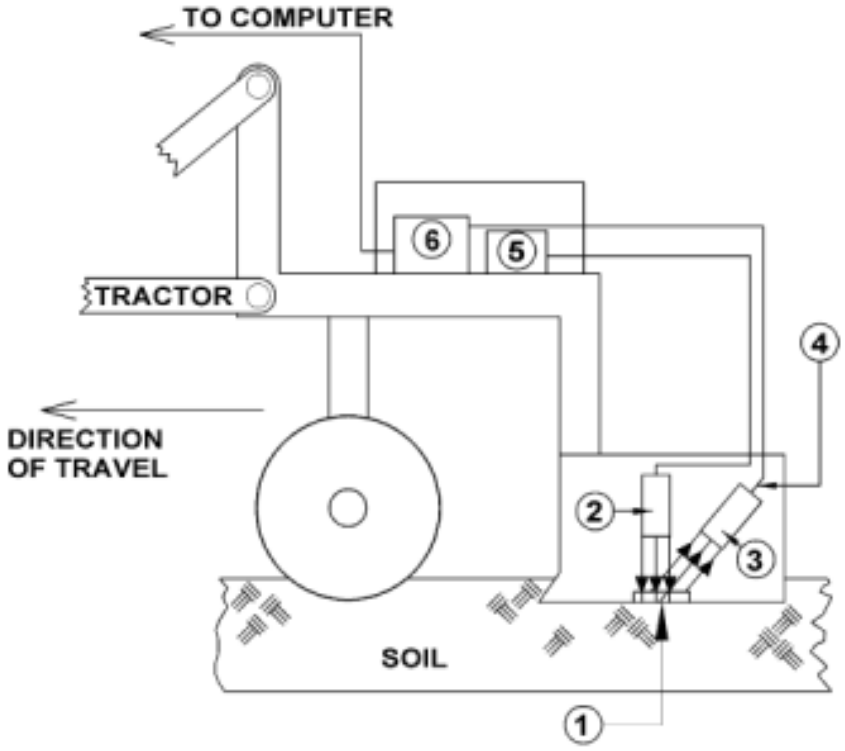

Figure 2-23 An on-line horizontal combined penetrometer for measurement of volumetric moisture content (θv) and penetration resistance (PR) (after, Sun et al. 2006).

They used locally weighted principal component regression calibration method with a leave-one-out cross-validation. The mapping system achieved R^2 values of 0.65, 0.80, 0.80, 0.60 and 0.92 for soil moisture content, organic matter, P, K and total carbon, respectively, and RMSE values of 2.8, 0.40, 30.0, 107 and 0.15, respectively.

Adamchuk et al. (2009) have developed a combined mapping system of soil physical properties (Figure 2-24) that consists of an instrumented blade for measurement of mechanical resistance, optical and capacitance sensors. The

latter operating frequency of the capacitance was 12.7 and 18.9 MHz for the dry and wet soil conditions, respectively. They reported R^2 values between laboratory and sensor-based measurements of 0.57 for both θv and ω. However, the data fusion of soil mechanical resistance and capacitance sensors was capable to predict soil BD with $R^2 = 0.71$ (Adamchuk et al. (2009).

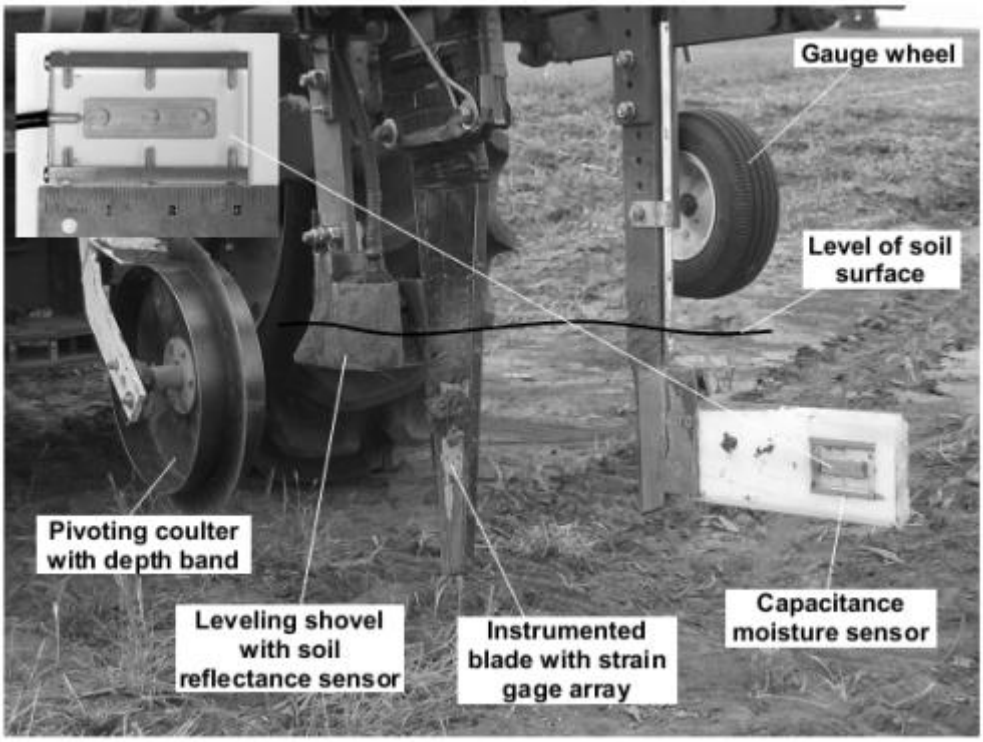

Figure 2-24 A Combined on-line mapping system (after, Adamchuk et al., 2009).

Kweon et al (2008) developed soil profile array sensors (Figure 2-25) which consisted of a vis-NIRS of 450 nm to 2200 nm wavelength spectrum to measure ω, a string potentiometer to measure PR, a soil conductivity probe, a GPS and a thermometer. PLSR was used to develop calibration models based on the leave-one-out-validation. They concluded that three of the six fields measured in Kansas State showed satisfactory results for estimating soil BD with R^2 value as high as 0.78 and lowest RMSE of 0.07 g cm^{-3}.

Figure 2-25 Soil profile array sensors (after Kweon et al., 2008).

Based on the on-line sensing platform of Mouazen et al. (2006), and algorithms to predict BD produced by Mouazen and Ramon (2006) and Mouazen and Ramon (2009), Quraishi and Mouazen (2013b) expanded the algorithms to estimate soil BD to the majority of soil types in the UK. This was done by developing a correction factor of the BD estimation for each soil texture class based on ANN analysis with input data on soil gravimetric water, texture, draught and depth obtained from the on-line multi-sensor mapping system. The ANN analysis resulted in the best model to predict a correction factor as function of moisture content and soil texture fractions (R^2 = 0.96), which allowed the utilisation of the on-line measurement system for any field having any texture and average moisture content. The on-line BD sensor showed good capability of predicting field BD rapidly for a large number of samples with high accuracy with a high R^2 value of 0.81 and a low RMSEp of 0.11 Mg m^{-3}.

Dhillon et al., (2010) presented an on-line soil mapping system, which integrated an optical sensor with only two wavelengths (505±10 and 880±10

nm) detection capabilities, ahead of a capacitance probe in addition to a load cell sensor. The mapping system can be towed by a pick-up truck (Figure 2-26). Based on laboratory calibration, the capacitance probe predicted θv and ω with standard errors of 0.016 cm^3 cm^{-3} and 0.014 g g^{-1}, respectively, whereas, the optical sensor accurately predicted soil OM with $R^2 = 0.74$ and standard error of 0.41%. Despite the high accuracy during the laboratory calibration, the system revealed low measurement accuracy for soil mechanical resistance under field conditions, when a comparison was made between the data collected by the load cell and a standard cone penetrometer ($R^2 = 0.28$). The main criticism of this system was that none of the data fusion techniques to improve the prediction accuracy of the soil mechanical resistance have been applied.

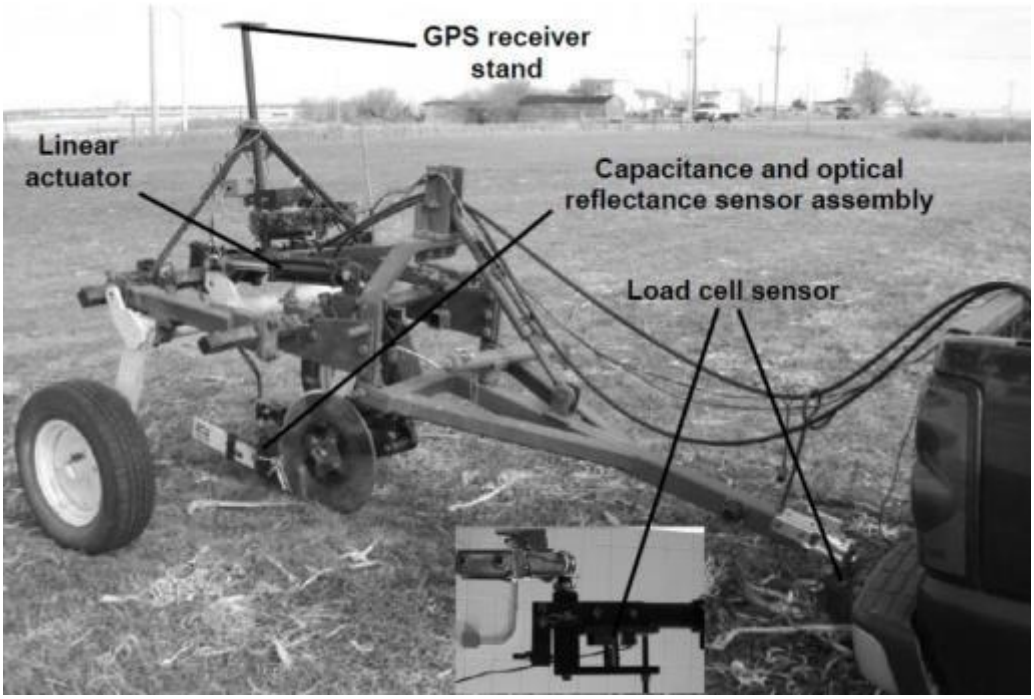

Figure 2-26 Integrated on-line sensing system for some soil properties mapping (after, Dhillon et al, 2010).

Naderi-Boldaji et al. (2011) developed and evaluated a multi-sensor probe for on-line measurement of soil moisture content and soil compaction. The combined probe consisted of a strain-gauge load cell with a horizontal dielectric

sensor, assembled on a tine of 55cm in length, for the measurements of soil mechanical resistance and soil θv, respectively. The dielectric probe operates by means of a sinusoidal signal with a 100 MHz frequency generated by an oscillator and propagates into the soil by two copper half ring electrodes insulated electrically by a Teflon insulator (Figure 2-27). The standing voltage is generated from the propagated signal measured by a digital oscilloscope connected with the electrodes via coaxial cable. They showed that measurement of θv is affected by soil properties such as BD, organic matter, moisture content and CC. The results achieved of the relationship between the output voltage (V) and θv were of R^2 values of 0.98 and 0.91 for bulk densities of 1.5 and 1.2 g cm^{-3}, respectively.

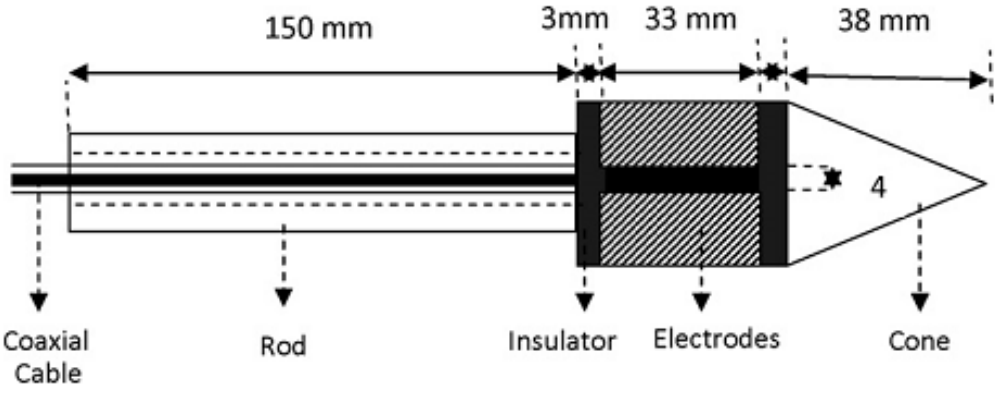

Figure 2-27 Schematic illustration and dimensions of the multi-sensor probe (after, Naderi-Boldaji et al., 2011).

In a latter study, Naderi-Boldaji et al. (2013) examined the potential of an on-line mapping system to measure soil compaction. They stated that soil compaction can be measured as a function of soil PR and θv. The upgraded mapping system consisted of a horizontal penetrometer connected to a load cell, and a dielectric-based sensor soil and a gamma-ray (the Mole) sensor (Figure 2-28) to measure simultaneously PR, θv and CC, respectively. They developed a soil BD estimation model as a function of PR, θv and CC using a multivariate

statistical analysis. Results showed this model to provide reasonable estimation of BD with R^2= 0.72 and RMSE=0.06 g cm^{-3}, as compared to soil core samples.

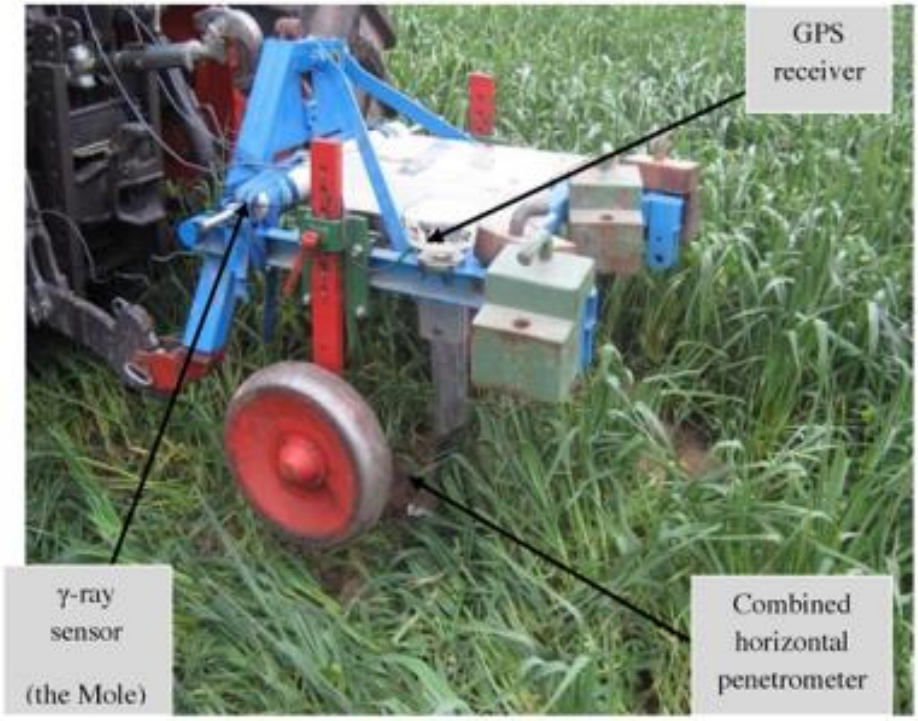

Figure 2-28 Triple sensor fusion mapping system (after, Naderi-Boldaji et al., 2013).

2.4.2. Historical developing of the *in-situ* multi-sensors

With this category of sensors data collection is made once at a particular point. They are either portable or be driven by a mobile vehicle. The main sensor is a penetrometer to penetrate the soil vertically through the soil profile. In addition to the penetrometer other sensors are combined in one system.

Vaz et al. (2001) reported soil strength measured by the penetrometer is affected by soil BD and soil moisture. For that, they combined a TDR and penetrometer to predict soil strength and moisture content simultaneously. The TDR electrodes were shaped as a pair of parallel copper wires with 0.5 (mm) in diameter and 15 (cm) in length, wound around a PVC insulated cone of a penetrometer (Figure 1-3). The TDR electrodes were connected to a cable

tester (model Tektronix 1502C) using a coaxial cable running inside the penetrometer steel tube. A personal laptop used to store the TDR readings. They concluded that soil resistance measuring accuracy was improved by adding soil moisture to a prediction model.

Peter and Yurui (2004) designed a combined capacitance sensor with a cone penetrometer (Figure 2-29). They achieved a R^2 = 0.94 for the linear relationship between the capacitance sensor's V and θv in a silt loam soil texture under laboratory conditions. The Peter and Yurui (2004) system overestimated PR compared to the readings of the standard cone penetrometer.

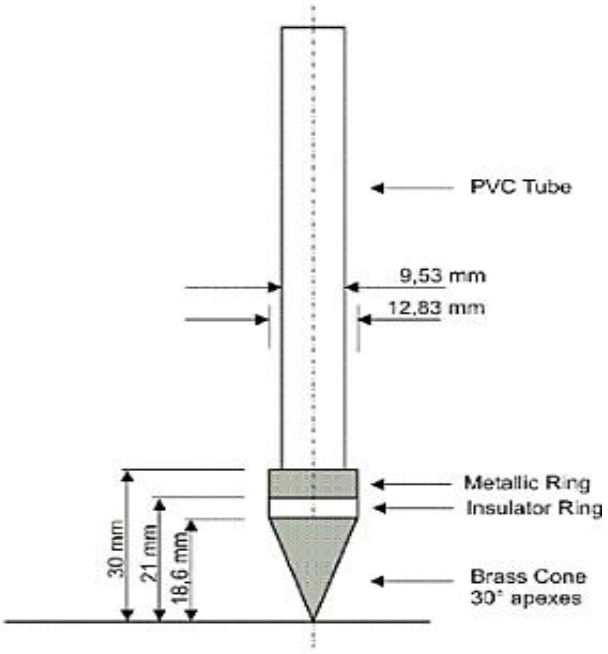

Figure 2-29 A combined sensor of cone penetrometer and capacitance probe with its electrodes shape and dimensions (after, Peter and Yurui, 2004).

Hummel et al. (2004) presented a combined probe consisting of a cone penetrometer and NIR spectrometer (Figure 2-30). They achieved a R^2 of 0.90 and SD of calibration and prediction of soil ω of 1.97% and 2.38%, respectively. Their combined system has predicted the cone index with R^2 = 0.86 compared

to the standard cone index, using all the data from clay loam, silt loam and sandy loam soil textures and the whole the range of soil moisture content. However, they did not attempt to measure soil BD.

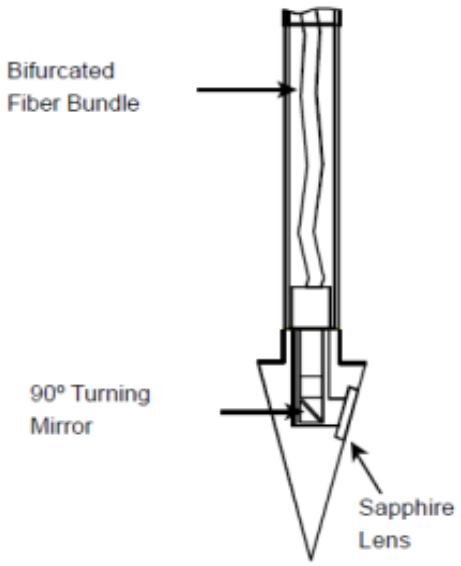

Figure 2-30 A combined probe of cone penetrometer and NIR spectrometer for the measurement of soil penetration resistance (PR) (after, Hummel et al., 2004).

Generally, the *in-situ* measuring applications are considerably more accurate than the on-line measuring applications of soil compaction, for example, Hall and Raper (2005) reported weak correlation results for an on-line soil strength sensor test in a sandy loam soil bin, to distinguish between compacted soil layers in comparison with the standard penetrometer. They found that soil strength measured by the mobilised system is closely correlated to soil BD measured by core sampling rather than the PR measured by penetrometer, with R^2 = 0.74 and 0.53, respectively. Andrade-Sánchez et al. (2003) evaluated an on-line soil conductance sensor system under laboratory and field conditions, with R^2 values of 0.87 and 0.78, respectively. These estimated values of R^2 were rather low for soil θv. This is might be due to the low sensor frequency adopted in their experiment with the range of 5.25 to 7.25 MHz.

Sheng et al., (2011) developed a monitoring system for soil water dynamics at two different soil depths (shallow: 16 cm; deep: 36 cm) (Figure 2-31), which consisted of two impedance soil moisture sensors with a 100 MHz operating frequency, two soil temperature sensors, an EC sensor, an optical sensor (photo-resistance type), a microcontroller, a 1 (MB) flash memory chip, a wireless transmitter, a solar panel and a rechargeable battery. The monitoring system was connected wirelessly to a laptop via a receiver to exchange data. The microcontroller functions as a data logger for every sensor and manages the data transmission, regulates power consumption between the batteries and the solar panel and controls data transmission wirelessly, keeping a data backup stored in the flash memory. The calibration results of the soil moisture sensors under laboratory conditions fit a linear relationship of R^2= 0.99 with RMSE of 0.03 (cm^3 cm^{-3}).

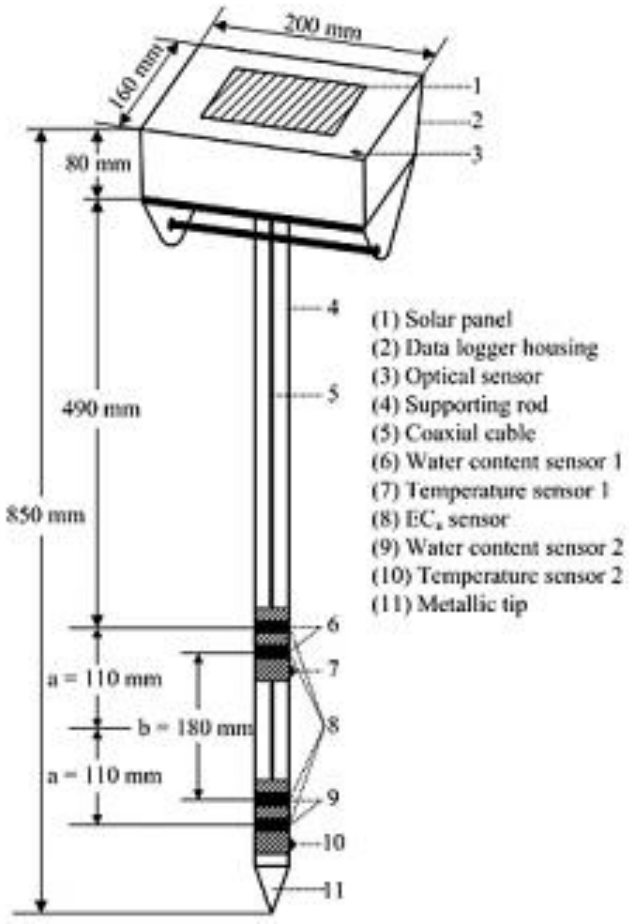

Figure 2-31 Soil water dynamics monitoring system (after, Sheng et al., 2011).

Quraishi and Mouazen (2013c) developed and tested a prototype soil BD multi-sensor kit (Figure 2-32). It consisted of a digital penetrometer (Eijkelkamp penetrologger) combined with a NIR spectrophotometer (1650-2500 nm) (Avantes, Eerbeek, The Netherlands), fibre optics, which was connected to a 10 watt halogen lamp and reflection fibres were connected to 256 pixel Indium Gallium Arsenide (InGaAs) detector. Their multi-sensor measuring system was controlled using AvaSoft 7.7 software (Avantes, Eerbeek, The Netherlands) through Universal Serial Bus (USB) cable connected to a personal laptop. They used ANN to model BD as a function of ω, CC and organic matter content. ANN was also used to predict moisture content, and CC based on vis-NIR spectra. Encouraging ANN results for the prediction of soil water content, organic matter, CC and BD were reported with R^2 values of 0.94, 0.96, 092 and 0.94, and for RMSE values of 2.60, 0.82, 4.53 (%) and 0.04 Mg m^{-3}, respectively.

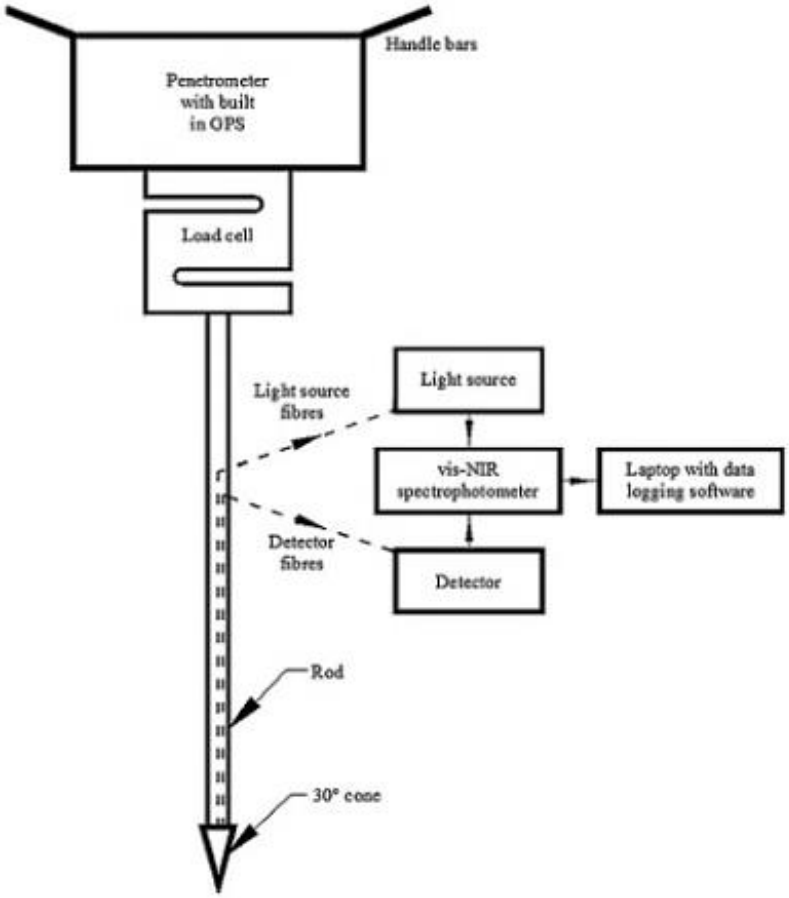

Figure 2-32 Schematic diagram of prototype of a soil bulk density multi-sensor (after, Quraishi and Mouazen, 2013c).

Liu et al. (2008) evaluated the thermo-TDR technique to estimate soil BD (Figure 2-33), the technique is based on the theory that the volumetric heat capacity (ρ_c) of the soil can be determined by summing the heat capacities of the solids, water, and air. Since the density and specific heat capacity of air are relatively very small to the other terms, the contribution of soil air is negligible, then soil BD can be calculated using the following equation:

$$\rho_c = \mathrm{BD} * C_s + \rho_w * C_w * \theta \mathrm{v} \qquad 2\text{-}6$$

Then soil BD can be estimated by:

$$\mathrm{BD} = \frac{\rho_c - \rho_w * C_w * \theta \mathrm{v}}{C_s} \qquad 2\text{-}7$$

Where BD is soil bulk density (Mg m^{-3}), $\theta \mathrm{v}$ is soil volumetric moisture content (m^3 m^{-3}), ρ_w (1.0 Mg m^{-3}) and C_w (4.18 kJ kg^{-1} K^{-1}) are the density and the specific heat capacity of water, respectively, and C_s (kJ kg^{-1} K^{-1}) is the specific heat capacity of the soil solids, which they are 0.791, 0.875 and 0.833 (kJ kg^{-1} K^{-1}) for sandy, silt loam and clay loam soil textures.

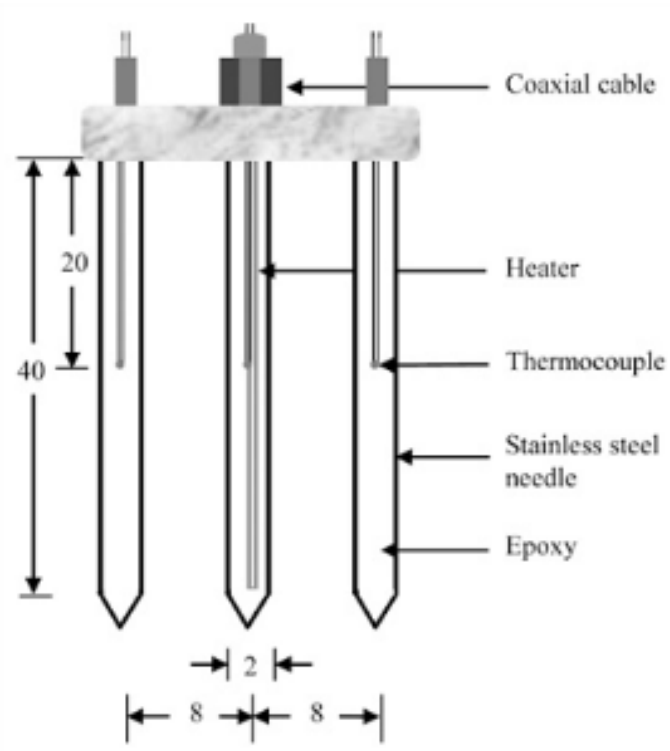

Figure 2-33 Schematic view the thermo-TDR probe (after, Liu et al. 2008).

They reported RMSE values of BD prediction compared with the core sample measures in laboratory evaluations were 0.055, 0.051, and 0.046 Mg m^{-3} for a silt loam, a clay loam, and a sand soil, respectively, and was 0.095 Mg m^{-3} for *in-situ* evaluation.

2.5. Research gaps

The current measurement methods for soil compaction in the field have shortcomings. For instance, soil strength based methods are affected simultaneously by many factors, such as moisture content, BD, OM, texture and gravel availability. While, the traditional method of measuring soil BD in-situ by core sampling method (e.g. with Kopecki ring method) is time consuming, expensive for large number of soil samples and vulnerable to errors as soil cores have to be transferred to laboratory for 24 hours, be dried before the results can be shown. This is the reason why it can be concluded that the main research gaps highlighted with the literature review is that there is no laboratory or *in-situ* soil BD measuring system using only vis-NIRS and dielectric sensor without depending on the soil strength. In this thesis the author will discuss the accuracy, design, prototyping and evaluation of a combined sensor for the *in-situ* measurement of soil BD. The combined senor introduced earlier by the publication of Al-Asadi and Mouazen (2014), consisted of a FDR sensor to measure soil θv and a vis-NIR spectrophotometer to measure soil ω simultaneously for same soil sample. The proposed technique will provide a new sensing methodology to overcome the shortcomings of the existing methods of measuring soil BD and by using well-established formulae, BD indicating soil compaction will be calculated as a function of θv and ω of the same point. Measurements will be carried out at wide range of soil textures, moisture content, BD and different land use including arable and grasslands, since the understanding of soil chemical and physical properties affecting the new measuring system of soil BD is vital, in order to improve the system accuracy and to provide precise calibration models.

2.6. Conclusions

Soil compaction is among the most important factors that cause the deterioration of farmland and lower quantity and quality of crops and also can lead to increase the power requirements for the agricultural soil preparations. There are several factors that lead to soil compaction, and those the most affective once are soil moisture content and weight of agricultural machinery. Good land management of field operations is the key factor to control and eliminate the problem of soil compaction. One of the most important land management tools is the use of innovative methods of measuring soil compaction rather than traditional methods. Several sensors to measure various properties of the soil been reviewed and the focus was on dielectric and vis-NIR spectroscopy, the latter has been presented as a powerful analytical technique for both laboratory and field applications, it showed high accuracy of measuring ω in the soil and it has been used in both on-line and *in-situ* modes. Dielectric sensors also showed high accuracy of measuring soil θv. Different combined measuring systems of soil compaction have been reviewed and its ability to predict soil BD was presented. A conclusion has drawn on the need of an objective, cost effective, accurate and rapid measuring system of soil compaction. This new measuring system of soil compaction should indicate soil BD and avoid relying on soil strength for its limitation factors.

Chapter 3

3. Materials and Methods

This section provides detailed information on the vis-NIRS and the dielectric sensors, which were used to measure soil spectra and output voltage of the reflected sinusoidal wave data, respectively. The predicted values of ω and θv were then substituted in Eqn. 1-9 to estimate soil BD. This chapter also explains the methods used to calibrate both sensors and the measurements conditions at the laboratory and *in-situ*. The affecting factors on the measurement accuracy with both sensors were identified and the impacts were evaluated. These included among other affecting factors, soil texture, land use and soil moisture content. A prototype measuring system of topsoil soil bulk density consisting of a portable near infrared spectrophotometer and dielectric sensor was developed and tested under laboratory and field conditions. Finally, an explanation of the method of producing field maps was presented.

3.1. Experimental sites and soil sampling

The experimental sites used in this study are distributed across eight locations in England namely: Silsoe (Cranfield University experimental farm) and Wilstead in central Bedfordshire, Haversham and Gayhurst in Buckinghamshire, Flawborough in Nottinghamshire, Nafferton and Morpeth in Northumberland and from one location in Wales, namely, Aberbran farm, Brecon. A total of 1013 undisturbed soil samples were collected from 32 fields, at the same time as the sensor field measurement, during the period from May 2011 -September 2013. Detailed information about these fields is shown in Table 3-1.

The new concept of measuring soil bulk density tested in the laboratory and on fields using wide range of soil textures, various soil moisture content and different land use.

Table 3-1 Detailed information of the sites, where soil samples were collected from the top layer of 10–20 cm during 2011 -2013.

Field name	County	Field location [a]	Soil type [b]	SN	Soil texture [c]	Clay %	Silt %	Sand %	OM %	Crops
Avenue, Silsoe	Beds	52° 0'33.77"N, 0°26'23.59"W	Gleyic Cambisols	45	Sandy loam	16	20	63	3.6	Oilseed rape
Avenue, Silsoe		52° 0'33.70"N, 0°26'17.08"W		80	Sandy loam	29	19	51	3	Grassland
Beechwood, Silsoe		52° 0'6.95"N, 0°26'2.78"W		40	Clay	66	11	23	5.8	Oilseed rape
Chilpolea, Silsoe		52° 0'34.27"N, 0°26'35.78"W		20	Loam	21	30	49	2.5	Oilseed rape
Clover Hill, Silsoe		51°59'57.63"N, 0°25'56.12"W		20	Clay loam	35	24	41	4.8	Oilseed rape
Copse, Silsoe		52° 0'22.10"N, 0°26'12.57"W		40	Clay loam	38	26	36	4.8	Wheat
Dowing, Silsoe		52° 0'30.71"N, 0°26'44.24"W		20	Sandy clay loam	28	19	53	4.1	Wheat
Far Warden, Silsoe		52° 0'4.52"N, 0°26'32.02"W		20	Clay	59	27	14	5.1	Wheat
Ive, Silsoe		52° 0'17.28"N, 0°26'0.06"W		40	Clay	53	19	28	3	Wheat
Middle , Silsoe		52° 0'0.67"N, 0°26'24.38"W		20	Clay	55	25	15	4.7	Field beans
Mound, Silsoe		52° 0'30.06"N, 0°26'22.78"W		38	Sandy loam	16	21	63	3.5	Arable land
Near Warden, Silsoe		52° 0'11.32"N, 0°26'18.03"W		20	Clay	54	25	16	5.5	Barley
Onley, Silsoe		52° 0'11.01"N, 0°25'48.33"W		51	Clay	60	30	10	5.4	Grassland
Orchard, Silsoe		52° 0'29.13"N, 0°26'32.82"W		20	Clay loam	33	26	41	4.2	Wheat
Showground, Silsoe		52° 0'29.21"N, 0°26'7.02"W		40	Sandy clay loam	24	17	59	3.3	Wheat
Upbury, Silsoe		51°59'58.31"N, 0°26'13.72"W		20	Clay	54	24	22	4.5	Field beans
Field 1, Wilstead		52° 5'40.73"N, 0°27'9.18"W	HaplicLuvisols	32	Clay loam	32	27	40	3.5	Oilseed rape
Field 2, Wilstead		52° 5'51.54"N, 0°27'19.22"W		20	Clay	47	38	15	3.8	Wheat
Field 3, Wilstead		52° 5'35.89"N, 0°26'55.93"W		20	Clay	48	31	15	5.3	Wheat
10 Acres, Wilstead		52° 5'27.27"N, 0°26'54.18"W		20	Clay	50	28	22	3.5	Field beans
Hownsand, Wilstead		52° 5'26.93"N, 0°27'21.86"W		53	Sandy loam	14	18	68	3.3	Barley
Runway, Wilstead		52° 5'37.51"N, 0°27'17.07"W		90	Clay loam	35	25	40	4.2	Grassland
Barn right, Wilstead		52° 5'33.97"N, 0°27'19.09"W		60	Clay loam	30	30	40	3.6	Wheat
Barn left, Wilstead		52° 5'25.13"N, 0°27'8.22"W		25	Loam	18	35	47	3.5	Wheat
Gayhurset	Bucks	52° 6'38.23"N, 0°45'51.67"W	Calcic Xerosols	25	Clay	44	35	21	5.4	Grassland
Haversham		52° 4'52.51"N, 0°47'6.11"W		34	clay loam	37	27	36	4.6	Grassland
Flawborough	Nottingham-shire	52°58'35.53"N, 0°50'17.64"W	EutricGleysols	20	Clay	51	33	15	7.2	Grassland
Flawborough		52°58'46.42"N, 0°50'32.80"W	Calcic Luvisols	20	Clay	51	35	14	5.4	Wheat
Longfarmlington, Morpeth	Northumbe-rland	55°17'34.96"N, 1°45'48.69"W	CalcicLuvisols	47	Clay	52	22	26	7.1	Wheat
Longfarmlington, Morpeth		55°17'31.04"N, 1°45'26.65"W		45	Clay	55	23	22	8	Grassland
Nafferton		54°59'8.23"N, 1°53'44.23"W	EutricGleysols	28	Sandy loam	13	22	65	7.5	Grassland
Aberbran	Brecon, Wales	51°56'56.23"N, 3°28'10.61"W	LuvicXerosols	40	Silt loam	21	65	14	5.9	Grassland
			Total	1013						

[a] Google Earth, [b] Soil type classification is according to the Food and Agriculture Organisation (FAO), [c] Soil texture classification is according to the United States Department of Agriculture (USDA), SN is the number of soil samples.

Figure 3-1 shows texture classes of the soil samples illustrated on the soil texture triangle of the United States Department of Agriculture (USDA). The minimum number of soil samples collected from each field was 20 and the maximum was 90 soil samples (Table 3-1). This number of samples enabled the validation of the measurement accuracy under different field conditions.

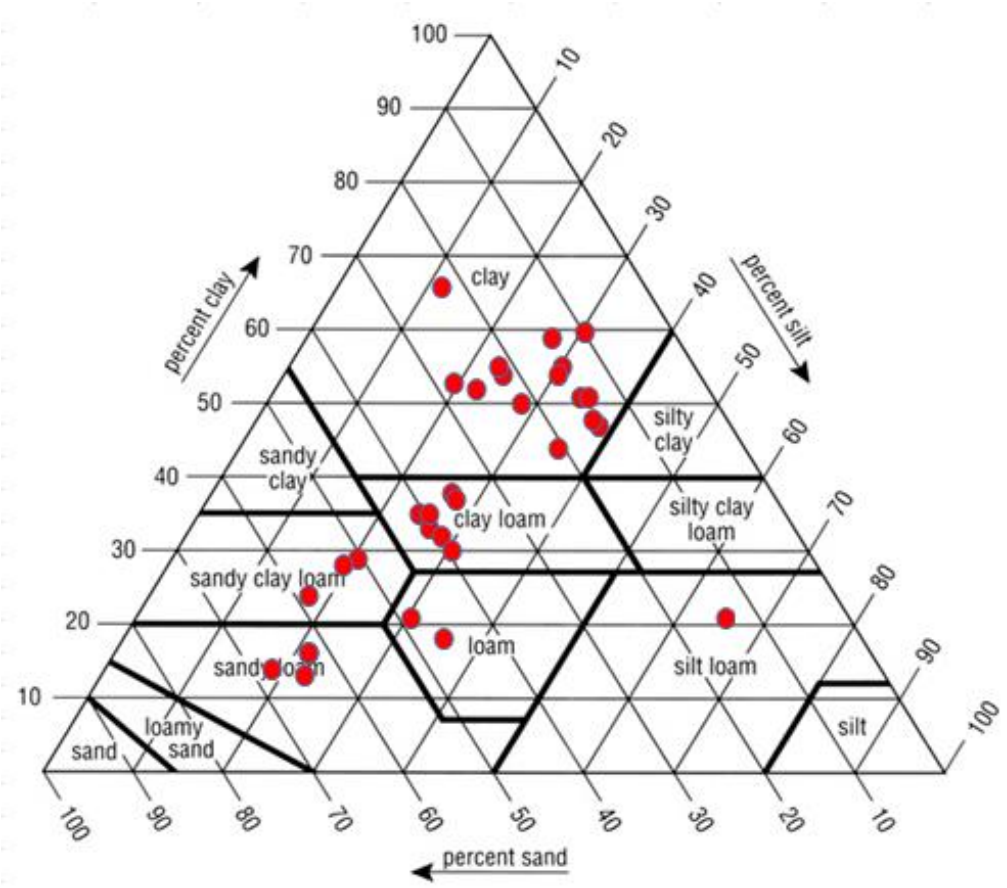

Figure 3-1 Soil texture classes distribution according to the United States Department of Agriculture (USDA) classification; the red points indicate soil texture of each field used in this study.

The study used undisturbed soil samples (cores), which were collected in a rigid ploy vinyl chloride (PVC) cylinder of 60 mm and 50 mm in height and diameter, respectively (117.75 cm^3 in volume). A sharp metal cylinder (51 mm and 55 mm of inside and outside diameters, respectively, and 35 mm of height) attached to one end of the PVC cylinder formed a cutting and supporting edge (51 mm and

55 mm of inside and outside diameters, respectively, and 30 mm of height), while on the other end a metal cover was constructed to help with hammering the cylinder into the ground, until the inter height of the collecting cylinder (60 mm) is inserted (Figure 3-2).

All the dielectric sensor readings were performed *in-situ* by recording the output voltage of the core sample (used for laboratory analysis), and three additional readings taken around the core sample position within 50 cm diameter spot. An average reading of the four readings was calculated and was considered as the final value of the output voltage reading at a measurement point. Similarly four vis-NIR spectrophotometer scans were collected from three equally divided soil volumes from every core sample collected at the laboratory. The four spectra were then averaged in one representative spectrum of a core soil sample.

After the sensor readings were recorded *in-situ*, the cores were transferred to the laboratory for further analysis. All soil cores were kept in the PVC cylinders and sealed in plastic pages to prevent moisture escaping. In the laboratory the soil samples were stored at 4 °C from the time of collection until the time of laboratory analysis.

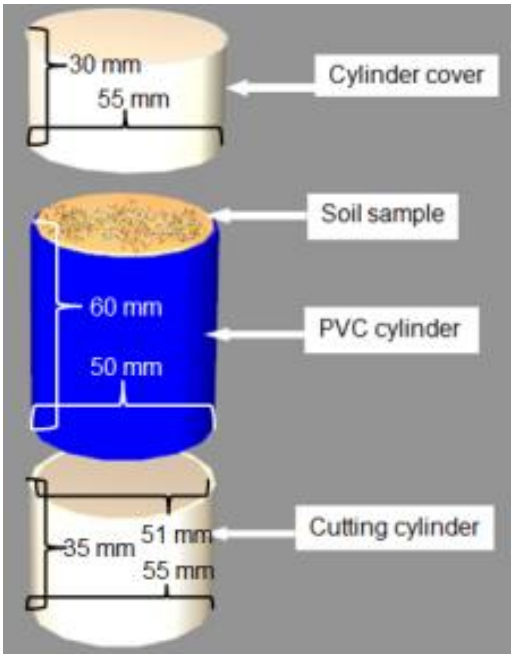

Figure 3-2 Undisturbed soil sample collecting cylinder shape and dimensions.

3.2. Laboratory analyses

Soil θv, ω and BD for all 1013 samples were measured by first oven drying the soil samples at 105 °C for 24 h (British Standards, 2007). The average field particle size distribution (PSD) and the average OM were measured, by mixing various numbers of soil samples from each field, depending on the field size, normally 20 soil samples considered to be representing the soil properties at each field and the required amount to conduct soil PSD and OM was taken from the field representing soil mix. The PSD was measured using the sieving and sedimentation method (British Standards, 1998). Soil OM was measured with a TrusSpecCNS spectrometer (LECO Corporation, St. Joseph, MI, USA), using the Dumas combustion method (British Standards, 2000). Table 3-1 shows the results of the laboratory analyses.

3.3. Optical instrumentation and scanning

There are two main types (among others) of sampling configuration with spectrometers depending on the nature and the position of the testing sample, namely, transmittance and reflectance. Although the arrangement of the main components differs between instruments, the basic configuration of both spectrophotometer types is shown in Figure 3-3.

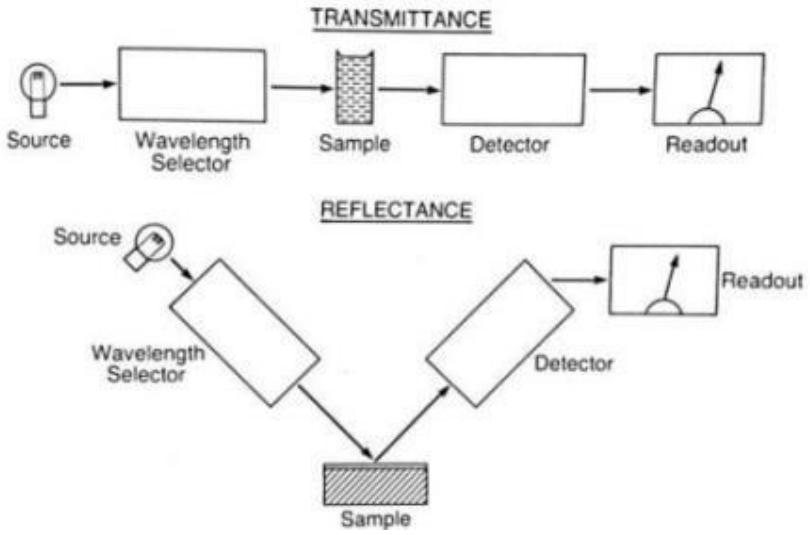

Figure 3-3 Basic instrument configurations for transmittance and reflectance spectrometers (after, Osborne et al., 1993).

In this study, two types of reflectance instrument, fibre type and standalone spectrophotometers, have been used, namely:

- LabSpec® 2500 vis-NIR portable spectrophotometer (LabSpec Pro Near Infrared Analyzer, Analytical Spectral Devices, Inc, USA) (ASDi), covering the spectrum range of 350-2500 nm. This was used for the pilot study fields and to understand the effect of moisture content, texture and land use on the accuracy (Figure 3-4).
- Avantes® NIR portable spectrophotometer (Avantes, Eerbeek, The Netherlands) covering the spectrum range 1650-2500 nm. This was used as part of the prototype combined probe (Figure 3-5).

3.3.1. ASDi LabSpec® 2500 spectrophotometer:

The instrument (Figure 3-4) has rapid data collection rate at 10 spectra per second, and sampling intervals of 1.4 nm and 2 nm for the spectral regions 350-1000 nm and 1000-2500 nm, respectively. Its main components are:

- Light source: The light source is a high intensity quartz-halogen lamp, built in a high intensity hand-held probe, which operates on 10 VDC and 18.6 Watt output. Its output light correlated colour temperature is 2,975 K° and 231.22 Lumens. The illumination and detection fibers were gathered in the high intensity probe enclosed at a 35° angle from the vertical line.
- Optical cables: Two fiber optic cables are deployed; the internal one is made up of thirty seven (37) randomly distributed, ultra-low-OH, silica glass fiber optics. Nineteen of these fibers are 100 micron in diameter and are used for the vis-NIR spectrum (350-1000 nm). The remaining eighteen fibers are 200 micron diameter and are divided equally between two NIR spectral regions of 1000-1800 nm and 1800-2500 nm. The external optical cable conveys the reflected light from the probe to the wavelength filter through a group of lenses. It consists of forty four randomly distributed, ultra-low-OH silica glass fibers, which are 200

micron in diameter. The cable is 1 meter in length and protected by a metal spiral inside the black PVC cable casing.

- Three prisms and a group of focusing lenses are used to filter out and redirect three groups of the reflected light to each different detector.
- Detectors: ASDi has three separate holographic diffractions with three separate detectors as follows:
  - Vis-NIR: 512 element silicon photo-diode array for the spectrum region from 350 to1000 nm.
  - NIR: cooled InGaAs, photo-diodes detector for the spectral region from 1000 nm to 1800 nm.
  - NIR: cooled InGaAs, photo-diodes detector for the spectral regionfrom1800 nm to 2500 nm.
- Data readout, storage and control device: A laptop is used to monitor and store the spectra data. An Ethernet cable connects the laptop and ASDi spectrometer, which is controlled by the Indico® Pro application software and easily converts the spectral readouts (ASD coded files) about the soil samples collected using the ASD instrument to a recognized file format (DX format file) for statistical analysis by The Unscrambler® version 7.8 by Camo Software (Camo Inc.; Oslo, Norway)

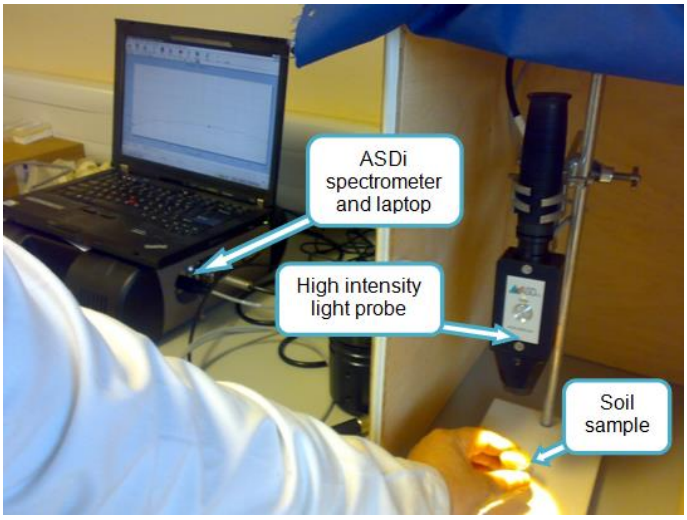

Figure 3-4 The ASDi LabSpec® 2500 spectrometer and the high intensity probe during the laboratory soil sample scanning at the Soil Laboratory, Cranfield University.

3.3.2. Avantes® spectrophotometer:

The portable system has a wavelength measurement range of 1650-2500 nm and was used for the prototype combined probe (Figure 3-5). It is consists of the following components:

- Inserting probe: This consists of a 13 mm diameter and 1 m in height stainless steel rod, which is used to insert the Avantes spectrometer's optical probe to 20 cm depth in the soil. The rod protects the optical fibers, which run inside it to a highly reflective surface internal chamber open to the soil through a sapphire window (Figure 3-5).
- Fiber optic cables: Two external fiber optic cables are used. The first connects the light from the light source to the internal chamber and the second cable transfers the diffuse reflected spectra from the soil to the Avantes spectrometer. Both external fiber optic cables are protecting by steel coil and PVC shielding.
- Spectrometer: The Avantes model NIR200-2.6 has a dual stage thermo-electrical Peltier-cooled InGaAs single detector with 256 pixels and 7 nm resolution. The Avantes spectrometer is connected to a laptop through a high-speed USB2.0 interface. AvaSoft 8.0 software (Avantes, Eerbeek, The Netherlands) is used for controlling, analysing and converting the spectra data collected from soil scanning. A lead-acid battery with 12VDC and 14 AVh is used as a power source during the field measurement.
- Light source: A stabilized halogen lamp through an electronic circuit is used as a light source, with adjustable light focusing of the fiber optic connection to control the output light illumination at the desired wavelength via a filter-slot mounted on the front. The light source operates from a 24VDC and 20 Watts lead-acid battery, with a bulb colour temperature of 3000 °K.

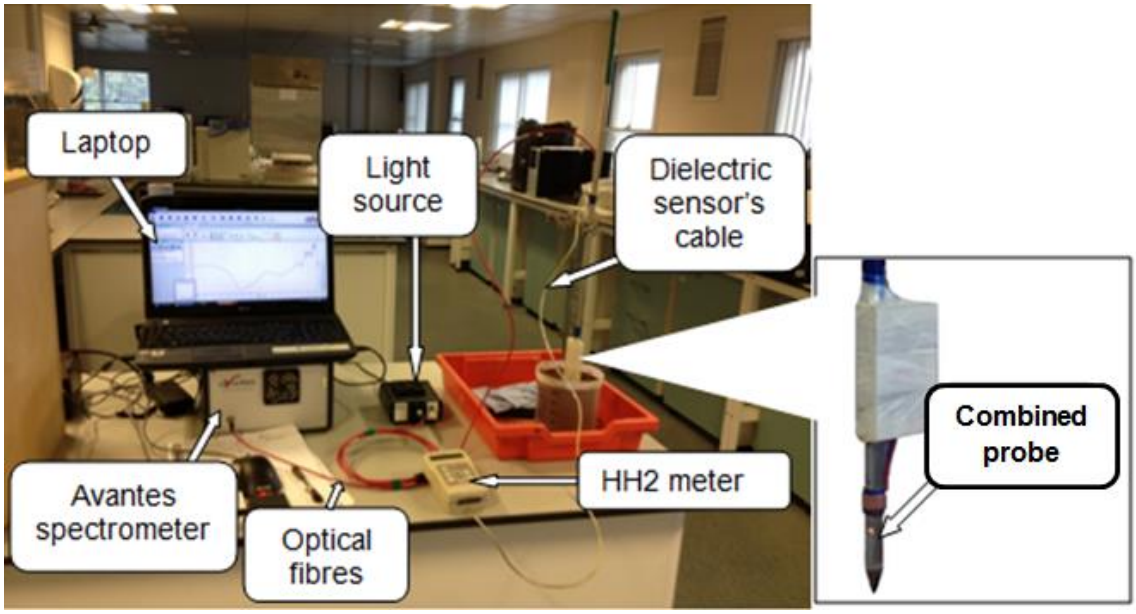

Figure 3-5 Avantes model NIR200-2.6 spectrometer with the prototype combined probe during the laboratory calibration, at Soil Laboratory, Cranfield University.

3.3.3 Optical scanning

The fresh (undisturbed) and remoulded soil samples were scanned in diffuse reflectance mode in the laboratory and *in-situ*. Three replicate scans were taken from each soil sample using the LabSpec® vis-NIR and Avantes portable spectrophotometer and the average of those three scans was used for spectra pre-treatment and model establishment.

Before scanning, only large plant remains, debris and stones were removed from the fresh soil samples (Mouazen et al., 2005a). Various weights of non-sieved soil according to different textures and moistures were packed into Petri dishes of a 1.0 cm height by 3.6 cm in diameter. The soil in a Petri dish was mixed properly and gentle pressure was applied on the surface with a spatula to generate a levelled and smooth surface to ensure maximum diffuse reflection and thus a good signal-to-noise ratio (Mouazen et al., 2007; Kuang et al., 2012). Before the soil samples were scanned and at intervals of 30 min, a white

reference Spectralon disc was scanned to generate the baseline of a 100 % reflected spectra.

3.3.4. Pre-treatments of the spectra data

Spectra pre-treatment aimed to reduce spurious peaks that do not contain any physical or chemical spectra information and to correct the physical scatter effects, Figure 3-6A shows the raw reflectance spectra data plotted against the full wavelength range (350-2500 nm) of the ASDi spectrometer. The same pre-treatments were applied on all spectra data collected from both spectrometers, except for the spectra range reduction, whereas, it was reduced from 500 to 2200 nm wavelength range of the ASDi spectrophotometer, as Figure 3-6B showing and reduced from 1650 to 2225 nm wavelength range of the Avantes spectrophotometer . The aim of reducing the spectra wavelength range is to eliminate noise at both edges of the detection scale and to enhance calibration accuracy for ω measurement (Mouazen et al., 2005a). After noise elimination, spectra data were also reduced by means of averaging every 10 nm of the successive spectra readout to one, the final reduction results of the spectra observations were in the range of n= 169-172 after the two pre-treatments mentioned above. A maximum normalisation was followed, which is typically used to get all data to approximately the same scale (Figure 3-6C), or to get a more even distribution of the variances and the average values. The maximum normalisation is a normalisation that “polarizes” the spectra. The peaks of all spectra with positive values were scaled to + 1, while spectra with negative values were scaled to − 1. Since soil spectra have maximum positive values, the peaks of these spectra were scaled to + 1 (Mouazen et al., 2005a). The maximum normalisation led to better results for ω measurement, compared to other pre-treatment options tested. Spectra were then subjected to the Savitzky–Golay first derivation transformation (Martens and Naes, 1989), which enables the transformation of spectra data to the first or higher order derivatives, including a smoothing factor. This method determines how many adjacent variables will be used to estimate the polynomial approximation used for derivatives. A second order polynomial approximation was selected due to

its performance in producing more accurate calibration models using this study data. The final process of the pre-treatment was smoothing carried out at 2:2 rate, in order to produce even more noiseless spectra from the measured soil samples. All pre-treatment steps were carried out using the Unscrambler 7.8 software (Camo Inc.; Oslo, Norway).

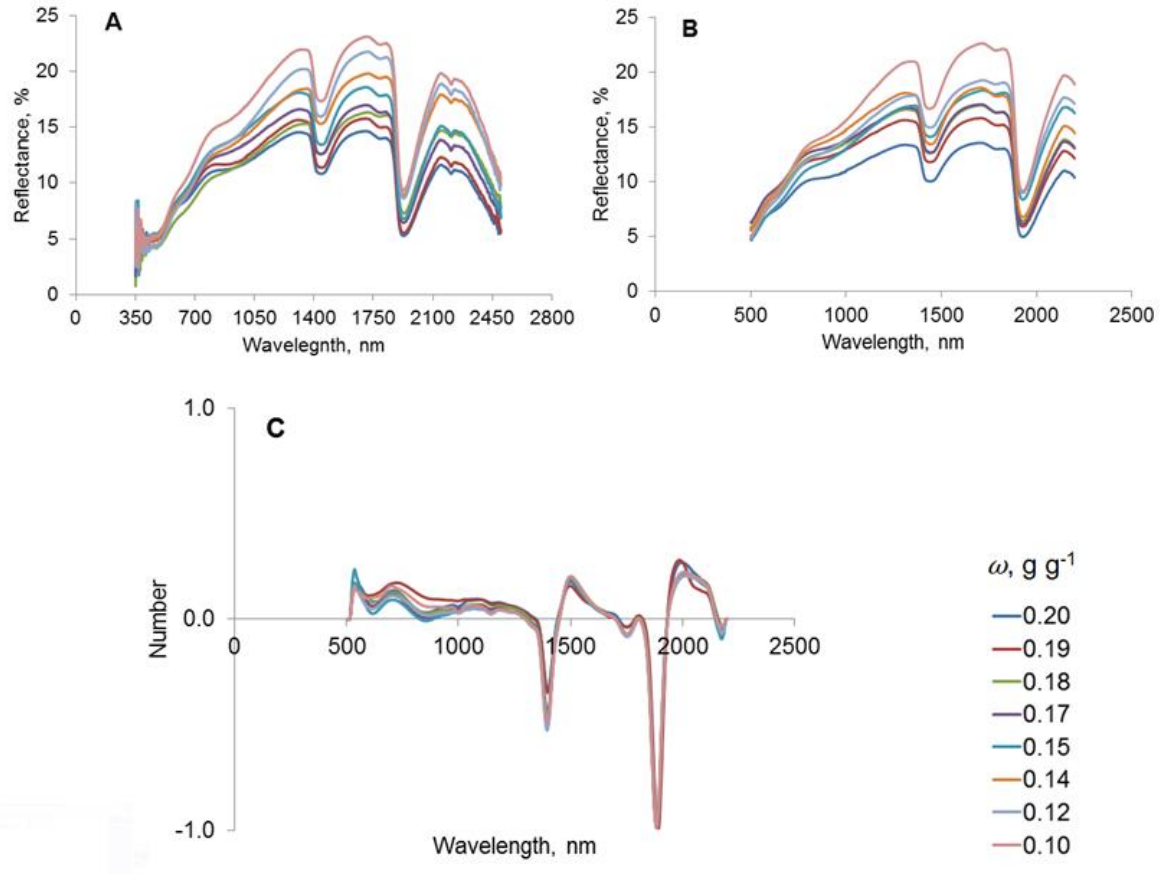

Figure 3-6 The pre-treatments of the reflectance spectral data, (A) the original full range, (B) noise reduction at the edges of the spectrum range, averaging every 10 reading to 1 and smoothing and (C) normalisation.

3.3.5. Establishment of vis-NIRS calibration models

The entire 1013 soil spectra data generated from each soil sample scan were arranged in ascending order according to ω, then a three out of every four readings (75% of the spectra data) were chosen to be used in the process of generating the calibration model, while the remainder (25% of the spectra data)

was used as independent validation set. The ascending order process for spectra data before choosing the calibration and validation sets ensures that the range of moisture is represented in both sets. Two different calibration techniques were tested namely: Artificial Neural Networks (ANN) and partial least squares regression (PLSR).

- **Artificial Neural Networks**

The ANN toolbox from the Statistica software version 11 (StatSoft, USA, 2011) package was used to generate calibration models for ω. This was done for all affecting factor case studies investigated in this study (point 3.3.5) and for the general calibration model using the whole soil samples. The ANN method is a simplified model of the biological structure of human brains (Günaydin, 2009). It has three main layers of structure, namely, input nodes, one or more layers of hidden nodes and a set of output nodes (Figure 3-6).

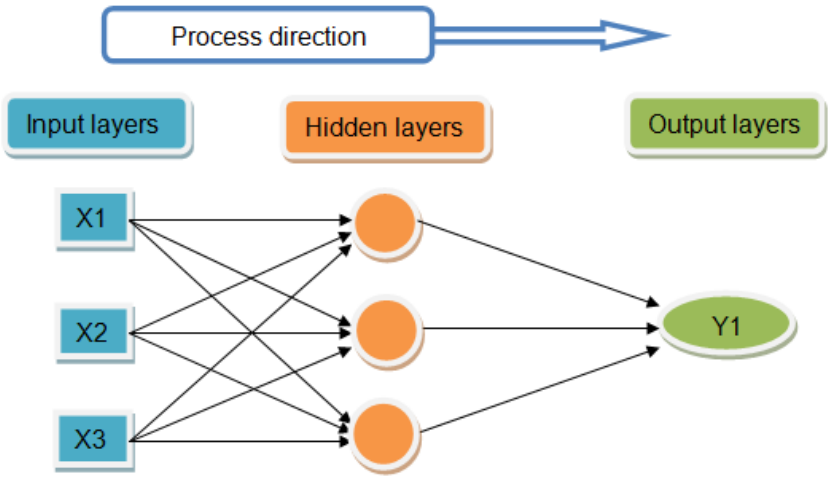

Figure 3-7 A simple feed-forward Artificial Neural Networks (ANN).

All the modelling cases were developed using the powerful second order Broyden–Fletcher–Goldfarb–Shanno (BFGS) training algorithms, with different transfer functions used for hidden and output layers. The transfer functions included hyperbolic tangent (Tanh), logarithmic (Log) and exponential (Exp). The number of neurons in the hidden layer is established by training several networks with different numbers of hidden neurons, and comparing the

predicted with measured values. In this study, the hidden layers were varied between five to twenty one neurons depending on the best results obtained from the calibration models. Spectra data for each category of soil sample were pre-treated and divided into a training set (60%), test set (15%) and independent validation set (25%). The input data were soil diffuse reflectance spectra, whereas the output was ω.

- **Partial Least Square Regression**

The partial least squares regression (PLSR) toolbox of the Unscrambler 7.8 software (Camo Inc.; Oslo, Norway) was applied on the calibration set of the spectra data and the calibration model validity was tested with the independent validation set. The PLSR technique was implemented to relate the variation in one variable (e.g. ω) responding to the variation in multi-spectra reflected frequencies. It is a bilinear modelling method where information in the original x data is projected onto a small number of underlying ("latent") variables called PLS components, in other words, reducing the quantity of the spectra data and thus decreasing over-fitting problems without discarding any important information. The y data are actively used in estimating the "latent" variables to ensure that the first components are those that are most relevant for predicting the y variables. Interpretation of the relationship between the x and y data of the calibration set data (75%) is then simplified as this relationship is concentrated on the smallest possible number of components leading to the production of the PLSR calibration model, which can be used to predict y variables (e.g. ω) from any given x data (spectra data). More detailed information about the PLSR can be found in Martens and Naes (1989) and Osborne et al (1993).

3.4. Frequency domain reflectometry (FDR) measurement with ThetaProbe

3.4.1. ThetaProbe description

ThetaProbe (Delta-T Devices Ltd.) is the commercial name of a dielectric probe for the field measurements of soil θv. It has been developed jointly by the Macaulay Land Use Research Institute, Scotland and Delta-T Devices Ltd, Cambridge. ThetaProbe consists of a waterproof hard plastic housing, which

contains the electronic circuitry and provides a solid base for the four parallel stainless steel rods of 65 mm length and 3.3 mm diameter, which are inserted into the soil. At the other end of the probe is the input/output cable (Figure. 3-7). The electronic circuit generates and emits an electromagnetic signal of sinusoidal shape, which is applied to an internal transmission line to the array of four rods. The impedance of this array varies according to the impedance of the soil, which has two components, namely, the apparent dielectric constant (*K*) and the ionic conductivity. 100 MHz was chosen as the operating frequency in order to minimise the effect of ionic conductivity, so that changes in the transmission line impedance was dependent almost solely on the soil's apparent *K*. Water content determines the *K* of the soil, as the *K* of the water (~81) is much higher than the *K* of the soil (3 to 5) and that of the air (1). The travelling electromagnetic wave through the soil mass will cause a voltage standing wave to be set up from the interference of the emitted signal and its reflected component. By measuring this voltage amplitude, the *K* of the soil can be obtained and thus θv. More details can be found in Gaskin and Miller (1996) and Miller and Gaskin (1997). Kaleita et al. (2005) studied the effect of soil temperature on laboratory calibration of the ThetaProbe, and found insignificant differences in the accuracy for a temperature range of 10 to 40 °C. An insignificant effect from soil salinity in the range of 250 - 2000 mS m^{-1} was confirmed by the ThetaProbe manufacturer (Delta-T Devices Ltd., 1999).

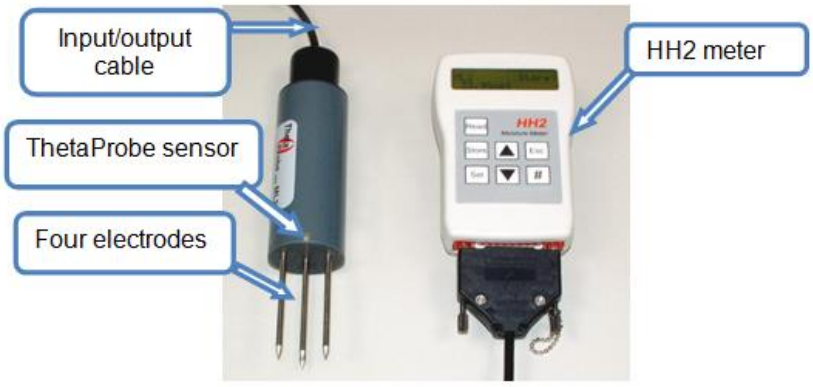

Figure 3-8 ThetaProbe and the HH2 meter.

3.4.2. Establishment and testing of calibration models of ThetaProbe

Three ThetaProbe readings were recorded *in-situ* from the same spot (e.g. 50 cm in diameter), where the soil core was collected and these three readings were recorded before extracting the core sample. An Additional reading was also recorded from the soil core itself after been extracted from the ground. These four readings were averaged to one final reading.

In this study, five methods for the calibration of the ThetaProbe were tested, namely, manufacturer (M), specific soil calibration (SSC), general formula (GF) (Topp et al. 1980), and ThetaProbe output voltage (V) and ANN. The input for all calibrations was the readout of the ThetaProbe only. In the following subsections, the five calibration methods are explained.

- **Manufacturer calibration method (M):**

The general calibration by the manufacturer of the device is a pre-set programme at ThetaProbe digital moisture meter type (HH2), which provides an instant readout of θv in $cm^{-3}cm^{-3}$ and also output voltage (V) in mv. It comprises two calibration options for mineral (OM<7%) and organic (OM>7%) soils (Delta-T Devices Ltd., 1999). It is based on the following third order relationship between *K* and V:

$$\sqrt{K} = 1.07 + 6.4\mathrm{V} - 6.4\mathrm{V}^2 + 4.7\mathrm{V}^3 \qquad (3\text{-}1)$$

Where $\sqrt{K}$ is the square root of the dielectric constant (dimensionless) and V is the output voltage reading of the ThetaProbe in mv.

By substituting $\sqrt{K}$ into the following equations, θv can be calculated for mineral and organic soils, respectively:

$$\theta\mathrm{v} = \frac{\sqrt{k}-1.6}{8.4} \qquad (3\text{-}2)$$

$$\theta\mathrm{v} = \frac{\sqrt{k}-1.3}{7.7} \qquad (3\text{-}3)$$

- **Specific soil calibration method (SSC):**

This method relies on Eqn. 3-1, but is used for specific soil types. To calculate θv for a specific soil, the following linear relationship between $\sqrt{K}$ and θv was established (Delta-T Devices Ltd., 1999):

$$\theta \mathrm{v} = \frac{\sqrt{K} - a_0}{a_1} \qquad (3\text{-}4)$$

Where a_1 and a_0 are coefficients for wet and dry soil samples, respectively. a_0 is considered equal to $\sqrt{K_0}$ (Gaskin and Miller, 1996). However, a_1 is calculated from the following equation:

$$a_1 = \frac{\sqrt{K_1} - \sqrt{K_0}}{\theta \mathrm{vt}} \qquad (3\text{-}5)$$

$\sqrt{K_1}$ is the square root of the dielectric constant of the wet undisturbed soil sample, $\sqrt{K_0}$ is the square root of the dielectric constant of the dried undisturbed soil sample. Both $\sqrt{K_1}$ and$\sqrt{K_0}$ were measured using Eqn. 3-1. θvt is the measured volumetric moisture content by oven drying of samples at 105 °C for 24 h.

- **General formula calibration method (GF):**

This method relies on the concept that *K* can be measured from the standing voltage of the soil matrix and thus indicates θv. Topp et al., (1980) established the universal equation to express the relation between θv and *K* of many soil types, collected from all over the world, which is written as follows:

$$\theta \mathrm{v} = -0.053 + 0.0292K - 0.00055K^2 + 0.0000043K^3 \qquad (3\text{-}6)$$

The *K* value is derived based on average measured V, which is substituted into Eqn. 3-6 to calculate θv.

- **Output voltage calibration method (OV):**

In this method a direct relationship between V and θv was established based on *in-situ* measurements from the ThetaProbe of soils collected in the current work. The average spot ThetaProbe output voltage readings of 1013 samples were divided into two sets, namely, calibration (75%) and independent validation set

(25%). The former was used to generate the relationship between θv and V based on the equation of the best fit line calculated by Microsoft Excel program, whereas the latter was used to validate the calibration equation developed.

- **Artificial neural networks (ANN) method:**

Here, the same ANN as that used for the prediction of ω (Section 3.3.2) was used. However, the input data is the readout V of the ThetaProbe, whereas the output is θv.

3.5. Data fusion and soil bulk density estimation

Methods adopted in Section 3.3.2 and Section 3.4.2 for the measurement of ω and θv, respectively, were based solely on the vis-NIRS spectra data, and the output voltage of the ThetaProbe, respectively, and the calibration models of each sensor were generated separately. In this section, the measurement of θv and ω is explained based on a fusion of the readout data from both sensing techniques (V and spectra), which were obtained for the 1013 soil samples, with or without including data obtained from laboratory analysis on sand (S in %), silt (SL in %), C in % and OM in %, which they were represented by the average values of each field involved in this study. However, in order to compare with other data fusion models, the input data of V (Section 2.4.2) or soil spectra (Section 3.3.2) were used to produce ANN calibration models for the measurement of θv and ω, respectively (Table 3-2).

Table 3-2 Different inputs used for different artificial neural networks (ANN) analysis for the measurement of volumetric (θv) and gravimetric (ω) moisture content. Data used as input are output voltage (V), visible and near infrared spectra (Spec), sand (S), clay (C), silt (SL) and organic matter (OM).

Table 3-2 Different inputs used for different artificial neural networks (ANN) analysis for the measurement of volumetric (θv) and gravimetric (ω) moisture content. Data used as input are output voltage (V), visible and near infrared spectra (Spec), sand (S), clay (C), silt (SL) and organic matter (OM).

Model	Input	Output
I	V, Spec, S, SL, C, OM	θv, ω
II	V , Spec, C, OM	θv, ω
III	V , Spec, OM	θv, ω
IV	V , Spec, C	θv, ω
V	V , Spec	θv, ω
VI	Spec	ω
VII	V	θv

One of the tools available for data fusion is the ANN. Similar ANN to that used in Section 3.3.2. Section 2.4.2 was used here too. In this study, different numbers of hidden nodes were selected automatically by the Statistica software (data mining toolbox) in each ANN calibration model depending on the input data used (Figure 3-8).

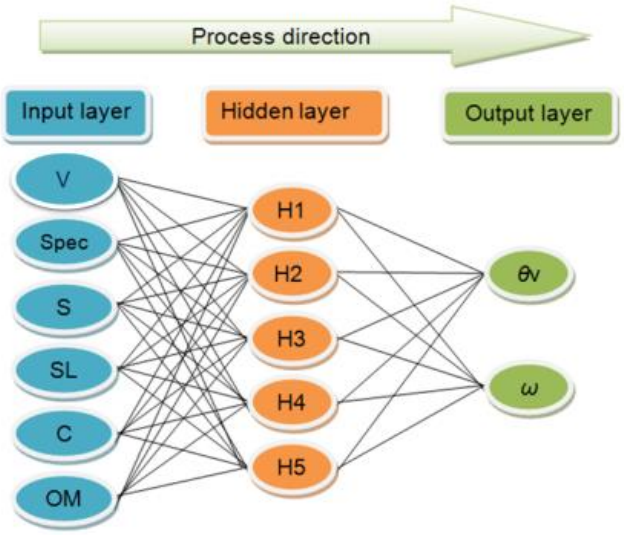

Figure 3-9 The of an ANN calibration model I for predicting θv and ω architecture.

For instance, the number of nodes of the hidden layer for θv based on V only was two nodes (Table 3-2). Five ANN analyses were performed to develop

different calibration models, according to the different multi-input variables used (Table 3-2). The output targets for the different input combinations were θv or ω (based on one input; soil spectra or V), or both (based on data fusion of soil spectra, V, soil texture components and OM). In this study, a hidden layer with five neurons showed the best results. All the texture classes were included in the calibration set so that the resulted models are valid for all textures.

Having data on θv measured with a ThetaProbe and ω measured with a vis-NIR spectrophotometer, or by a fusion of data from both instruments, these are substituted into Eqn. 1-9 to derive BD values for all combinations of input data (Table 3-2). The estimation accuracy of BD is estimated by comparing with the oven drying method of soil samples at 105 °C for 24 h.

The performance of the developed models was evaluated by means of the higher coefficient of determination (R^2) values alongside the root mean square error of prediction (RMSEp) values of the independent validation set. The residual prediction deviation (RPD), which is the ratio of standard deviation (SD) values of the laboratory measured ω, θv and BD divided by RMSEp of the independent validation set, were also considered to evaluate the performance of the calibration models (Mouazen et al., 2010). Mouazen et al. (2006b) proposed the following classes of RPD values: an RPD value below 1.5 indicates poor model predictions and that such a value wouldn't be useful; an RPD value between 1.5 and 2.0 indicates a possibility of distinguishing between large and small values, while a value between 2.0 and 2.5 makes approximate quantitative predictions possible. For RPD values between 2.5 and 3.0 and above 3.0, the prediction is classified as good and excellent, respectively. This classification system of RPD was adopted in this study. Generally, a good model performance would have high R^2 and RPD values, and a small value of RMSEp.

- **Potential error estimation**

Analysis the RMSE values of ThetaProbe and ASDi spectrometer of current study with other researchers results of the RMSE values of predicting both θv

and ω, showing the capability of the new measuring system to predict soil BD at lower potential error. The linear formula used to estimate DB contains only two parameters of θv and ω, which leads to simplified potential error relation of DB prediction, as follow:

$$\text{Potential BD estimation error} = \frac{\text{RMSE of } \theta\text{v}}{\text{RMSE of } \omega} \qquad 3\text{-}7$$

Where: Potential BD estimation error is the expected error of estimating BD relaying on the errors of θv and ω readings, it has no unites or dimension as $\text{BD potential error} = \frac{\text{RMSEp of } \theta\text{v}}{\text{RMSEp of } \omega} = \frac{\frac{\text{cm}^3}{\text{cm}^3}}{\frac{\text{g}}{\text{g}}} = 1$, RMSE of θv cm^3 cm^{-3} is the root mean square error of prediction θv using dielectric sensor and RMSE of ω g g^{-1} is the root mean square error of prediction ω using vis-NIRS.

3.6. Factors affecting measurement accuracy

Literature documented influences of soil conditions on the performance of the vis-NIR and dielectric sensors for the prediction of soil ω and θv and subsequently the estimation of BD. Among these factors, soil water content (Mouazen et al., 2005; Robinson et al., 2003) soil texture (Quraishi and Mouazen, 2013a; Rowlandson et al., 2013) and land use probably the most significant factors. So far, the influences of these factors were studied separately and to a given extent on ThetaProbe and ASDi sensors performance. In this thesis the combined influences of these factors on the prediction of ω and θv and the estimation of BD will be investigated.

3.6.1. The effect of soil moisture level

The effect of soil moisture content on the prediction accuracy of θv or ω with both sensors was studied by conducting the field measurements during different seasons (representing different moisture content levels) using the same five fields with arable lands only (Table 3-3). Three field measurements were carried out within the period from July, 2011 to October, 2012. A total of 100 soil samples were collected for each of the three experimental visits, divided to 20 soil samples per field per visit. All precautions have been taking in order to

conduct measurements and core sampling before soil tillage took place, to avoid the effect of soil disturbance on the readings. The same procedures explained previously (Point 3.1) were followed to obtain the readings from sensors and collecting the soil samples. The following three average levels of soil moisture content (L) of the 100 soil samples were obtained during the three field measurement occasions:

- L 1 with 0.11 g g^{-1} and 0.15 cm^3 cm^{-3} gravimetric and volumetric moisture content, respectively, during the period from 11th to 15th of July, 2011.
- L 2 with 0.20g g^{-1} and 0.23 cm^3 cm^{-3} gravimetric and volumetric moisture content, respectively, during the period from 15th to 21st of May, 2012.
- L 3 with 0.28g g^{-1} and 0.32 cm^3 cm^{-3} gravimetric and volumetric moisture content, respectively, during the period from 1st to 5th of October, 2012.

Table 3-3 Detailed information about the five experimental fields in Silsoe experimental farm, where soil samples were collected during 2011 and 2012, for investigating the influence of soil moisture content on the prediction accuracy.

Fields	Soil texture	Clay, %	Silt, %	Sand ,%	OM, %	L1		L2		L3	
						Crop	SN	Crop	SN	Crop	SN
Avenue	Sandy loam	16	20	63	3.6	Wheat	20	Barley	20	Harvested Wheat	20
Beechwood	Clay	66	11	23	5.8	Beans	20	Wheat	20	Harvested Wheat	20
Clover hill	Clay loam	35	24	41	4.8	Wheat	20	Beans	20	Harvested Barley	20
Orchard	Clay loam	33	26	41	4.15	Barley	20	Wheat	20	Beans	20
Showground	Sandy clay loam	24	17	59	3.34	Wheat	20	Barley	20	Harvested Wheat	20
						Sum	100		100		100
						Total			300		

SN is sample number; OM is soil organic matter content.

Table 3-4 provides basic statistics of the 300 soil samples used for the analysis of the effect of the soil moisture content. Data were obtained from the laboratory oven drying method at 105 °C for 24 h.

Table 3-4 Sample statistics of the laboratory analysis of three levels and the collective soil volumetric moisture content (θv) (cm^3 cm^{-3}), gravimetric moisture content (ω) (g g^{-1}) and soil bulk density (BD) (g cm^{-3}) used for the analysis of the effect of soil moisture content on the prediction accuracy.

Category	Level	Minimum	Maximum	Average	SD	Range
θv	L 1	0.080	0.222	0.147	0.044	0.142
	L 2	0.130	0.410	0.231	0.077	0.28
	L 3	0.136	0.512	0.321	0.135	0.376
	Collective	0.035	0.44	0.197	0.117	0.405
ω	L 1	0.062	0.145	0.107	0.026	0.083
	L 2	0.114	0.394	0.196	0.085	0.28
	L 3	0.120	0.44	0.28	0.133	0.32
	Collective	0.08	0.512	0.236	0.119	0.432
BD	L1	1.092	1.671	1.359	0.133	0.579
	L2	0.913	1.423	1.219	0.126	0.51
	L3	0.879	1.529	1.192	0.153	0.65
	Collective	0.852	1.671	1.258	0.163	0.819

SD is standard deviation; θv is volumetric moisture content (cm^3 cm^{-3}); ω is gravimetric moisture content (g g^{-1}); BD is soil bulk density (g cm^{-3}), Collective is the total of the three soil moisture levels.

Among all calibration methods the ANN method was selected to perform data fusion of both sensors, due to its high performance (Al-Asadi and Mouazen, 2014), for each of the three levels of moisture content, a performance comparison was made between the ANN calibration models for θv and ω predictions using V and vis-NIR spectra data, respectively. The same data (75 soil samples) from each moisture level was used separately to generate calibration models using the above calibration method. The calibration models accuracies were tested using the same independent validation spectra data (25 soil samples). Similar procedure followed with the collective model (L1+L1+L3).

The final output was four different ANN analyses, carried out for L1, L2, L3 and L1+L2+L3 (the collective model) with V and vis-NIR spectra data were used as input, whereas the output was θv and ω, respectively.

3.6.2. The effect of soil texture

Three soil texture classes were selected to understand the effect of texture class on the measurement accuracy of θv or ω. These are sandy loam, clay loam and clay. A total of 100 soil samples from each of the three soil textures (300 samples) were used, which were collected from arable lands and grasslands, during the period from December, 2011 to November, 2012, from different locations in the UK (Table 3-4). The same number of soil samples was used for each texture as to eliminate the influence of the sample number on prediction accuracy of the vis-NIR spectroscopy (Kuang and Mouazen, 2012).

Table 3-5 provides detailed information about the location, growing crop and number of soil samples collected from each field. For each soil texture class, calibration models for the prediction of θv or ω were developed using ANN, by dividing the 100 samples into calibration (60%), cross-validation (15%) and test (25%) sets. In addition, models for all texture classes were developed using the same division of the sample sets.

Table 3-6 provides basic statistics of the laboratory analysis of the 600 soil samples, used for the analysis of the effect of the soil texture on the prediction accuracy of θv, ω and BD.

Table 3-5 Field location, land use and number of soil samples used to study the soil textures effect on the measurement of volumetric (θv) and gravimetric (ω) moisture content.

Texture class	Field	Agriculture practice and crops		Clay %	Silt %	Sand %	OM %	Sample number
Clay	Ive, silsoe, Beds	Arable land	Winter wheat	53	19	28	2.96	15
	Far Warden, silsoe, Beds		Oil seed ripe	59	27	14	5.1	20
	Flawborough, Nottinghamshire		Winter wheat	51	35	14	5.4	20
	Morpeth, Northumberland		Oil seed ripe	52	22	26	7.08	45
Clay loam	Copse, Silsoe, Beds		Winter wheat	38	26	36	4.83	33
	Field 1, Duck End, Wilstead, Beds		Winter wheat	32	27	40	3.45	32
	Barn Right, Duck End, Wilstead, Beds		Barley	30	30	40	3.6	35
Sandy loam	Avenue, Silsoe , Beds		Winter wheat	16	20	63	3.6	45
	Mound, Silsoe , Beds		Barley	16	21	63	3.5	38
	Showground, Silsoe , Beds		Winter wheat	24	17	59	3.6	17
							Sum	**300**
Clay	Flawborough, Nottinghamshire	Grassland		51	33	15	7.2	20
	Morpeth, Northumberland			55	23	22	8.04	45
	Gayhurst, Bucks			44	35	21	5.4	15
	Olney, Silsoe, Beds			60	30	10	5.4	20
Clay loam	Harversham, Bucks			37	27	36	4.6	40
	Runway, Duck End, Wilstead, Beds			35	25	40	4.2	60
Sandy loam	Nafferton, Northumberland			13	22	65	7.5	28
	Avenue, Silsoe, Beds			29	19	51	3.1	32
	Brecon, Wales			21	65	14	5.94	40
							Sum	**300**
							Total	**600**

Table 3-6 Samples statistics of laboratory measured volumetric moisture content (θv) in cm^3 cm^{-3}, gravimetric moisture content (ω) in g g^{-1} and bulk density (BD) in g cm^{-3}, used for the analysis of the effect of soil texture classes.

		Arable lands			Grasslands		
Soil class	statistic factor	θv	ω	BD	θv	ω	BD
Clay	Maximum	0.53	0.38	1.58	0.53	0.34	1.70
	Minimum	0.37	0.27	1.12	0.20	0.12	0.88
	Range	0.16	0.11	0.46	0.33	0.22	0.82
	Average	0.44	0.32	1.36	0.35	0.25	1.39
	SD	0.04	0.03	0.15	0.09	0.06	0.20
Clay loam	Maximum	0.45	0.36	1.88	0.40	0.25	1.79
	Minimum	0.19	0.12	1.10	0.18	0.11	1.35
	Range	0.26	0.24	0.78	0.22	0.14	0.44
	Average	0.30	0.20	1.58	0.29	0.19	1.57
	SD	0.06	0.05	0.19	0.07	0.05	0.12
Sandy loam	Maximum	0.36	0.24	1.81	0.46	0.36	2.08
	Minimum	0.14	0.11	1.09	0.25	0.12	1.18
	Range	0.21	0.13	0.72	0.21	0.24	0.91
	Average	0.21	0.15	1.41	0.36	0.23	1.68
	SD	0.05	0.03	0.17	0.06	0.08	0.31
Collective	Maximum	0.53	0.40	1.89	0.53	0.42	2.07
	Minimum	0.16	0.11	1.00	0.19	0.12	0.88
	Range	0.37	0.29	0.89	0.34	0.30	1.19
	Average	0.32	0.23	1.45	0.33	0.23	1.52
	SD	0.10	0.09	0.20	0.09	0.07	0.25

SD is standard deviation; θv is volumetric moisture content (cm^3 cm^{-3}); ω is gravimetric moisture content (g g^{-1}); BD is soil bulk density (g cm^{-3}), Collective is the total of the three soil textures.

3.6.3. Effect of light and heavy soils

A total of 440 soil samples collected from arable lands only have been used to study the effect of dividing samples into the light and heavy soils (Figure 3-9) on the measurements accuracy of both sensors. The light soil class included loam, sandy loam, sandy clay loam, silt loam, silt, sand and loam sand textures, whereas the heavy soil class included clay loam, silty clay loam, silty clay, sandy clay and clay soils. In corresponding to the CC fraction obtained after the PSD analysis, Table 3-7 provides detailed information of the 440 soil samples including the number of samples, field location, texture class and soil texture fractions.

Table 3-7 Detailed information of the fields, where soil samples were collected to study the effect of dividing samples into light and heavy soil textures on the measurement accuracy of volumetric (θv) and gravimetric (ω) moisture content.

Soil category	Field	Samples number	Soil texture	Clay %	Silt %	Sand %	OM %
Light	Avenue, Silsoe, Beds	45	Sandy loam	16	20	63	3.6
	Barn left, Wilstead, Beds	25	Loam	18	35	47	3.5
	Dowings, Silsoe, Beds	20	Sandy clay loam	28	19	53	4.1
	Howne sand, Wilstead, Beds	52	Sandy loam	14	18	68	3.3
	Mound, Silsoe, Beds	38	Sandy loam	16	21	63	3.5
	Showground, Silsoe, Beds	40	Sandy clay loam	24	17	59	3.34
	Sum	220					
Heavy	Clover Hill, Silsoe, Beds	20	Clay loam	35	24	41	4.8
	Beechwood, Silsoe, Beds	40	Clay	66	11	23	5.8
	Ive, Silsoe, Beds	40	Clay	53	19	28	2.96
	Near Warden, Silsoe, Beds	20	Clay	54	25	16	5.53
	Orchard, Silsoe, Beds	20	Clay loam	33	26	41	4.15
	Upbury, Silsoe, Beds	20	Clay	54	24	22	4.5
	Flawborough, Nottinghamshire	20	Clay	51	35	14	5.4
	Morpeth, Northumberland	40	Clay	52	22	26	7.08
	Sum	220					
	Total	440					

OM is soil organic matter content.

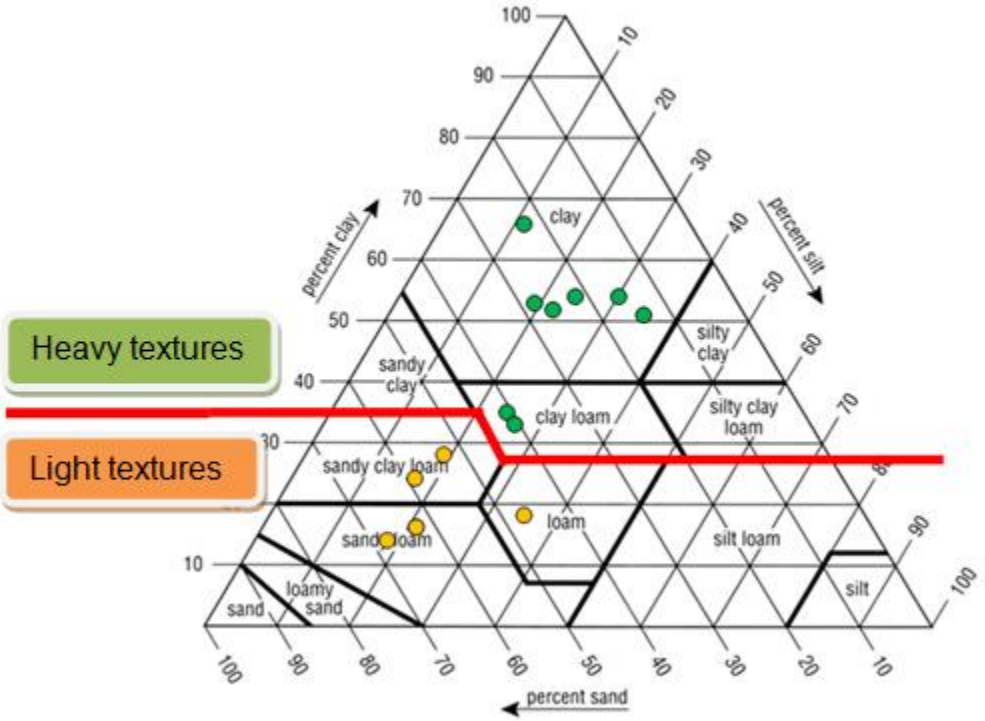

Figure 3-10 Average field texture, classified into heavy and light soil texture classes, according to the United States Department of Agriculture (USDA).

Table 3-8 provides basic statistics of the 440 soil samples used in the analysis of the effect of the light and heavy soils. The values of θv, ω and BD were obtained from the laboratory oven-drying method at 105 °C for 24 h. Two separate ANN calibration models were developed to analyse the effect of grouping soils into light and heavy classes on the measurement accuracy of θv and ω. The effect of the number of soil samples on the perdition accuracy of both sensors were diminished by selecting equal number of soil samples of 220 samples for the light and another 220 soil samples for the heavy soils. In addition, a total of 440 soil samples were used to produce the overall calibration model of all textures. Soil samples in all sets were divided into calibration (60%), test (15%) and validation (25%) sets. The prediction of θv and ω has been managed with input variables on V and the pre-treated vis-NIR spectra data.

Table 3-8 Sample statistics of laboratory measured volumetric moisture content (θv) in $cm^3\ cm^{-3}$, gravimetric moisture content (ω) in $g\ g^{-1}$ and bulk density (BD) in $g\ cm^{-3}$, used for the analysis of the influence of classification of soil samples into light and heavy soils on the prediction accuracy.

Soil type	Category	Maximum	Minimum	Range	Average	SD
Light	θv	0.38	0.14	0.24	0.23	0.06
	ω	0.29	0.10	0.19	0.15	0.04
	BD	1.81	1.15	0.67	1.52	0.17
Heavy	θv	0.53	0.18	0.35	0.40	0.07
	ω	0.45	0.14	0.31	0.28	0.08
	BD	1.75	1.11	0.64	1.44	0.18
Collective	θv	0.53	0.14	0.39	0.32	0.11
	ω	0.45	0.10	0.35	0.23	0.10
	BD	1.81	0.97	0.85	1.41	0.20

SD is standard deviation; θv is volumetric moisture content ($cm^3\ cm^{-3}$); ω is gravimetric moisture content ($g\ g^{-1}$); BD is soil bulk density ($g\ cm^{-3}$), Collective is the total of light and heavy soil textures.

3.6.4. The effect of land use

The majority of agricultural fields in the UK are cultivated with arable crops. However, grasslands are of wide spread practice that have proven environmental benefits in particular. The effect of land use (e.g. arable fields or grassland fields) on the prediction accuracy of θv and ω was investigated by dividing the collected soil samples into the following two groups of different sites:

- Arable lands soil samples: where fields were planted with different arable crops e.g. barely, wheat and oil seed rape.
- Grasslands soil samples: where fields were planted with grass crops.

A total of 616 soil samples were used for this analyses, with 308 samples collected each from arable and grassland fields. Table 3-9 shows the detailed information about the sample division, for different land use of the experimental sites including texture classes and texture fractions.

Table 3-9 Detailed information about experimental fields, where soil samples were collected to study the effect of land use on the measurement accuracy of volumetric (θv) and gravimetric (ω) moisture content.

Land use		Sites	Sample number	Soil texture	Clay %	Silt %	Sand %	OM %
Grassland		Avenue, Silsoe, Beds	40	Sandy loam	29	19	51	2.98
		Onley, Silsoe, Beds	20	Clay	60	30	10	5.4
		Morpeth, Northumberland	45	Clay	55	23	22	8.04
		Nafferton, Northumberland	28	Sandy loam	13	22	65	7.5
		Brecon, Wales	40	Silt loam	21	65	14	5.94
		Runway, Wilstead, Beds	60	Clay loam	35	25	40	4.2
		Gayhurset, Bucks	21	Clay	44	35	21	5.4
		Haversham, Bucks	34	Clay loam	37	27	36	4.6
		Flawborough, Nottinghamshire	20	Clay	51	33	15	7.2
		Sum	308					
Arable land	winter wheat	Beechwood, Silsoe, Beds	40	Clay	66	11	23	5.8
	winter wheat	Far Warden, Silsoe, Beds	20	Clay	59	27	14	5.1
	oil seed rape	Avenue, Silsoe, Beds	40	Sandy loam	16	20	63	3.6
	oil seed rape	Ive, Silsoe, Beds	40	Clay	53	19	28	2.96
	winter wheat	Near Warden, Silsoe, Beds	20	Clay	54	25	16	5.53
	Barley	Orchard, Silsoe, Beds	20	Clay loam	33	26	41	4.15
	winter wheat	Showground, Silsoe, Beds	40	Sandy clay loam	24	17	59	3.34
	Barley	10 Acres, Wilstead, Beds	21	Clay	50	28	22	3.5
	oil seed rape	Flawborough, Nottinghamshire	20	Clay	51	35	14	5.4
	winter wheat	Morpeth, Northumberland	47	Clay	52	22	26	7.08
		Sum	308					
		Total	616					

Table 3-10 provides the basic statistics of the 616 soil samples, used for the analysis of the effect of land use on the prediction accuracy. The values of θv, ω and BD were obtained with the oven-drying method at 105 °C for 24 h.

Table 3-10 Samples statistic of the laboratory measured volumetric moisture content (θv), in cm^3 cm^{-3}, gravimetric moisture content (ω) in g g^{-1} and bulk density (BD) in g cm^{-3}, the samples used for the analysis of the effect of land use on the measurement accuracy.

Land use	Category	Statistics factor				
		Maximum	Minimum	Range	Average	SD
Arable lands	θv	0.51	0.14	0.38	0.28	0.12
	ω	0.39	0.10	0.29	0.20	0.09
	BD	1.79	1.07	0.72	1.40	0.15
Grasslands	θv	0.53	0.19	0.34	0.32	0.09
	ω	0.41	0.12	0.29	0.22	0.08
	BD	2.08	0.89	1.19	1.48	0.24
Collective	θv	0.55	0.14	0.41	0.30	0.10
	ω	0.39	0.10	0.29	0.21	0.08
	BD	2.08	1.03	1.05	1.46	0.20

SD is standard deviation; θv is volumetric moisture content (cm^3 cm^{-3}); ω is gravimetric moisture content (g g^{-1}); BD is soil bulk density (g cm^{-3}), Collective is the total of the two land use practices.

The ANN calibration method was used to establish calibration models to predict θv and ω for arable lands and grasslands using the readout data produced from the dielectric and the vis-NIRS sensors, with equal soil sample number (308 soil samples for each class). Another ANN calibration models to predict θv and ω using both data sets of 616 soil samples were developed. Similar to the above ANN models, the soil samples were divided into calibration (60%), cross-validation (15 %) and test (25%) and independent validation sets for the three modelling scenarios.

3.7. Development of a soil bulk density prototype sensor

After providing a proof of concept of the new measurement system of BD and understanding the most affecting factors on the measurement accuracy of θv and ω and consequently of BD. The plan was to test this new concept in real situation *in-situ*. In order to do so, a new penetration probe was design and developed. It is a portable prototype measuring system, consisting of a combination of a NIR spectrophotometer (Avantes spectrometer), a dielectric sensor, a standard penetrometer, a battery and a laptop (Figure 3-13).

The dielectric sensor used in this prototype measuring system has an electronic circuit generating a 100 MHz electromagnetic sine wave, which is propagated into the soil body through a central electrode in the form of a copper ring with a 10, 15 and 1.5 mm height, diameter and wall thickness, respectively. The copper ring is insulated from the probe body, which forms two shielding electrodes as they are connected to the electronic circuits' negative. Each shielding electrode has a cylinder shape with a 13 and 50 mm diameter and height, respectively. The readout pin of the electronic circuit is connected to the HH2 meter from Delta-T devices, which at the time of reading acts as a power supply and provides data storage.

Although the same electronic circuit of ThetaProbe was used for the prototype sensor, V values of ThetaProbe and the prototype sensor are not comparable, due to the differences in the dimensions and the shapes of the probe's electrodes, which in turn lead to significant differences in the sinusoidal wave reflection measurements. From the above, it can be concluded that it is necessary to calibrate the prototype sensor in the laboratory using different moisture levels and different types of soils (as explained in more details in point 3.7.1.), to figure out the relationship between these factors and V for the prototype, before carrying out the measurements in the field.

V is a direct readout of ThetaPobe's electronic circuit, which was preferred to be used in this study as no need for further transformation formula to be used to record the dielectric constant values, for example.

The probe body also provides protection for the optical fibres, as they run inside its cavity. The optical fibres open in the centre of a high reflection chamber, with a sapphire round window mounted on the top. The sapphire window is located in a small grove made in the probe body to prevent scratches that might form on its surface by the direct contact with the soil (Figures 3-10 and 3-11). The other ends of the optical fibres are connected to the Avantes spectrophotometer and the light source.

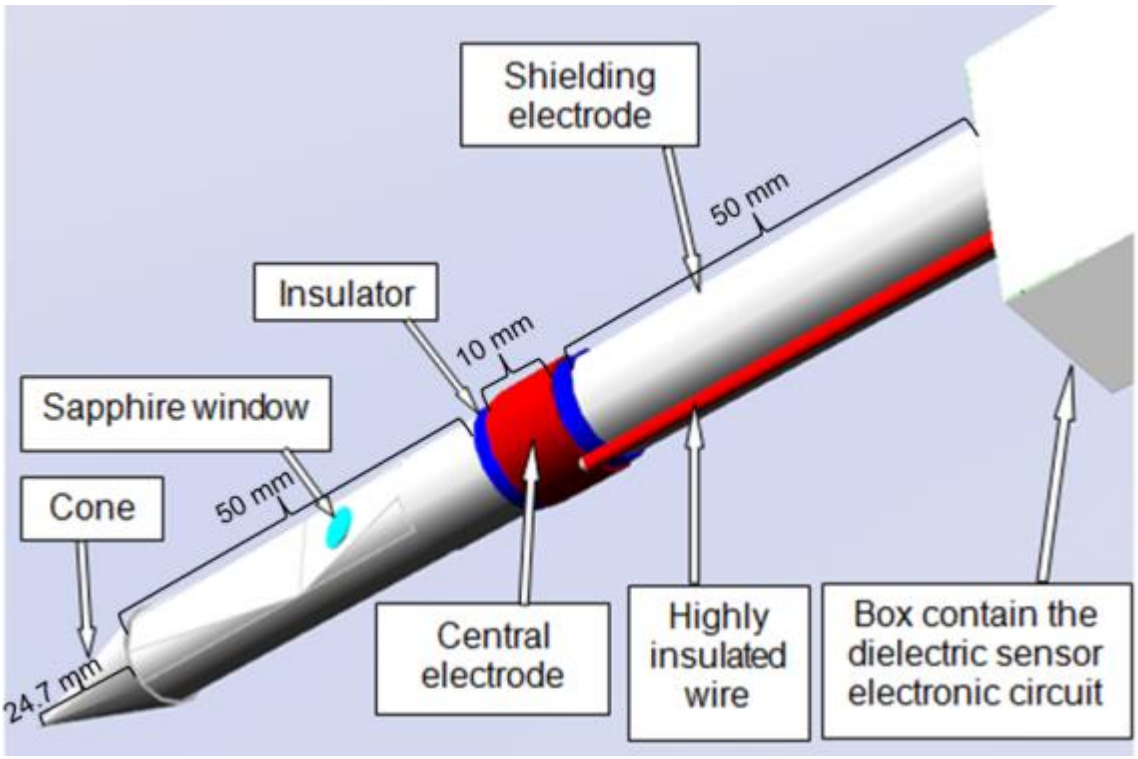

Figure 3-11 The combined portable probe of a near infrared (NIR) spectrophotometer and a dielectric sensor, for the measurement of soil volumetric moisture content (θv), gravimetric moisture content (ω) and bulk density (BD).

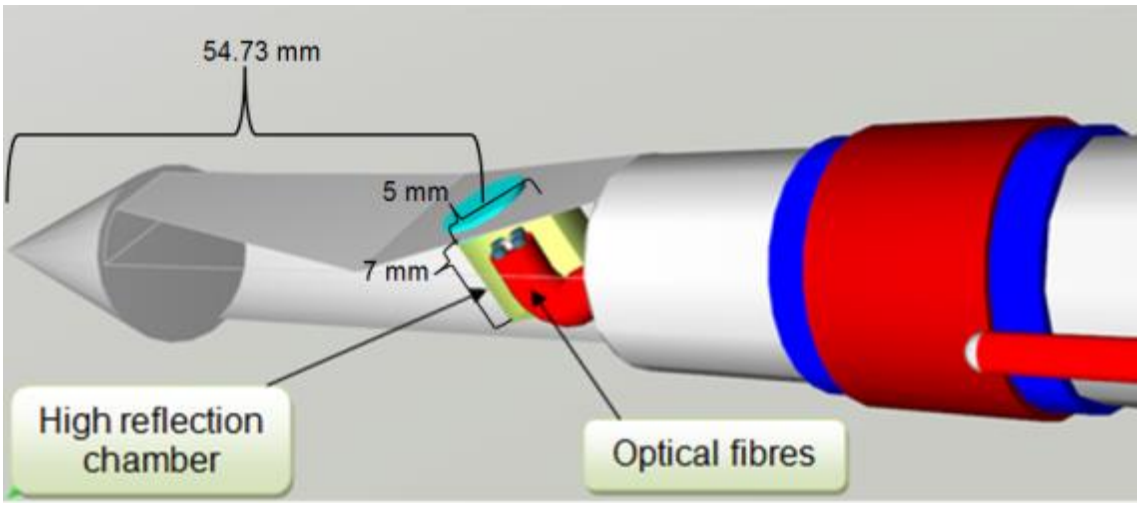

Figure 3-12 The reflection chamber of the combined probe.

As the combined probe inserted into the soil vertically, the surrounding soil in contact with probe electrodes will be affected by the fringe fields of the propagated signal, resulting from the two capacitors (Figure 3-12).

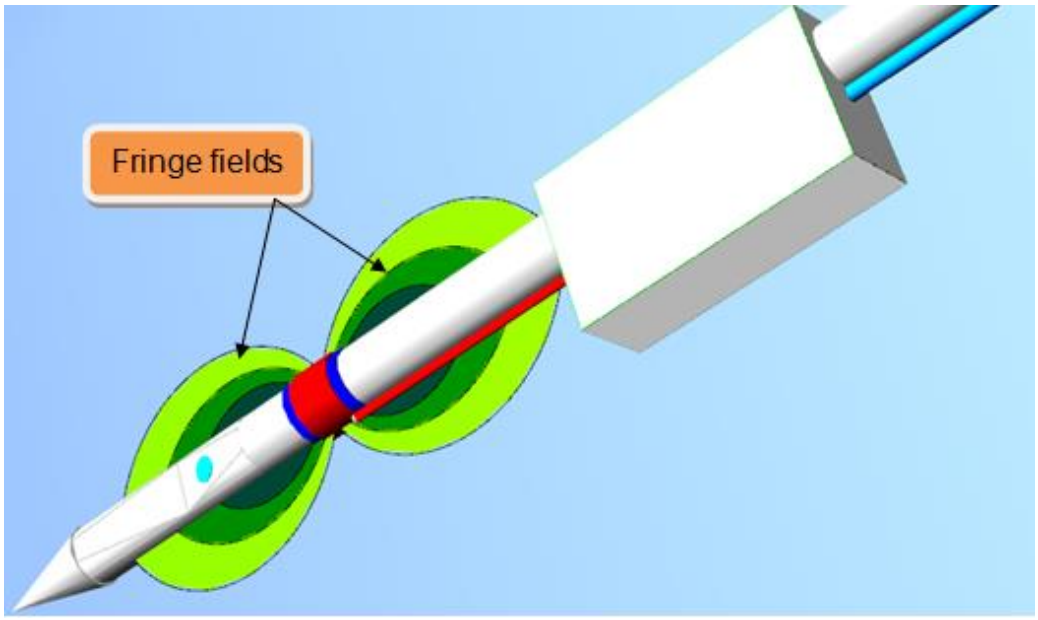

Figure 3-13 Shows the electromagnetic fringe fields around the dielectric sensors' electrodes.

3.7.1. Laboratory testing of the prototype measuring system

The prototype of the portable soil BD measuring system was first tested in the laboratory using two soil textures, namely, sandy loam and clay loam (Table 3-11). Each soil texture was oven dried for 24 hours at a 105 °C. Stones and large plant residuals were removed and the dry weight of the soil was recorded. Different measured volumes of distilled water were added to the dry soils and mixed properly in order to artificially produce various soil moisture contents. Then, instantly the wet soils were placed in a 1 litre volume plastic packet and the wet weight was recorded. A total of 50 soil samples of each soil texture were prepared to perform the laboratory testing. Three replicates were recorded for vis-NIR spectra and V readings obtained with the NIR spectrophotometer and the dielectric sensor, respectively, from each soil sample with different moisture content and BD.

Table 3-11 Information of the soil textures of soils used in the laboratory test of the prototype measurement system.

Soil texture	Samples number	Clay %	Silt %	Sand %	OM %
Sandy loam	50	30	18	52	3.00
Clay loam	50	60	29	11	5.50

The entire spectra data were pre-treated as explained in the point 3.3.4. using the Unscrambler® version 7.8 (Camo Inc.; Oslo, Norway), except for the spectra data noise at the high edge of the frequency, which was made negligible by reducing the spectra data range from 1650 to 2225 nm. Later on, the ANN calibration method was used to analyse the data produced in the laboratory for each soil texture and for both textures. The entire data set (e.g. 50 or 100 samples) were divided into calibration (60%), cross-validation (15%) and test (25%). The ANN analyses included the prediction of θv and ω, using input readings on V and vis-NIR spectra. Finally, BD was estimated using Eqn. 1-9.The prediction accuracy of

θv, ω and BD of the prototype measuring system was evaluated in terms of R^2 and RMSEP values of the independent data sets.

3.7.2. *In-situ* test of the prototype

- ***In-situ* measurement**

The prototype portable measurement system was tested for *in-situ* measurement in five fields with various textures and growing crops. At each point in the field, three V and NIR spectra were measured with the prototype's dielectric sensor and vis-NIR spectrometer. Average values of the three V and vis-NIR spectra were calculated afterwards. The experiment ran from August, 2013 to December, 2013, at the Silsoe experimental farm of Cranfield University. These fields are the same as those used to study the effect of moisture content of the measurements of output voltage and spectra. However, two more fields were used, namely, Avenue and Onley fields with grass grown. Table 3-12 shows information about the test fields where the prototype was tested.

Table 3-12 Information of the fields, where the prototype measuring system was tested.

Fields	SN	Soil texture	Clay%	Silt%	Sand%	OM%	Crop
Avenue	20	Sandy loam	16	20	63	3.6	Barley
Beechwood	20	Cay	66	11	23	5.8	Wheat
Clover hill	20	Clay loam	35	24	41	4.8	Barley
Orchard	20	Clay loam	33	26	41	4.15	Wheat
Showground	20	Sandy clay	24	17	59	3.34	Barley
Sum	100	loam					
Avenue	50	Sandy loam	0.29	0.19	0.51	2.98	Grass
Onley	50	Clay	0.60	0.30	0.10	5.40	
Sum	100						

SN is samples number; OM is the organic matter content.

Table 3-13 provides basic statistics of the 200 soil samples, used for the field testing of the portable prototype sensor. Values of θv, ω and BD were obtained with the oven-drying method at 105 °C for 24 h, from soil samples extracted from 5 – 10 cm from the soil top surface, the top of the soil was removed before the readings were recorded and the soil were collected to avoid effect of the high percentage of plants residuals.

Table 3-13 Sample statistics of the soil samples, used for testing the new prototype measuring system. Values were obtained from laboratory measured volumetric moisture content (θv), in cm^3 cm^{-3}, gravimetric moisture content (ω) in g g^{-1} and bulk density (BD) in g cm^{-3}.

Statistic factor	Arable lands			Grasslands		
	θv	ω	BD	θv	ω	BD
Maximum	0.55	0.41	1.60	0.46	0.36	1.78
Minimum	0.12	0.10	1.08	0.24	0.15	1.20
Range	0.43	0.31	0.52	0.22	0.21	0.58
Average	0.34	0.26	1.34	0.35	0.25	1.49
SD	0.14	0.11	0.11	0.09	0.08	0.24

SD is standard deviation, ω is gravimetric moisture content (g g^{-1}), θv is the volumetric moisture content (cm^3 cm^{-3}) and BD is soil bulk density (g cm^{-3}).

The light weight and compact size of the prototype *in-situ* measurement system made it easy to move through the growing crops and carry out the measurements either by assembling the system on a sackbarrow (Figure 3-13) or carrying in a rucksack (Figure3-14).

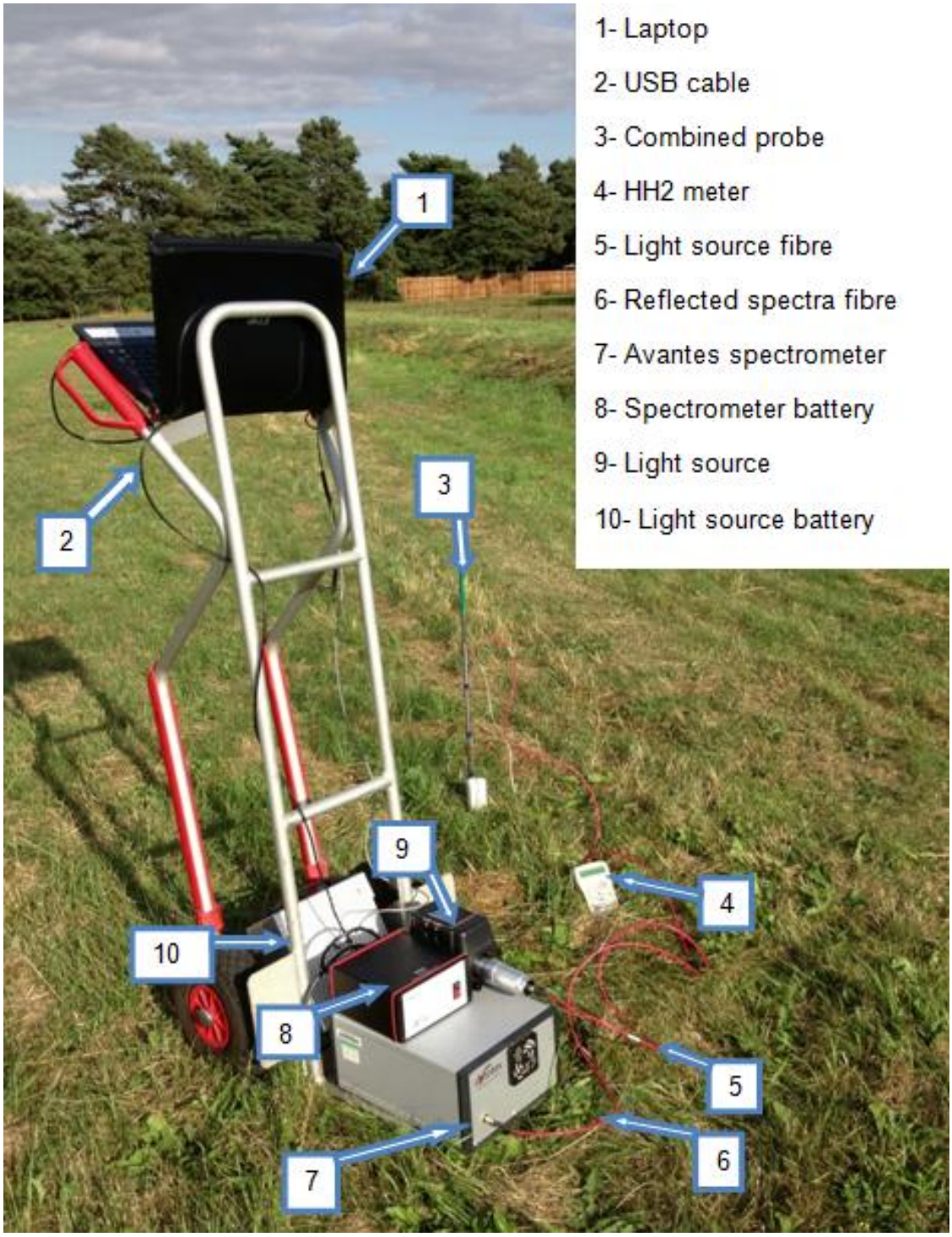

Figure 3-14 The prototype of the field measuring system of soil of volumetric moisture content (θv), gravimetric moisture content (ω) and bulk density (BD) assembled on a wheelbarrow.

Figure 3-15 The prototype of the field measuring system of volumetric moisture content (θv), gravimetric moisture content (ω) and bulk density (BD) carried in a rucksack.

The ANN technique was deployed to generate calibration models for θv and ω based on 75% of the vis-NIR spectra and V by the prototype sensors (75 soil samples). BD was then estimated using Eqn. 1-9 for the arable, grasslands and individual fields. All estimated BD values obtained by applying the ANN calibration models on the independent validation set (25% = 25 soil samples) were compared with the independent measured BD values (25% = 25 soil samples) using core sampling method. Before running the ANN analyses, the entire spectra data was pre-treated as explained in the Point 3.3.4 using the Unscrambler® version 7.8 (Camo Inc.; Oslo, Norway), except for the noise removing at the higher edge of the operating frequency of the Avantes spectrometer, which has been neglected by limiting the spectra data detection range from 1650 to 2225 nm.

3.7.3. Development of soil maps

Out of the 7 fields sampled with the prototype portable system, two fields were randomly selected for mapping. These were the Avenue arable and grassland fields. Three types of maps for the Avenue fields were developed for each soil property, namely, θv, ω and BD. These three maps are of the measured θv, ω and BD by the oven-drying of the core soil samples as a reference maps, the predicted maps of θv, ω and BD using the prototype combined sensor (for selected points) and predicted maps θv, ω and BD using full-data point maps. The reference and the predicted maps are used for a visual comparison of the prototype measuring system accuracy, the number of the soil samples and the position of the readouts for the reference and the 20 soil samples predicted maps were identical, while the full-data point maps were generated using a double number of the readouts of spectra and V data (A 40 readouts for a 40 different positions per field), as compared to the former two maps. The inverse distance weighing (IDW) interpolation method was used to develop the former two groups of maps using ArcGIS 10.2 (ESRI, USA) software. It was deployed to provide histogram of the prediction errors of the difference between oven-drying measured and the prototype predicted values of soil θv, ω and BD. Based on semivariogram

parameters and kriging interpolation methods, ArcGIS 10.2 (ESRI, USA) was used to produce the full-data point maps of the field predicted θv and ω from V and vis-NIR spectra, respectively. Then field BD was calculated using Eqn. 1-9, by substituting the predicted values of θv and ω obtained with ANN calibration method and comparison was made between the calculated BD and independent measured BD using core samples method.

Chapter 4

4. Results

In this chapter the validation results of both dielectric and vis-NIRS techniques for the measurement of θv and ω, respectively, will be presented. Results of the potential error for soil BD estimation resulted from using both ThetaProbe and ASDi sensors will be introduced. Finally, the results of both sensors as affected by the four affecting factors will be provided. To evaluate the performance of the methodology used in the current work the following main comparisons were considered in this chapter:

- **Effect of modelling approach**

Where a comparison was made between different calibration models adopted for ThetaProbe sensor, namely,

  - Manufacturer (M)
  - General formulae (GF),
  - Soil specific calibration (SSC),
  - Output voltage calibration (OV),
  - Artificial neural networks (ANN).

Two calibration techniques were tested for ASDi spectrometer, namely,

  - Partial least squares regression (PLSR)
  - Artificial neural networks (ANN).

The last comparison regarding the modelling approach was preformed between ANN data fusion method and SSC and PLSR calibration methods of ThetaProbe and ASDi spectrometer, respectively. With the ANN data fusion method a multiple data layers of both ThetaProbe and ASDi spectrometer readouts of V and spectra data, respectively, were used as input in addition to other properties of the soil (Table 4-1).

- **Effect of moisture level**

Here the results of effect of three different soil moisture levels on performances of both ThetaProbe and ASDi sensors were presented. The Three levels of soil moisture content and their averages values of gravimetric and volumetric moisture content were as follows:

  - L1 = 0.11 g g^{-1} and 0.15 cm^3 cm^{-3}
  - L2 = 0.20 g g^{-1} and 0.23 cm^3 cm^{-3}
  - L3 = 0.28 g g^{-1} and 0.32 cm^3 cm^{-3}

- **Effect of soil texture**

Here the results of soil texture effect on ThetaProbe and ASDi sensors accuracies were compared using three different soil types, namely,

  - Clay
  - Clay loam
  - Sandy loam

In addition the results of both sensors accuracies, obtained after dividing the soil types into two soil textures classes were compared. These classes were:

  - Light textures
  - Heavy textures

- **Land use effect**

Here the results of different land use effect on ThetaProbe and ASDi sensors performance and estimated BD were presented, comparing the accuracy obtained in arable land soils with grassland soils.

- **Laboratory test and calibration of the prototype combined probe**

The results of the prototype system performance to measure θv, ω and BD are represented under the laboratory conditions.

- ***In-situ* test of the prototype combined probe**

The capability of the data fusion calibration technique implemented on data collected with the prototype combined probe to eliminate BD under field conditions of five arable fields is evaluated.

- **The potential error for soil BD estimation**

The potential error for the estimation of soil BD calculated as RMSEp values of θv and ω estimation, obtained from current work was compared with the average published values reported by other researchers.

- **Mapping using the prototype portable measuring system**

Finally, maps of θv and ω, and soil BD developed with the prototype combined sensor are compared with the corresponding maps developed based on the core sampling method. In addition variation of these three properties will be examined using full-point maps provided for selected arable and grassland soils.

4.1. Effect of modelling

- **Accuracy of ThetaProbe measurement for volumetric moisture content**

Table 4-1 shows the measurement accuracy of θv with the ThetaProbe compared to the oven drying method using M, SSC, GF, OV and ANN calibration models with one input parameter (e.g. output voltage V). The results suggest that the ThetaProbe is capable of measuring θv with high accuracy even with the M calibration method, without the need for additional calibration. However, slight differences can be observed between these methods. With the M method, the measured values of θv over-estimate the oven drying measured values. The scatter plot of the ThetaProbe-M predicted versus oven drying measured θv illustrates a slope with the x axis with a value of 1.12 cm^3 cm^{-3}, indicating over-estimation of the M model (Figure 4-1A). The SSC calibration method performs equally well as that of the M method. However, the GF calibration method provides

an improved measurement accuracy (R^2 = 0.96 and RMSEp = 0.020 cm^3 cm^{-3}) (Table 4-1). The RMSEp obtained with these three methods (e.g. M, SSC and GF) is still larger than 0.01 m^3 m^{-3}, which contradicts the instruction provided by the ThetaProbe's manufacturer. The OV calibration method leads to further improvement (R^2 = 0.97 and RMSEp = 0.019 cm^3 cm^{-3}), as compared to the M, SSC and GF methods. ANN analysis with one input (e.g. V) does not perform as well as the OV method (R^2 = 0.96 and RMSEp = 0.021 cm^3 cm^{-3}). However, the ANN performance is the second best after the OV method. The worst performing methods are the SSC and M with the largest RMSEp values of 0.026 and 0.025 cm^3 cm^{-3}, respectively.

Table 4-1 Measurement accuracy of volumetric moisture content (θv), gravimetric moisture content (ω) and bulk density (BD) using the ThetaProbe or visible and near infrared (vis-NIR) spectra data (Spec), based on one input and data fusion with multiple inputs.

		θv		*ω*		BD	
Calibration method	Input	R^2	RMSEp, cm^3 cm^{-3}	R^2	RMSEp, g g^{-1}	R^2	RMSEp, g cm^{-3}
PLSR & M	One - V or Spec	0.95	0.025	0.91	0.027	0.50	0.160
PLSR & GF	One - V or Spec	0.96	0.020	0.91	0.027	0.23	0.187
PLSR & SSC	One - V or Spec	0.95	0.026	0.91	0.027	0.53	0.190
PLSR & OV	One - V or Spec	0.97	0.019	0.91	0.027	0.47	0.165
ANN	One - V or Spec	0.96	0.021	0.95	0.020	0.69	0.122
	V, Spec, S, SL, C & OM	0.97	0.019	0.95	0.020	0.70	0.120
	V, Spec, C & OM	0.96	0.020	0.94	0.022	0.65	0.127
	V, Spec & OM	0.97	0.018	0.96	0.018	0.78	0.101
	V, Spec & C	0.97	0.019	0.96	0.018	0.76	0.106
	V and Spec	0.98	0.015	0.98	0.014	0.81	0.095

M is manufacturer, GF is general formulae, SSC is soil specific calibration, OV is output voltage calibration, PLSR is partial least squares regression, OM is organic matter content, C is clay content, S is sand content, SL is silt content, V is readout voltage of ThetaProbe, Spec is spectra data, ANN is artificial neural networks, RMSEp is root mean square error of prediction and R^2 if coefficient of determination.

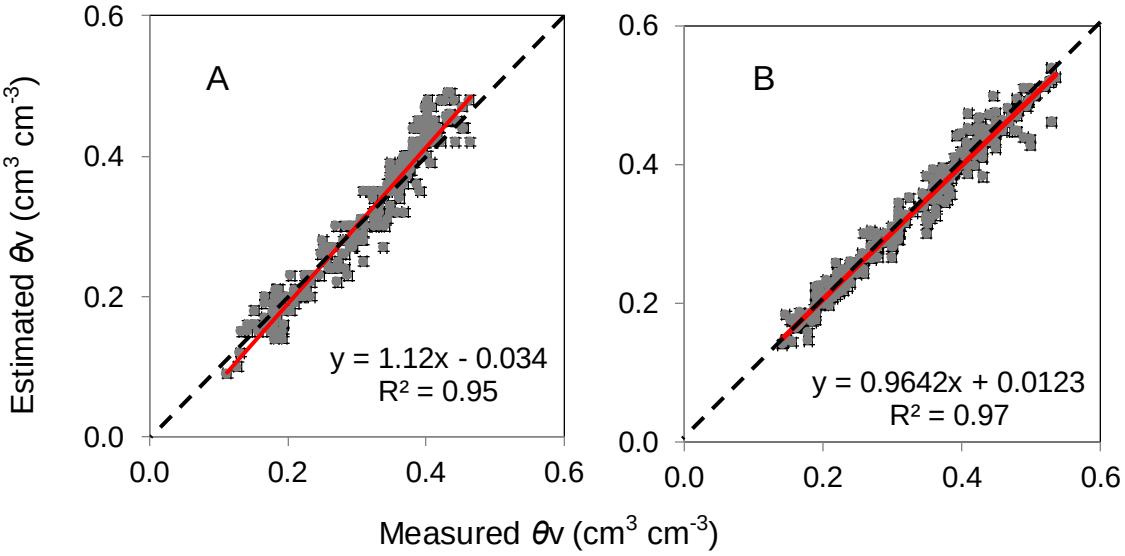

Figure 4-1 Scatter plots between ThetaProbe predicted volumetric moisture content (θv) and volumetric moisture content (θv) measured by oven drying method, using ThetaProbe's manufacturer (M) calibration (A) and artificial neural networks (ANN) calibration (B). Dashed line = 1:1 line; bold red line = line of best fit; ⊢ = error bars.

The ANN calibration model V, which is based on data fusion generally provides better measurement of θv, the Model showed the best results obtained from the effect of modelling, only V and vis-NIR spectra were used as input data to generate the Model V (Table 4-2) with R^2 = 0.98 and RMSEp = 0.015 cm^3 cm^{-3} of testing Model V on the independent validation set (Table 4-1), in comparison with the M, GF, SSC, OV and ANN-V models. Furthermore, this ANN-data fusion analysis with V and spectra only is the best performing among other ANN data-fusion analyses, where texture fractions and OM were used as input together with V and Spec (Table 4-1). In addition to the fact that the ANN – data fusion model results in the best measurement accuracy of θv, a shorter time was needed to conduct the ANN calibration-prediction, as compared to the single input modelling methods. This

technique requires only V and soil spectra to be used as input data, which are measured anyway by the ThetaProbe and vis-NIRS, respectively.

Table 4-2 Model specifications used for different artificial neural networks (ANN) analyses for the measurement of volumetric (θv) and gravimetric (ω) moisture content. Data used as input are output voltage (V), visible and near infrared spectra (Spec), sand (S), clay (C), silt (SL) and organic matter (OM).

Model	Input	Structure	Training algorithm	Hidden function	Output function	Output
I	V, Spec, S, SL, C, OM	176-5-2	BFGS 208	Log.	Exp.	θv, ω
II	V , Spec, C, OM	174-7-2	BFGS 92	Log.	Exp.	θv, ω
III	V , Spec, OM	173-6-2	BFGS 119	Exp.	Exp.	θv, ω
IV	V , Spec, C	173-4-2	BFGS 105	Exp.	Tanh	θv, ω
V	V , Spec	172-8-2	BFGS 188	Exp.	Tanh	θv, ω
VI	Spec	171-7-1	BFGS 202	Tanh	Tanh	ω
VII	V	1-2-1	BFGS 65	Exp.	Tanh	θv

BFGS: Broyden-Fletcher-Goldfarb-Shanno algorithm (Günaydin, 2009); Tanh: Hyperbolic tangent is a symmetric S-shaped (sigmoid) function; Exp.: Exponential function; Log.: Logarithmic function.

After the ANN – data fusion model, the OV calibration model with one input variable (e.g. V) can be ranked as the second best predictor of θv (Table 4-1), when validated with the independent validation set. By using 75% (759 samples) of the total 1013 soil samples, the following 2nd order polynomial equation was established using the OV method (Table 4-2):

$$\theta \mathrm{v} = 0.52\mathrm{V}^2 - 0.161\mathrm{V} + 0.141 \qquad (4\text{-}1)$$

Where, θv is soil volumetric moisture content cm^3 cm^{-3} and V is ThetaProbe output voltage (v).

The GF regression equation results in a slightly less accuracy (RMSEp = 0.020 $cm^3\ cm^{-3}$), as compared to that (RMSEp = 0.019 $cm^3\ cm^{-3}$) obtained with Eqn. 4-1, as shown in Table 4-1.

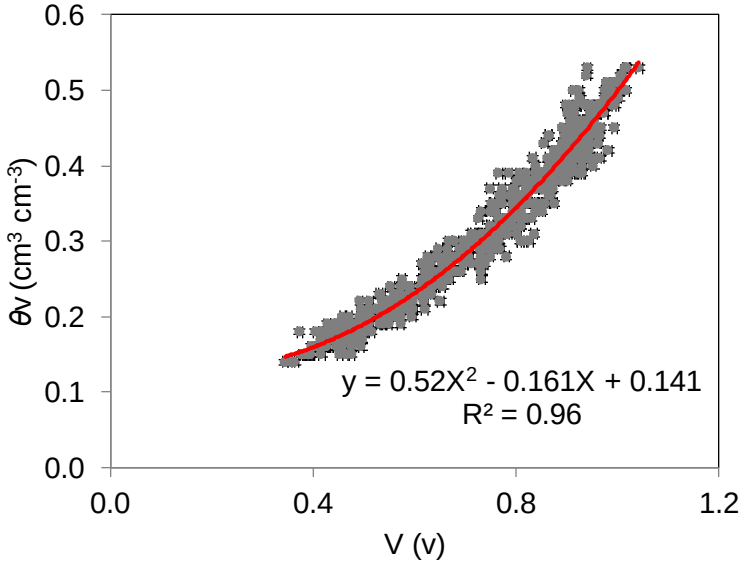

Figure 4-2 The relationship between the output voltage of ThetaProbe (V) and the soil volumetric moisture content (θv) measured by oven drying method. Bold red line = line of best fit; ⊢⊣ = error bars.

- **Accuracy of visible and near infrared spectroscopy measurement for gravimetric moisture content**

When only the vis-NIR spectra were used as input data, a smaller measurement accuracy of ω was obtained with the PLSR model (R^2 = 0.91 and RMSEp = 0.027 g g^{-1}), as compared to the ANN model (R^2 = 0.95 and RMSEp = 0.020 g g^{-1}) (Table 4-1). These results were expected, as ANN has been proved to out-perform PLSR for the measurement of soil properties with vis-NIRS (Khalilmoghadam et al., 2009; Mouazen et al., 2010; Viscarra Rossel and Behrens, 2010; Quraishi and Mouazen, 2013b). However, this is a clear contradiction of the measurement derived for θv. ANN – data fusion based analysis results in much improved measurement performance of ω, as compared to the PLSR technique. Furthermore, ANN – data fusion modelling based on V and spectra, out-performs (R^2 = 0.98 and RMSEp =

0.014 g g^{-1}) all other ANN – data fusion analyses based not only on V and spectra only, but laboratory measured texture fractions and OM (Table 4-1). After ANN – data fusion model based on V and spectra, the second best performing techniques are those based either on the fusion of V, spectra and OM or V, spectra and C (R^2 = 0.96 and RMSEp = 0.018 g g^{-1}).

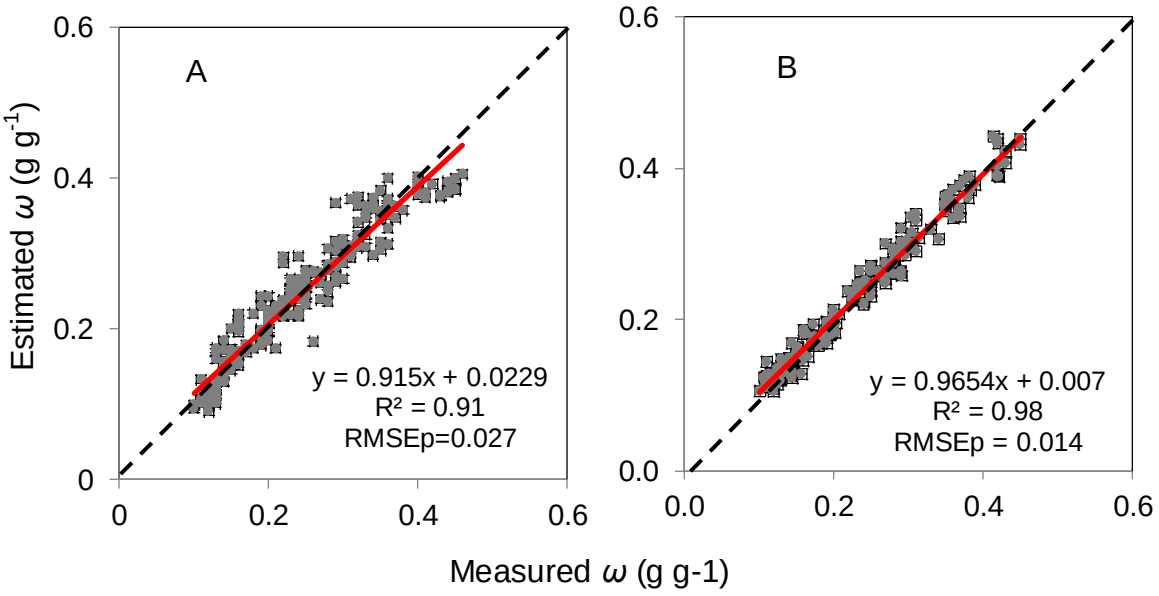

Figure 4-3 Scatter plot of independent validation between the estimated ω with vis-NIRS and measured ω with oven drying, using the PLSR calibration method (A); and the ANN – data fusion calibration method (B). Dashed line = 1:1 line; bold red line = line of best fit; ⊢⊣= error bars.

- **Bulk density assessment**

Having ω and θv measured accurately, respectively with the vis-NIRS and ThetaProbe, they are substituted in Eqn. 1-9 to derive BD. The accuracy of BD assessment with a single input variable (e.g. V or soil spectra) or with multiple input variables (e.g. V, soil spectra, C, S, SL and OM) (Table 4-2) is discussed in the following sections.

- **Accuracy of bulk density assessment with a single input variable**

Under this BD modelling category, ω is measured based on vis-NIR spectra - PLSR, whereas θv is measured based on V only and by means of the five calibration techniques of ThetaProbe discussed above. Generally, the BD assessment in this category is not encouraging (R^2 = 0.23 – 0.53 and RMSEp = 0.160 – 0.190 g cm^{-3}). The best assessment is obtained with the ANN - moisture content model (R^2 = 0.69 and RMSEp = 0.122 g cm^{-3}), however, this still has a relatively high RMSEp (Table 4-1). Figure 4-4A illustrates the scatter plots of estimated BD with ANN – single input variable moisture content models versus oven-drying measured BD. This is still a valuable result, as the analysis is capable of predicting BD of soils with a wide range of BD variation between 1.0 and 2.0 g cm^{-3}. The intercept of the linear regression equation reveals that the new system under-estimates BD, which might be attributed to the relatively low accuracy of the vis-NIRS for the measurement of ω, as compared to the ThetaProbe for the measurement of θv.

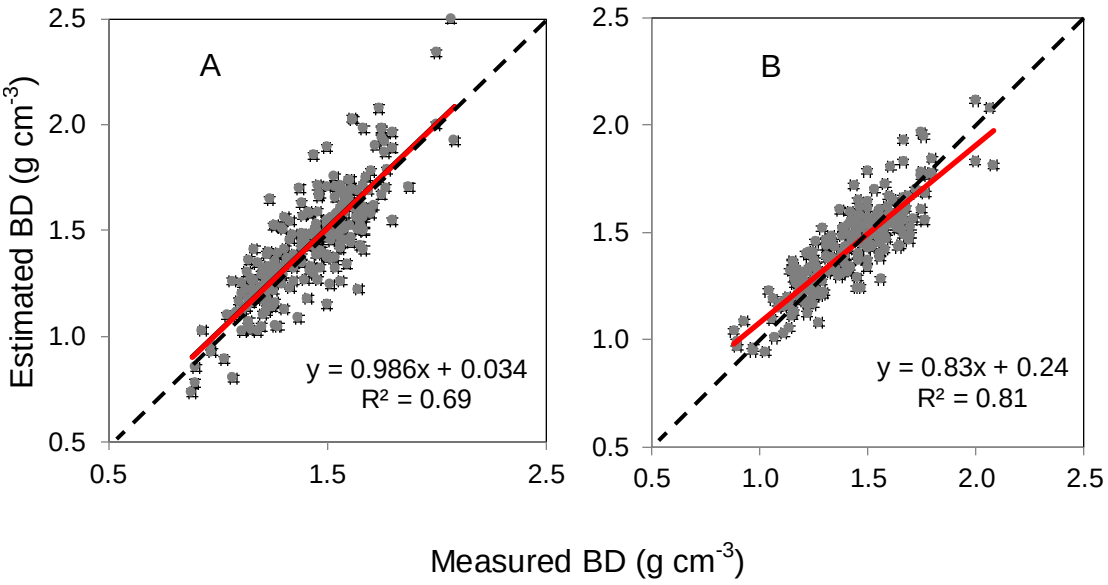

Figure 4-4 Scatter plot between estimated and oven drying measured soil bulk density (BD) based on artificial neural networks (ANN) with single input variable (A) and ANN – data fusion modelling (B). Dashed line = 1:1 line; bold red line = line of best fit; ⊢⊣= error bars.

- **Accuracy of bulk density assessment with multiple input variables (data fusion)**

Under this modelling category, both ω and θv are predicted with ANN based on different combinations of input variables of vis-NIR spectra: V, S, SL, C and OM (Table 4-2). Generally, as for the measurement performance of ω and θv, the assessment of BD (using Eqn. 1-9) with ANN – data fusion techniques (R^2 = 0.65 – 0.81 and RMSEp = 0.127 – 0.095 g cm^{-3}) out-performs the corresponding assessments obtained with the single input variable methods (R^2 = 0.23 – 0.53 and RMSEp = 0.160 – 0.187 g cm^{-3}) (Table 4-1). These results are in agreement with those reported by Quraishi and Mouazen (2013b). Although high assessment accuracy of BD is obtained with different ω and θv models of ANN – data fusion with different combinations of input variables, the accuracy increases with the decrease in the number of input variable used for ω and θv analyses. This trend is clearly illustrated by the increase in RMSEp values with the number of input variables used during ANN analyses (Figure 4-5C) of the independent validation set. However, R^2 values decrease with the increase in the number of input variables (Figure 4-6). This trend can be attributed to a similar trend observed for θv (Figures 4-5A and 4-6) and ω (Figures 4-5B and 4-6). One exception is for the ANN model based on V, spectra, C and OM input variables, for which a smaller accuracy can be observed, as compared to those obtained with a larger number of input variables (Figures. 4-5 and 4-6). Furthermore, the ANN – data fusion model with V, Spec and C performs less well, as compared to that with V, Spectra and OM (Figures 4-5 and 4-6).

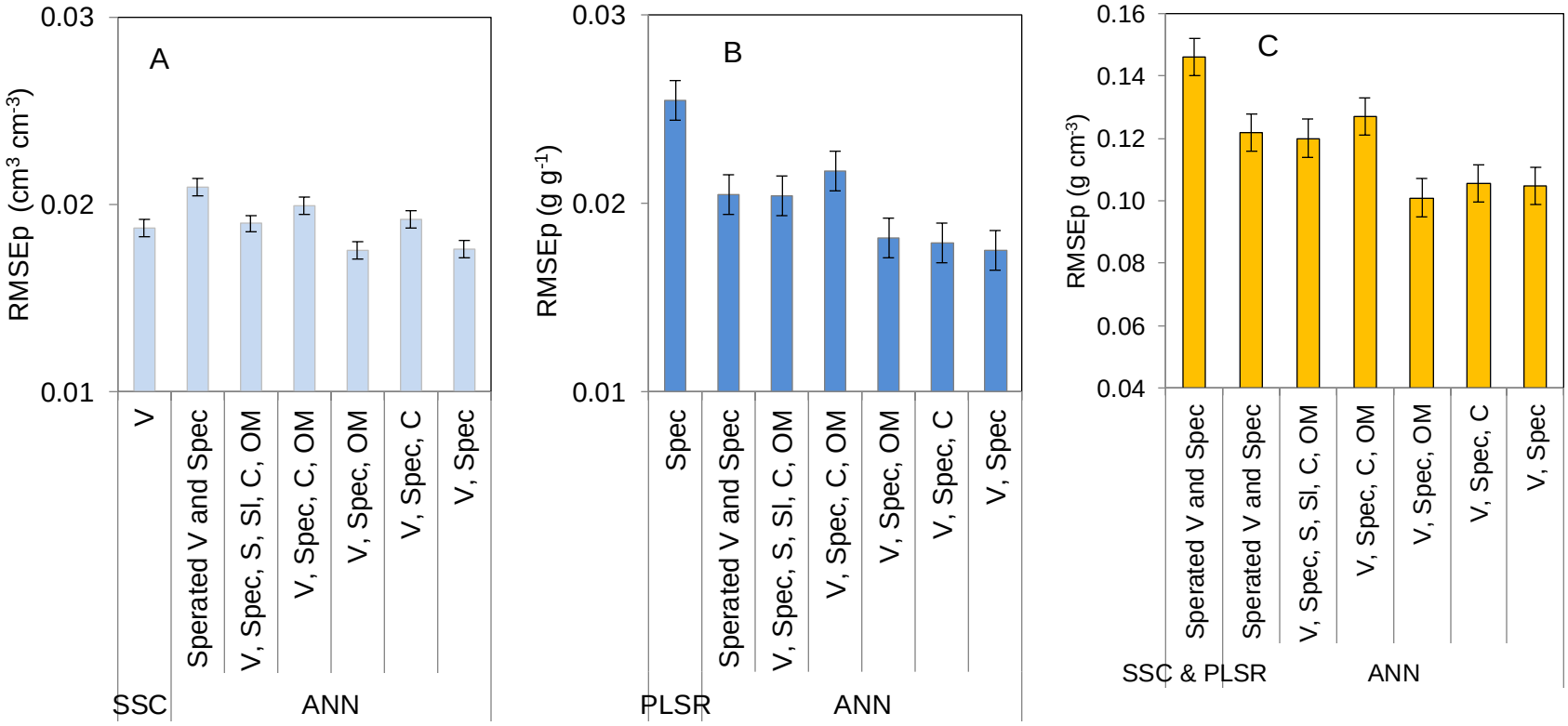

Figure 4-5 Variation of root mean square error of prediction (RMSEp) for the independent validation set with the number of input variable (soil spectra (Spec), readout voltage (V), sand (S), silt (SL), clay (C) and organic matter content (OM) used for artificial neural networks (ANN) to predict volumetric moisture content (θv) (A); gravimetric moisture content (ω) (B), and bulk density (BD) (C). The results of ANN – data fusion are compared to those obtained with single-variable input model (taken as an example), based on partial least squares regression (PLSR) to predict ω and specific soil calibration (SSC) to predict θv.

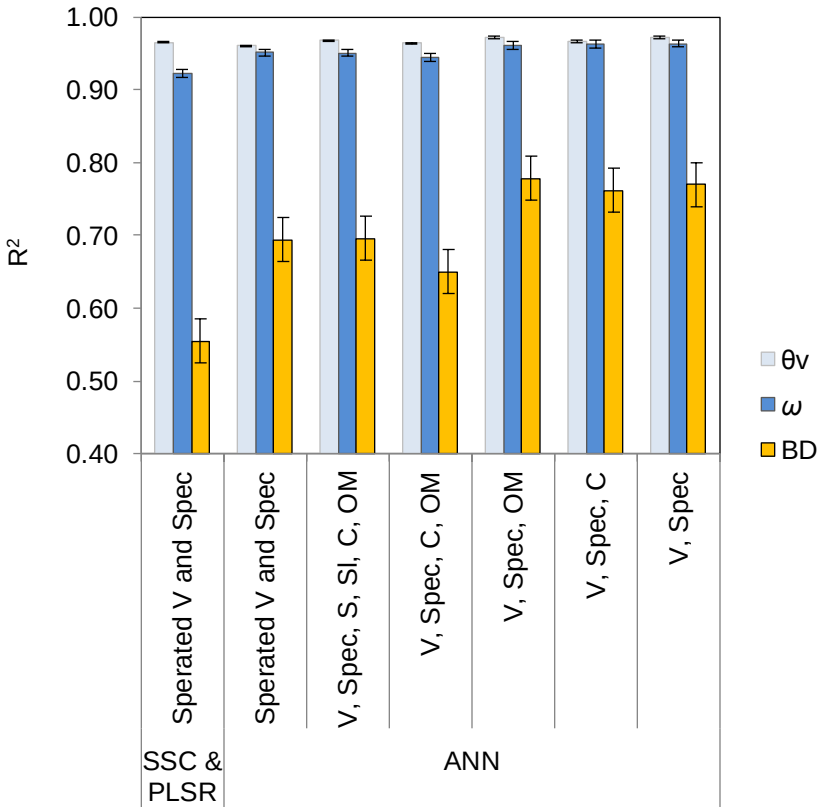

Figure 4-6 Variation of coefficient of determination (R2) of the independent validation set with the number of input variables (soil spectra (Spec), readout voltage (V), sand (S), silt (SL), clay (C) and organic matter content (OM) used for artificial neural neural networks (ANN) to predict volumetric moisture content (θv) (A); gravimetric moisture content (θv) (B), and bulk density (BD) (C). The results of ANN – data fusion are compared to those obtained with single-variable input model (taken as an example), based on partial least squares regression (PLSR) to predict ω and specific soil calibration (SSC) to predict θv.

4.2. Effect of moisture level

Appendix 1 shows the ANN results of θv and ω for three individual moisture levels and for all three moisture content levels (collective calibration) models based on data collected from arable lands only. Different network structures were generated automatically by the Statistica software, where the input layer

for all models contained 172 neurons (171 neurons of spectra data and one neuron of V) and the output layer of all models generated contained two neurons of θv and ω. Eight neurons in the hidden layers were used with all three individual moisture content models, whereas 18 neurons were used with the collective model. Most non-linear functions were chosen automatically in the hidden and output activations, except for the L3 output activation where it was linear (identity function).

All three individual moisture content models performed satisfactorily in cross-validation and training (R2 = 0.95 – 1) (Appendix 1). The performance improved of both training and cross-validation with soil moisture content increasing, but with different rates. While slight improving observed between L2 and L3, performance difference was obvious when comparing between L1 and other two moisture levels. The collective moisture content model show similar results to the individual moisture content analyses.

- **Accuracy of ThetaProbe measurement for volumetric moisture content**

The results of four different ANN calibration models, which were developed for three levels of moisture content and the collective model (Appendix 1), revealed high performance for each calibration model tested. However, the accuracy for the training and cross-validation of θv increased accordingly with increasing soil moisture level. Similar behaviour can be observed in the test sets (Appendix 3), where, for example, RPD and R^2 increased with moisture content level with 4.00, 7.00 and 10.38 $cm^3\ cm^{-3}$ and 0.94, 0.98 and 0.99 values at L1, L2 and L3, respectively. The RMSEp values showed a slight decrease from L1 to L2 and no difference between L2 and L3 could be observed (Table 4-3), this is in-line with Mittelbach (2011) when field tested four installed dielectric soil sensors down to 110 cm of depth, resulting lower absolute error of θv prediction during the dry conditions comparing to the measurements near or at the saturation conditions of the soil.

The scatter plots of measured versus estimated θv for the test sets showed the points are distributed closer to the 1:1 line with small slope and intercept values,

confirming high prediction accuracy (Appendix 2). However, soil texture at L2 and more clearly at L3 effected the distribution of the points, which resulting a wider range or variability of soil moisture across the fields (Appendix 2 B and C).

Table 4-3 Results of volumetric moisture content (θv) (cm^3 cm^{-3}), gravimetric moisture content (ω) (g g^{-1}) and soil bulk density (BD) (g cm^{-3}) prediction in the validation sets, based on artificial neural networks (ANN) calibration methods for the soil moisture level effect experiment of level 1 (L1), level 2 (L2), level 3 (L3), and the collective model.

Moisture level	θv			ω			BD		
	R^2	RMSEp cm^3 cm^{-3}	RPD	R^2	RMSEp g g^{-1}	RPD	R^2	RMSEp g cm^{-3}	RPD
L1	0.94	0.011	4	0.89	0.009	2.89	0.58	0.081	1.64
L2	0.98	0.011	7	0.98	0.012	7.08	0.74	0.068	1.85
L3	0.99	0.013	10.38	1	0.008	16.63	0.86	0.061	2.51
Collective	0.99	0.013	9	0.98	0.018	6.61	0.57	0.104	1.57

R^2: coefficient of determination; RMSEp: root mean square error of prediction; RPD: residual prediction deviation (Standard deviation/root mean square error of prediction).

- **Accuracy of visible and near infrared spectroscopy measurement for gravimetric moisture content**

The results of prediction accuracy of ω with the ANN analysis showed high performance (Table 4-3), using the independent validation sets of the three moisture levels plus the collective model. The accuracy improved with increasing soil moisture level. For example, the RPD and R^2 values increased with moisture content level with 2.89, 7.08 and 16.63 g g^{-1} and 0.89, 0.98 and 1 values at L1, L2 and L3, respectively. However, RMSEp responses to the moisture levels were different, where the largest value (0.012 g g^{-1}) was calculated for L2, as compared to those of L1 (0.09 g g^{-1}) and L3 (0.08 g g^{-1}).
The collective model preformed slightly better (RMSEp = 0.018 g g^{-1} comparing to Quraishi (2013), who reported RMSEp value of 0.024 g g^{-1} of ω prediction using the ANN method (Appendix 3D), although both studies used same fields

with similar variability in the data sets. The improved results of the current work might be attributed to the fusion of ThetaProbe and vis-NIR spectral data when used as input to ANN analysis. Appendix 3 shows ANN predicted ω values using ASDi spectrophotometer versus the oven drying measured ω values of the three moisture levels and collective model. Again the points distributed close to the 1:1 line with small slope and intercept values (particularly for L2 and L3). The x intercept and slope values were 0.007, 0.0042, 0.0045 and 0.027 g g^{-1} and 0.99, 1.00, 1.01 and 0.95, for L1, L2, L3 moisture content levels and for the collective model, respectively. For the same reason mentioned above of ThetaProbe measurements, soil texture at L2 and more clearly at L3 effected the distribution of the points, which resulting a wider range or variability of soil moisture across the fields, as soil fine textures tend to hold the moisture for a longer time, this phenomena was not clearly observed with L1, where the measurements were conducted in the fields after a long period in which the rain did not fall, making the soil moisture more homogeneous in L1 comparing to L2 and L3 (Appendix 2 A, B and C).

- **Accuracy of bulk density assessment with soil moisture level**

The estimated values of θv and ω using the ThetaProbe and vis-NIRS, respectively, were substituted into Eqn. 1-9 to derive soil BD for the three moisture levels and the collective models. Table 4-5 shows the prediction results of soil BD for the independent validation sets, where the accuracy improves significantly with increasing soil moisture. With increasing the moisture content level, R^2 and RPD values increased, while RMSEp decreased. The highest prediction accuracy was with L3 (R^2 = 0.86, RMSEp = 0.61 g cm^{-3}; and RPD = 2.51).

Figures 4-7 shows scatter plots of soil BD measured by the oven drying method against soil BD predicted using the two sensors with the ANN calibration technique. The scattered points of the distribution lie nearer to the 1:1 line as the moisture level increased. The prediction results of θv and ω were improved with soil moisture increasing with R^2 and RPD values raising (Table 4-3).

However, it was observed that ω prediction accuracy is the most influential of BD prediction accuracy, despite that RMSEp value of θv at L3 was the highest, with the lowest RMSEp value of ω. This supports the author hypothesis that the vis-NIRS data are the key factor when different levels of soil moisture are used to predict BD.

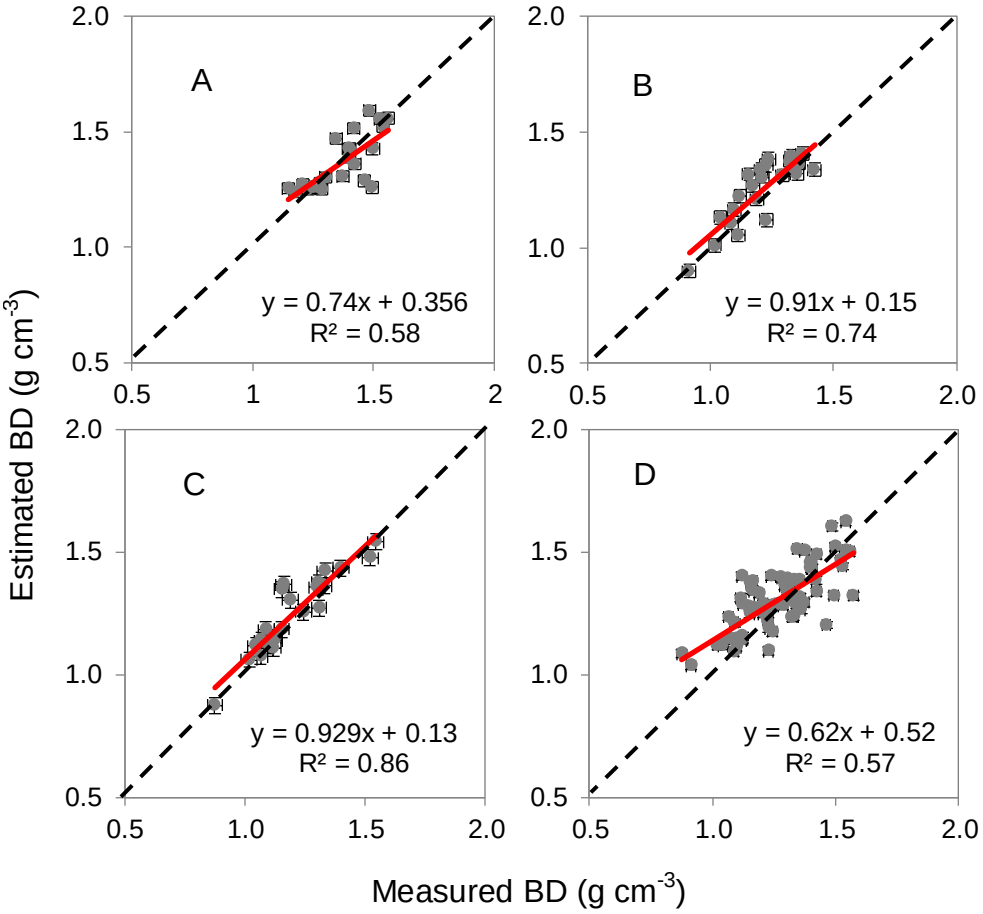

Figure 4-7 Core sampling versus predicted soil bulk density (BD) with the artificial neural networks (ANN) calibration method, for the soil moisture levels effect experiment of level 1 (L1) (A), level 2 (L2) (B), level 3 (L3) (C), and the collective model (D). Dashed line = 1:1 line; bold red line = line of best fit; ⊢⊣= error bars.

4.3. Effect of soil texture

The effect of soil texture class on the measurement accuracy of θv and ω and subsequently on BD was evaluated based on data fusion with ANN analysis. Which is over the past two decades has been subject of great interest among all

other statistical analysis. ANN success can be attributed to power, versatility, and ease of use, its ability to learn from examples is one of the many features of building neural networks that enable the user to generate accurate models of the underlying relationship between various data sets, although the representative data used to invoke the training algorithms is the key factor to generate accurate models. Although the Statistica software can be run automatically to learn the structure of the data, the user essentially needs to have some previous knowledge of how to select and prepare the training and the test data sets, and how to interpret the results, after all, the level of user knowledge needed to successfully build ANN models is considerably lower than those needed in most traditional statistical tools and techniques, specifically when ANN models are hidden behind the well designed and intelligent computer programs (StatSoft, 2012).

ANN analysis results for arable lands were presented separately than those for grassland data, as to avoid the effect of different land use. Appendix 4 shows the ANN analysis results for clay, clay loam, and sandy loam soil textures, and the total collected from arable land and grassland. Different network structures resulted, where the input layer for all models contained 172 neurons (171 neurons of spectra data and one neuron of V) and the output layer of all models generated contained two neurons of θv and ω. Various numbers of neurons, ranging from 8 to 24, were in the hidden layer. Mix linear and non-linear functions were chosen automatically by the Statistica software in the hidden and output activations, however, the majority of these functions were non-linear. In general, the performance of the training and validation sets of soil textures from grassland was better than those from arable land.

- **Accuracy of ThetaProbe measurement of volumetric moisture content as affected by soil texture class**

The effect of texture class was tested on the prediction accuracy of θv using three texture classes and the collective model using the ANN calibration method (Table 4-4). Results showed the performance of ThetaProbe calibration models was affected by the soil texture class; similar findings were reported by

Ponizovsky et al., (1999) and Sarani and Afrasiab (2012). The highest R^2 and lowest RMSEp values from the clay loam texture indicated the most accurate measurement with values of 0.89 and 0.018 cm^3 cm^{-3}, respectively, on the arable land and values of 0.99 and 0.008 cm^3 cm^{-3}, respectively, on the grassland. Similarly, the RPD of the clay loam texture was the best in grassland with a value of 8.75 and arable lands with a value of 3.33.

The second best accuracy was obtained for the collective texture model. The accuracy in the sandy loam texture was the third best for arable land model, giving the third best RPD value of 2.38, instead of the clay loam texture as expected, as it had the highest SD value among the other textures tested (Table 3-6). The collective model containing all three textures from arable land was less accurate compared to the collective model of the same soil textures from grassland, with RPD values of 4.35 and 6.43, respectively.

Table 4-4 Artificial neural networks prediction results of volumetric moisture content (θv) (cm^3 cm^{-3}) based on input of ThetaProbe output voltage (V) and visible and near infrared spectra (Spec) for different soil textures collected from arable land and grassland fields.

Soil textures	Arable land			Grassland		
	R^2	RMSEp, cm^3 cm^{-3}	RPD	R^2	RMSEp, cm^3 cm^{-3}	RPD
Clay	0.80	0.019	2.11	0.96	0.018	5.00
Clay loam	0.89	0.018	3.33	0.99	0.008	8.75
Sandy loam	0.87	0.021	2.38	0.90	0.019	3.16
Collective	0.95	0.023	4.35	0.97	0.014	6.43

R^2: coefficient of determination; RMSEp: root mean square error of prediction; RPD: residual prediction deviation (Standard deviation/root mean square error of prediction).

Appendix 5 and Appendix 6 show the scatter plots of the predicted and measured θv for clay (A), clay loam (B), sandy loam (C) soil textures and the collective (D) models for arable land and grassland, respectively, where the

points scattered closest to the 1:1 line have a clay loam texture and from both types of land use. Also of note is that the x intercept decreases with decreasing CC in the arable soils (Appendix 5). The ANN models for clay and clay loam textures from grassland predicted θv more accurately and the x intercepts were better than those of the same textures from arable land. However, θv was under-estimated for the sandy loam texture on grassland. Both collective models from arable land and grassland textures showed good prediction accuracy of θv (Appendix 6).

- **Accuracy of visible and near infrared spectroscopy for gravimetric moisture content measurement as affected by texture classes**

The effect of the same three soil textures, namely, clay, clay Loam and sandy loam was evaluated on the prediction accuracy of ω using the ANN calibration method. The results presented in Table 4-5, generally showed a good performance of ω model for each soil texture. Eight different ANN calibration models were generated from the arable land and grassland texture classes (Appendix 4).

Table 4-5 Artificial neural networks (ANN) results of gravimetric moisture content (ω) (g g^{-1}) prediction based on input data of visible and near infrared (vis-NIRS) spectra and ThetaProbe output voltage (V) for different soil textures collected from arable land and grassland fields.

Texture class	Arable land			Grassland		
	R^2	RMSEp, g g^{-1}	RPD	R^2	RMSEp, g g^{-1}	RPD
Clay	0.83	0.015	2.00	0.97	0.011	5.45
Clay loam	0.87	0.018	2.78	1.00	0.004	12.50
Sandy loam	0.89	0.013	2.31	0.95	0.019	4.21
Collective	0.96	0.018	5.00	0.98	0.011	6.36

R^2: determination coefficient; RMSEp: root mean square error of prediction; RPD: residual prediction deviation (Standard deviation/root mean square error of prediction).

Generally, the calibration models of soil textures collected from the grassland fields were more accurate than those collected from the arable land fields. The lowest accuracy of ω prediction using the independent validation was for clay

on arable land with the highest RMSEp of 0.018 g g^{-1} and the lowest RPD of 2.00. The measurement in the grassland textures showed a clay loam texture RPD value of 12.50, which is the highest accuracy among all. However, the rest of the RPD values show good to excellent prediction accuracy of ω, according to Viscarra Rossel et al. (2006).

Grassland RMSEp results showed considerably larger values for sandy loam textures (0.019 g g^{-1}), as compared to the remaining two textures and the collective texture model. A similar result is reported by Dalal and Henry (1986), who found larger RMSEp values associated with ω prediction for coarsely textured and low OM soils. The RMSEp of the collective model in arable soils (0.018%) was close to the RMSEp value of 0.021% reported by Mouazen et al., (2006) for arable soils, where 360 soil samples were used from different fields with various soil textures. The collective texture model performed satisfactorily in grassland soils too, suggesting a mixed texture model to perform well for the prediction of ω.

The RMSEp values of the ANN prediction of ω using the ASDi spectrometer revealed mixed results regarding the soil texture effect, where the best accuracy of prediction was obtained with the clay loam texture from grassland (RMSEp = 0.004 g g^{-1}) and the lowest prediction accuracy was gained from clay loam textures collected from arable land (RMSEp = 0.018 g g^{-1}). The collective texture model of arable land results of R^2, RMSEp and RPD of 0.96, 0.018 g g^{-1} and 5.00, respectively, which are slightly more accurate from those reported by Mouazen et al. (2005) with R^2, RMSEp and RPD values of 0.75, 0.025 and 3.38 kg kg^{-1}, respectively.

Appendix 7 and Appendix 8 show the scatted plots of predicted and measured ω of soil textures namely, clay (A), clay loam (B), sandy loam (C) and the collective texture (D) collected for arable land and grassland, respectively, where the points are closer to the 1:1 line for all individual soil texture models and the collective model of grassland compared to the all individual soil texture models and the collective texture model of arable land.

- **Accuracy of soil BD with soil texture classes effect**

The results of soil BD prediction with data fusion of V and vis-NIR spectra data gained from the dielectric and ASDi sensors, respectively, using Eqn. 1-9 can be found in Table 4-6. The highest accuracy of soil BD prediction was recorded for the sandy loam texture from grassland soils with R^2 of 0.95, RMSEp of 0.075 g cm^{-3} and RPD value of 4.13, and the lowest accuracy was with the clay loam texture from arable land with R^2 of 0.42, RPD of 1.65, and RMSEp of 0.115 g cm^{-3}. Although excellent prediction results e.g. RPD values were found with most soil textures, RPD values of soil textures from grassland were better than those from arable land, except for the clay texture where the arable land was better with an RPD value of 3.26 compared to a clay texture from grassland with a RPD value of 2.44. A similar trend dominated the values of RMSEp for BD prediction (Table 4-6). RPD values in grassland soils showed improving BD prediction with decreasing CC. This is not true for arable land soils (Table 4-6).

Table 4-6 Prediction results for soil bulk density (BD) for different soil textures collected from arable land and grassland soils.

Texture class	Arable lands			Grasslands		
	R^2	RMSEp, g cm^{-3}	RPD	R^2	RMSEp, g cm^{-3}	RPD
Clay	0.90	0.046	3.26	0.85	0.082	2.44
Clay loam	0.42	0.115	1.65	0.77	0.048	2.50
Sandy loam	0.49	0.083	2.05	0.95	0.075	4.13
Collective	0.68	0.079	2.53	0.91	0.066	3.79

R^2: determination coefficient; RMSEp: root mean square error of prediction; RPD: residual prediction deviation (Standard deviation/root mean square error of prediction).

Figures 4-8 and 4-9 illustrate the scatter plots of estimated BD versus oven drying measured BD. The intercept of the linear regression equation reveals that the new system considerably under-estimates BD with all texture models except for sandy loam soils for grassland soils. This is in agreement with findings of Quraishi (2013), who reported BD prediction accuracy in a clay soil texture was less accurate comparing to the BD estimation in the sandy loam texture, using an on-line system (Mouazen et al., 2006) to predict soil BD with sensor array including: vis-NIRS, load cell and depth wheel. However, the

measurements of the current work were of less under-estimation for clay textures comparing to clay loam textures, and the only exceptional over-estimated BD was found for sandy loam texture of grassland (Figure 4-9), which might be attributed to the relatively lower accuracy of the vis-NIRS for the measurement of ω, as compared to the ThetaProbe for the measurement of θv (Tables 4-4 and 4-5).

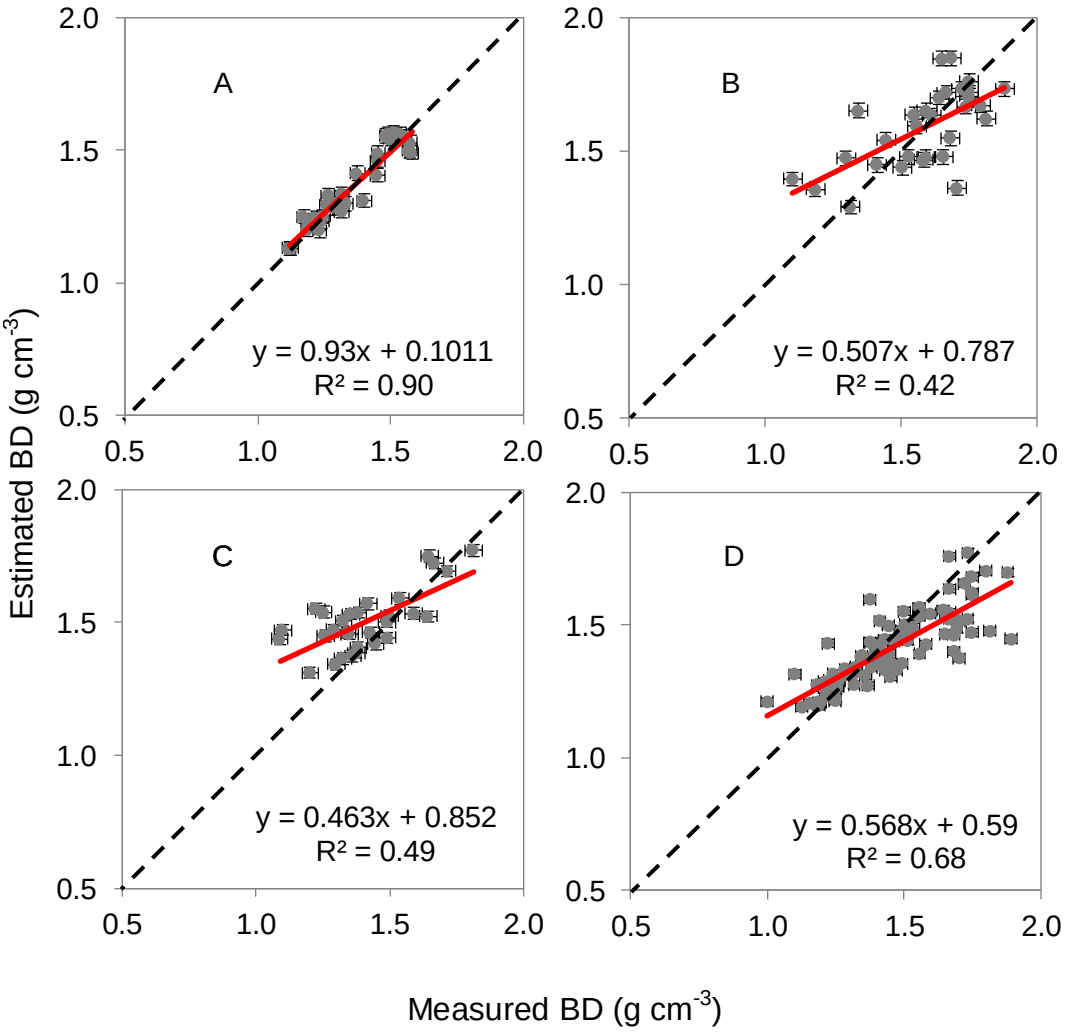

Figure 4-8 Scatter plots of core sampling measured versus sensor fusion predicted soil bulk density (BD) for clay (A), clay loam (B) and sandy loam (C) textures and the collective texture model (D), for samples collected from arable land fields. Dashed line = 1:1 line; bold red line = line of best fit; ⊢⊣ = error bars.

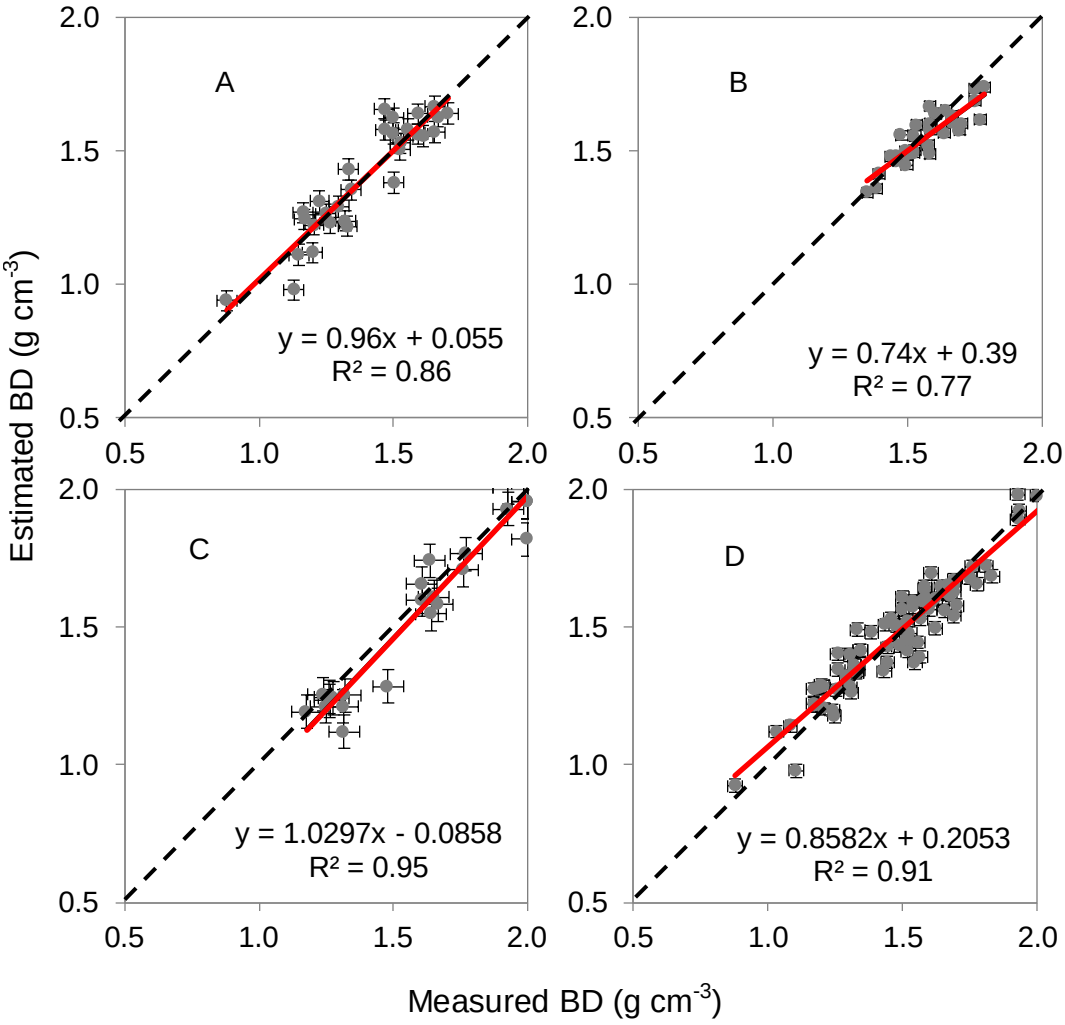

Figure 4-9 Scatter plots of core sampling measured versus sensor fusion predicted soil bulk density (BD) for clay (A), clay loam (B) and sandy loam (C) textures and for the collective texture model (D), of samples collected from grassland fields. Dashed line = 1:1 line; bold red line = line of best fit; ⊢⊣ = error bars.

4.4. Light and heavy soils effect

Appendix 9 provides the ANN analysis results for light soils, heavy soils and the collective, for samples collected from arable lands only. The purpose behind using arable land samples was to reduce the number of factors that affect the measurement accuracy of the new system (e.g. agriculture practice) and to provide more specific calibration models that can be used to predict θv and ω

on arable lands. In addition, arable soils are more affected by soil compaction problem than grassland soils, due to the use of heavy agriculture machinery and the intensive use of the land. Various network structures resulted, where the input layer for all models contained 172 neurons (171 neurons of spectra data and one neuron of V) and the output layer of all models generated contained two neurons of θv and ω. The number of neurons in the hidden layer ranged from 8 to 21. Linear and non-linear functions were chosen automatically by the Statistica software in the hidden and output activations. Generally, the training performance for the light soils was slightly better than those for the heavy soils (Appendix 9). Alternatively, the validation of the models using the validation set showed models for the heavy soils have outperformed those of the light soils (Appendix 14).

- **Accuracy of ThetaProbe measurement of volumetric moisture content for the light and heavy soils**

Although high accuracy resulted from the ThetaProbe calibration models for both light and heavy soils, the independent validation of the heavy soils showed a better prediction accuracy of θv (Appendix 14), as compared to the training set (Appendix 9). The higher R^2 (0.96) and RPD (4.38) values for the heavy soils indicate more accurate measurement as compared to lower R^2 (0.93) and RPD (3.75) for the light soils. The effect of light and heavy soils was not obvious in the RMSEp values, hence, they were 0.016 cm^3 cm^{-3} for both soil categories (Table 4-7). In this case, the use of RPD for the comparison is essential to identify the better accuracy. The highest RPD value of 5.24 was obtained for the collective model of both light and heavy soils (Table 4-7). However, the collective model resulted in the highest RMSEp, suggesting the use of individual texture class (heavy or light) to provide the smallest error and the best model performance.

Table 4-7 Artificial neural networks prediction results for the prediction of soil volumetric moisture content (θv) (cm^3 cm^{-3}), gravimetric moisture content (ω) (g g^{-1}) and bulk density (BD) (g cm^{-3}) based on the output voltage (V) of the dielectric sensor and visible and near infrared spectra (Spec) used as an input for the artificial neural networks (ANN) analyses of the light and heavy soils and collective soil textures.

Index	θv			ω			BD		
	R^2	RMSEp cm^3 cm^{-3}	RPD	R^2	RMSEp g g^{-1}	RPD	R^2	RMSEp g cm^{-3}	RPD
Light	0.93	0.016	3.75	0.9	0.012	3.33	0.49	0.106	1.6
Heavy	0.96	0.016	4.38	0.96	0.016	5	0.92	0.053	3.4
Collective	0.96	0.021	5.24	0.96	0.018	5.56	0.71	0.092	2.17

R^2: determination coefficient; RMSEp: root mean square error of prediction; RPD: residual prediction deviation (Standard deviation/root mean square error of prediction).

Appendix 10 shows the scatter plots of the predicted versus measured θv by oven drying for light soils (A), heavy soils (B) and the collective soil models (C), where the points are aligned best close to the 1:1 line for the heavy soils independent prediction. However, among the three models of θv, the smallest intercept with x axis of 0.009 cm^3 cm^{-3} and the best slope of 0.98 were obtained for heavy soils model, ensuring the best prediction performance. The positive values of the intercepts of all three models indicate under-estimation, a result that contradicts to that of Robinson et al. (1999), who reported over-estimation of θv obtained with a ThetaProbe for sandy and sandy loam soil textures.

- **Accuracy of visible and near infrared spectroscopy for gravimetric moisture content measurement for light and heavy soils**

The effect of light and heavy soils on the prediction accuracy of ω with the ANN calibration method was studied. The results of the independent validation sets including statistical factors: R^2, RMSEp and RPD are presented in Table 4-7. Generally, the performance of vis-NIRS to predict ω, using the ANN technique for both soils (light and heavy) was excellent with the collective texture model giving the best RPD value of 5.56, but again the largest RMSEp of 0.018 g g^{-1}.

Similar finding was reported by Mouazen et al. (2007) for a collection of soil samples from Belgium and Northern France, who explained that the high accuracy to predict ω using vis-NIRS can be attributed to the clear influential on the spectra data by the O-H bond energy absorbance in the second overtone region at 1450 nm. Although, the RMSEp values indicates that the accuracy was higher with light soils compared to the heavy soils (Table 4-7).

Appendix 11 shows the scatter plots between the predicted and measured ω, respectively, for light soils (A), heavy soils (B) and the collective soil texture class (C), where the points are closest to the 1:1 line with the heavy soils. The smallest x axis intercept and the perfect slope of 0.0008 g g^{-1} and, respectively suggest the best prediction is obtained for the heavy soils, although the root mean square error was slightly larger than that of the light soils (Appendix 14).

- **Accuracy of soil bulk density estimation with light and heavy soils effect**

The independent validation results of soil BD prediction with data fusion of V and spectra data using the dielectric and vis-NIRS sensors, respectively, and based on the ANN calibration method are shown in Table 4-7. All statistical factors including, R^2, RMSEp and RPD, which have been used to compare light, heavy and the collective models, indicate that the measurement of soil BD for the heavy soils gave the best accuracy of prediction, with R^2, RMSEp and RPD values of 0.92, 0.053 g cm^{-3} and 3.40, respectively. The lowest accuracy was with light soils and the second best was the collective texture model (Table 4-7).

Figure 4-10 shows the scatter plots of the predicted versus measured soil BD by data fusion and oven drying methods, for light soils (A), heavy soils (B) and the collective (C), where the points are closest to the 1:1 line with the heavy soils of the independent validation data set. The lowest x intercept (0.023 g cm^{-3}) and best slope of 0.98 of the heavy soils indicate the best performance compared to the other models. This suggests dividing samples into heavy and light soils when estimation of BD is required for heavy soils. For light soils, however, merging heavy and light soils in a collective texture model is expected to result in much improved estimation performance

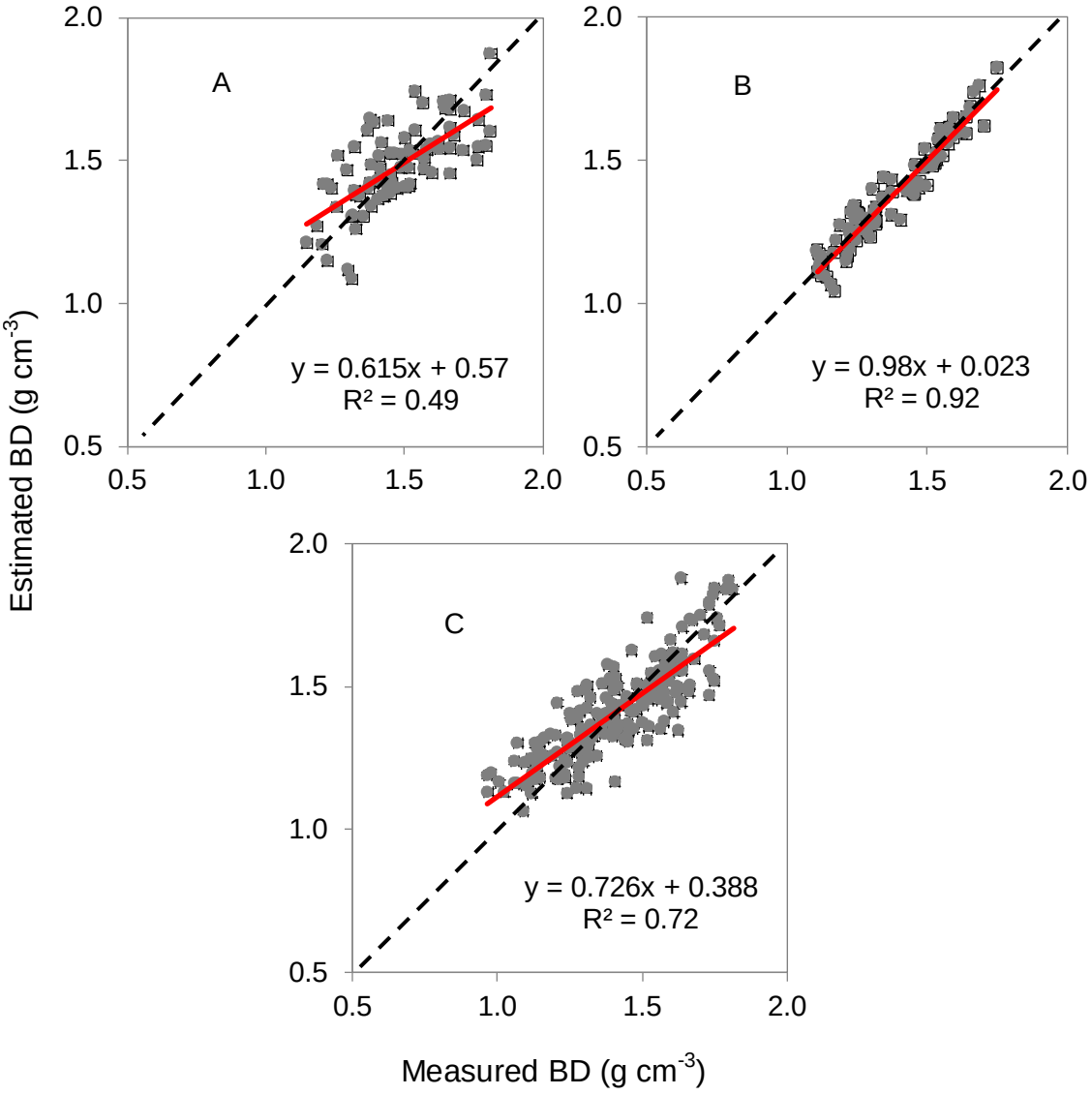

Figure 4-10 Scatter plots of core sampling measured versus artificial neural networks (ANN) predicted soil bulk density (BD) for the light soils (A), the heavy soils (B) and the collective texture soil samples (C). Dashed line = 1:1 line; bold red line = line of best fit; ⊢⊣ = error bars.

4.5. Effect of land use

Appendix 12 provides the ANN analysis results for arable land, grassland and the collective land use. Different network structures resulted, where the input layer for all models contained 172 neurons (171 neurons of spectra data and one neuron of V) and the output layer of all models generated contained two

neurons of θv and ω. The numbers of neurons in the hidden layer were 24, 21 and 18 for arable land, grassland and the collective models, respectively. All models used non-linear functions and were chosen automatically by the Statistica software in the hidden and output activations. The performance of the three ANN model categories in the training and cross-validation provided comparable performance.

- **Accuracy of ThetaProbe measurement for volumetric moisture content for the land use effect**

The ThetaProbe measurement of θv gave high accuracy results in both arable and grassland soils. However, the independent validation of the arable soils revealed the highest prediction accuracy of R^2 and RPD, with values of 0.99, and 8.23, respectively (Table 4-8). However, the grassland model has predicted θv with less error with RMSEp value of 0.013 cm^3 cm^{-3}. The R^2, RMSEp and RPD values of 0.97, 0.018 cm^3 cm^{-3} and 5.29 of the collective model indicates the lowest prediction accuracy of θv, (Table 4-8).

Appendix 13 shows the scatter plots of predicted versus measured θv for arable land soils (A), grassland soils (B) and the collective scenario (C), where the points closest to the 1:1 line are found in the grassland soils of the independent validation data set. However, the arable land soils and the collective models also predicted θv accurately.

Table 4-8 Artificial neural networks (ANN) results for the prediction of soil volumetric moisture content (θv) (cm^3 cm^{-3}) based on the output voltage (V) of the ThetaProbe and visible and near infrared spectra (Spec) used as an input for ANN analyses.

Land use	θv			Ω			BD		
	R^2	RMSEp cm^3 cm^{-3}	RPD	R^2	RMSEp g g^{-1}	RPD	R^2	RMSEp g cm^{-3}	RPD
Arable land	0.99	0.014	8.23	0.97	0.015	5.73	0.67	0.097	2
Grassland	0.98	0.013	6.19	0.98	0.01	7.31	0.91	0.083	3.18
Collective	0.97	0.018	5.6	0.98	0.012	6.86	0.77	0.079	2.4

R^2: determination coefficient; RMSEp: root mean square error of prediction; RPD: residual prediction deviation (Standard deviation/root mean square error of prediction).

- **Accuracy of visible and near infrared spectroscopy for gravimetric moisture content measurement for the land use effect**

The ANN results of the independent validation sets including statistical factors: R^2, RMSEp and RPD are shown in Table 4-8. All the three calibration models have predicted ω with excellent performance. The prediction of ω for the grassland soils was slightly better than arable soils and the collective model had the second best results with RMSEp value of 0.012 g g^{-1}. The R^2, RMSEp and RPD results of this analysis with values of 0.97, 0.015 g g^{-1} and 5.73, respectively, for arable soils, are over preformed of R^2, RMSEp and RPD values, for the measurements of ω from a multiple field reported by Mouazen et al. (2006b) of 0.88, 0.021 g g^{-1} and 2.87, respectively, when they used PLSR calibration method.

Appendix 14 shows the scatter plots of the predicted versus measured ω, respectively, for arable soils (A), grassland soils (B) and the collective soil (C) models, where the points closest to the 1:1 line are found in the grassland soils of the independent validation data set (Appendix 14B). Also, the grassland model resulted in the smallest intercept of 0.0021 g g^{-1} and the perfect slope, indicating the best performance among the other two models. However, the differences between the three models were minimal indicating no clear effect of

land use of measurement accuracy on ω. This result does not in line for the measurement of ω, where the best accuracy was found for grassland soils (Table 4-12).

- **Accuracy of data fusion for soil bulk density estimation for the land use effect**

The predicted values of θv and ω using the ThetaProbe and vis-NIRS, respectively, substituted into Eqn. 1-9 to derive soil BD using samples of the independent validation sets are shown in Table 4-8. All statistical factors including, R^2, RMSEp and RPD, which have been used to compare between the three models, indicate that the estimation of soil BD from grassland soils achieved the highest accuracy, with R^2, RMSEp and RPD values of 0.91, 0.083 g cm^{-3} and 3.18, respectively. The lowest accuracy was with arable soils and the second best was the collective model. Unfortunately, no results could be found in the literature about the prediction accuracy of θv and ω using dielectric probe and vis-NIRS, respectively, separately for arable lands and grasslands.

Figure 4-11 shows the scatter plots of measured versus predicted BD using the two sensors. The points distributed nearer to the 1:1 line are found in the soils from grasslands. However, all three ANN models underestimated soil BD, with x axis intercept values of 0.438, 0.079 and 0.35 g cm^{-3} for the arable land, grassland and the collective models, respectively. The overall conclusion in this section is that splitting samples into arable and grassland does not lead to improved estimation accuracy of BD. On the contrary, RMSEp (Table 4-6), intercept and slope values (Figure 4-11B) indicate the grassland model to perform the best as compared to the other two models.

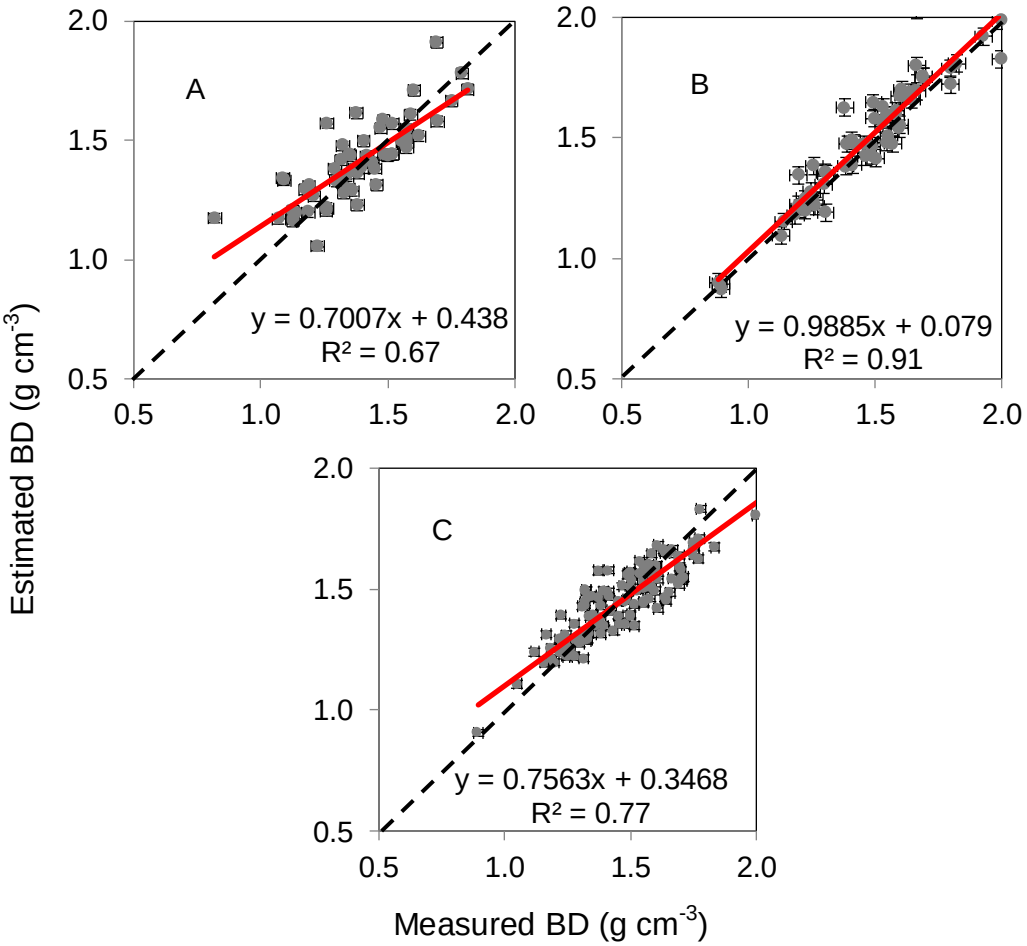

Figure 4-11 Scatter plots of core sampling measured versus artificial neural networks (ANN) predicted soil bulk density (BD) for arable land (A), grassland (B) and the collective sample (C) models. Dashed line = 1:1 line; bold red line = line of best fit; ⊢⊣= error bars.

5.6. Evaluation of the prototype combined probe

5.6.1. Laboratory test and calibration of the prototype combined probe

The output voltage (V) of the dielectric sensor, which was assembled on a standard penetrometer, was tested in the laboratory using two soil textures namely, sandy loam and clay loam, where three repeated readouts were recorded and the average was considered. Figure 4-12 shows the relationship between V of the dielectric probe and θv measured by the oven drying method for the two soil textures, where, different relationships can be observed, including: linear and 3rd order polynomials, respectively. Similar observations

were reported by Seyfried et al. (2005) when they studied the effect of a range of soil textures on a dielectric sensor. Both relations gave high R^2 values of 0.98 and 0.99 for sandy loam and clay loam textures, respectively.

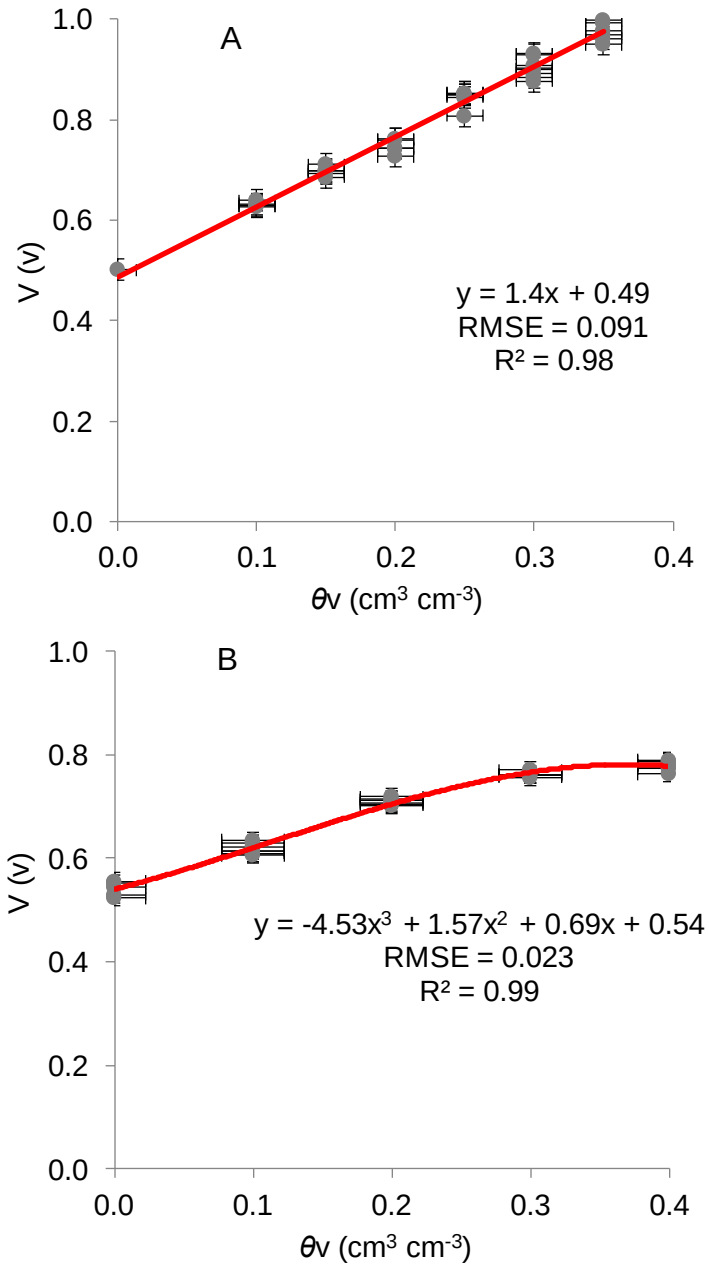

Figure 4-12 Laboratory measured relationship between the output voltage (V) and volumetric moisture content (θv) of the dielectric sensor of the prototype combined sensor, in sandy loam (A) and clay loam (B) textures. Bold red line = line of best fit; ⊢⊣= error bars.

The RMSE value from the laboratory test revealed smaller error of measurement with the clay loam texture (RMSE = 0.023 cm^3 cm^{-3}) than with the sandy loam (RMSE = 0.091 cm^3 cm^{-3}). The reason for this is mainly related to the structural failure of the sandy loam texture, associated with the addition of moisture to the test samples, especially, with θv above 0.20 cm^3 cm^{-3} (Figure 4-12A). This phenomena was less noticeable with the clay loam texture (Figure 4-12B), which can naturally hold more moisture before failure compared to the sandy loam texture.

Figure 4-12 Laboratory measured relationship between the output voltage (V) and volumetric moisture content (θv) of the dielectric sensor of the prototype combined sensor, in sandy loam (A) and clay loam (B) textures. Appendix 15 shows the results of the ANN calibration models of sandy loam and clay loam soil textures, using V and spectra data only, obtained from the dielectric and vis-NIRS sensors, respectively. A total of 170 neurons were used in the input layer, divided into 169 neurons of vis-NIR spectra and one neuron of V. All of the calibration models generated performed well as indicated by the R^2 values of each training and validation data set, and for both soil textures and for the collective sample model.

- **Dielectric sensor performance under laboratory conditions**

Generally, high accuracy of θv prediction using the independent validation sets was obtained from the laboratory test of the dielectric sensor of the combined probe, where three repeated readouts were recorded and the average was considered of V values of each prepared soil sample with various MC, with both soil textures used in the test. However prediction in the sandy loam texture was better with a RMSEp of 0.009 cm^3 cm^{-3} and RPD = 10.21 compared to a RMSEp = 0.040 cm^3 cm^{-3} and RPD = 3.36 for the clay loam texture (Table 4-9). This is due to the formation of air pockets around the central electrode ring of the dielectric sensor in the clay loam texture more than the sandy loam texture. Naderi-Boldaji et al. (2012) reported a rather low correlation between oven dried and dielectric sensor measured values of θv (R^2= 0.544). They used a linear calibration formula for the soil moisture range of 0.20 to 0.40 cm^3 cm^{-3}, under

laboratory conditions. Adamchuk et al. (2009) evaluated a capacitance based dielectric sensor for on-line mapping applications. They reported a R^2 value of 0.79 for the measurements of θv under laboratory conditions, while they observed a 57% reduction of θv for field readings by using the laboratory calibration model.

Table 4-9 Volumetric moisture content (θv) prediction results using dielectric probe under laboratory conditions of the independent validation sets, of sandy loam, clay loam textures and the collective sample model.

	Sandy loam	Clay loam	Collective
R^2	0.99	0.92	0.94
RMSE, $cm^3\ cm^{-3}$	0.009	0.040	0.030
RPD	10.21	3.63	3.82

R^2: coefficient of determination. RMSE: root mean square error of prediction and RPD: residual prediction deviation. A RPD value larger than 2.5 indicates excellent model prediction (Viscara Rossel et al., 2006).

The scatter plots of measured versus predicted θv for sandy loam, clay loam and collective samples, shown in Figure 4-13 indicate excellent prediction performance in the three cases. All three cases indicate small intercept, high R^2 and almost perfect slope.

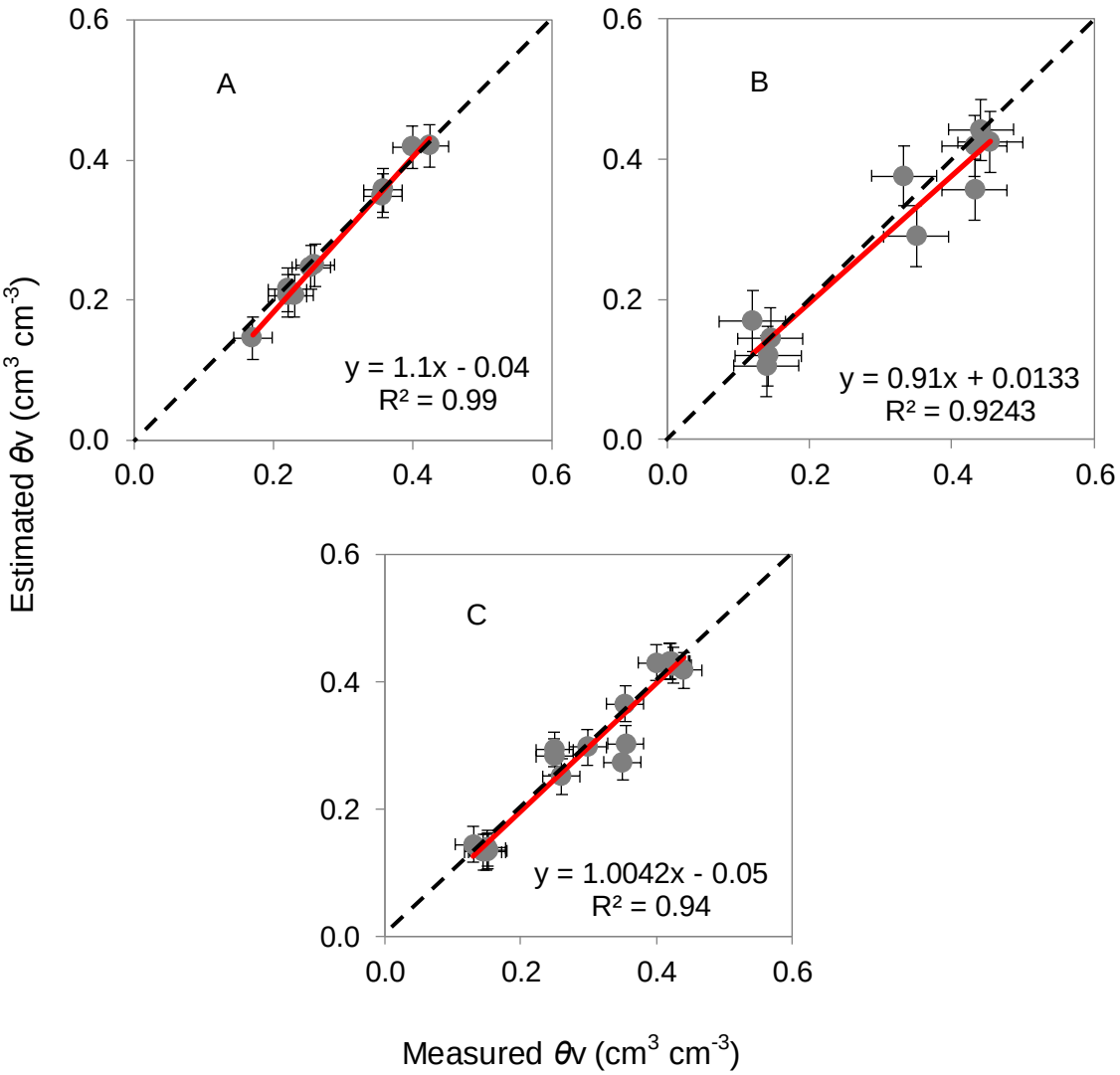

Figure 4-13 Scatter plots core sampling measured versus artificial neural networks (ANN) predicted soil volumetric moisture content (θv) using the prototype combined senor for laboratory measurements in sandy loam soils (A), clay loam soils (B) and the collective sample (C) models. Dashed line = 1:1 line; bold red line = line of best fit; ⊢⊣ = error bars.

- **Vis-NIR spectrophotometer performance under laboratory conditions:**

The results of ω prediction reveal that the performance of all NIR models of sandy loam and clay loam textures and the collective samples are classified as excellent (RPD > 2.5) according to Viscarra Rossel et al. (2006), which is

expected due to the fact that the test is carried out under controlled laboratory conditions. However, the collective model resulted in the smallest RPD value, as compared to the other two models. Furthermore, small differences are apparent between soil textures, particularly with R^2 and RMSEp values (Table 4-10).

Table 4-10 Gravimetric moisture content (ω) prediction results under laboratory conditions of the independent validation sets, of sandy loam, clay loam textures and the collective sample set.

	Sandy loam	Clay loam	Collective
R^2	0.99	0.94	0.94
RMSE, g g^{-1}	0.007	0.037	0.029
RPD	12.67	3.90	4.09

R^2: coefficient of determination. RMSE: root mean square error of prediction; and, RPD: residual prediction deviation.

The scatter plots of measured versus predicted ω for sandy loam, clay loam and collective samples, shown in Figure 4-14 indicate excellent prediction performance in the three cases. All three cases indicate small intercept, high R^2 and almost perfect slope.

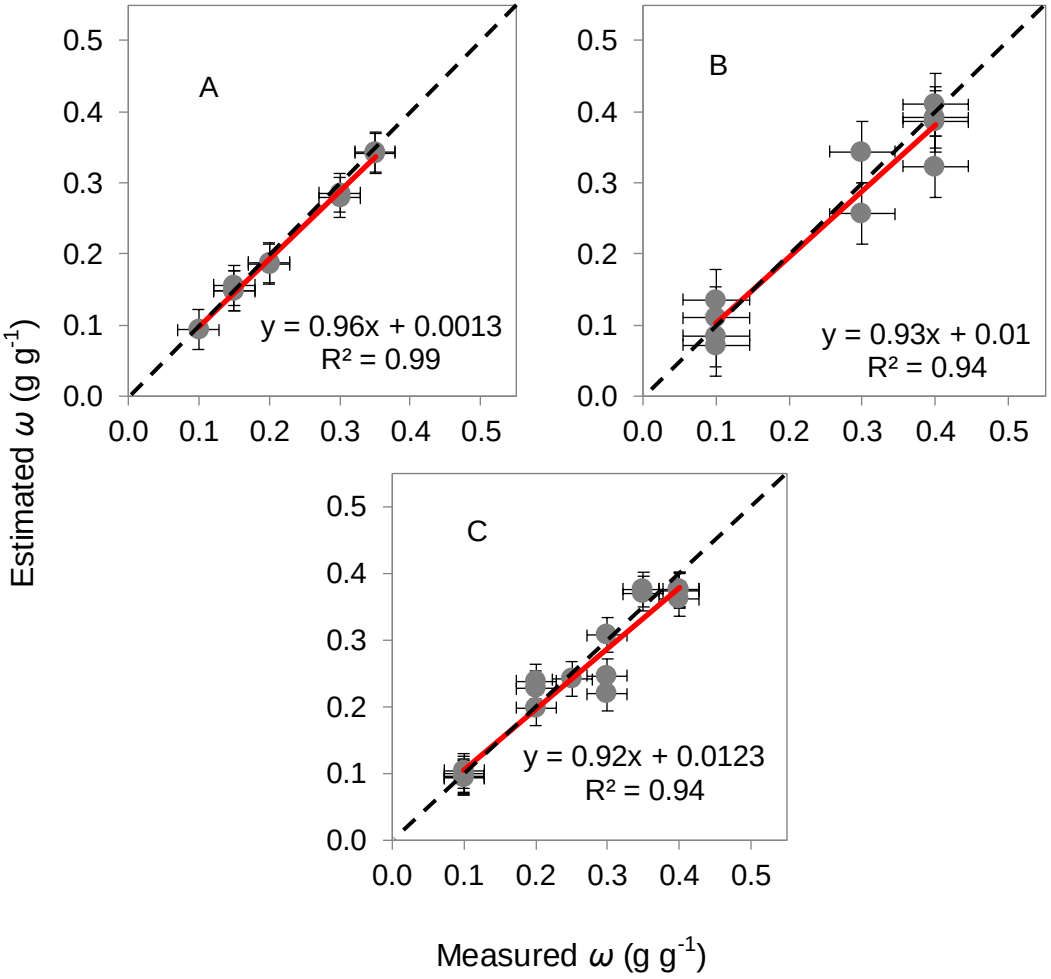

Figure 4-14 Scatter plots of core sampling measured versus artificial neural networks (ANN) predicted soil gravimetric moisture content (ω) using the prototype combined sensor from laboratory measurements in sandy loam soils (A), clay loam soils (B) and the collective sample (C) models. Dashed line = 1:1 line; bold red line = line of best fit; ⊢⊣ = error bars.

- **Estimation of bulk density under laboratory conditions**

The results of BD prediction show good accuracy for the sandy loam texture with R^2, RMSEp and RPD values of 0.92, 0.031 g cm^{-3} and 5.88, respectively, compared to the clay loam texture (Table 4-11), where the prediction of BD was relatively lower. Quraishi (2013) reported a similar but rather better result for BD

prediction using a prototype BD sensor under laboratory conditions for a sandy loam (RMSEp = 0.02 g cm^{-3}) and clay (RMSEp = 0.04 g cm^{-3}) textures, respectively. Both the current work and that of Quraishi (2013) show that BD is better estimated with lower CC soils.

Table 4-11 Soil bulk density (BD) prediction results under laboratory conditions of the independent validation sets for sandy loam, clay loam and the collective sample set.

	Sandy loam	Clay loam	Collective
R^2	0.92	0.84	0.83
RMSE, g cm^{-3}	0.031	0.061	0.044
RPD	5.88	2.43	3.66

R^2: coefficient of determination. RMSE: root mean square error of prediction; and, RPD: residual prediction deviation. A RPD value larger than 2.5 indicates an excellent model prediction (Viscara Rossel et al., 2006).

The scatter plots of measured versus predicted BD (Figure 4-15) under laboratory condition show moderate prediction accuracy, although the measurement accuracy of both θv and ω were better. One reason could be the small number of soil samples used for this test.

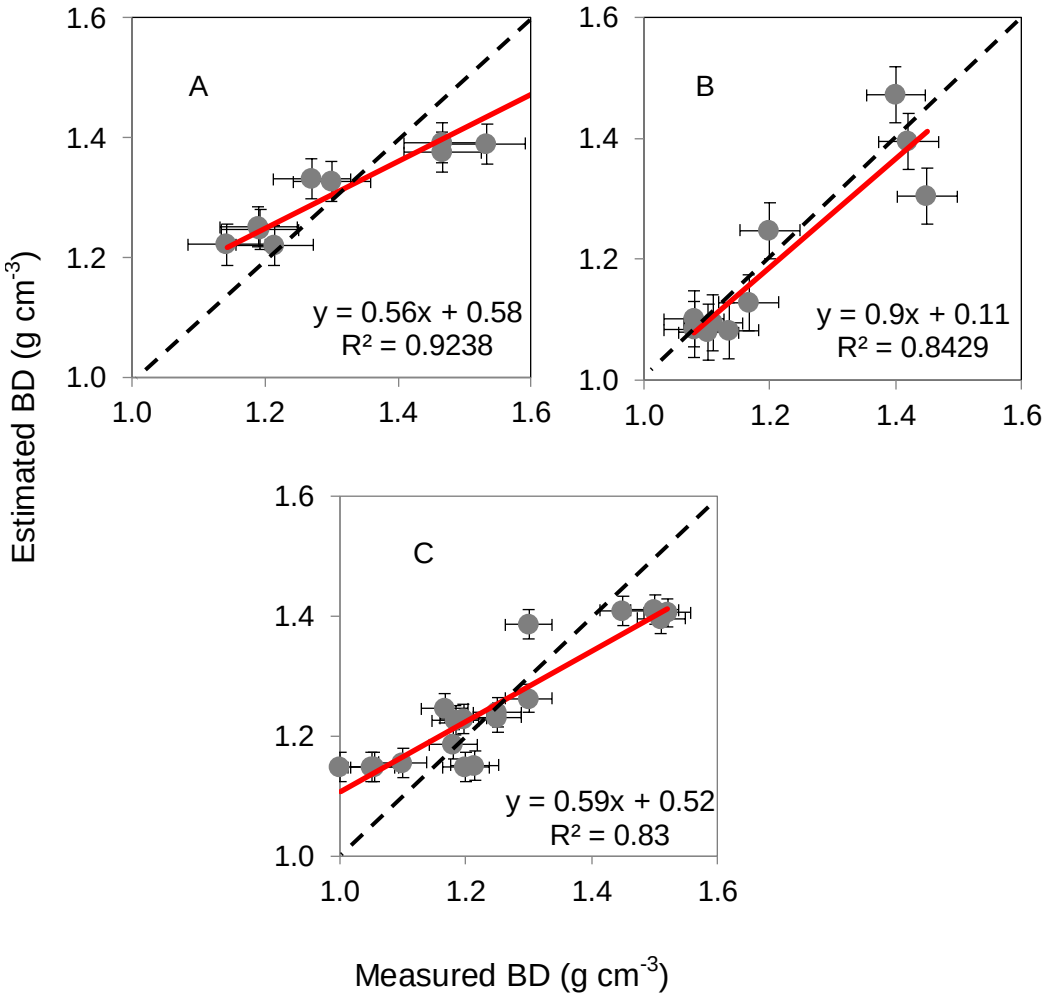

Figure 4-15 Scatter plots of core sampling measured versus predicted soil bulk density (BD) using the prototype combined sensor under laboratory testing conditions for sandy loam soil (A), clay loam (B) and the collective sample set (C). Dashed line = 1:1 line; bold red line = line of best fit; ⊢⊣ = error bars.

5.6.2. *In-situ* test of the prototype combined probe

Appendix 16 shows the results of the ANN calibration models using soil samples collected from arable and grassland fields, using V and spectra data only, which were obtained from the dielectric and vis-NIRS sensors, respectively. A total of 170 neurons were used as the input layer, divided into 169 neurons of vis-NIR spectra and one neuron of V. All of the calibration models generated performed well as indicated by the R^2 values for each

training and validation data set, and for both arable and grassland soils. However, the collective calibration model performance is relatively lower than those of the individual land use models.

- **Dielectric sensor performance under field conditions**

The relation between the dielectric sensor V and θv in this study was somewhat weaker when the measurements were taken in the arable fields rather than grassland soils. However, this is likely to be due to the heterogeneous nature of topsoil layer of arable soils. While the R^2, RMSEp, and RPD values for arable soils may be lower than grassland soils, but they are both considered to be within the excellent prediction level (Table 4-10), with values of R^2, RMSE and RPD are 0.97, 0.024 cm^3 cm^{-3} and 5.80, 1.00, 0.005 cm^3 cm^{-3} and 13.72, 0.94, 0.039 cm^3 cm^{-3} and 3.67 for arable, grassland soils and the collective scenarios, respectively. Similarly, Figure 4-12 the slope and x intercept of the scatter plots show grassland is in advance of other two models.

The prediction accuracy of θv using the assembled dielectric probe on the prototype combined system may be lower than controlled laboratory experiments (Table 4-12), however, the field measurements may better reflect the ability of the prototype to measure under real-world conditions. The same conclusion emerged to Kaleita et al., (2005) who calibrated a dielectric sensor for laboratory and field use and obtained R^2 values of 0.87 and 0.77, respectively. The results of this work, was more accurate than those reported by Andrade-Sanchez et al. (2001), who developed and tested a dielectric sensor and reported acceptable correlation with θv with (R^2 values of 0.87 and 0.78 under laboratory and field tests, respectively).

Table 4-12 Field results of volumetric moisture content (θv) prediction using the prototype's dielectric sensor in arable, grassland and collective land use soils.

	Arable land	Grassland	Collective
R^2	0.97	1.00	0.94
RMSE, $cm^3\ cm^{-3}$	0.024	0.005	0.039
RPD	5.80	13.72	3.67

R^2: coefficient of determination. RMSE: root mean square error of prediction; and, RPD: residual prediction deviation. A RPD value larger than 2.5 indicates an excellent model prediction (Viscara Rossel et al., 2006).

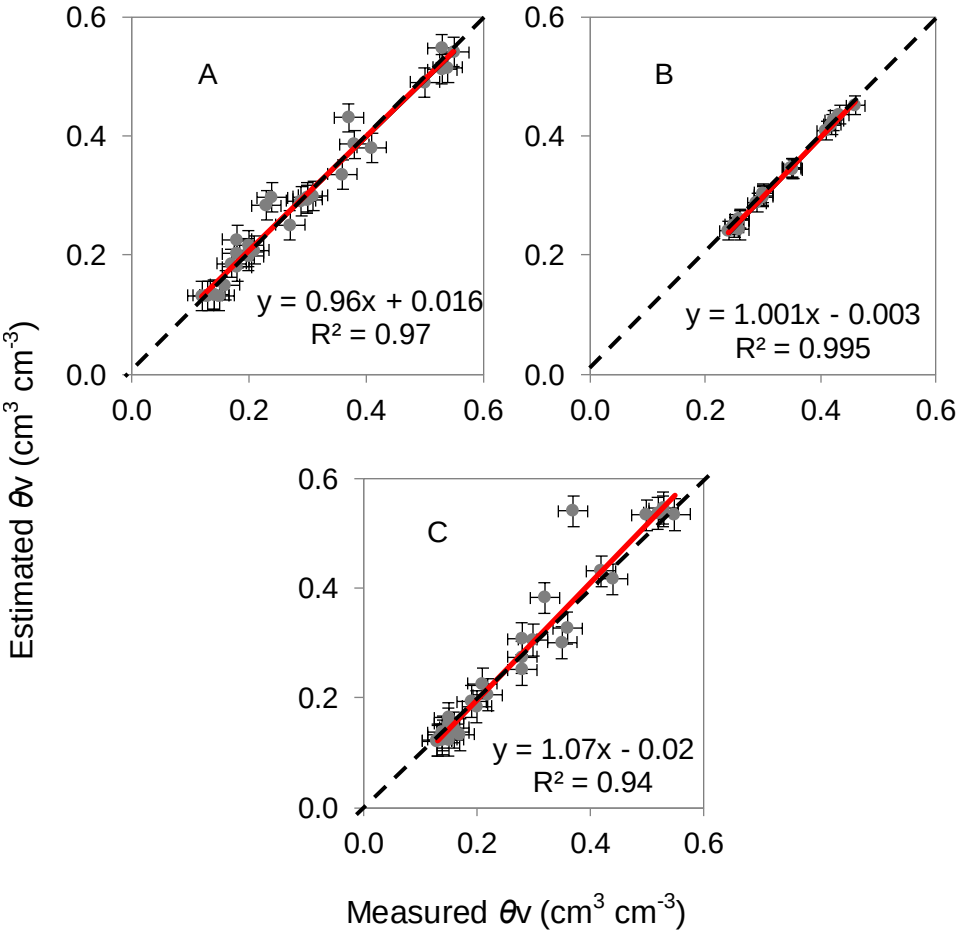

Figure 4-16 Scatter plots of core sampling measured versus artificial neural networks (ANN) predicted soil volumetric moisture content (θv) using the prototype combined senor for field measurements in arable land soils (A), grassland soils (B) and the collective soils (C). Dashed line = 1:1 line; bold red line = line of best fit; ⊢⊣ = error bars.

- **Vis-NIR spectrophotometer performance under field conditions**

Generally, field measurements revealed lower accuracy (Table 4-13) compared to the laboratory measurements (Table 4-10), as expected. The main reason is the variability of soil properties under field conditions, including texture, OM and presence of gravels, which may raise the need for calibration models derived from soils with less diverse properties if precise accuracy is demanded, for example, generate a calibration model for each specific field. Values of R^2, RMSE and RPD for the prediction of ω using the vis-NIR spectrophotometry are 0.97, 1.9 g g^{-1} and 5.46, and 0.96, 1.1 g g^{-1} and 4.73, for arable and grassland soils, respectively, and 0.96, 2.3 g g^{-1} and 4.56 for the collective model, respectively, which are of similar magnitude to those obtained by Mouazen at al. (2006b) and closer to those reported by Quraishi and Mouazen (2013b), who found 0.94, 2.6 g g^{-1} and 4.03 values, respectively. This is despite the fact that spectra data collected from multiple fields would be less accurate, Table 4-13 shows excellent accuracy of prediction ω, with five arable and two grasslands fields, with R^2 and RPD values close if not better than those reported by Quraishi (2013), however, RMSEp values of Quraishi (2013) ranged from 0.32 to 0.60 % from single arable fields with a wide range of textures.

Table 4-13 Field results of gravimetric moisture content (ω) prediction using the prototype's visible and near infrared (vis-NIR) spectrophotometer, in arable, grassland and collective land use soils.

	Arable land	Grassland	Collective
R^2	0.97	0.96	0.96
RMSEp, g g^{-1}	0.019	0.011	0.023
RPD	5.46	4.73	4.56

R^2: coefficient of determination. RMSE: root mean square error of prediction. RPD: residual prediction deviation. RPD values larger than 2.5 indicate an excellent model prediction (Viscara Rossel et al., 2006).

The scatter plots of measured versus predicted ω shown in Figure 4-17 indicate excellent measurement accuracy for the three sampling scenarios.

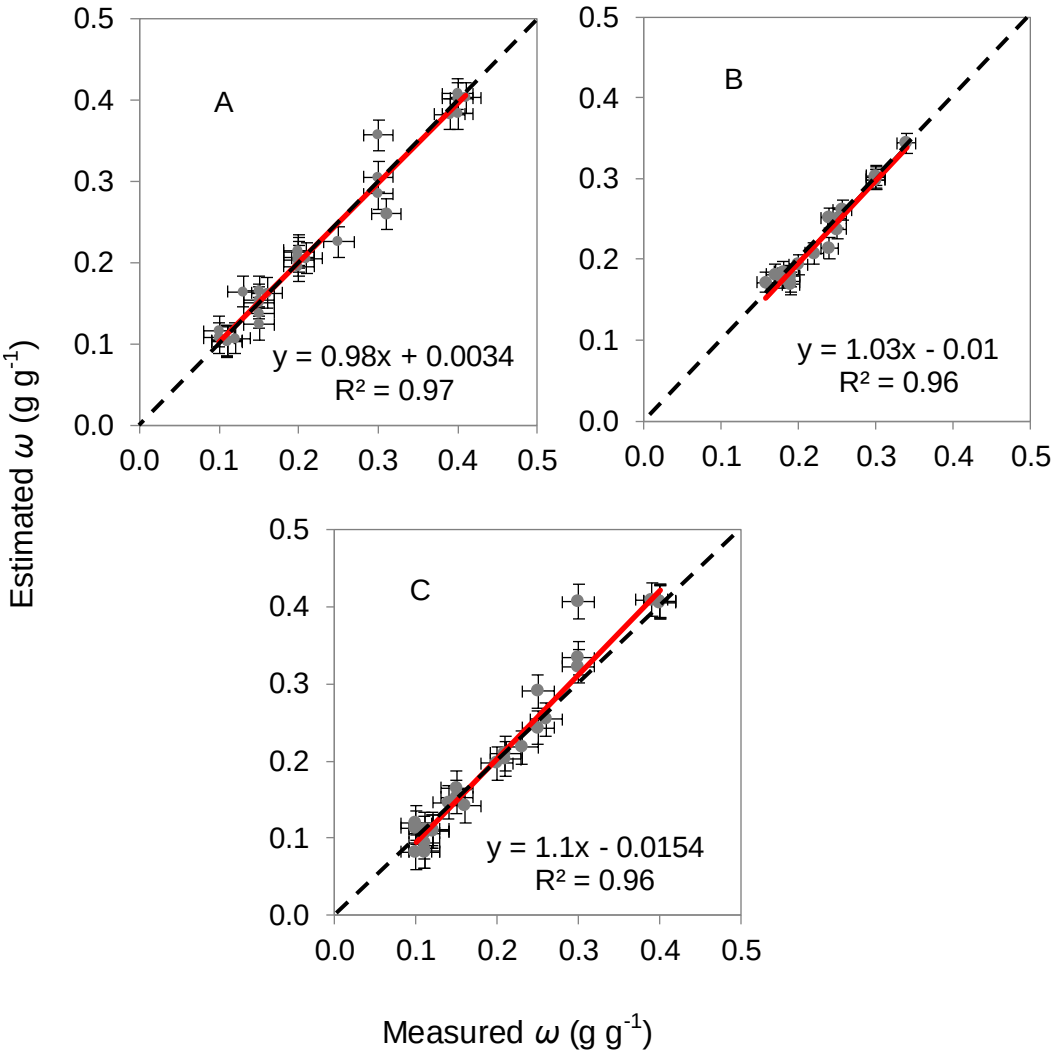

Figure 4-17 Scatter plots of core sampling measured versus artificial neural networks (ANN) predicted soil gravimetric moisture content (ω) using the prototype combined senor for field measurements with arable land soils (A), grassland soils (B) and the collective land use samples (C). Dashed line = 1:1 line; bold red line = line of best fit; ⊢⊣ = error bars.

The results of this research were more accurate than that of Christy et al. (2003) who obtained R^2 = 0.82 for ω prediction using a prototype soil reflectance mapping unit equipped with a NIR spectrophotometer, in a single field in central Iowa, USA. Also, the results of the collective model presented in Table 4-11 for R^2 = 0.96 and RMSEp = 2.3 %, are better from those reported by Christy et al. (2008), who obtained R^2 = 0.40 and RMSEp = 3.6 %, for the ω

prediction with an on-line measuring system. However, it is worth noting that results of Christy et al. (2008) were reported for on-line measurement in contrary to that of the current work.

- **Estimation of bulk density under field conditions**

The prediction of BD in the arable land revealed rather lower accuracy results with values of R^2 = 0.34 and RMSEp = 0.104 g cm^{-3} (Table 4-14) compared to R^2 = 0.94 and RMSEp = 0.04 g cm^{-3} reported by Quraishi and Mouazen (2013b), who used a prototype measuring system that combined a vis-NIRS sensor and penetrometer for the measurement of soil BD. The grassland results show better accuracy of soil BD prediction in comparison with the measurements from arable land, with the validation R^2, RMSEp (%) and RPD values of 0.47, 7.7 g cm^{-3} and 1.36, respectively.

The collective model for predicting soil BD in situ revealed encouraging results of R^2 = 0.52 and RMSEp = 0.102 g cm^{-3} and they are in line with those reported by Kweon et al. (2008), who measured BD with the use of vis-NIR and insertion force measurements in six fields in Kansas, USA. Their cross-validation R^2 values ranged from 0.21 to 0.78 and RMSE values ranged from 0.07 to 0.13 g cm^{-3}.

Table 4-14 Field results of bulk density (BD) prediction using the prototype combined sensor tested in arable, grassland and collective soils.

	Arable land	Grassland	Collective
R^2	0.34	0.47	0.52
RMSEp	0.104	0.077	0.102
RPD	1.08	1.36	1.21

R^2: coefficient of determination; RMSE: root mean square error of prediction; and, RPD: residual prediction deviation. A RPD value larger than 2.5 indicates an excellent model prediction (Viscara Rossel et al., 2006).

Comparing the scatter plots revealed that BD points are closer to the 1:1 line for grassland soils (Figure 4-18B), while BD points from arable soils seem to be

more scattered (Figure 4-18A). The smaller intercept of 0.2 g cm^{-3} and the better slope of 0.84 of the collective sample model (Figure 4-18C), as compared to the other two models indicate a better estimation performance, suggesting the use of large number of soil samples collected from arable and grassland soils has improved the prediction accuracy of BD.

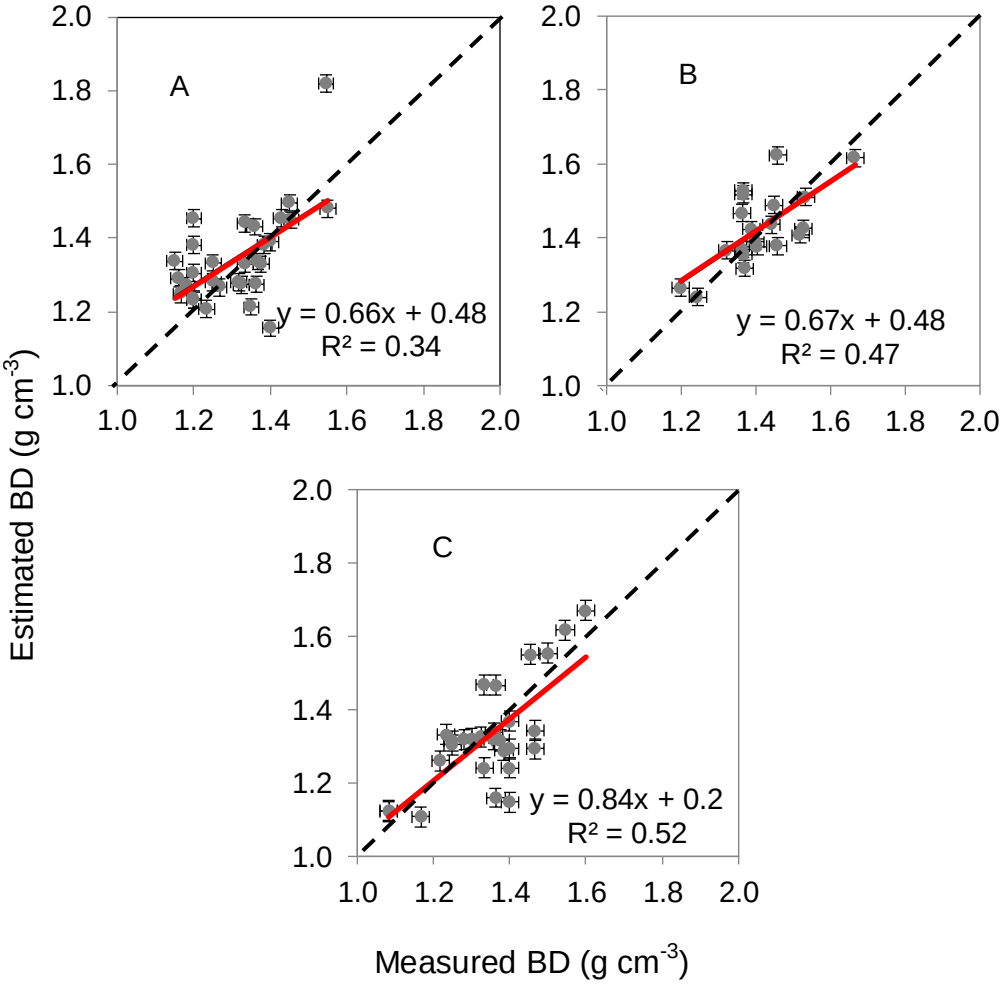

Figure 4-18 Scatter plots of core sampling measured versus artificial neural networks (ANN) predicted soil bulk density (BD) using the prototype combined sensor with arable land soils (A), grassland soils (B) and the collective land use samples (C). Dashed line = 1:1 line; bold red line = line of best fit; ⊢⊣ = error bars.

- **Estimation of soil bulk density for individual fields**

The accuracy of the prototype measuring system during the field measurements shows higher accuracy of soil BD estimation for any individual field tested in this experiment, this effect is expected and in line with other research groups results of using vis-NIRS to predict soil properties. Table 4-15 shows the RMSEp results of the experiment was conducted in five fields and two pastures, which clearly shows that the measurement of any single field operation came with high accuracy and short range of variation between RMSEp values for all fields tested, ranging RMSEp values to estimate soil BD between 0.009 and 0.032 g cm^{-3}, the results of this work is in line with the findings of Quraishi 2014 who reported better prediction accuracy of soil BD for an individual fields comparing to the collective model. The RMSEp results of the field experiment for individual fields are classified excellent to estimate soil BD using the prototype measuring system under field conditions.

Table 4-15 Field results of RMSEp of the prototype measuring system to predict soil BD of five arable fields and two grasslands as an individual analysis.

Field	Land use	Sample number		RMSEp g cm^{-3}
		Model	Test	
Avenue	Arable land	180	20	0.027
Showground				0.017
Orchard				0.032
Clover Hill				0.008
Beechwood				0.021
Avenue	Grassland	150	50	0.006
Olney				0.028

Literature shows no similar studies about the assessment of BD, as a function of θv and ω measured with a dielectric probe and vis-NIR spectrophotometer, respectively. Therefore, the prototype combined system introduced in the current study proves to be unique in the assessment of BD, and also the prediction of other soil properties that are important for land management.

However, further development is needed so as to improve the estimation performance obtained so far. This might concern improvement in the technical specification or calibration procedure followed in the current work.

4.7. Estimation of the potential error of soil BD predicted using Eqn. 3-7

From the literature review, it was observed that the range of RMSEp values of each θv and ω measured by the dielectric constant and vis-NIRS techniques vary as shown in Table 4-16.

Table 4-16 Summery of RMSEp values of θv and ω predictions using the dielectric constant and visible and near infrared (vis-NIRS) techniques.

	θv		ω	
	Researchers	RMSEp*	Researchers	RMSEp**
1	Rowlandson et al. (2013)	0.034	Christy et al. (2003)	0.030
2	Sheng et al., (2011)	0.030	Mouazen and Ramon (2006)	0.024
3			Christy (2008)	0.028
4			Quraishi and Mouazen (2013c)	0.026
	Average	0.032	Average	0.027

RMSEp* is the root mean square error of prediction of θv ($cm^3\ cm^{-3}$) and RMSEp** is the root mean square error of prediction of ω ($g\ g^{-1}$).

Table 4-17 shows the results of the potential error of estimation of soil BD calculated using RMSEp values of θv and ω estimated by ThetaProbe and ASDi sensors, respectively, for the 1013 soil samples tested during this study, using different calibration methods, compared with potential error of BD prediction using other researchers findings of θv and ω RMSEp values (Table 4-15).

Table 4-17 the results of potential error of soil BD estimation, showing a comparison between published RMSE values and RMSEp values of the current study obtained with different calibration methods of ThetaProbe and ASDi sensors.

	θv RMSEp $cm^3\ cm^{-3}$	ω RMSEp $g\ g^{-1}$	calibration method	BD potential error*
literature values	0.032	0.027	-	1.185
Current study values	0.026	0.027	PLSR and SSC	0.963
	0.015	0.014	ANN	1.071

RMSEp is the root mean square error of prediction; PLSR is partial least squares regression; ANN is artificial neural networks; * : the BD potential error does not have unites since it derived from Eqn. 1-9, which expresses the error ratio for both sensors.

The results of error of soil BD estimation, calculated by Eqn. 3-7, indicating smaller error values of current study of 0.963 and 1.071 obtained with PLSR and SCC and ANN, respectively, compared with the average error value of 1.185 reported in the literature, calculated from the average values of RMSE of θv and ω prediction of other researchers publications. These positive results have proved the quality of the current work and encouraged further tests to understand more the factors affecting the accuracy of the BD measurements using the dielectric and vis-NIRS sensors as a combined measuring system.

4.8. Mapping of soil bulk density, gravimetric and volumetric moisture content on selected arable and grassland soils using the new prototype portable measuring system

Comparison maps of reference and predicted θv, ω and BD were generated for Avenue field, Silsoe, as an example of field testing of the prototype. This field is or two plots, with one used for arable crops and the other used for grassland crops. A total of 40 points were measured using the prototype combined probe,

from which 20 points were selected to collect core samples using the undisturbed soil sample collecting cylinder (Figure 3-2). These 20 cores were used to validate the prototype measurement. Three types of mapping product were developed for θv, ω and BD, namely, comparison maps, full-point maps and error maps. Figure 4-19 shows the layout of Avenue field used to derive the full-point maps based on 40 readings and the comparison maps based on 20 points. The error maps developed are based on the absolute error between the predicted and measured of the 20 points.

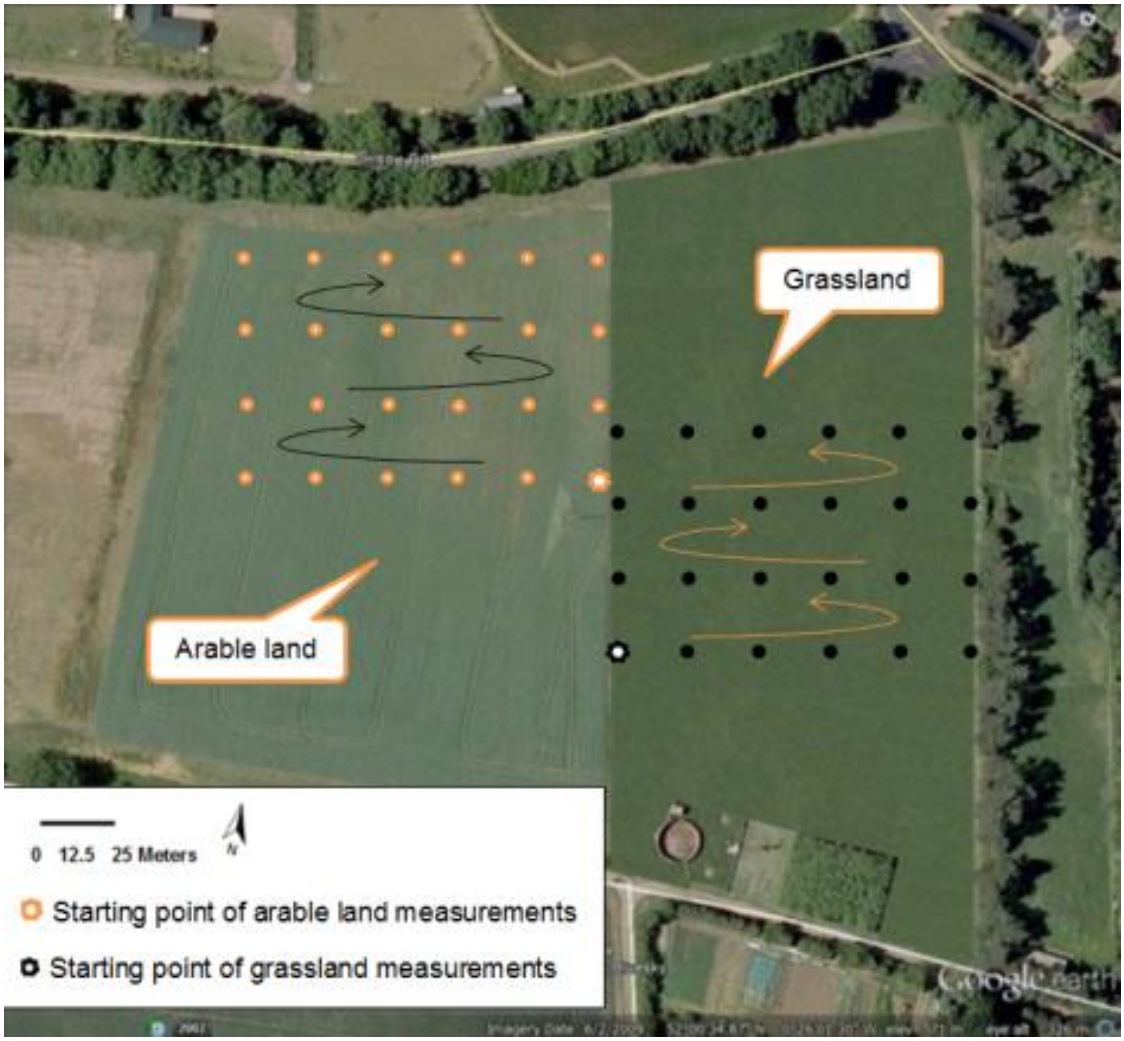

Figure 4-19 Sampling layout of samples collected in Avenue arable field and grassland with the prototype combined probe.

Figure 4-20 compares the spatial distributions of the measured θv by core sampling and predicted θv by the dielectric sensor of the prototype, for arable land (Figure 4-20 A and B, respectively) and grassland (Figure 4-20 C and D, respectively) plots of the field. The full-points maps are shown in Figure (4-20 E and F). Figures show that the dielectric sensor is capable of mapping wide ranges of variability of θv throughout the field with high accuracy, as shown by the pattern of predicted θv (Figures 4-20B and 4-20D) which mirrors that of the core sampled map (Figures 4-20A and 4-20C), with a similar θv range from 0.12 to 0.46 cm^3 cm^{-3} The full-points maps of arable plot (Figure 4-20 E) and grassland plot (Figure 4-20 F) show similar spatial distribution of θv comparing to the references maps (Figure 4-20 A and C), particularly in the grassland plot.

Figure 4-21 demonstrates a comparison between measured and predicted ω on arable land (Figure 4-21 A and B, respectively), grassland (Figure 4-21 C and D, respectively) and full-points on arable land and grassland plots (Figure 4-21 E and F, respectively). The similar spatial patterns seen when comparing the measured and predicted ω are attributed to the high prediction accuracy of the NIR spectrophotometer. However, there are slight differences in spatial pattern between measured and predicted ω can be observed (Figure 4-21).The full-points maps of arable (Figure 4-21 E) and grassland plots (Figure 4-21 F) soils show similar spatial patterns of ω to the references maps (Figure 4-21 A and C).

The comparison maps of measured (Figure 4-22 A and C) and predicted BD from the prototype (Figure 4-22 B and D), and full-points maps (Figure 4-22 E and F) developed for arable land and grassland plots, respectively, show a degree of similarity. The spatial similarity in the arable plot (Figure 4-22 A and B) is clearer than that in the grassland plot (Figure 4-22 C and D). In general the new measuring system was able to indicate the major soil BD spatial patterns (Figure 4-22).

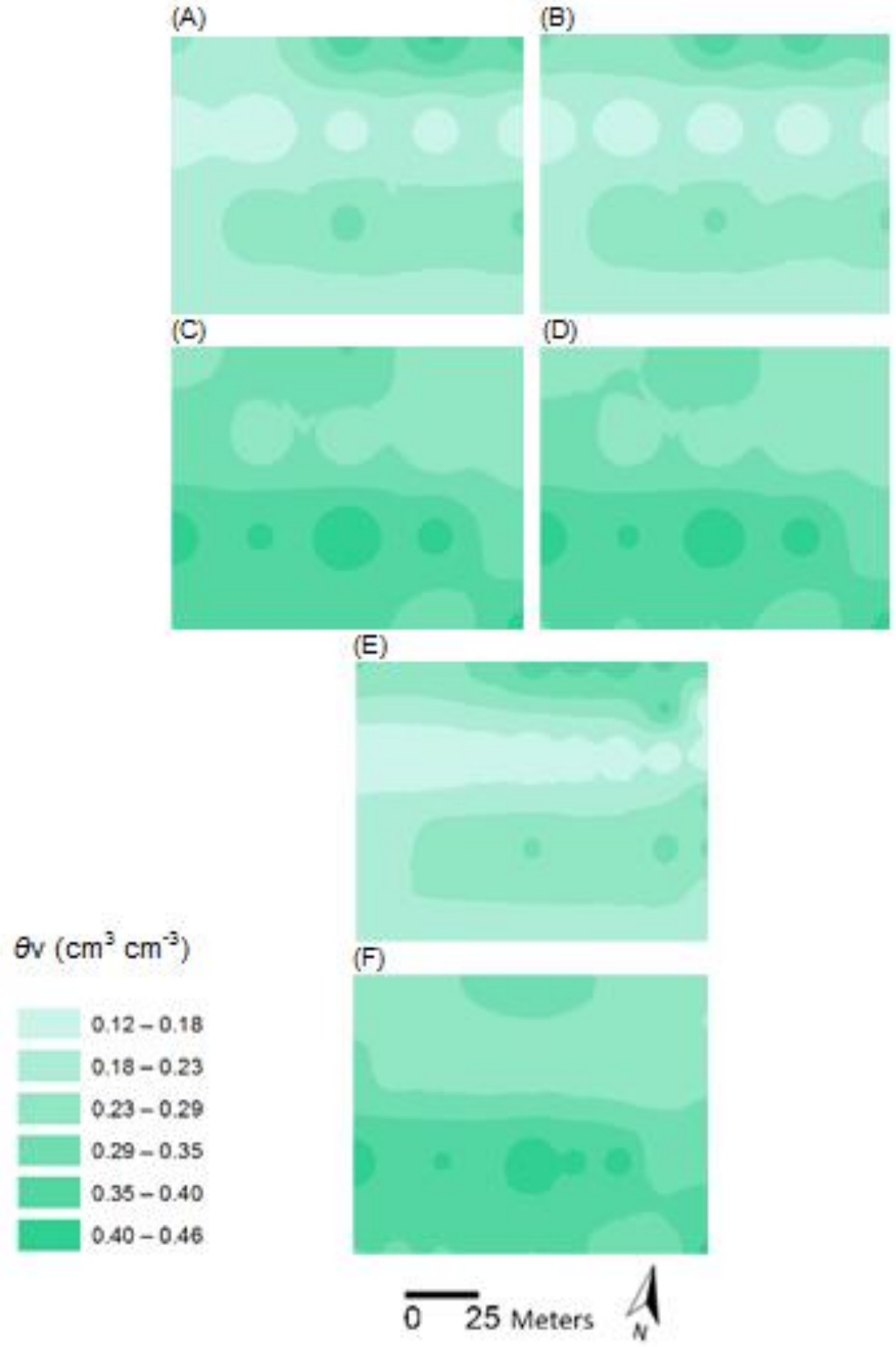

Figure 4-20 Comparison θv maps between measured (A and C) and predicted (B and D), and full-points maps (E and F) using ArcGIS 10.2 (ESRI, USA) software with the readouts of the prototype measuring system in arable and grassland plots, respectively, in Avenue field, Silsoe, UK.

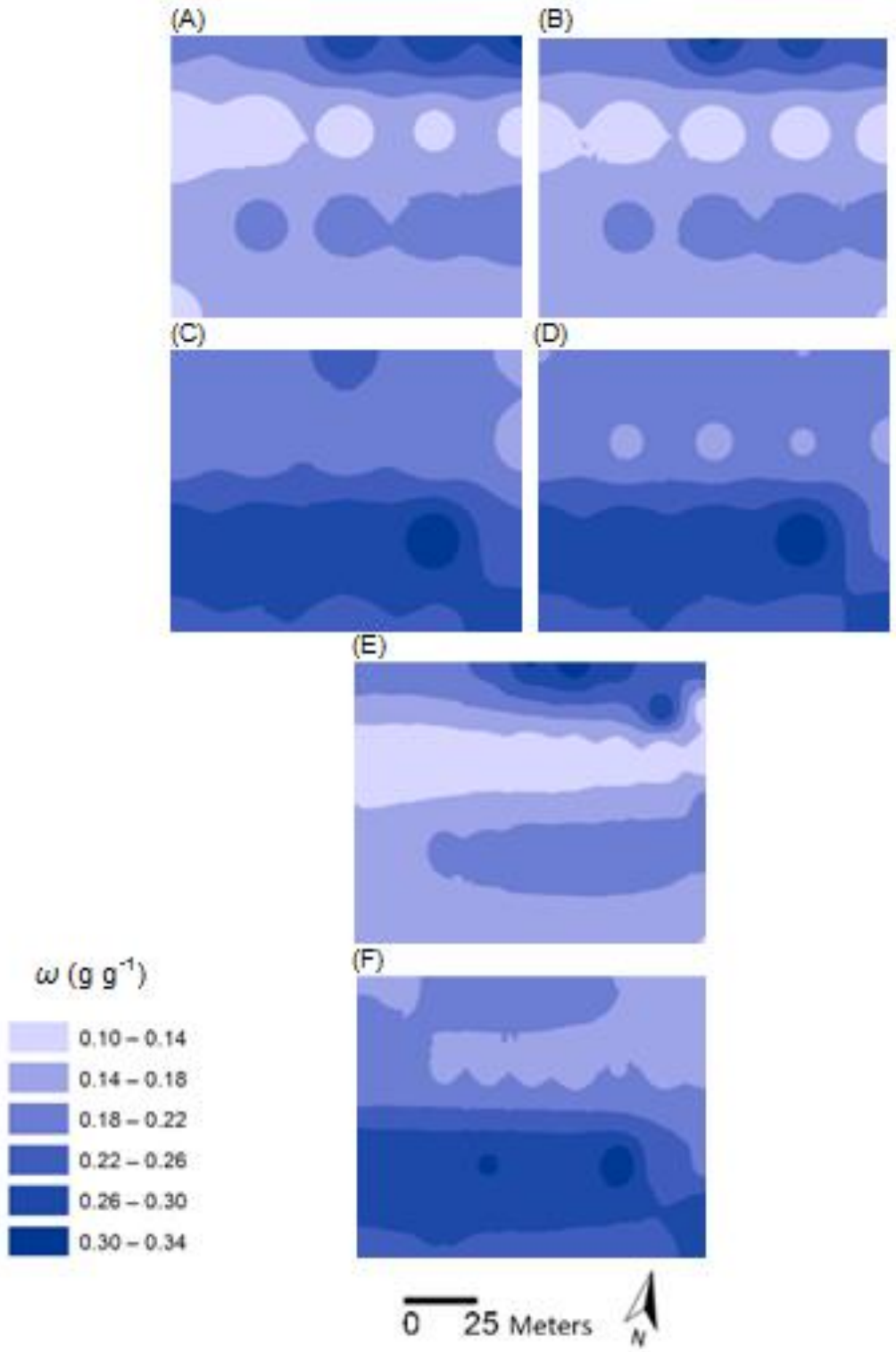

Figure 4-21 Comparison ω maps between measured (A and C) and predicted (B and D), and full-points maps (E and F) using ArcGIS 10.2 (ESRI, USA) software with the readouts of the prototype measuring system for arable and grassland plots, respectively, in Avenue field, Silsoe, UK.

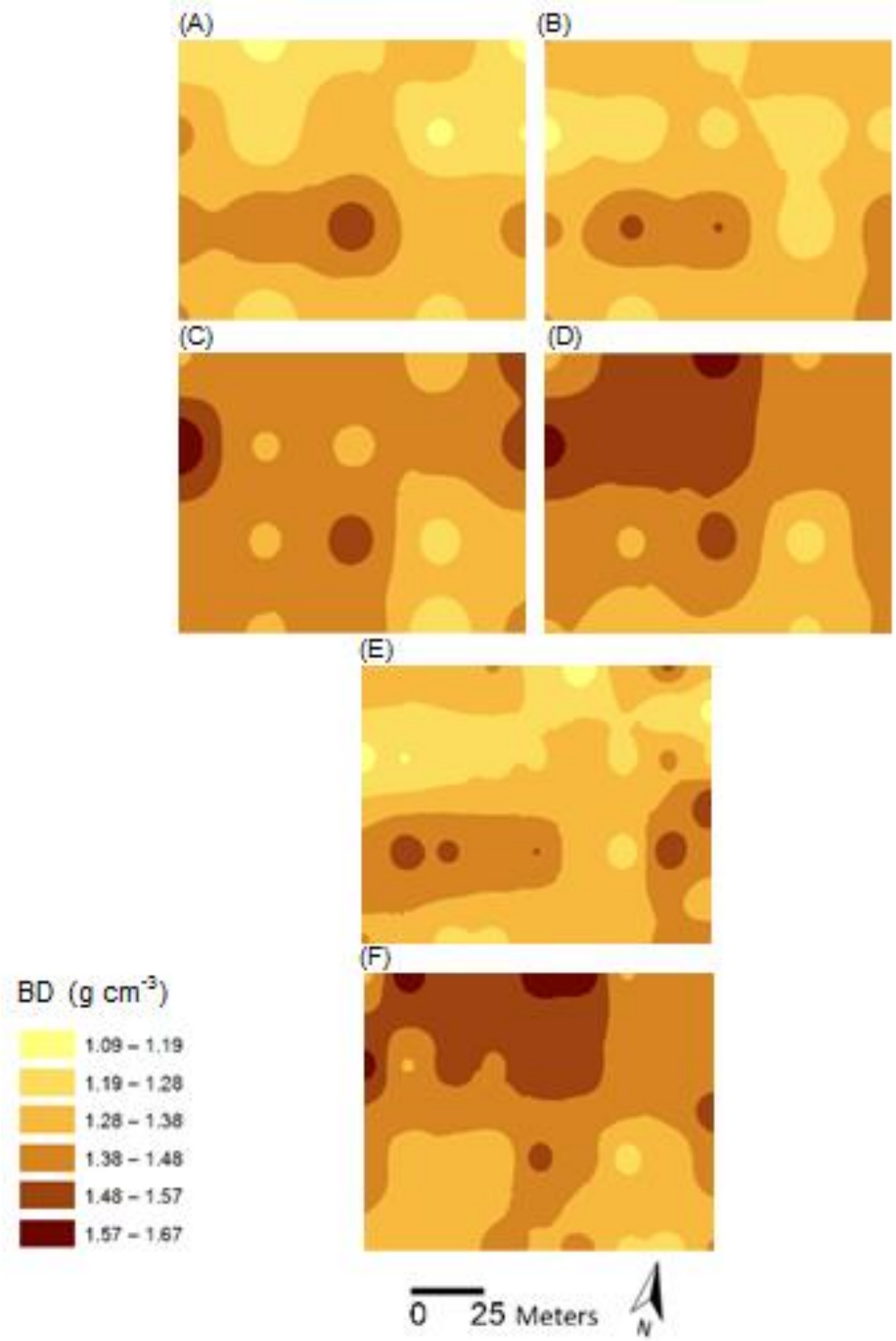

Figure 4-22 Comparison bulk density (BD) maps between measured (A and C) and predicted (B and D) and full-points maps (E and F) using ArcGIS 10.2 (ESRI, USA) software with the readouts of the prototype measuring system for arable land and grassland plots, respectively, in Avenue field, Silsoe, UK.

- **Error analysis**

The error map of θv measurements on arable land plot is shown in Figure 4-23A, which illustrates that the maximum error is encountered in the north west and south west corners of the field, where the dielectric probe over-estimated θv. The north east corner of the field exhibited under-estimation of θv, but to a lesser degree than those areas exhibiting over-estimation. The over-estimation errors correlate with compacted areas in the field. The grassland error map of θv measurements (Figure 4-23B) shows lower error rates compared to the arable land error map. Furthermore, fewer spatial patterns of error are evident in the grassland map, while each colour pattern in both error maps represents the same rate of θv prediction absolute error.

The absolute error histograms of θv in the arable soil (Figure 4-24A) shows that the majority of the errors were between -0.020 and 0.020 cm^3 cm^{-3} and the error distribution shows that the dielectric sensor have skewed towards over-estimation end. The grassland histograms of θv error (Figure 4-24B) show that most of the error of prediction is within a range from -0.004 to 0.005 cm^3 cm^{-3} and under-estimation error was the dominant feature.

The error map of ω measurements in arable land illustrated in Figure (4-25A) shows the maximum negative error (predicted ω > measured ω) in the south west corner and the maximum positive error is observed in the north east corner of the field. The negative errors resulting from over-estimation of ω were considerably more the positive errors. This is shown in the error histograms of the measurements taken in the arable land (Figure 4-26A). The majority of the errors were found between -0.020 and 0.020 g g^{-1}. The grassland error map of θv measurements (Figure 4-26B) shows lower rates, compared to the arable land error map. Furthermore, fewer spatial patterns of error are observed in the grassland map; however, most of errors were positive, with a range between 0.00 and 0.020 g g^{-1}.

BD error maps of arable land and grassland are shown in Figure 4-27 A and B, respectively, where the maximum errors occur at the borders of measured area

of both arable land and grassland, which might be attributed to a systematic error of the NIR spectrophotometer or it could be related to the irregularity of the top soil layer at the field edges. Kuang (2012) reported similar error locations during field mapping using an on-line vis-NIR spectrophotometer (Mouazen et al., 2005b). Figure (4-28A) shows a histogram of BD error, where most of the errors found in the BD map from the arable land are between -0.20 and 0.10 g cm^{-3}. Figure 4-38B shows the grassland error map of BD. Lower rates of error are observed compared to the arable land error map and fewer spatial patterns of error are observed in the grassland map.

Analysis of comparison maps, full-point maps and error maps of BD including normal distribution of error confirms the potential of the prototype sensor to map θv, ω and BD. Although spatial distribution of these properties were possible to map for the top soil layer only, the potential of utilising the sensor to map these soil properties through the soil profile is possible, after technical modification to the dielectric constant sensor to measure θv is undertaken.

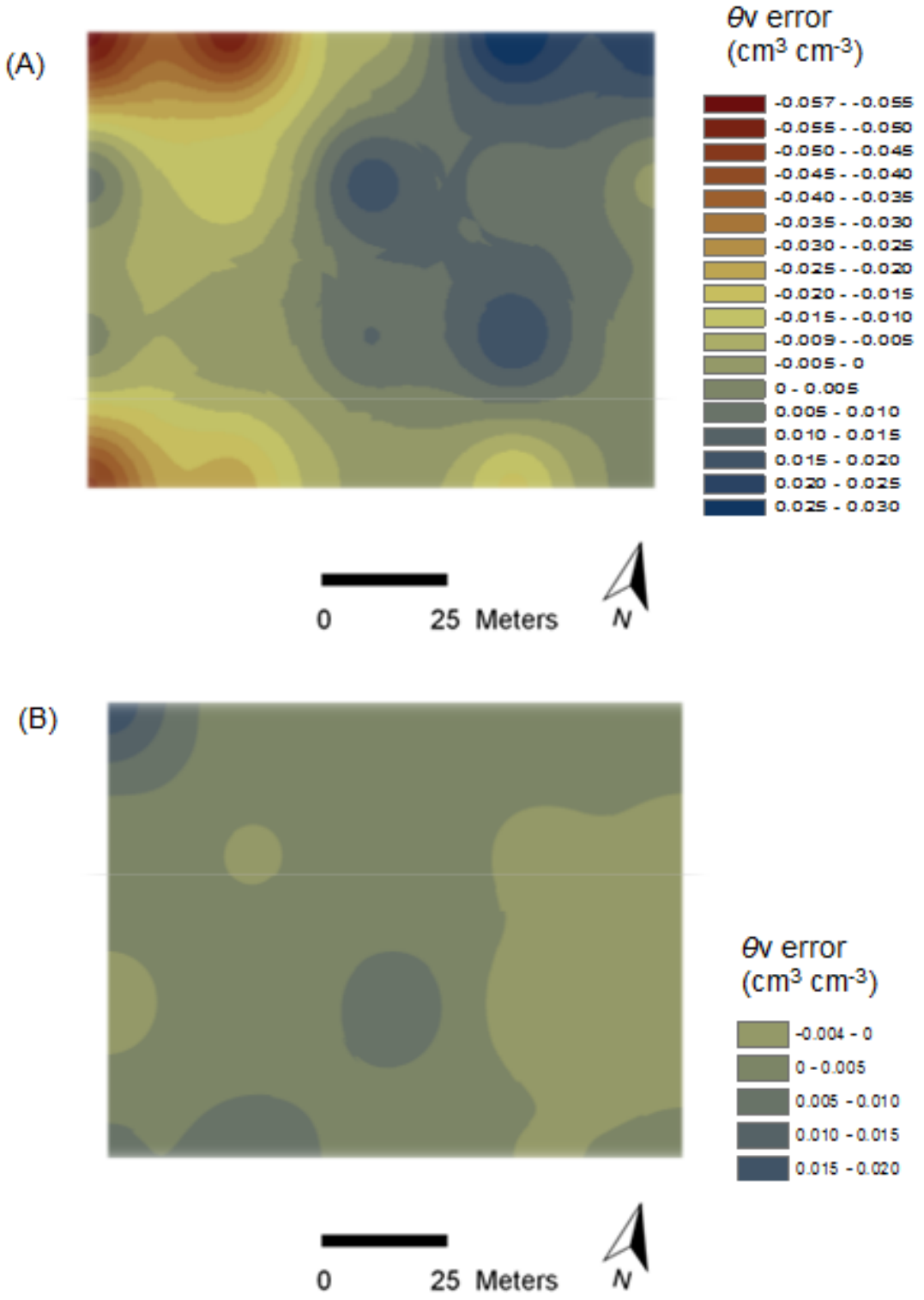

Figure 4-23 Volumetric moisture content (θv) error between oven drying method and predicted using the prototype combined probe, in the arable land (A) and grassland (B) plots, in Avenue field, Silsoe, UK. The error maps were created by using the ArcGIS 10.2 (ESRI, USA) software.

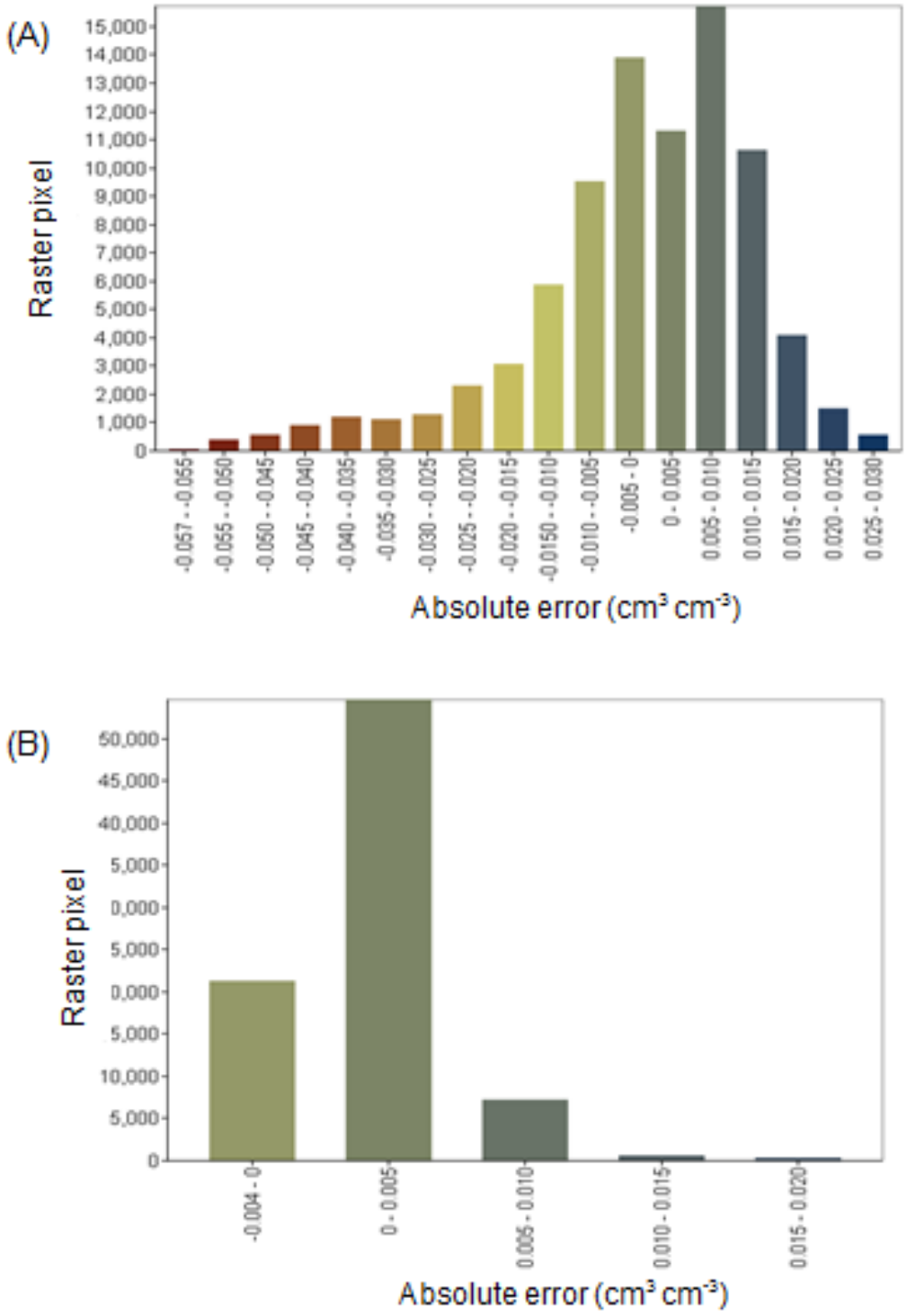

Figure 4-24 Volumetric moisture content (θv) error between oven drying method and predicted using the prototype combined probe, in the arable land (A) and grassland (B) plots, in Avenue field, Silsoe, UK. The error histograms were created by using the ArcGIS 10.2 (ESRI, USA) software.

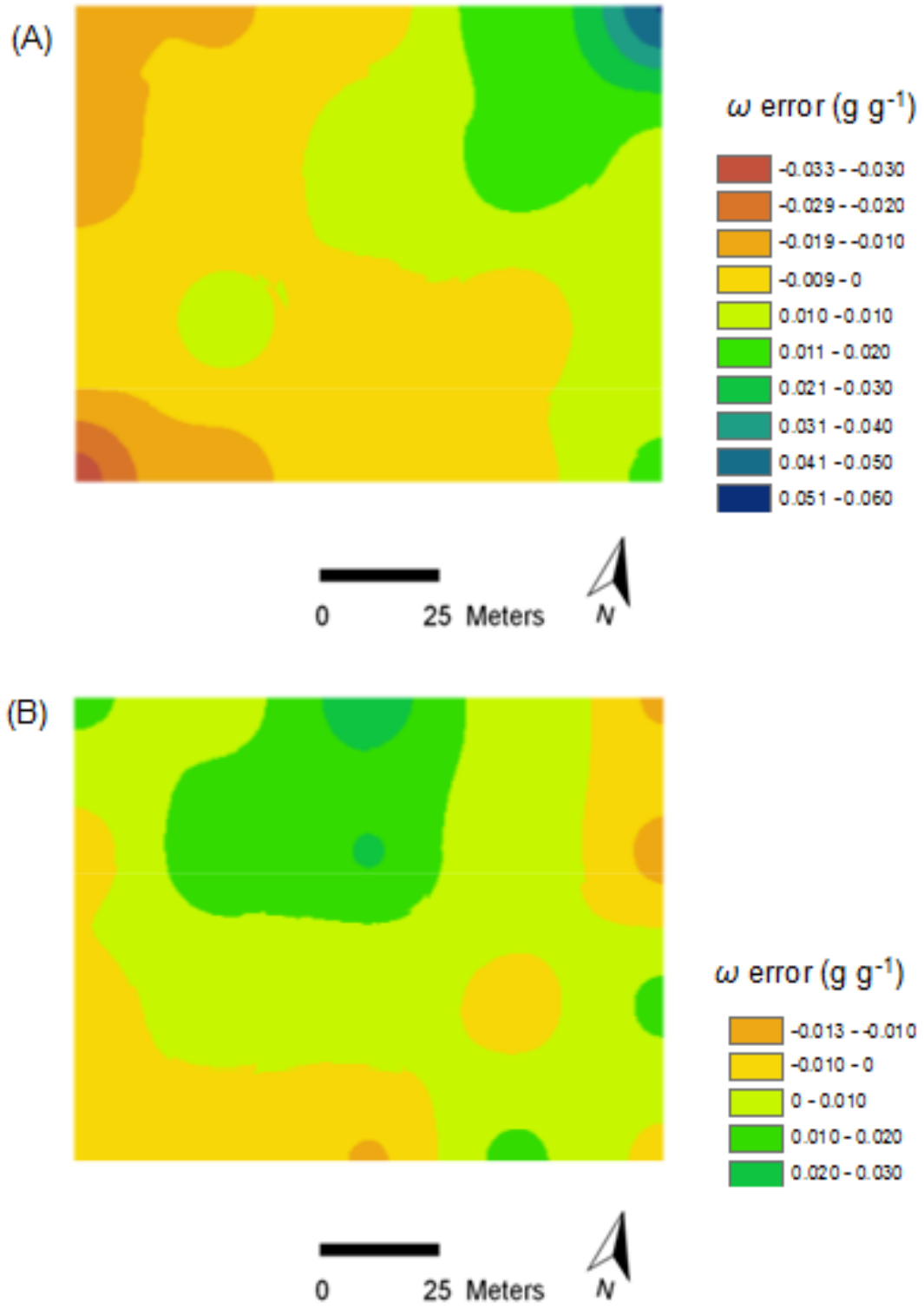

Figure 4-25 Gravimetric moisture content (ω) error between oven drying method and predicted using the prototype combined probe, in the arable land (A) and grassland (B) plots, in Avenue field, Silsoe, UK. The error maps were created by using the ArcGIS 10.2 (ESRI, USA) software.

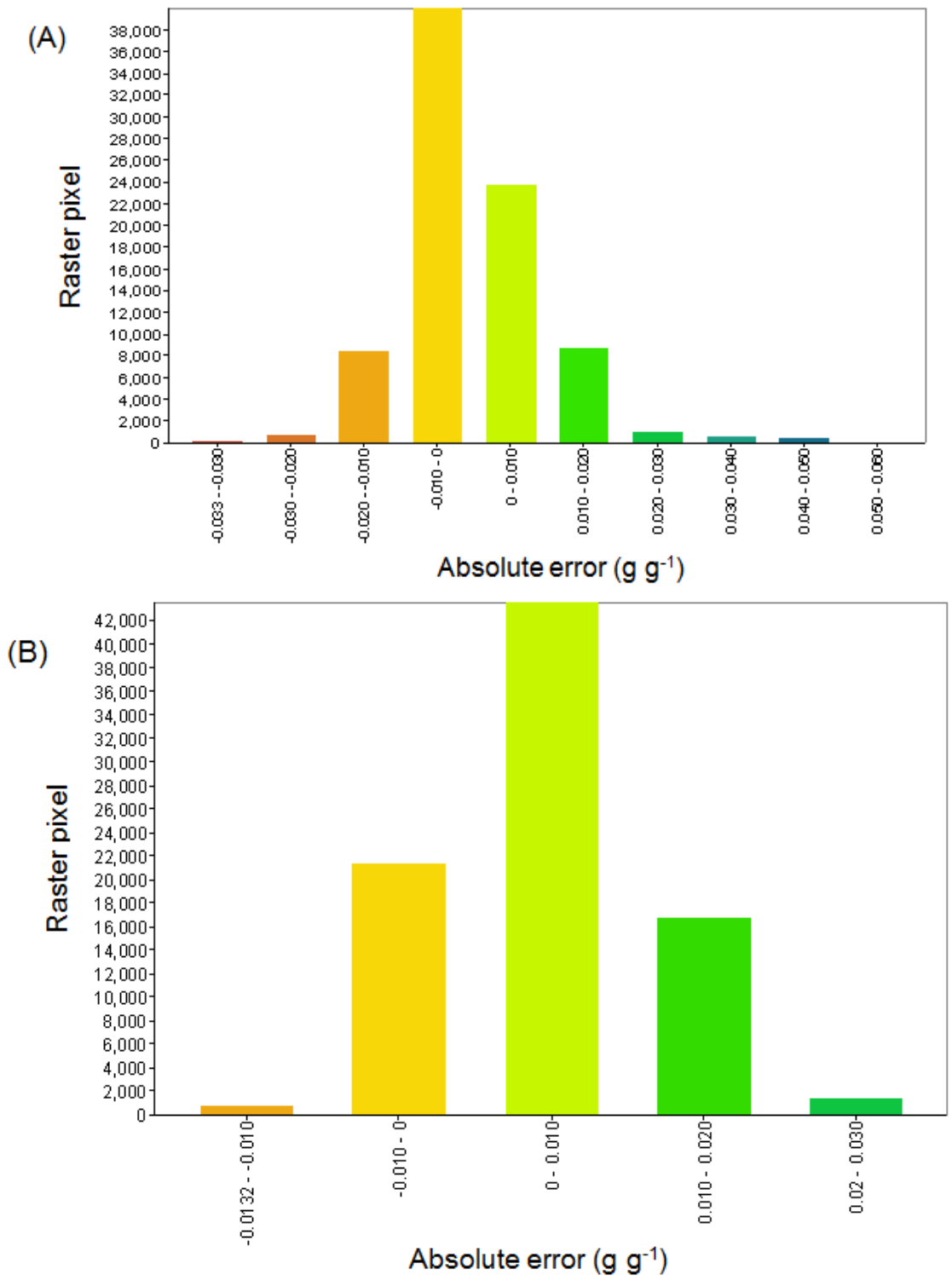

Figure 4-26 Absolute error between measured and predicted gravimetric moisture content (ω) using the prototype combined probe for arable land (A) and grassland (B) plots in Avenue field, Silsoe, UK. The error histograms were created by using the ArcGIS 10.2 (ESRI, USA) software.

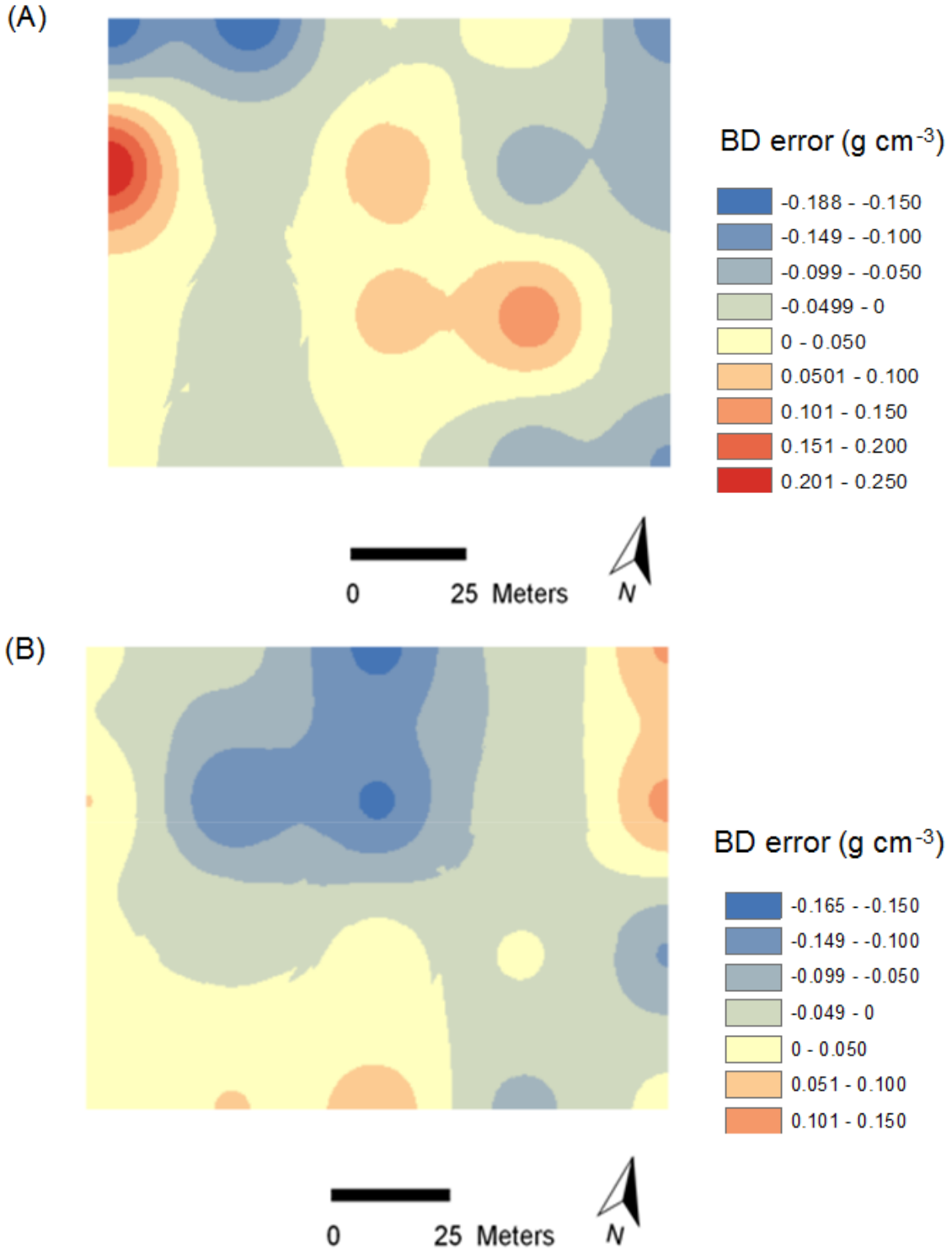

Figure 4-27 Soil bulk density (BD) error between core sampling and predicted using the prototype combined probe, in the arable land (A) and grassland (B) plots, in Avenue field, Silsoe, UK. The error maps were created by using the ArcGIS 10.2 (ESRI, USA) software.

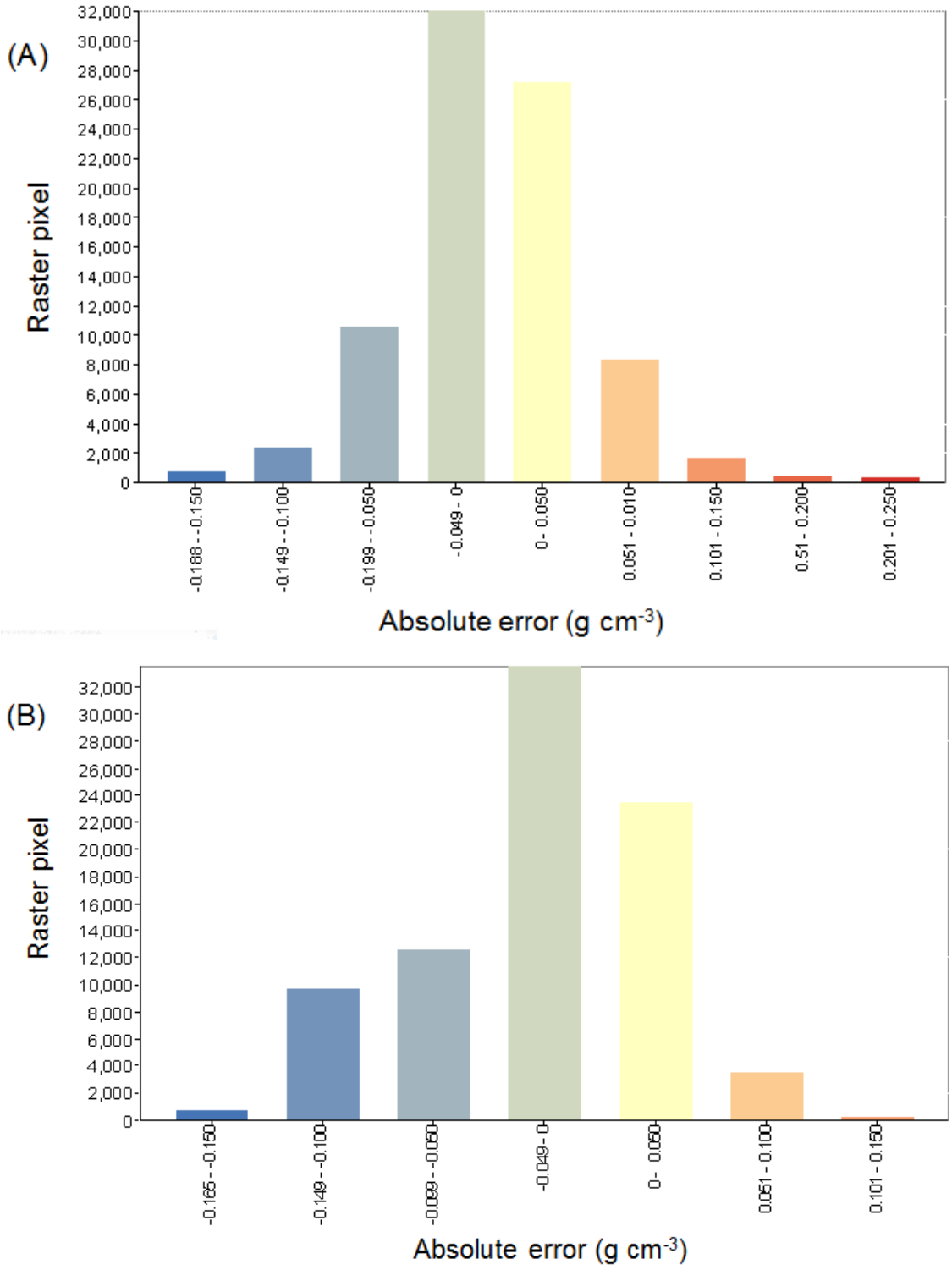

Figure 4-28 Absolute error between core sampling and predicted using the prototype combined probe, in the arable land (A) and grassland (B) plots, in Avenue field, Silsoe, UK. The error histograms were created by using the ArcGIS 10.2 (ESRI, USA) software.

Chapter 5

5. Discussion

Modern agricultural production of crops and animals is often linked to negative impacts on soil and the environment. Large volumes of data are required for successful land management particularly where precision farming is used. The only realistic way to obtain this valuable data for soil or plants is with the use of sensors (Dworak et al., 2010). A characteristic of the current agricultural era is increased soil BD due to intensive agricultural operations. Soil BD is known to be the one of the key soil physical properties alongside soil structure, aeration and compaction (Lal, 2006). Soil compaction can be measured by both direct methods, namely, soil BD and PR; and indirect methods that depend on air and water movements in the soil. Although there have been many attempts by researchers to provide a measurement system for soil compaction, only limited success was reported for portable, simple and fast sensing systems. The main criterion for evaluating these systems is the measurement accuracy. However, different accuracy levels can be achieved using the prototype measuring system with implementing lower cost and shorter spectrum detector for different end-users requirements.

This chapter is about discussing how valuable of the findings of the current study in the context of other studies, identifying where the strengths and weaknesses lie with the techniques developed for measuring soil BD and attempt to recognise where research work is still required to create a robust, repeatable and operational system of measurement appropriate to land managers. The new measuring system developed and evaluated in this thesis consists of the dielectric constant and vis-NIRS sensors. Chapter 4 presented the experimental results, demonstrated the systems' ability to provide accurate readings, evaluated under various soil conditions and different calibration techniques and provided a brief discussion of the experimental results with details of the factors that affect the measurement accuracy. Thus, this chapter focuses on providing relevant scientific reasoning, wherever appropriate, to

explain the effect of different factors on the measurement accuracy. It also discusses the prototyping of the measuring system, with its new combined probe using both sensing techniques, including its design, manufacture, and laboratory and field testing, and the situations where it can be used and its commercially availability. The discussion, therefore, will be divided into four main topics, namely:

1. Prediction accuracy comparison between the results of the new measuring system and the established measuring systems of soil compaction. This will include the influences of modelling method, moisture, texture and land use. Discussion will separately tackle θv, ω and BD.
2. The new combined probe sensing technique design, manufacture and laboratory and field validation.
3. Advantages and practical challenges associated with the use of the new system.
4. The implementation and commercialisation of the new measuring system.

5.1. Prediction accuracy comparison

The new measuring system has been tested under laboratory and field conditions. The impact of four factors namely, modelling, soil moisture level, soil texture and land use, were evaluated on the measurement accuracy of soil θv, ω and BD using the new system. The results revealed that the accuracy of each single sensor may often be low compared to data fusion of multiple sensors, due to the fact that soil sensors are sensitive to more than one soil property of interest. In these instances, data fusion is the key to overcoming the shortcomings of a single sensor and useful and integrated information can be extracted from multiple sensors (Mahmood et al., 2012).

5.1.1. Modelling effect

In this study, the M method revealed an over-estimation for a group of soil samples across a full range of moisture contents, similar findings observed by

Robinson et al. (1999) and Kaleita et al. (2005). Both research groups indicated that the accuracy of the ThetaProbe declined with moisture content (Table 4-1and Figure 4-1A). Cosh et al. (2005) compared the performance of the M and SSC methods using 180 samples collected from arable and grassland sites with a wide range of soil textures. They reported a smaller RMSEp value with SSC (0.040 cm^3 cm^{-3}), as compared to M (0.053 cm^3 cm^{-3}). This RMSEp range is larger overall than that obtained in the current study, although we accounted for different textures, OM and land use (Table 4-1). Eqn. 4-1 is based on wide variations in soil type, moisture content, OM and land use (Table 3-1) of the UK soils. Therefore, it is an improved regression equation as compared, to that reported by Kaleita et al. (2005), who attempted to relate θv with K, using a smaller number of 100 samples only. Their regression models resulted in R^2 values of 0.85 and 0.77 for the laboratory and *in-situ* experiments, respectively. The GF regression equation (Eqn. 3-6) of Topp et al. (1980) based on soil samples collected from all over the world, provided an adequate estimation of θv in the range <0.5 cm^3 cm^{-3}, which covers the entire range of interest in most mineral soils, with a RMSEp of 0.013 cm^3 cm^{-3}. Jones et al. (2002) reported a shortcoming of the GF method for θv exceeding 0.5 cm^3 cm^{-3} in organic or mineral soils with high OM or C content.

Data fusion based on ANN analyses using data from the vis–NIR spectrophotometer and a dielectric sensor for the measurements of soil ω and θv, respectively, out preformed other calibration methods if data from both sensors was analysed separately. This is due to the ANNs' ability to deal with nonlinear behaviours, as the results from this study indicate the relationship between the soil spectra data and ω is nonlinear. Similar findings of the advantage of the ANN method over other linear calibration methods were also reported by others (Mouazen et al., 2010; Viscarra Rossel and Behrens, 2010; Quraishi and Mouazen, 2013b and Kuang, 2012). The results showed that the relationship between V and θv is also nonlinear. Wijaya et al. (2003) and Gaskin and Miller (1996) reported nonlinearity behaviour of K as a function of the soil moisture change. The ANN – data fusion results in a RPD value of 4.45 for the independent validation set, which can be classified as excellent measurement

performance according to Mouazen et al. (2006b), although the PLSR also results in an excellent but smaller RPD value of 3.57. Mouazen et al., (2006a) stated that the performance of vis-NIRS-PLSR to predict ω is influenced by the scale of modelling. They reported a lower validation accuracy for a sample set collected from multiple fields in Belgium and northern France (R^2 = 0.91 and RPD = 3.22), as compared to that of a single-field sample set (R^2 = 0.97 and RPD = 5.26). The accuracy of measurement obtained in the current study with both PLSR and ANN – data fusion for a sample set collected from 32 fields in the UK is higher than that reported by Mouazen et al. (2006a), which is an encouraging result and suggests using the current ω models for BD assessment. Likewise for θv measurement, ANN – data fusion technique provided the best ω measurement performance, and requires the same input of V and soil spectra only (Table 4-1).

The modelling effect shows that fusing data from both sensors further enhanced their prediction of θv and ω and therefore BD, which supports the author's hypothesis that the prediction accuracy of each sensor will be improved by deploying ANN. This also indicates the strength of ANN to handle data from multiple sensors and the ability to deal with non-linearity among sensor readouts, thereby enhancing the effectiveness of sensor data fusion. The highest accuracy was achieved for the θv, ω and BD predictions gained by using the ANN data fusion calibration model, with RMSEp values of 0.015 cm^3 cm^{-3}, 0.014 g g^{-1} and 0.095 g cm^{-3}, respectively and with R^2 values of 0.98, 0.98 and 0.81, respectively, compared to the lower values obtained by preforming separate calibration methods for each sensor (Table 4-1). The prediction result of BD using ANN is slightly better than Quraishi and Mouazen (2013), who achieved a BD prediction result with R^2 = 0.69 and RMSE = 0.11 g cm^{-3}, using soil PR and soil clay content as input parameters to an ANN model. Günaydin (2009) also attempted to predict soil BD by using an ANN model. His model inputs were: fine grained, sand, gravel, specific density, liquid limit, and plastic limit. The regression analysis revealed various correlations (R^2 = 0.70- 0.95) between different combinations of the inputs and predicted soil BD. However,

the large number of inputs could be the main practicality limitation of such a BD estimation methodology.

Although, most of the soil strength related BD measuring systems are less accurate than the new BD measuring system, they are not even close to the prediction accuracy of BD measurements achieved using the new concept. Quraishi and Mouazen (2013c) presented a prototype BD sensor, consisting of a penetrometer and NIR spectrometer, with prediction accuracies of R^2 = 0.94 and RMSE = 0.04 g cm^{-3}, using the ANN method. However, their measurements were conducted only in three arable fields in Silsoe, England, which express such high accuracy of BD prediction, where vis-NIRS is well known to be affected by soil variability in texture, colour alongside with moisture. Given that the results of BD prediction gained from the current study are obtained from soil readings of 32 fields distributed across England and Wales, the new system shows high accuracy when various soil types and conditions are taken into account. The previous research group also reported a higher prediction BD accuracy of one field with R^2 = 0.95 and RMSE = 0.02 Mg m^{-1}, which indicates that soil variability is the main limitation factor affecting prediction accuracy.

ANN has an extraordinary ability to derive and extract meaning, functions, and trends from complicated, noisy, and imprecise data. They have been considered as a standard nonlinear modelling method (StatSoft, 2012). Their predictive and generalisation capabilities have been developed to learn just like human brain from the presented data and dynamically modifying themselves accordingly. Statistica multilayer perceptron neural networks is one of the most useful toolbox of ANN, which been used to generate the calibration models and to perform the data fusion of the 2 variables in the input layer, where the input data of both sensors can be processed simultaneously. The use of ANN has led to better prediction performance due to the non-parametric nature of ANN multilayer perceptron and can approximate almost any function with high degree of precision. So, the main difference between ANN and any other calibration methods is that ANN in a real sense can learn by the given example

data rather than having to be programmed with specific, preconceived functions. In other words, ANN can be classified as a non-parametric statistical mechanism that uses the observations to predict the unknown function (Boguslauskas and Mileris, 2009; Singh et al., 2012). Among all models, the ANN - data fusion with V and soil spectra only used as input variables for the measurement of ω and θv performs the best for the assessment of BD using Eqn. 1-9 (R^2 = 0.81 and RMSEp = 0.095 g cm^{-3}). This is mainly attributed to a much larger improvement in ω measurement, as compared to θv (Table 4-1), when ANN is used. This model provides useful information about field BD with small RMSEp, to recommend practical application of the new proposed system of combining vis-NIRS and dielectric sensors for the assessment of BD.

This can answer the question of why ANN has been chosen for the complicated mathematical functions for the multisensory applications modelling and to perform multiple predictions. Even with single factor prediction (e.g. ω) ANN has showed higher performance comparing to the linear calibration (PLSR). Farifteh et al. (2007) similarly reported over performing of ANN compared to PLSR, when they developed predictive models of soil salinity based on soil spectral data. However, when ANN single factor prediction (e.g. θv), compared with multi-factor based prediction (e.g. M, GF, SSC and OV), there are no obvious prediction accuracy improvement (Table 4-1).

5.1.2. Soil moisture level effect

The accuracy of measurement of the three parameters improved considerably with increasing soil moisture, which is in line with many researchers who have demonstrated higher sensitivity of both sensors with rising soil moisture. Therefore, the highest moisture level (L3) was found to be the best to conduct the field measurements using both sensors to predict θv and ω and subsequently this positive effect resulted in the highest prediction accuracy of BD with R^2, RMSEp and RPD values of 0.86, 0.061 g cm^{-3} and 2.51, respectively (Table 4-3).

The relationship between soil θv and K is non-linear, which takes its characteristics from the forces between the water molecules and the soil

particles, where more energy is required to change the polarity of the water molecules dipoles in the case of dry soil. This reduces the reflection of the transmitted signal through the body of the soil. This forces decrease with soil moisture increases, comparing to the high dipolar moment of the free water molecules at the saturated soil condition (Fernández-Gálvez, 2008). Fernández-Gálvez (2008) studied the effect of the soil moisture level on θv prediction accuracy, using nine calibration models of different research groups. Consequently, 81 predicted θv values resulted from all possible combinations of calibration model, which their RMSE were used to identify effect of moisture levels (from 0 to 0.50 $m^3\ m^{-3}$) on the prediction accuracy. The retrieval soil moisture RMSE of the 81 cases, and the highest RMSE induced by using the two most inaccurate soil dielectric models are illustrated in Figure 5-1, which shows that the RMSE values are higher with low moisture content and the error of prediction decreases as the soil moisture increases (Figure 5-1), which is in line with the findings of the current research.

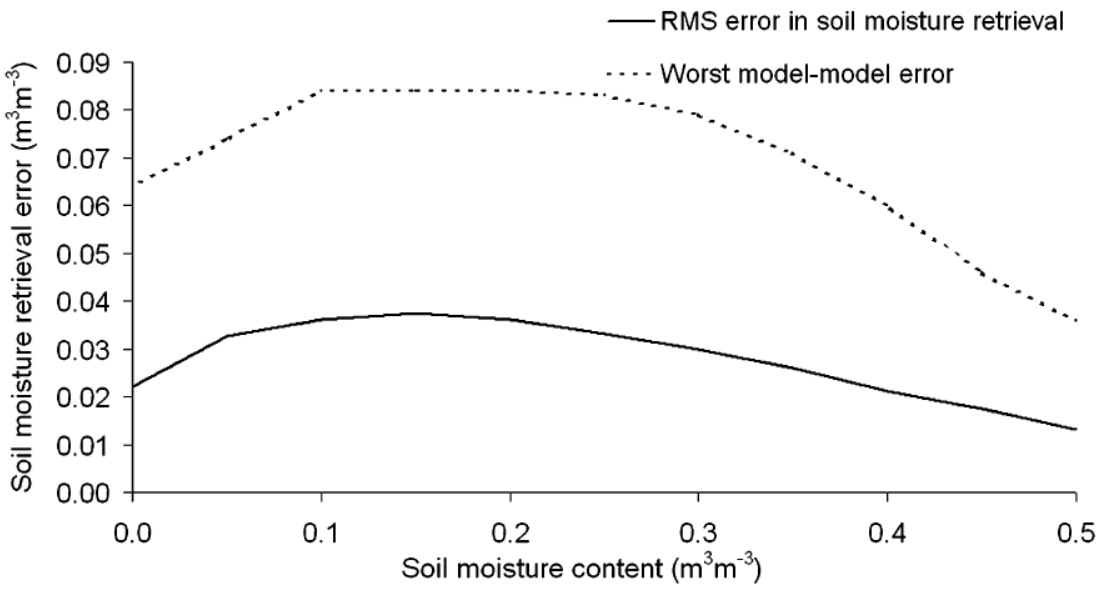

Figure 5-1 Retrieval errors of volumetric moisture content (θv) estimation using different calibration models (after, Fernández-Gálvez, 2008).

Arsoy (2014) compared the accuracy of three dielectric sensors to predict θv, reporting RMSE values of 0.012, 0.015 and 0.016 $m^3\ m^{-3}$, for TDR, ThetaProbe and WET sensor readings, respectively. These results were obtained under laboratory conditions using a wide range of soil textures, BD and 6 different moisture levels. The SSC method was adopted in the current study to calibrate ThetaProbe, comparing to the collective model of the 3 level moisture contents. Despite the fact that the measurement conducted at 5 fields with various soil textures, the accuracy achieved here is slightly better with RMSE of 0.013 $cm^3\ cm^{-3}$. Presumably the accuracy of the current study was improved with the use of ANN calibration method.

Soil moisture at different levels can be easily identified using vis-NIRS, due to the obvious influence of soil ω on the spectra data; however, this advantage can be a limitation factor in the prediction of other soil chemical properties (Nocita et al. 2013; Kuang and Mouazen, 2013). Literature shows that there is a clear effect of soil moisture level on the prediction of ω using vis-NIR spectrophotometer (Mouazen et al., 2005a; Viscarra Rossel and McBratney, 1998), in terms of increasing the level of soil moisture reflected positively in the prediction accuracy for the moisture levels investigated. This is particularly due to the good sensitivity of vis-NIR to the O-H bond in the soil samples. Dalal and Henry (1986) reported better results of predicting ω for eight profiles from each of three major soil series in Darling Down, Queensland, Australia, using NIR spectrophotometry within the wavelength range 1100 to 2500 nm than for L1 in the current work. An R^2 value of 0.93 and RMSE value of 0.6% was reported for samples ranging between 3.5% and 13% moisture content, which is close to the L1 range of moisture (e.g. 0.11 $g\ g^{-1}$).

Kodaira and Shibusawa (2013) reported that ω was the best predicted property using an on-line mapping system (Figure 5-2), equipped with a vis-NIR spectrometer with a wavelength range from 305 to 1700 nm and using a PLSR calibration method. They predicted ω with R^2, RMSEp and RPD values of 0.93, 0.0142 $g\ g^{-1}$ and 3.6, respectively. However, comparing to L2, which is the nearest range of soil moisture, the prediction accuracy of ω obtained in the current work for non-mobile measurement was better with R^2, RMSEp and RPD

values of 0.98, 0.012 g g^{-1} and 7.08, respectively. Although the on-line measurement system provides high resolution data at speedy way, in terms of the robustness, the new non-mobile BD measuring system showed high durability, as the combined probe can be inserted into the measuring layer easily and controllable, where no tolerance of the soil strength on the accuracy. However, software and hardware developments are essential to present mapping system for larger scale, although for *in-situ* application the new BD measuring system has showed simplicity of collecting the readings and high easiness of use.

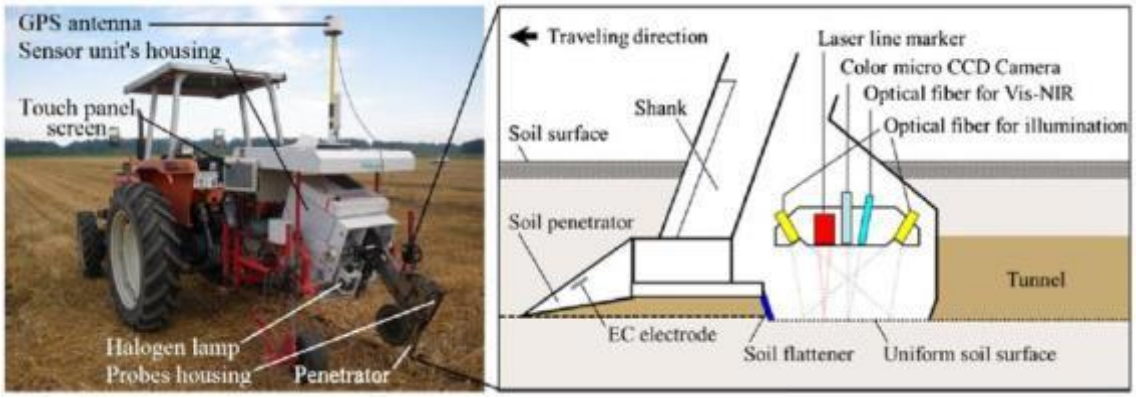

Figure 5-2 Real-time soil visible-near infrared mapping system (after, Kodaira and Shibusawa, 2013).

R^2 of BD prediction of the collective model was 0.57 (Table 4-3), which is an improved value compared to that (0.46), reported by Quraishi and Mouazen (2013b), when they used multiple linear regression (MLR) analysis. However, they reported a better R^2 value of 0.81 with the ANN method as compared to collective model of the current work (R^2 = 0.57). This confirms ANN to be the most favoured calibration method. But, the BD prediction accuracy for L3 moisture content (R^2 = 0.86) was the best obtained as compared to the remaining models, confirming the best measurement of BD is to be expected when the soil is wet enough to avoid error associated with soil disturbance while penetrating the soil.

When discussing the prediction errors of BD based under dry soil conditions affecting penetrometers, Quraishi (2013) stated this to be a limitation of soil related measuring tools of soil compaction. This is because of the additional force needed to insert the cone through the soil under dry soil conditions. Although the new measuring system proposed in the current work does not depend on the strength of penetrating the soil, the process of inserting the ThetaProbe electrodes in the dry soils is accompanied by great difficulties led to formation of air pockets around the central electrode and thus decreased measurement accuracy (Gaskin and Miller, 1996). The vis-NIRS is also affected by the soil moisture level, so that measurement accuracy increases with soil moisture. It's worth mentioning that measurements under dry soil conditions, using core sampling method as a comparator with the predicted soil BD values obtained by the new measuring system was difficult to preform and subjected to measurement errors (Holmes et al., 2011), which in return induces more prediction errors of soil BD at L1 soil moisture. Furthermore, the collective model showed lower accuracy compared to any moisture level. This suggests the need for the measurement of BD to be made for one measurement done in one time, and to avoid mixing measurement taken at different time intervals that may reflect different levels of moisture content in the soil.

5.1.3. Soil texture effect:

The soil texture class effect on the measurement accuracy of θv prediction shows that the range of RMSEp of θv was from 0.018 to 0.021 cm^3 cm^{-3} for all textures and from both arable and grassland soils. However, the best result was obtained from the measurement of grassland in heavy clay loam soils. Apart from this result, there were no clear impacts of soil texture on the ThetaProbe measurements, although, the results from grassland showed better accuracies. Further work is needed to consider more soil texture classes than those considered in the current work (e.g. three soil textures).

Using a Hydra probe, Rowlandson et al. (2013) showed that the measurement accuracy of θv for soil textures with clay contents less than 40% were higher than measurements of finer textured soils (Table 5-1). The various calibration

techniques revealed RMSEp values ranging from 0.0374 cm^3 cm^{-3} for the calibration of individual fields to 0.0623 cm^3 cm^{-3} for the whole dataset collected.

Table 5-1 Measurement accuracies of a dielectric soil moisture sensor (Hydra probe) with different modelling and for coarse and fine soil texture (after, Rowlandson et al., 2013).

Calibration technique	R^2	RMSE ($cm^3\ cm^{-3}$)	Models
General, linear	0.77	0.062	$\theta v = 0.0838\sqrt{K} - 0.0846$
General, 3rd order polynomial	0.77	0.062	$\theta v = 3.55 * 10^{-6}K^3 - 4.19 * 10^{-4}K^2 + 0.022K - 0.0024$
General, Linear with outliers removed	0.85	0.048	$\theta v = 0.0862\sqrt{K} - 0.0962$
General, 3rd order polynomial with outliers removed	0.85	0.047	$\theta v = 3.99 * 10^{-6}K^3 - 4.56 * 10^{-4}K^2 + 0.023K - 0.014$
Texture, coarse (<40% clay)	0.85	0.042	$\theta v = 0.0971\sqrt{K} - 0.1326$
Texture, fine (>40% clay)	0.81	0.051	$\theta v = 0.0787\sqrt{K} - 0.0626$

The results of the current study show no clear texture effect on the RMSEp values for the studied texture classes and heavy and light soil classification experiments. But, in general the RMSEp values ranged from 0.008 to 0.021 cm^3 cm^{-3}, which were considerably better than those reported by Rowlandson et al. (2013) and suggest that ThetaProbe is in advance of Hydra probe in terms of prediction accuracy with the use of data fusion performed by ANN technique. Similarly, no clear trend observed of the influence of clay percentage on the accuracy of measurement of the ThetaProbe. However, literature demonstrated negative correlation between CC and measurement accuracy of θv. Alizadeh et al., (2008) reported negative influence of CC with R^2 values of 0.91, 0.93 and 0.95 and RMSE values of 6.7%, 5.1% and 2.7%, for clayey, loamy and sandy loam soils, respectively. However, these authors only used 17 soil samples to represent each one of the three soil textures. Similarly, Hanson and Peters (2000) stated that the ThetaProbe accuracy decreases with increasing CC. They reported R^2 values of 0.87, 0.91 and 0.79 and average absolute differences (absolute percent volume) of 1.8, 2.5 and 3.0, for sandy loam, loam and clay textures, respectively. Sarani and Afrasiab (2012) reported better ThetaProbe accuracies, with R^2 and RMSEp values of 0.95, 0.93, 0.91 and 0.90, and 3.0, 2.9, 3.8 and 10.8 % for sandy, sandy loam, loam and clayey textures, respectively.

Wijaya et al. (2003) found ThetaProbe readings are significantly affected by the type of soil, where they reported RMSEp values of 0.014 and 0.008 cm^3 cm^{-3} for clay and clay loam soil textures, respectively. However, no clear difference of the RMSEp between the light and heavy soils was observed in the current study under the field conditions, which contradict the findings of Wijaya et al. (2003), who gained their results under laboratory conditions, where homogenous soil samples were used. Also, Wijaya et al. (2003) did not divide all texture classes into heavy and light soils. Both soil groups tested in this research resulted in RMSEp of 0.016 cm^3 cm^{-3}, which were within the range reported by the manufacturer (Delta-T devices, 1999), and is comparable to that of Wijaya et al. (2003) reported for clay

soil under laboratory conditions. This high accuracy expresses the reliability of ThetaProbe to predict θv under field conditions with ANN calibration method.

The ω prediction results did not show clear evidence of texture classes from both arable land and grassland. However, in most cases the prediction accuracy was within the range between good to excellent, which is not consistent with what Kuang and Mouazen (2011) reported. They found a negative influence of clay fractions when they studied ω prediction using vis-NIRS. They reported the highest RPD value of 3.01 measured in a single field with a sandy loam texture and the lowest RPD value of 2.5 was in a single field with clay loam texture. They attributed this trend to the combined effects of texture and moisture content on prediction accuracy. The effect of CC in most soil textures on prediction of ω using vis-NIRS was positive according to the current work results (Table 4-5), which is in-line with Quraishi (2013) who reported RPD values of 5.30, 3.09 and 3.68 in three fields with various textures, namely, clay, sandy loam and sandy loam, respectively. However, the RPD values of ω from this work, using the ANN method, are considered to be within the range of very good to excellent prediction models under soil texture effect, according to Viscarra Rossel et al. (2006) who classified RPD values between 2.0 to 2.5 as a very good quantitative model, while the RPD values larger than 2.5 are indicative of an excellent predictive model.

Mouazen et al. (2006) work on ω prediction with vis-NIR spectroscopy showed a less performing model (R^2 = 0.88; RMSEp = 2.5%) for data set collected from several fields in Belgium and Northern France, compared to single field prediction accuracy of about 7 ha area (R^2 = 0.98; RMSEp = 1.6%). They stated that the variability of soil samples in terms of colour, texture, and origin, attributed negatively to the prediction accuracy of soil ω under laboratory conditions. Kuang (2012) reported on the ability of vis-NIRS to measure ω in farms with different soil textures. The results revealed that ω could be predicted accurately with PLSR modelling, using soil samples with different soil textures collected from four farms across Europe, with R^2 values ranging from 0.74 to 0.92 and RPD from 1.63 to

4.57 for the independent validation sets. Better model performance was observed for heavy soils than for light soils. Kano et al. (1985) used a NIR soil sensor at two wavelengths of 1800 and 1940 nm to measure soil moisture. They reported soil texture influence on the accuracy, where a single calibration model could be used with clay and loam textures and another calibration model would be necessary for sand and sandy loam textures. Curcio et al. (2013) studied the interaction between the -OH group with clay and sand factions. They reported that the illite, kaolinite and montmorillonite minerals of clay have absorption peak around 2200 nm wavelength, whereas, the sand's silicates are liked to -OH stretch vibration of water observed around 1400 nm wavelength. They predicted clay, silt and sand accurately with R^2 and RMSEp values of 0.87, 0.60 and 0.80, respectively and RMSEp values of 5.8, 7.2 and 7.7, respectively, using PLSR calibration method under laboratory conditions. Sinha and Wang (2008) revealed a higher R^2 of 0.98 using the ANN technique for BD prediction as a function of soil solid particle density, fineness modulus, effective grain size, plastic and liquid limits. However, they measured the input variables under laboratory conditions, which could explain the high accuracy, although, such kinds of measurement of soil physical properties are time consuming and demand experienced individuals to conduct them.

The influence of CC on ω prediction was in line with the findings of other researchers, who reported the difficulty in predicting ω with the presence of high CC. This is due to the fact that the absorption bands of OH groups, which are associated with clay minerals and water bound in the clay lattice vary with mineral types (Clark, 1999) and coincide with the water removed upon oven drying. For this reason, quantity measurement of ω across different soil types is difficult (Ben-Dor et al., 1999). However, the R^2 and RPD value of a light soil was the lowest, which may be attributed to the large sample variation (e.g. SD and range of concentration) in heavy soils and collective soil texture, as compared to the light soils (Kuang and Mouazen, 2011). Qurishi and Mouazen (2013c) showed similar

trend of RPD and R^2 values, when they studied the effect of clay and sandy loam textures on ω prediction using vis-NIR portable system.

The findings of this section led to no clear conclusion on which texture model to provide the best accuracy. However, for both grassland and arable land fields, the collective texture model seem to provide more stable prediction results as compared to individual texture models. These results demonstrate that measurement in grassland fields is more robust and trusted than in arable land fields.

The final conclusion of the soil fraction effects on the spectra data can be that the soil minerals respond in different rates and it would be adequate to take into account the complex interaction between the –OH group and soil texture when vis-NIRS is used to predict soil moisture content.

5.1.4. Land use

The effect of land use on the measurement accuracy soil θv, ω and subsequently BD was evaluated. The prediction performance of BD on the grasslands was more accurate than on the arable lands. The reason behind this could be related to the larger heterogeneity of BD in grasslands (SD = 0.24 g cm^{-3}), as compared to the arable land (SD = 0.15 g cm^{-3}) sample sets considered in the current work (Table 3-10). This was true in spite of the fact that both sensors showed high prediction accuracy for θv and ω for the arable land soils, as compared to the grassland soils. Although the measurement conditions are different between the two land use scenarios investigated. For example, grassland soils tend to be more compacted in the measuring profile and with larger heterogeneity in the top soil BD, the system was able to predict BD accurately, which may be attributed to the good contact between the soil and dielectric probe, achieving an RMSEp = 0.013 cm^3 cm^{-3}. On the other hand, dividing the data according to the land use compared to the collective model, showed prediction improvement (Table 4-8). It was the spectra

data that outweighed the prediction accuracy for the grassland soils, where the RMSEp scored the lowest value (0.01 g g^{-1}). However, all RPD values fall under excellent classification category, according to the classification index of Viscara Rossel et al. (2006). The BD prediction of the grassland revealed the lowest x intercept value of 0.079 g cm^{-3} with the closest scattering of BD points around the 1:1 line. However, the encouraging results of the collective calibration model to predict soil BD using whole data was considered an advantage for the systems' ability to operate under different soil conditions. This suggests dividing sample set into arable and grass land is not recommended particularly for arable land soils. For grassland soils, splitting calibration models into two sets have a positive impact on accuracy.

- **Summary of Section 5.1**

In general, the soil BD measuring system developed and tested in the current work showed high capability to estimate soil θv, ω and BD, under various calibration methods, soil types and conditions, where the accuracy fluctuated under the factors tested, but in most cases was high. However, different levels or percentages of the tested affecting factors have helped to identify where and when the measurements would be consistent and more accurate. Starting with the modelling effect, the ANN method with data fusion was the best method to handle the data from both sensors and provided the best accuracy. The moisture level influence showed that soils with average moisture contents near high end at L3 were expected to achieve good prediction results. When it comes to the soil texture effect, it was concluded that clay minerals showed a positive interaction with the O-H bond, influencing the spectral data, which in turn led to high prediction accuracy for soils with high CC. The growing crop effect showed that grassland soils are in advance of arable land soils planted with different crops, but the author believes that there are no direct connections between the measuring system accuracy and the growing crops. The experimental results only demonstrated the relationship followed field operations and its impacts on the soil viability. Literature sources

indicated that many authors have attempted to provide an accurate soil BD measuring system, due to the importance of such a single soil physical property that has many environmental and economic impacts. The new measuring system has demonstrated that better results are achievable for measuring soil BD compared to many others reviewed work, where large data volumes and a wide range of soil types and conditions are experienced.

5.2. Evaluation of the prototype combined probe

5.2.1. Laboratory evaluation of the prototype combined probe

The prototype combined probe showed encouraging accuracy for measuring soil BD under field conditions (Table 4-14), although it was more accurate during laboratory test of two different soil textures, but soil texture effect was clear on RMSEp values 0.061 and 0.031 g cm^{-3} of BD with clay loam and sandy loam textures, respectively (Table 4-11), these findings are in-line with Liu et al. (2008) results of soil texture effect on the Thermo-TDR system accuracy to estimate BD in silt loam, clay loam and sandy textures under laboratory conditions with RMSEp values of 0.055, 0.051 and 0.046 Mg m^{-3}, respectively.

Clay fraction effect on the accuracy of the TDR sensors reported to be related to the attaching mechanism of the electrolytes to the clay fraction surface by static electrical force, leading to extra polarization, which would further interact with the electromagnetic wave that is travelling through the soil, in other words, CC impedes the electromagnet wave propagation in the clayey soils. The longer signal travel time leads to a higher output voltage, or overestimation of soil moisture reading (Sun and Young, 2015). Whereas, for the FDR sensors the effect of increasing CC lead to under-estimation of the V (Figure 4-12B), the reason behind such behaviour is due to decrease the bulk dielectric property of the soil matric with increase CC, the soil in FDR measuring systems represents the insulating material

between the electros of the dielectric sensor of the prototype combined probe. On the other hand, the linear relation between V and θv of the sandy loam soil texture expresses that the bulk dielectric of the soil matrix related to the *K* of the soil water solely (Figure 4-12A).

The accuracy of the dielectric probe depends on maintaining good contact between the probe's electrodes and the soil. For this reason, a penetrating cone is used as one of the shielding electrodes in addition to a second part above the central electrode, a similar approach was followed by Peter and Yurui (2004) for the design of a combined capacitance sensor with a cone penetrometer (Figure 2-29). They reported lower accuracy for the linear relationship between the capacitance sensor's V and θv using a silt loam soil texture under laboratory conditions, compared to the current prototype FDR sensor, which resulted in a better R^2 value of 0.99 and RMSEp = 0.023 cm^3 cm^{-3}, using a clay loam soil texture under laboratory conditions and the characteristics of the relationship between V and θv found to be expressed more accurately using a non-linearity function.

A vis-NIR spectrometer with a shorter spectrum was used for the prototype. The process of combining both sensors was the most challenging task of this work, as both sensors are very sensitive to any changes made to their sensing probes or heads. Delicate materials have to be used in the sensor manufacture, for example, using thin fibre optics in the limited space inside the steel shaft, upon which the combined probe is assembled and a sapphire material was used to ensure that no scratches would affect the probe windows' transparency.

5.2.2. *In-situ* evaluation of the prototype combined probe

The dielectric probe showed high accuracy in measuring θv in arable and grassland soils and even more accurate for a single field test using ANN technique. Similarly, Namdar-Khojasteh et al. (2010) studied the relationship between *K* measured by TDR and θv. Concluding ANN calibration method used to predict the *K*–θv relationship using 10 different soil textures (e.g. sand, loamy sand, sandy

loam, sandy clay loam and loam) provided considerably better prediction of θv comparing to GF of Topp (1980). However, he reported that the microscopic phenomena associated with *K* of clays are still a subject of considerable debate and more investigation studies are needed.

Soil temperature reported to be influential the dielectric accuracy (Robinson et al, 2003; Kaleita et al., 2005), Chow et al. (2009) concluded it is importance to include the soil temperature in the calibration model of the dielectric sensors, their study included nine dielectric sensors installed in the >50 cm soil layers. The effect of soil temperature on the dielectric property of the soil is complex due to the interferences of CC, electrical connectivity and BD (Seyfried and Murdock, 2004), It is reported that the *K* of water decreases approximately 0.7% $°C^{-1}$ for temperatures from 5 to 35°C, Hence, *K* of the soil had a temperature dependence related solely to *K* of the water, measurements of soil *K* would show a negative correlation with temperature (Campbell, 2015), for these reason adding temperature sensor to the prototype combined probe would improve the accuracy and provide more valuable information on the way of presenting compact mapping system.

The NIR spectrometer of the current prototype predicted ω accurately in arable and grassland soils with R^2 of 0.97 and 0.96 and RMSEp 0.019 and 0.011 g g^{-1}, respectively (Table 4-13), compared to a lower accuracy magnitude reported by Hummel et al. (2004) combined probe (Figure 2-30), the accuracy of the field measurements are in-line with Quraishi (2013) who used similar wavelength spectrum range for ω prediction.

RMSEp value of BD estimation for the five arable fields and two grasslands (Table 4-14) showed encouraging accuracy comparing to the lower RMSEp value of BD estimation obtained during the single field test (Table 4-15), these results suggesting a high sensitivity for the prototype combined probe to soil BD, however, the author believe the less variability of the soil at a single field contributed towards better BD prediction accuracy, same trend also observed when the RMSEp of the

arable lands compared with those of the grasslands, which naturally experience less soil variability providing that the grass established long enough. Quraishi (2013) reported considerable accuracy improvement of soil BD prediction at a single field comparing to the prediction of soil BD at multiple arable fields.

Field measurements of soil BD showed good accuracy when testing the prototype combined probe, which is composed of two sensors of dielectric and vis-NIRS to measure soil moisture only, Peter and Yurui (2004) concluded that adding the capacitance sensor electrode and insulator caused additional frictional resistance to soil penetration by the combined sensor. This led to deterioration in measurement accuracy for the soil strength related system, a problem which has no effect on the soil moisture related systems to measure soil BD designed and developed in the current thesis. This is in-line with the literature review, which showed shortcoming of soil strength related measuring systems. Furthermore, the available on-line mapping systems for soil properties are in general not accurate in comparison to *in-situ* measuring systems. For example, the low accuracies reported by Stombaugh (2014) on-line air permeability sensor (Figure 2-19) to estimated soil compaction and Adamchuk et al (2008) sensor array system (Figure 2-20) to map the spatial variability of soil mechanical resistance, which might be explained by a deficiency in their concept or design, even under soil bin conditions (Hall and Raper, 2005; Andrade-Sánchez et al., 2003).

The prototype measuring system showed better soil BD estimation accuracy with light soil textures (e.g. sandy loam), the process of inserting the combined probe was smoother and easier when the soil moisture is at the field capacity, which led to form a well-shaped walls of the measuring hole, these conditions were the best to gain stable and accurate readouts from both sensors, the well-shaped walls provided better contact area between the electrodes of the dielectric sensor, while the smooth and the well-shaped walls provided the better light reflectance for the NIRS measurements. The author recommend conducting the soil BD measurements after harvesting the crops and before ploughing the soil, as the

effect of soil disturbance at this time is minimum and also the results of soil BD measurements can provide a beneficial information for efficient land management, where for example a subsoiler can be used at specific parts in the field, whereas for the lower BD parts of the field a higher speed of the tractor may be selected for more efficient tillage.

From the above it is clear that the best time to conduct field measurements using the prototype combined probe when the heavy soils' moisture is ranging between 0.18 to 0.30 gg^{-1} and between 0.20 to 0.28 gg^{-1} in the light soils, in order to avoid the occurrence of air spaces around the dielectric probe' electrodes, as well as to prevent the overestimation of V when the soils at or near saturation status. Conducting field measurements also preferred when the soil temperature degree convergent with those in which the model calibration was generated, however, assembling a thermo-sensor on the combined probe and add the effect of soil temperature to the calibration models expected to improve the accuracy. Fields with light soil texture showed a tendency of better accuracy of estimation BD comparing to the fields with heavy soil texture (Table 4-15).

Many prediction models for soil physical or chemical properties have been extensively developed to be used with soil combined sensor applications. The data fusion technique is a powerful tool, when implemented for various multiple integrated sensors in a soil compaction measuring system, and has emerged as a promising approach (Mouazen and Ramon, 2008; Mouazen, 2009). Simultaneous mapping of soil compaction indicated as BD, alongside with θv and ω could considerably optimise future farming efficiency (Adamchuk et al., 2008).

It is understandable that *in-situ* mapping systems, such as the prototype system developed in the current work, are labour-demanding for a large field area, but this issue can be solved by providing, for example, a quad motorbike for easier movement around the fields during the measurements. However, the main important consideration about conducting such measurements is to ascertain the

measurement accuracy, which the literature has proved that the on-line mapping systems are not sufficiently accurate, due to many factor interactions associated with the measurement process, even the use of a relatively large number of sensors would not be able to solve this lack of accuracy.

5.3. Advantages and practical challenges associated with the use of the new concept and the prototype combined probe

The advantages of using the new concept to measure soil compaction indicated as BD with the implementation of dielectric and vis-NIRS sensors are as followed:

- The system is semi- non-invasive, whereas, the frequency domain sensor measures the dielectric constants of the compound by emitting an electromagnetic signal propagated through the soil body and the vis-NIRS sensor detects the diffused reflectance of electromagnetic wave from the soil samples surface down to the depth of 2 mm.
- The system is relatively small in size and light in weight: the ASDi spectrometer weights 5.44 kg with dimensions of 12.7 by 36.8 by 29.2 cm, of height, width and depth, respectively, whereas the ThetaProbe is a handheld with minor weight measuring device.
- The prototype soil compaction measuring system has an additional advantage by presenting a combined probe containing both sensors.
- Rapid readouts: The readings from both sensors can be recorded within few seconds.
- Robust design of the prototype combined probe in terms of the penetration rod geometrical structure, where the ability to easily penetrate the soil have been taken into account by this streamlined form.
- Cost effective, efficient and long lasting mapping system for BD and it has the potential to measure other soil physical and chemical properties.

- Adequate accuracy with wide a range soil types and conditions, providing accurate calibration models are used.

For further details of the up-to-date soil BD measuring systems, Table 5.2 shows a comparison between the prototype measuring system presented in this thesis and other prototypes, clearly, the prototype of the current work is among the best measuring systems from the accuracy point view (Table 4-14), Although these results are field measurements of the five different fields with different soil textures, the current results are encouraging when taking into account that the measurement accuracy under laboratory conditions of the prototype proved affected by the texture of soil (Table 4-11), which in the future requires calibration procedure depends on the type of soil to obtain a higher accuracy measurements. Both the current prototype and Liu et al. (2008) Thermo-TDR measuring systems of soil BD are non-soil-strength-depending systems sharing the high estimation accuracies and the simple operational principles, but the high electrical power of the probe's heaters and long time needed for a single readout are the main disadvantages of the Thermo-TDR probe, while the current prototype's probe consumes considerably less electrical power as no heating element is present and only around 5 seconds are needed for a single readout. Other soil-strength-depending soil BD measuring systems can be described as more complicated systems, which their accuracies are affected by soil moisture content, to solve this issue a moisture sensor should be added to the measuring system, among all these systems Quraishi and Mouazen (2013c) showed the highest accuracy of an *in-situ* measuring system of soil BD, aided by the ANN calibration technique they achieved RMSEp as low as 0.02 Mg cm^{-3} for a single field soil BD prediction, similarly the prototype measuring system of the current study showed considerably high accuracy to estimate soil BD in Clover Hill field with RMSEp value of 0.008 g cm^{-3}, furthermore for all individual field tested the results show excellent accuracy ranging from 0.008 to 0.032 g cm^{-3} (Table 4-15). However, the results of prediction soil BD during the individual field measurement show no clear effect of various soil

textures, which suggest that a calibration model from wide range of soil texture can predict BD with high accuracy.

The simplicity of the measuring system of soil BD is a key factor to present a practical, low cost and usable system, the prototype of the current system provide these advantages, however, the author believe that higher accuracy can be obtained when using calibration models of different soil textures, as the latter proved to affect the measurement accuracies of both dielectric (Liu et al., 2008; Rowlandson et al., 2013; Alizadeh et al., 2008) and vis-NIRS sensors (Kuang, 2012; Quraishi, 2013) (Table 4-9 and 4-10, respectively).

Table 5-2 provide a comparison between the prototype measuring system of soil BD and other measuring systems, the accuracy comparison shows that the new measuring system is among the most accurate systems with less than 0.01 g m^{-3} values of RMSEp for a single field measurement of soil BD. Furthermore, the prototype simple and robust design is the key feature of presenting the new system as affordable and accurate for the *in-situ* measurements, whereas the general disadvantage of the on-line system is the lower accuracy despite the use of multiple sensory systems, However, the radiation hazard of using the gamma ray source is the maim limitation of using Naderi-Boldaji et al. (2013) measuring system, which was the best among the on-line measuring systems of soil BD, with RMSE value of 0.06 g m^{-3}.

Table 5-2 Comparison between the prototype measuring system of soil BD and other measuring systems from the up to date literature.

Systems	Accuracy	Mobility	Complexity
The prototype of current thesis	RMSEp=0.01 g cm^{-3} of soil BD.	*In-situ*; portable system can be carried by a person.	Combined soil probe of dielectric sensor and vis-NIRS.
Kweon et al. (2008)	R^2=0.21 to 0.78 RMSE=0.07 to 0.13 g cm^{-3} of soil BD.	Mounted on a vertical frame is installed on a pick-up truck and has an assisting hydraulic system to help penetrate the soil profile.	Soil profile array sensors consisted of a vis-NIRS, a string potentiometer, a conductivity probe, GPS and a thermometer.
Adamchuk et al (2008)	R^2=0.32 of soil BD.	On-line; Compound on a platform carried on the three suspension points of a tractor.	Sensor array of an optical reflectance, dielectric probe and three sets of load cells.
Sun et al (2006)	R^2=0.51 of soil BD.	On-line; Compound on a platform carried on the three suspension points of a tractor.	Horizontal combined probe of a cone penetrometer and a FDR capacitance sensor.
Adamchuk et al. (2008)	R^2=0.71 of soil BD	On-line; Compound on a platform carried on the three suspension points of a tractor.	Combined mapping system consisting of a load cell, an optical sensor and a capacitance probe.
Dhillon et al.,	R^2 = 0.28 of the	On-line; mounted on a platform can	Integrated mapping system of an

(2010)	predicted soil mechanical resistance.	be towed by a pick-up truck	optical sensor with a capacitance probe, a load cell sensor and GPS.
Naderi-Boldaji et al. (2013)	R^2= 0.72 and RMSE=0.06 g cm^{-3} of soil BD.	On-line; Compound on a platform carried on the three suspension points of a tractor.	Mapping system consisted of a Horizontal penetrometer connected to a load cell, a dielectric probe and a gamma-ray sensor.
Quraishi and Mouazen 2013c	R^2=0.94 and RMSE=0.04 Mg m^{-3} of soil BD.	*In-situ*; portable system can be carried by a person.	Soil BD multi-sensor kit consisted of a digital penetrometer combined with an NIRS.
Liu et al. (2008)	RMSE=0.046 to 0.055 Mg m^{-3}	*In-situ*; portable system can be carried by a person.	TDR, thermometer and combined probe.

One of the challenges raised during the field measurements was the fact that agricultural soils are not naturally homogeneous and contain stones, gravels and plant residuals. These have a significant negative impact on the dielectric sensor, relating to the fact that the central electrode is very sensitive to air pockets when they present around it. Stones in the collected soil cores lead to soil moisture estimation error, as the stones do not hold any moisture inside them. Dry soil conditions make the measurements difficult and less accurate, while the very moist soil status could make it harder to conduct the readings. Excluding the soil sample outliers from the whole data could also improve the accuracy of prediction; however, a certain SD limit of soil sample groups can help solve this issue.

Technical challenges can be summarised as the necessity for a more compact system, which has the capability of recording the data from both sensors, as well as the ability to process the adapted calibration models and providing the desired output, which may include spatial maps or prediction values. Long life and light weight batteries are essential for the measuring system to be easily mobile and reliable for extended periods of field measurement. However, assembling the system on a quad motorbike could solve all of the above issues. Supplying the right coaxial cable for the dielectric sensor was the main challenge in the manufacture of the combined probe for the prototype measuring system. This was particularly due to the difficulty of dealing with the high frequency signals (100 MHz). With more research time and financial support a whole profile measuring probe instead of just the top 10 cm of depth measurements would have been developed.

5.4. Implementation and commercialisation of the new measuring system

The new measuring system has proved to measure soil BD as a function of the directly measured θv and ω. However, many soil physical and chemical properties can also be measured by the vis-NIR spectrometer, providing the right and accurate calibration models. The benefits of having this measuring system commercially available are expected to be multidisciplinary, including assisting

farmers from an economic point of view, where such a helpful and reliable system can by implemented for efficient application of fertilisers and this would lower the risk of surface and ground water contamination by the agrichemicals. Also, the identification of the compacted parts of the fields could direct compaction solution processes more specifically, which would save time and financial resources. Similarly, a considerable amount of energy can be saved if site-specific tillage is deployed (Andrade-Sanchez et al, 2008).

The author believes that the new measuring system will be a valuable tool to the environmental agencies, since speedy, high spatial resolution and low cost data about soil compaction will assist prediction and modelling of flood risk, while effective land management for flood defence can be established. In other words, the new measuring system can be a reliable and accurate mapping system to Natural England and Environmental Agency to support their two soil protection schemes of from runoff and erosion, by providing prediction models where soil erosion or floods might occur during heavy rains, due to the low infiltration rates, that are normally associated with compacted soils.

The new measuring tool can support the Catchment Sensitive Farming initiative by making a difference to local water quality by showing where improvements to soil bulk density (soil compaction) and rainfall infiltration are required, consistently, and in a targeted manner (DEFRA, 2008). Field measurement of soil compaction at high spatial resolution will assist successful implementation of Unilever sustainable agriculture by enabling a better management of land for sustainable production (Unilever, 2010). Finally, to improve compaction management, site specific tillage systems can be adopted based on high resolution measurement output of bulk density as the main indicator of soil compaction.

Chapter 6

6. Conclusions and future work

6.1. Conclusions

The visible and near infrared spectroscopy (vis-NIRS) for the measurement of the gravimetric moisture content (ω) was combined with the ThetaProbe for the measurement of the volumetric moisture content (θv) for *in-situ* assessment of soil bulk density (BD). Influences of modelling technique, moisture content, texture and land use on measurement accuracy of the three properties were evaluated. Based on successful results obtained for 32 fields in England and Wales with different textures, organic matter percentages, moisture contents, and various land use, a prototype measuring system for soil BD, with its combined probe of two sensing techniques, was designed, manufactured and tested in the laboratory and field. The following conclusions can be drawn from the results of the tests:

- Soil BD can be assessed with the proposed new approach by substituting the vis-NIR measured ω and the ThetaProbe measured θv into an existing BD model with high accuracy.
- Artificial neural networks (ANN) methods were proven to provide high performance as a calibration technique for both the dielectric sensor and vis-NIR spectrophotometer, with only spectra and V used as input variables to generate separate calibration models of θv and ω, respectively. However, the ANN - data fusion models are generally better than when used separately, due to the unique ability of the multilayer perceptron neural networks to deal with the most complex data, which were obtained from multiple variables in the input layer, and its capability to process the input data, using nonlinear functions rather than only linear processing calibration methods.

- The accuracy of BD assessment depends on the measurement accuracy of ω and θv. The highest accuracy (R^2 = 0.81 and RMSEp = 0.095 g cm^{-3}) was based on ω and θv values predicted with the artificial neural networks (ANN) – data fusion models with ThetaProbe output voltage (V) and vis-NIRS spectra used as input variables. A total of 1013 soil samples with wide ranges of soil moisture, texture, colour and two different cropping systems were used in the analysis. This demonstrated the good reliability of the new measuring system to predict soil BD, compared to other measuring systems reported in the literature (Quraishi and Mouazen, 2013c; Hummel et al., 2004; Sun et al., 2011; Lin et al., 2014), where their reported results were not able to achieve a similar magnitude of prediction accuracy under the same conditions.
- The performance of the BD model based on the ANN – data fusion approach deteriorated with an increase in the number of input variables e.g. clay, silt, sand or OM, used to predict ω and θv, which supports the author hypothesis of presenting a soil BD measuring system depends on ω and θv only. From statistics point view it can concluded that the additional soil properties are not relevant to the prediction ω and θv and subsequently have no effects on BD prediction. The reliance on a small number of input variables can be considered an advantage of the measuring system making the prediction of soil BD lower in cost as there is no need for laboratory analysis of soil properties.
- The influence of soil moisture level on accuracy of θv, ω and BD prediction revealed lower accuracy at the lowest soil moisture level and the accuracy improved as soil moisture levels increased. This is because literature showed that soil moisture content is one of the most influential factors on the vis-NIR spectra data (Stenberg et al., 2010; Mouazen et al., 2005a; Viscarra Rossel and McBratney, 1998). Similar conclusion can be drawn from moisture level effect experiment of the current work, for that, predicting ω accurately was the key to obtain higher BD measurement accuracy.

Furthermore, results also showed that accuracy of θv measurement with ThetaProbe depends on obtaining good contact with the soil. For dry soil condition, a poor contact between the soil and ThetaProbe's electrodes might also affect the accuracy of θv measurement and hence the prediction of BD. The implication of this fact leads to preferable soil moisture range, where precise soil BD estimation can be certain.

- A smaller effect of texture as compared to moisture content on prediction accuracy of BD was seen from clay on the dielectric sensor compared to the vis-NIRS measurements. In fact, no clear effect of texture was observed, which was attributed to the small number of soil textures (3 textures) compared in the current work. The results of the ω prediction for the soil texture effect experiment showed that root mean square error of prediction (RMSEp) in most cases decreased with lower clay content. However, in most soil textures a good to excellent BD prediction accuracy levels were obtained for arable and grassland soils, according to the residual prediction deviation (RPD).
- The collective texture models of heavy and light soils appears to provide more stable soil BD prediction results, as compared to individual texture model of light soils. However, the heavy soil model performed better than the collective soil model. This suggests dividing samples into heavy and light soils when estimation of BD is required for heavy soils. For light soils, however, merging heavy and light soils in a collective texture model is expected to result in much improved estimation performance. However, results show that measurement in grassland soils is more robust and accurate than in arable land fields. Furthermore, the analysis also showed that there was no measurable effect on the dielectric sensor readings, but in contrast, a clear impact on the vis-NIR spectrophotometer measurements. The BD prediction on heavy soils showed the best accuracy, which is particularly related to the higher prediction accuracy of ω. The positive interaction effect of CC and moisture content on the spectral data leading to

better ω prediction. This revealed the need for further study of the interaction between soil fractions and moisture content and the identification of the most sensitive wavelength band that could be used for this combination.

- The land use effect experiment indicated more accurate assessment of BD in Grassland fields than in arable fields. This was true for R^2 and RPD values. However, the RMSEp values were similar in both arable land and grassland fields, suggesting that splitting samples into arable and grassland does not lead to improved estimation accuracy of BD. The higher R2 and RPD values obtained in the grassland field were attributed to the higher SD that increased R^2 and RPD values. This is particularly due to the natural differences of the two grassland locations, where the samples were collected.
- The prototype portable combined sensor can be used successfully for the measurements of θv, ω and BD across a wide range of soil textures and land uses. However, the laboratory test gave better results compared to the in-situ measurements. The field test of the prototype in selected arable and grassland sites to predict θv and ω provided excellent results, and the BD results were encouraging. The best topsoil BD predicted was for grassland soils (R^2 = 0.47, RMSEp = 0.077 g m^{-3} and RPD = 1.36). It can be concluded that a narrow band wavelength spectrometer or even mono optical detectors of a certain wavelength can also be used to predict ω effectively, which would considerably lower the cost of the new measuring system and would present it as replacement for the high cost of traditional laboratory measuring methods.
- The highest accuracy of the prototype measuring system was achieved with single field measurements, where BD predicted as low as 0.01 g cm^{-3} of the RMSEp.
- The data of the field test of the prototype combined sensor were successfully utilised to produce maps of measured and predicted θv, ω and

BD. These derived products were capable of showing accurate spatial variation for each parameter mapped, although, the full-points maps were more clear image as double readings number were used to generate θv, ω and BD maps. These BD maps can be of particular interest for land managers, where soil compaction or traffic have to managed site specifically.

- The new measuring system has proven good capability to measure soil compaction indicated as a soil BD, using the combined probe. Unlike measuring soil compaction systems that rely on the strength of the soil, the new measuring system depends on the moisture content measurements of the soil only. From an economic perspective the new measuring system can be an effective tool for land managers to determine soil deterioration areas of the field due to compression and then directing tillage operations to those areas specifically, and that leads to reduce expenses when compared to apply tillage to the whole field. At the same time environmental organizations can benefit from the new system to conduct surveys to the problem of soil compaction, which is one of the most important factors that increase the risk of flooding during heavy rain seasons.

6.2. Future work

This thesis provided a first step of developing a prototype combined sensor for the assessment of BD. However, further development should be considered as to cover the following points:

- It is proposed that further development of the prototype combined sensor software programming and hardware components be carried out, where one platform containing both sensors would be an advantage and substituting the laptop with a suitable data logger capable of device control, data storage

and data display. This arrangement would result in a more compact system and one that is more practical for field based measurements.

- The dielectric sensor electrodes need an improved design, in order to achieve better contact with the soil. The current prototype is capable of measurement to a soil depth of 10 cm, but with further development, the combined probe has the potential to become a whole profile probe, enabling the system to measure soil BD at various soil depths.
- The NIR spectrophotometer is a robust tool that can provide rapid measurements of many physical and chemical soil properties, if accurate calibration models are used. The following points need to be considered for the development of the prototype:
  1. New calibration models can be developed for different physical and chemical soil properties (e.g. organic carbon, N, P, pH and C) using the ANN calibration method.
  2. More compactness and less weight spectrophotometer are needed for easier in-situ measurements.
  3. Software development is essential for fast measurement of both sensors and output interpretations, for example, an automatic generation of output maps from the measurements would be beneficial to present mapping system.
  4. A quad motorbike would be needed for mapping large areas and it would provide additional power source for the system operation.
  5. Develop the combined probe further to achieve soil profile measuring capability through different soil depth down to 30 cm.

References

Abu-Hamdeh, N.H. 2003. Soil compaction and root distribution for okra as affected by tillage and vehicle parameters. Soil & Tillage Research 74 (2003) 25–35.

Abu-Hamdeh, N.H. 2004. THE EFFECT OF TILLAGE TREATMENTS ON SOIL WATER HOLDING CAPACITY AND ON SOIL PHYSICAL PROPERTIES. International Soil Conservation Organisation Conference – Brisbane, July 2004. website: http://www.tucson.ars.ag.gov/isco/isco13/PAPERS%20A-E/ABU-HAMDEH.pdf.

Adamchuk, V. I., Hummel, J.W., Morgan, M.T., Upadhyaya, S.K. 2004. On-the-go soil sensors for precision agriculture. Computers and Electronics in Agriculture 44 (2004) 71–91.

Adamchuk, V.I., Hempleman, R.C., Jahraus, D.G. 2009. On-the-Go Capacitance Sensing of Soil Water Content. ASABE, Paper Number: MC09-201.

Adamchuk, V.I., T.I. Ingram, K.A. Sudduth, and S.O. Chung. 2008. On-the-go mapping of soil mechanical resistance using a linear depth effect model. Transactions of the ASABE 51(6): 1885-1894.

Adelakun, A. and Ranjan, R. S. 2013). DESIGN OF A MULTILEVEL TDR PROBE FOR MEASURING SOIL WATER CONTENT AT DIFFERENT DEPTHS. American Society of Agricultural and Biological Engineers. Vol. 56(4): 1451-1460.

Alakukku, L. 1999. Subsoil compaction due to wheel traffic. In: Agricultural and Food Science in Finland. 8: 333-351.

Alakukku, L. and Elonen, P. 1995. Long-term effects of a single compaction by heavy field traffic on yield and nitrogen uptake of annual crops. Soil & Tillage Research 36 (1995) 141-152.

Alakukku, L., Weisskopf, P., Chamen, , W.C.T., Tijink, F.G.J., van der Linden, J.P., Pires, S. Sommer, C., Spoor, G. 2003. Prevention strategies for field traffic-induced subsoil compaction: a review Part 1. Machine/soil interactions. Soil & Tillage Research 73 (2003) 145–160.

Al-Asadi, R. A. and Mouazen, A. M. 2014. Combining frequency domain reflectometry and visible and near infrared spectroscopy for assessment of soil bulk density. Soil & Tillage Research 135 (2014) 60–70.

Andrade-Sanchez, P., Upadhyaya, S. K., Plouffe, C., Poutre, B. 2008. DEVELOPMENT AND FIELD EVALUATION OF A FIELD-READY SOIL COMPACTION PROFILE SENSOR FOR REAL-TIME APPLICATIONS. American Society of Agricultural and Biological Engineers. Vol. 24(6): 743-750.

Andrade-Sanchez, P., Aguera, J., Upadhyaya, S.K., Jenkins, B.M., Rosa, U.A., Josiah, M., 2001. Evaluation of a dielectric based moisture and salinity sensor for in-situ applications. Paper No. 01-1010, ASAE, St. Joseph, Michigan.

Andrade-Sánchez, P., Upadhyaya, S. K., Agüera.Vega, J., Jenkins, B. M. 2003. EVALUATION OF A CAPACITANCE.BASED SOIL MOISTURE SENSOR FOR REAL.TIME APPLICATIONS. American Society of Agricultural Engineers. Vol. 47(4): 1281.1287.

Ansorge, D. and Godwin, R.J. 2007. The effect of tyres and a rubber track at high axle loads on soil compaction, Part 1: Single axle-studies. BIOSYSTEMS ENGINEERING 98 (2007) 115– 126.

Aragón, A., García, M.G., Filgueira, R.R., Pachepsky, Y.A., 2000. Maximum compactability of Argentine soils from the Proctor test; the relationship with organic carbon and water content. Soil Tillage Res. 56, 197-204.

Arsoy, S. 2014. Constant energy calibration for permittivity based moisture probes. Journal of Hydrology 510 (2014) 79–91.

Arvidsson, J. 2001. Subsoil compaction caused by heavy sugarbeet harvesters un southern Sweden. I. Soil physical properties and crop yield in six field experiments. In: Soil Tillage Research 60: pp. 67-78.

Arvidsson, J. and Håkansson, I. 2014. Response of different crops to soil compaction—Short-term effects in Swedish field experiments. Soil & Tillage Research 138 (2014) 56–63.

Arvidsson, J., Håkansson. I. 1996. Do effects of soil compaction persist after ploughing? Results from 21 long-term field experiments in Sweden. Soil & Tillage Research 39 (1996) 175-197.

ASTM D3385. 2014. Standard Test Method for Infiltration Rate of Soils in Field Using Double-Ring Infiltrometer. website : http://enterprise.astm.org/filtrexx40.cgi?+REDLINE_PAGES/D3385.htm.

Bardy, N. C., 1984. The Nature and Properties of Soils. 9th Ed. MacMillan Publishing Co, New York, USA.

Ben Dor, E.; Banin, A. (1995). Near-infrared analysis as a rapid method to simultaneously evaluate several soil properties. Soil Science Society of America Journal 59, 364-372.

Ben-Dor, E., Irons, J. R., and Epema, G. F. (1999). Soil reflectance. In "Remote Sensing for the Earth Sciences: Manual of Remote Sensing" (A. N. Rencz, Ed.), Vol. 3, pp. 111–188. (3rd edn.). Wiley, New York.

Blue-Jet. 2014. Soil compaction: Causes and Effects. Web-based document accessed on 17/02/2014 at: http://www.blu-jet.com/soilcompaction.htm.

Boguslauskas, V., and Mileris, R. 2009. Estimation of Credit Risk by Artificial Neural Networks Models. ECONOMICS OF ENGINEERING DECISIONS. ISSN 1392 – 2785.

Boivin, P., Schäffer, B., Temgoua, E., Gratier, M., Steinman. G. 2006. Assessment of soil compaction using soil shrinkage modelling: Experimental data and perspectives. Soil & Tillage Research 88 (2006) 65–79.

Botta, G.F., Jorajuria, D., Rosatto, H., Ferrero, C. 2006. Light tractor traffic frequency on soil compaction in the Rolling Pampa region of Argentina. Soil & Tillage Research 86 (2006) 9–14.

Botta, G.F., Tolon-Becerra, A., Tourn, M., Lastra-Bravo, X., Rivero, D. 2012. Agricultural traffic: Motion resistance and soil compaction in relation to tractor design and different soil conditions. Soil & Tillage Research 120 (2012) 92–98.

Bowers, S.A., Hanks, R.J. 1965. REFLECTION OF RADIANT ENERGY FROM SOILS. Agricultural Research Service U.S. Department of Agriculture. Vol. 100, No. 2.

British Standards, 1998. Soil Quality: BS 7755: Section 5.4: 1998. Part 5: Physical Methods. Section 5.4: Determination of Particle Size Distribution in Mineral Soil Material – Method by Sieving and Sedimentation. British Standards Institution, UK.

British Standards, 2000. Soil Improvers and Growing Media: BS EN 13039:2000. Determination of Organic Matter Content and Ash. British Standards Institution, UK.

British Standards, 2007. Soil Improvers and Growing Media: BS EN 13040:2007. Sample Preparation for Chemical and Physical Tests, Determination of Dry Matter Content, Moisture Content and Laboratory Compacted Bulk Density. British Standards Institution, UK.

Burns, D.A. and Circzak, E.W. 2008. Handbook of Near-Infrared Analysis. Taylor and Francis Group. ISBN: 978-0-8493-7393-0.

Canarache, A. & Van den Akker, J.J.H. (2003). SOCOLIT and SOCODB, two European databases on soil compaction. Proceedings of the International Soil Tillage Research Organization 16th Triennial conference, Brisbane, 13–18 July, pp. 265–270.

Canillas, E. C. and Salokhe, V. M. (2002). Modeling compaction in agricultural soils. Journal of Terramechanics 39 (2002) 71–84.

Cantero-Martı´nez, C., Angas, P., Lampurlane´s, J. 2003. Growth, yield and water productivity of barley (*Hordeum vulgare* L.) affected by tillage and N fertilization in Mediterranean semiarid, rainfed conditions of Spain. Field Crops Research 84 (2003) 341–357.

Chamen, T., Alakukku, L., Pires, S., Sommer, C., Spoor, G., Tijink, F. and Weisskopf, P. 2003. Prevention strategies for field traffic-in -duced subsoil compaction: a review, Part 2. Equipment and field practices. In: Soil Tillage Research 73: 161-174.

Chamen, W.C.T. 2011. The effects of low and controlled traffic systems on soil physical properties, yields and the profitability of cereal crops on a range of soil types. School of Applied Sciences, Cranfield University thesis, 2011.

Chamen, W.C.T., Audsley, E., 1993. A study of the comparative economics of conventional and zero traffic systems for arable crops, Soil and Tillage Research, 25 (4), pp. 369-396.

Chang, C. W., Laird, D. A., Mausbach, M. J., and Hurburgh, C. R. (2001). Near-infrared reflectance spectroscopy-principal components regression analyses of soil properties. Soil Sci. Soc. Am. J. 65, 480–490.

Chen, G. and Weil, R. R. 2011. Root growth and yield of maize as affected by soil compaction and cover crops. Soil & Tillage Research 117 (2011) 17–27.

Chow, L., Xing, Z., Rees, H. W., Meng, F., Monteith, J. and Stevens, L. 2009. Field Performance of Nine Soil Water Content Sensors on a Sandy Loam Soil in New Brunswick, Maritime Region, Canada. Sensors 2009, 9, 9398-9413; doi:10.3390/s91109398.

Christy, C. D., Drummond, P., Laird, D. A., 2003. An on-the-go spectral reflectance sensor for soil. Paper No. 03-1044, ASAE, St. Joseph, Michigan.

Christy, C.D. 2008. Real-time measurement of soil attributes using on-the-go near infrared reflectance spectroscopy. Computers and electronics in agriculture 61 (2008) 10–19.

Clark, R. N. (1999). Spectroscopy of rocks and minerals and principles of spectroscopy. In "Remote Sensing for the Earth Sciences" (A. N. Rencz, Ed.), pp. 3–58. John Wiley & Sons, Chichester, UK.

Cosh, M. H., Jacksona, T. J., Bindlish, R., Famiglietti, J. S., Ryu, D. 2005. Calibration of an impedance probe for estimation of surface soil water content over large regions. Journal of Hydrology 311 (2005) 49–58.

Curcioa, D., Ciraolob, G., D'Asaroa, F., Minacapilli, M. 2013. Prediction of soil texture distributions using VNIR-SWIR reflectance spectroscopy. Procedia Environmental Sciences 19 (2013) 494 – 503.

Dalal, R.C., Henry, R.J., 1986. Simultaneous determination of moisture, organic carbon, and total nitrogen by near infrared reflectance spectrophotometer. Soil Sci. Soc. Amer. J. 50, 120-123.

Daniel Hillel (1998) Environmental Soil Physics. Academic Press, An Imprint of Elsevier. http://www.apnet.com. ISBN-13: 978-0-12-348525-0.

Daum, D. R. 2014. Soil Compaction and Conservation Tillage. Penn Tate Extension. College of Agricultural Science. Website: http://extension.psu.edu/plants/crops/soil-management/conservation-tillage/soil-compaction-and-conservation-tillage . visited at 21/04/2014.

Défossez, P., Richard, G., 2002. Models of soil compaction due to traffic and their evaluation. Soil Tillage Res. 67, 41–64.

Défossez, P., Richard, G., Keller, T., Adamiade, V., Govind, A., Mary, B. 2014. Modelling the impact of declining soil organic carbon on soil vcompaction: Application to a cultivated Eutric Cambisol with massive straw exportation for energy production in Northern France. Soil & Tillage Research 141 (2014) 44–54.

Department for Environment, Food and Rural Affairs (DEFRA), 2008. ENGLAND CATCHMENT SENSITIVE FARMING DELIVERY INITIATIVE. Website: http://archive.defra.gov.uk/foodfarm/landmanage/water/csf/documents/ecsfdi-phase1-report.pdf

DeJong-Hughes, J. F. Moncrief, W. B. Voorhees, and J. B. Swan. Soil compaction: causes, effects and control. University of Minnesota extension. WW-03115 2001. Website: http://www.extension.umn.edu/ agriculture/Tillage/soil-compaction/index.html.

Delta-T Devices Ltd. 1996. Theta Probe Soil Moisture Sensor Type ML1 User Manual. Delta-T Devices, Inc., Cambridge, England.

Delta-T Devices Ltd. 1999. Theta Probe Soil Moisture Sensor Type MLx2 User Manual. Delta-T Devices, Inc., Cambridge, England.

Dhillon, R. S., Adamchuk, V. I., Holland, K. H., Hempleman, C. R. 2010. Development of an Integrated On-the-Go Sensing System for Soil Properties. American Society of Agricultural and Biological Engineers. Paper Number: 1009817

Douglas, E. and McKyes, E. (1978). Compaction effects on the hydraulic conductivity of a clay soil. Soil Science 125(5), 278-282.

Duiker, S. 2004. Avoiding Soil Compaction. Information and Communication Technologies in the College of Agricultural Sciences. The Pennsylvania State University; www.cas.psu.edu.

Dworak, V., Selbeck, J., Ehlert, D. 2010. RANGING SENSORS FOR VEHICLE-BASED MEASUREMENTOF CROP STAND AND ORCHARD PARAMETERS: A REVIEW. American Society of Agricultural and Biological Engineers. Vol. 54(4): 1497-1510.

FAO, 2003. Soil compaction. Conservation of natural resources for sustainable agriculture. Website: http://www.fao.org/ag/ca/doc/soil_compaction.pdf . visited 1/3/2014.

Farifteh, J., Van der Meer, F., Atzberger, C., Carranza, E.J.M. 2007. Quantitative analysis of salt-affected soil reflectance spectra: A comparison of two adaptive methods (PLSR and ANN). Remote Sensing of Environment 110 (2007) 59–78.

Fernández-Gálvez, J. 2008. Errors in soil moisture content estimates induced by uncertainties in the effective soil dielectric constant. International Journal of Remote Sensing. Vol. 29, No. 11, 10 June 2008, 3317–3323.

Ferrero, A., Lipiec, J., 2000. Determining the effect of trampling on soils in hillslope woodlands. Int. Agrophys. 14, 9–16.

Fleige, H., Horn, R., 2000. Field experiments of the effect of soil compaction on soil properties, runoff, interflow and erosion. In: Horn, R., et al. (Eds.), Subsoil Compaction Distribution, Processes and Consequences. Advance in GeoEcology, vol. 32. Catena Verlag, Reiskirchen, Germany, pp. 258–268.

Foley, J.L., Harris, E. 2007. Field calibration of ThetaProbe (ML2x) and ECHO probe (EC-20) soil water sensors in a Black Vertosol. Australian journal of soil research, 45(3), 233-236.

Franzen, H., Lal, R., Ehlers, W., 1994. Tillage and mulching effects on physical properties of a tropical Alfisol. Soil & Tillage Research 28, 329–346.

Frey B., Kremer J., Rüdt A., Sciacca S., Matthies D., Lüsche P., 2009. Compaction of forest soils with heavy logging machinery affects soil bacterial community structure. European Journal of Soil Biology 45 (2009) 312–320.

Fullen, M. A. 1985. COMPACTION, HYDROLOGICAL PROCESSES AND SOIL EROSION ON LOAMY SANDS IN EAST SHROPSHIRE, ENGLAND. Soil & Tillage Research, 6 (1985) 17-29.

Gaskin, G. J. and Miller, J. D. 1996. Measurement of Soil Water Content Using a Simplified Impedance Measuring Technique. J. agric. Engng. Res. (1996) 63, 153 – 160.

Gauglitz, G. and Vo-Dinh, T. 2003. Handbook of Spectroscopy. WILEY-VCH Verlag GmbH & Co. ISBN: 3-527-29782- 0.

Glancey, J. L., Upadhyaya, S. K., Chancellor, W. J., Rumsey, J. W., 1989. An instrumented chisel for the study of soil-tillage dynamics. Soil & Tillage Research, 14, 1-24.

Grossman, R.B., 1981. Bulk Density: Application, Estimation, and Field Management (second approximation). Nat. Soil Survey Lab., Soil Cons. Survey, Lincoln, NE.

Günaydin, O., 2009. Estimation of soil compaction parameters by using statistical analyses and artificial neural networks. Environmental Geology 57, 203–215.

Hakansson, I., 1990. A method for characterizing the state of compactness of the plough layer, Soil Tillage Research, 16: 105-120.

Hall, H. E., and Raper, R. L. 2005. DEVELOPMENT AND CONCEPT EVALUATION OF AN ON-THE-GO SOIL STRENGTH MEASUREMENT SYSTEM. American Society of Agricultural Engineers. Vol. 48(2): 469−477.

HALLIKAINEN, M. T., ULABY, F. T., DOBSON, M. C., EL-RAYES, M. A., WU, L. 1985. Microwave Dielectric Behavior of Wet Soil-Part 1: Empirical Models and Experimental Observations. TRANSACTIONS ON GEOSCIENCE AND REMOTE SENSING, VOL. GE-23, NO. 1, JANUARY 1985.

Hamza, M.A. and Anderson, W.K. 2005. Soil compaction in cropping systems A review of the nature, causes and possible solutions. Soil & Tillage Research 82 (2005) 121–145.

Hanson, B. R. and Peters, D. 2000. Soil type affects accuracy of dielectric moisture sensors. California Agriculture, May-June 2000, website: http://cekings.ucanr.edu/files/19211.pdf .

Haynes, M. A. 2010. Comparison of Methods to Remediate Compacted Soils for Vegetative Establishment. North Carolina State University, Soil Science, MSc thesis.

Hemmat, A., and Adamchuk, V.I. 2008. Sensor systems for measuring soil compaction: Review and analysis. Computers and electronics in agriculture 6 3 (2 0 0 8) 89–103.

Hemmat, A., Khorsandy, A., Masoumi, A.A., Adamchuk, V.I. 2009. Influence of failure mode induced by a horizontally operated single-tip penetrometer on measured soil resistance. Soil & Tillage Research 105 (2009) 49–54.

Hester, R.E. and Harrison, R. M. 2012. Soils and Food Security. The Royal Society of Chemistry. Vol. 35. ISBN: 978-1-84973-426-4.

Hollas, J. M. 2004. Modern Spectroscopy. Fourth edition, John Wiley & Sons, Inc. ISBN 0 470 84416 7.

Holmes, K. W., Wherrett, A., Keating, A., Murphy, D. V. 2011. Meeting bulk density sampling requirements efficiently to estimate soil carbon stocks. Soil Research 49(8) 680-695.

Horn, R, van den Akker, J.J.H., Arvidsson, J., 2000. Subsoil compaction: Distribution, processes and consequences. Deutsche Bibliothek, Germany.

Horn, R., Domial, H., Anna Slowihka-Jurkiewicz, van Ouwerkerk, C. 1995. Soil compaction processes and their effects on the structure of arable soils and the environment. Soil & Tillage Research 35 (1995) 23-36.

Horn, R., Way, T., Rostek, J., 2001. Effect of repeated wheeling on stress/strain properties and ecological consequences in structured arable soils. Revista de la Ciencia del Sueloy Nutricion Vegetal 1, 34–40.

Hummel, J. W., Ahmad, I. S., Newman, S. C., Sudduth, K. A., Drummond, S. T. 2004. SIMULTANEOUS SOIL MOISTURE AND CONE INDEX MEASUREMENT. American Society of Agricultural Engineers. Vol. 47(3): 607−618.

Jones, S. B., Wraith, J. M. and Or, D., 2002. Time domain reflectometry measurement principles and applications. Hydrol. Process. 16, 141–153.

Kaleita, A. L., Heitman, J. L., Logsdon, S. D. 2005. FIELD CALIBRATION OF THE THETAPROBE FOR DES MOINES LOBE SOILS. American Society of Agricultural Engineers, Applied Engineering in Agriculture, Vol. 21(5): 865−870.

Kano, Y., W. F. McClure, and R. W. Skaggs. 1985 A near infrared reflectance soil moisture meter. Transactions of the ASAE 28(6): 1852–1855.

Keller, T and Arvidsson, J. 2004. Technical solutions to reduce the risk of subsoil compaction: effects of dual wheels, tandem wheels and tyre inflation pressure on stress propagation in soil. Soil & Tillage Research 79 (2004) 191–205.

Kelly, K.B. (1985). Effects of soil modification and treading on pasture growth and physical properties of an irrigated red-brown earth. Australian Journal of Agricultural Research 36: 799-807.

Khalilmoghadam, B., Afyuni, M., Abbaspour, K.C., Jalalian, A., Dehghani, A.A., Schulin, R., 2009. Estimation of surface shear strength in Zagros region of Iran – a comparison of artificial neural networks and multiple-linear regression models. Geoderma 153, 29–36.

Kodaira, M. and Shibusawa, S. 2013. Using a mobile real-time soil visible-near infrared sensor for high resolution soil property mapping. Geoderma 199 (2013) 64–79.

Kuang, B. 2013. On-line Measurement of Some Selected Soil Properties for Controlled Input Crop Management Systems. PhD Thesis, School of Applied Sciences. Cranfield University.

Kuang, B. and Mouazen, A.M. 2011. Effects of soil moisture content and soil texture on Vis-NIR spectroscopy prediction of key soil properties at field scale. Geophysical Research Abstracts. Vol. 13, EGU2011-7703, 2011.

Kuang, B. and Mouazen, A.M. 2012. Influence of numbers of samples on prediction error of visible and near infrared spectroscopy of selected soil properties at farm scale. European Journal of Soil Science, 2012, volume 63, Issue 3, pp421-429.

Kuang, B. and Mouazen, A.M. 2013. Non-biased prediction of soil organic carbon and total nitrogen with viseNIR spectroscopy, as affected by soil moisture content and texture. Biosystems Engineering 114 (2013) 249 – 258.

Kuang, B.; Mahmood, H. S.; Quraishi, Z.; Hoogmoed, W. B.; Mouazen, A. M.; van Henten, E. J., 2012. Sensing soil properties in the laboratory, in situ, and on-line: a review. In Donald Sparks, editors: Advances in Agronomy, 114, AGRON, UK: Academic Press, 155-224.

Kunwar, P., Singh, Gupta, S., Kumar, A., Shukla, S. P. 2012. Linear and nonlinear modelling approaches for urban air quality prediction.

Kweon, G., Lund, E., Maxton, C., Drummond, P., Jensen, K. 2008. In Situ Measurement of Soil Properties Using a Probe-Based VIS- NIR Spectrophotometer. Paper Number: 084399, ASABE, USA.

Lal, R. 2006. Encyclopaedia of Soil Science. Taylor & Francis Group, LLC. ISBN: 0-8493-5053-0.

Lal, R. and Shukla, M. K. 2004. Principles of soil physics. Marcel Dekker, Inc. ISBN: 0-8247-5324-0. Website: http://books.google.co.uk/

books?id=3IeGCMKvPZwC&pg=PA197&dq=soil+strength&hl=en&sa=X&ei=2LtTU5uJI7GV7AbBjoCYAw&redir_esc=y#v=onepage&q&f=true.

Lamers, J.G., Perdok, U.D., Lumkes, L.M., Klooster, J.J., 1986. Controlled traffic farming systems in the Netherlands, Soil and Tillage Research, 8, pp. 65-76.

Lee, K. S., Lee, D. H., Sudduth, K. A., Chung, S. O., Kitchen, N. R., Drummond, S.T. 2009. WAVELENGTH IDENTIFICATION AND DIFFUSER EFLECTANCE ESTIMATION FOR SURFACE AND PROFILE SOIL PROPERTIES. Transactions of the ASABE, Vol. 52(3): 683-695.

Lemus, R. 2011. Breaking Down Soil Compaction: Does It Increase Forage Production? Mississippi State University Extension Service. website: http://msucares.com/pubs/publications/p2657.pdf .

Li, D., Chen, X., Peng, Z., Chen, S., Chen, W., Han, L., Li, Y. 2012. Prediction of soil organic matter content in a litchi orchard of South China using spectral indices. Soil & Tillage Research 123 (2012) 78–86.

Lin, J., Sun, Y., Lammers, P.S. 2014. Evaluating model-based relationship of cone index, soil water content and bulk density using dual-sensor penetrometer data. Soil & Tillage Research 138 (2014) 9–16.

Lipiec, J. and Stępniewski, W. 1995. Effects of soil compaction and tillage systems on uptake and losses of nutrients. Soil & Tillage Research 35 (1995) 37-52.

Lipiec, J., Arvidsson, J., E. Murer. 2003. Review of modelling crop growth, movement of water and chemicals in relation to topsoil and subsoil compaction. Soil & Tillage Research 73 (2003) 15–29.

Lipiec, J., Wȯjciga, A. and Horn, R. 2009. Hydraulic properties of soil aggregates as influenced by compaction. Soil & Tillage Research 103 (2009) 170–177.

Liu X., Ren T. and Horton R. 2008. Determination of Soil Bulk Density with Thermo-Time Domain Reflectometry Sensors. Soil Science Society of America Journal: Volume 72: Number 4 • July–August 2008.

Mahmood, H. S., Hoogmoed, W. B., van Henten, E. J. 2012. Sensor data fusion to predict multiple soil properties. Precision Agric (2012) 13:628–645.

Martens, H. & Naes, T. (1989). Multivariate Calibration, 2nd edition. John Wiley & Sons, Ltd., Chichester. ISBN: 978-0-471-93047-1.

Marín-González, Boyan Kuang, Mohammed Z. Quraishi, Miguel A´ngel Muno´z-Garcı´a, Mouazen, A. M. 2013. On-line measurement of soil properties without direct spectral response in near infrared spectral range. Soil & Tillage Research 132 (2013) 21–29.

Miller, C.E., 2001. Chemical principles on near-infrared technology. In: Williams, P. Norris, K., (Eds.). Near-Infrarde Technology in the American Association of Cereal Chemists, Inc. St. Paul, Minnesota, USA, 19-37.

Miller, J.D., Gaskin, G.J., 1997. The Development and Application of the ThetaProbe Soil Water Sensor. MLURI Technical note.

Mitchel, J., Jackson, L., Miyan, G. 2004. Minimum Tillage Vegetable Crop Production in California, Division of Agriculture and Natural Resources, University of California, Publication 8132.

Mittelbach, H. 2011. Soil Moisture in Switzerland: Analyses from the Swiss Soil Moisture Experiment. DOCTOR OF SCIENCES thesis submitted to ETH ZURICH, Diss. ETH No. 20114. Website: http://e-collection.library.ethz.ch/eserv/eth:5423/eth-5423-02.pdf

Moret-Fernández, D., Vicente, J., Aragüés, R., Peña, C., López, M.V. 2012. A new TDR probe for measurements of soil solution electrical conductivity. Journal of Hydrology 448–449 (2012) 73–79.

Morgan, C.L.S., Waiser, T. H., Brown, D. J., Hallmark, C. T. 2009. Simulated in situ characterization of soil organic and inorganic carbon with visible near-infrared diffuse reflectance spectroscopy. Geoderma 151 (20 09) 249–256.

Mosaddeghi, M.R., Koolen, A.J., Hajabbasi, M.A., Hemmat, A., Keller, T., 2007. Suitability of pre-compression stress as the real critical stress of unsaturated agricultural soils. Biosyst. Eng. 98, 90–101.

Motavalli, P.P., Anderson, S.H., Pengthamkeerati, P., Gantzer, C.J. 2003. Use of soil cone penetrometers to detect the effects of compaction and organic amendments in claypan soils. Soil & Tillage Research 74 (2003) 103–114.

Mouazen, A.M. and Ramon, H. 2006. Development of on-line measurement system of bulk density based on on-line measured draught, depth and soil moisture content. Soil & Tillage Research 86 (2006) 218–229.

Mouazen, A.M., 2009. The future for on-line measurement of soil properties with sensor fusion systems. Landwards, IAgrE Professional Journal. 64(1), 14-16.

Mouazen, A.M., Dumont, K., Maertens, K., Ramon, H., 2003. Two-dimensional prediction of spatial variation in topsoil compaction of a sandy loam field-based on measured horizontal force of compaction sensor, cutting depth and moisture content. Soil Till. Res. 74, 91–102.

Mouazen, A.M., Karoui, R., De Baerdemaeker, J. & Ramon, H. 2006. Characterization of soil water content using measured visible and near infrared spectra. Soil Science Society of America Journal, 70, 1295-1302.

Mouazen, A.M., Kuang, B., De Baerdemaeker, J., Ramon, H. 2010. Comparison among principal component, partial least squares and back propagation neural network analyses for accuracy of measurement of selected soil properties with visible and near infrared spectroscopy. Geoderma 158 (2010) 23–31.

Mouazen, A.M., Maleki, M.R., Breadmaker, J.D., Ramon, H. 2007. On-line measurement of some selected soil properties using a VIS–NIR sensor. Soil & Tillage Research 93 (2007) 13–27.

Mouazen, A.M., Maleki, M.R., De Baerdemaeker, J., Ramon, H. 2007. On-line measurement of some selected soil properties using a VIS–NIR sensor. Soil & Tillage Research 93 (2007) 13–27.

Mouazen, A.M., Ramon, H., Baerdemaeker, J.D., 2002. Effects of bulk density and moisture content on selected mechanical properties of sandy loam soil, Biosystems Engineering, 83, 217-224.

Mouazen, A.M.; De Baerdemaeker, J. Ramon, H., 2005b. Towards development of on-line soil moisture content sensor using a fibre-type NIR spectrophotometer. Soil & Tillage Research, 80(1-2), 171-183.

Mouazen, A.M.; De Baerdemaeker, J.; Ramon, H., 2006b. Effect of wavelength range on the measurement accuracy of some selected soil properties using visual-near infrared spectroscopy. Journal of Near Infrared Spectroscopy, 14(3), 189-199.

Mouazen, A.M.; Karoui, R.; De Baerdemaeker, J.; Ramon, H., 2005a. Classification of soil texture classes by using soil visual near infrared

spectroscopy and factorial discriminant analysis techniques. Journal of Near Infrared Spectroscopy. 13(4), 231-240.

Mouazen, A.M.; Karoui, R.; De Baerdemaeker, J.; Ramon, H., 2006a. Characterization of soil water content using measured visible and near infrared spectra. Soil Science Society of America Journal, 70, 1295-1302.

Mouazen, A.M.; Kuang, B.; De Baerdemaeker, J.; Ramon, H., 2010. Comparison between principal component, partial least squares and back propagation neural network analyses for accuracy of measurement of selected soil properties with visible and near infrared spectroscopy. Geoderma, 158(1-2): 23-31.

Mouazen, A.M.; Ramon, H., 2006. Development of on-line measurement system of bulk density based on on-line measured draught, depth and soil moisture content. Soil & Tillage Research, 86 (2), 218-229.

Mouazen, A.M.; Ramon, H., 2009. Expanding implementation of an on-line measurement system of topsoil compaction in loamy sand, loam, silt loam and silt soils. Soil & Tillage Research, 103(1): 98-104.

Mouazen, A.M.; Ramon, H., 2009. Expanding implementation of an on-line measurement system of topsoil compaction in loamy sand, loam, silt loam and silt soils. Soil & Tillage Research, 103 (1): 98-104.

Naderi-Boldaji, M. Alimardani, R., Hemmat, A., Sharifi, A., Keyhani, A., Dolatsha, A., Keller, T. 2012a. Improvement and field testing of a combined horizontal penetrometer for on-the-go measurement of soil water content and mechanical resistance. Soil & Tillage Research 123 (2012) 1–10.

Naderi-Boldaji, M., Sharifi , A., Alimardani, R., Hemmat, A., Keyhani, A., Loonstra , E.H., Weisskopf, P., Stettler, M., Keller, T. 2013. Use of a triple-sensor fusion system for on-the-go measurement of soil compaction. Soil & Tillage Research 128 (2013) 44–53.

Naderi-Boldaji, M., Sharifi, A., Jamshidi, B., Younesi-Alamouti, M., Minaee, S. 2011. A dielectric-based combined horizontal sensor for on-the-go measurement. Sensors and Actuators A 171 (2011) 131– 137.

Namdar-Khojasteh, D, Shorafa, M. and Omid, M (2010). Using of Artificial Neural Networks for Evaluation Soil Water Content with Time Domain Reflectometry. Modern Applied Science, Vol. 4, No. 10; October 2010.

Nevens, F. and Reheul, D. 2003. The consequences of wheel-induced soil compaction and subsoiling for silage maize on a sandy loam soil in Belgium. Soil & Tillage Research 70 (2003) 175–184.

Newell-Price, J.P., Whittingham, M.J., Chambers, B.J., Peel, S. 2013. Visual soil evaluation in relation to measured soil physical properties in a survey of grassland soil compaction in England and Wales. Soil & Tillage Research 127 (2013) 65–73.

Nocita, M., Stevens, A., Noon, C., Wesemael, B. 2013. Prediction of soil organic carbon for different levels of soil moisture using Vis-NIR spectroscopy. Geoderma 199 (2013) 37–42.

Nocita, M., Stevens, A., Toth, G., Panagos, P., Wesemael, B., Montanarella, L. 2014. Prediction of soil organic carbon content by diffuse reflectance spectroscopy using a local partial least square regression approach. Soil Biology & Biochemistry 68 (2014) 337-347.

Osborne, B. G., Fearn, T., Hindle, P. H. 1993. Practical Spectroscopy. Longman Scientific & Technical, The UK, ISBN: 0-582-09946-3.

Patel, S.K., Mani, I. 2011. Effect of multiple passes of tractor with varying normal load on subsoil compaction. Journal of Terramechanics 48 (2011) 277–284.

Peter, S. L. and Yurui, S. 2004. Combined Sensor for Simultaneous Investigation of Cone Index and Soil Water Content. ASAE/CSAE. Paper Number: 041046.

Pietrzykowski, M and Chodak, M. 2014. Near infrared spectroscopy—A tool for chemical properties and organic matter assessment of afforested mine soils. Ecological Engineering 62 (2014) 115– 122.

Ponizovsky, Chudinova, S.M., Pachepsky, Y.A. 1999. Performance of TDR calibration models as affected by soil texture. Journal of Hydrology 218 (1999) 35–43.

Presbitero, A.L., Rose, C.W., Yu, B., Ciesiolka, C.A.A., Coughlan, K.J., Fentie, B., 2005. Investigation of soil erosion from bare steep slopes of the humid tropic Philippines, Earth Interactions, volume 9, paper 5.

Quraishi, M. Z. 2013. EVALUATION OF FIELD SOIL COMPACTION USING INNOVATIVE SENSORS AND TECHNIQUES. EngD THESIS. SCHOOL OF APPLIED SCIENCES. Cranfield University.

Quraishi, M.Z.; Mouazen, A.M., 2013a. Calibration of an on-line sensor for measurement of topsoil bulk density in all soil textures. Soil & Tillage Research, 126: 219-228.

Quraishi, M.Z.; Mouazen, A.M., 2013b. Development of a methodology for in situ assessment of topsoil dry bulk density. Soil & Tillage Research, 126: 229-237.

Quraishi and Mouazen (2013c). A prototype sensor for the assessment of soil bulk density . Soil & Tillage Research 134 (2013) 97–110.

Radford, B.J., Yule, D.F., McGarry, D., Playford, C. 2001. Crop responses to applied soil compaction and to compaction repair treatments. Soil & Tillage Research 61 (2001) 157–166.

Raper, R.L., Schwab, E.B., Dabney. S.M. 2005. Measurement and variation of site-specific hardpans for silty upland soils in the Southeastern United Statess. Soil & Tillage Research 84 (2005) 7–17.

Richard, G., Cousin, I., Sillon, J.F., Bruand, A., Gue´rif, J., 2001. Effect of compaction on the porosity of a silty soil: influence on unsaturated hydraulic properties. Eur. J. Soil Sci. 52, 49–58.

Robinson, D. A., Jones, S. B., Wraith, J. M., Or, D. and Friedman, S. P. 2003. A Review of Advances in Dielectric and Electrical Conductivity Measurement in Soils Using Time Domain Reflectometry. Vadose Zone Journal 2:444–475 (2003).

Robinson, D.A., Gardner, C.M.K., Cooper, J.D. 1999. Measurement of relative permittivity in sandy soils using TDR, capacitance and theta probes: comparison, including the effects of bulk soil electrical conductivity. Journal of Hydrology 223 (1999) 198–211.

Rodríguez, L. A., Valencia. J. J, Urbano, J A. 2012. Soil compaction and tires for harvesting and transporting sugarcane. Journal of Terramechanics 49 (2012) 183–189.

Rosolem, C.A., Foloni, J.S.S. and Tiritan, C.S. 2001. Root growth and nutrient accumulation in cover crops as affected by soil compaction. Soil & Tillage Research 65 (2002) 109–115.

Rowlandson, T. L., Berg, A. A., Bullock, P. R., Ojo, E. R., McNairn, H., Wiseman, G., Cosh, M. H. 2013. Evaluation of several calibration procedures for a portable soil moisture sensor. Journal of Hydrology 498 (2013) 335–344.

Sarani, N and Afrasiab, P. (2012). Effect of soil texture on moisture measurement accuracy with Theta probe ML2 in Sistan region. International Conference on Chemical, Ecology and Environmental Sciences (ICEES'2012) march 17-18, 2012 Bangkok. Website: psrcentre.org/images/extraimages/phpPv.pdf .

Schmutz, P. P. 2007. INVESTIGATION OF UTILITY OF DELTA-T THETA PROBE FOR OBTAINING SURFICIAL MOISTURE MEASUREMENTS ON BEACHES. MSc Thesis, Agricultural Mechanical College, Louisiana State University, USA.

Schnaid, F. 2009. In Situ Testing in Geomechanics. The main tests. Taylor and Francls. ISBN: 0-203-93133-5. website: http://books.google.co.uk/books?id=IdvAUPwHzhsC&pg=PA151&dq=shear+vane&hl=en&sa=X&ei=lAlUU5PZIMyg7Abos4BQ&ved=0CDUQ6AEwBjgK#v=onepage&q=shear%20vane&f=true .

Schäffer, B., Attinger, W., Schulin, R. 2007. Compaction of restored soil by heavy agricultural machinery—Soil physical and mechanical aspects. Soil & Tillage Research 93 (2007) 28–43.

Servad, P., Marsili, A., Vignozzi, N., Pellegrini, S., Pagliai, M. 2005. Effects on some soil qualities in central Italy following the passage of four wheel drive tractor fitted with single and dual tires. Soil & Tillage Research 84 (2005) 87–100.

Seyfried, M. S., Grant, L. E., Du, E. and Humes, K. 2005. Dielectric Loss and Calibration of the Hydra Probe Soil Water Sensor. Vadose Zone Journal 4:1070–1079 (2005).

Shaxson, F. and Barber, R. 2003. Optimizing Soil Moisture for Plant Production. FOOD AND AGRICULTURE ORGANIZATION OF THE UNITED NATIONS (FAO). ISBN 92-5-104944-0. website: http://www.fao.org/docrep/006/y4690e/y4690e00.htm#Contents .

Sheng, W., Sun, Y., Schulze Lammers, P., Schumann, H., Berg, A., Shi, C., Wang, C. 2011. Observing soil water dynamics under two field conditions by a novel sensor system. Journal of Hydrology 409 (2011) 555–560.

Sherman, D. M., Waite, T.D. (1985). Electronic spectra of Fe^{3+} oxides and oxide hydroxides in the near-IR to near-UV, Am. Mineral. 70 1262–1269.

Shonk, J. L, Gaultney L. D, Schulze D. G, Scoyoc, G. E. V. (1991). Spectroscopic sensing of soil organic matter content.Trans. ASAE,34: 1978-1984.

Siczek, A., and Lipiec, J. 2011. Soybean nodulation and nitrogen fixation in response to soil compaction and surface straw mulching. Soil & Tillage Research 114 (2011) 50–56.

Singh, K.K., Colvin, T.S., Erbach, D.C., Mughal, A.Q., 1992. Tilth index: an approach to quantifying soil tilth. Transactions of ASAE 35 (6), 1777–1785.

Singh, K.P. Gupta, S., Kumar, A., Shukla, S.P. 2012. Linear and nonlinear modeling approaches for urban air quality prediction. Science of the Total Environment 426 (2012) 244–255

Sinha, S.K. and Wang, M.C. 2008. Artificial neural network prediction models for soil compaction and permeability. Geotechnical and Geological Engineering 26, 47–64.

Smith, K. A. and Mullins, C. E. 2000. Soil and Environmental Analysis Physical Methods. Second Edition, Marcel Dekker, Inc. ISBN: 0-8247-0414-2.

Soane, B.D. and van Ouwerkerk, C. 1995. Implications of soil compaction in crop production for the quality of the environment. Soil & Tillage Research 35 (1995) 5-22.

SOANE, B.D., DICKSON, J.W. and CAMPBELL, D.J. 1982. COMPACTION BY AGRICULTURAL VEHICLES: A REVIEW III. INCIDENCE AND CONTROL OF COMPACTION IN CROP PRODUCTION. Soil & Tillage Research, 2 (1982) 3-36.

Soehne, 1958. Journ. of Agr. Eng.

Spoor, G., Tijink, F.G.J. and Weisskopf, P. 2003. Subsoil compac-tion: risk, avoidance, identification and alleviation. In: Soil Tillage Research 73: 175-182.

StatSoft, 2012. STATISTICA 12 – Data Analysis Software System.

Stenberg, B. 2010. Effects of soil sample pretreatments and standardised rewetting as interacted with sand classes on Vis-NIR predictions of clay and soil organic carbon. Geoderma 158 (2010) 15–22.

Stenberg, B.; Viscarra Rossel, R.; Mouazen, A.M.; Wetterlind, J., 2010. Visible and near infrared spectroscopy in soil science. Advances in Agronomy, 107: 163-215.

Stiegler, J. H. 2014. Soil Compaction and Crusts. Oklahoma Cooperative Extension Service. PSS-2244. website: http://soilwater.okstate.edu/cropland-soil- management/compaction/factsheets/pss2244web.pdf .

Stombaugh, T. S. 2014. Soil Sensor. University of Kentucky, USA. Website: https://www.bae.uky.edu/tstomb/soil_sensor.htm.

Strudley, M. W., Green, T. R. and Ascoug, J. C. 2008. Tillage effects on soil hydraulic properties in space and time: State of the science. Soil & Tillage Research 99 (2008) 4–48.

Sun, Y., Cheng, Q., Lin, J., Schulze, P., Lammers Berg, A., Meng, F., Zeng, Q., Li, L., 2011. Energy-based comparison between a dynamic cone penetrometer and a motor-operated static cone penetrometer. Soil & Tillage Research 105–109, 115–116.

Sun, Y., Ma, D., Lammers, P. S., Schmittmann, O., Rose. M. 2006. On-the-go measurement of soil water content and mechanical resistance by a combined horizontal penetrometer. Soil & Tillage Research 86 (2006) 209–217.

Sun, Z.J., Young, G.D. 2015. A COST EFFECTIVE SOIL MOISTURE INSTRUMENT BASED ON TIMEDOMAIN TRANSMISSION MEASUREMENT. E.S.I. Environmental Sensors Inc.,100-4243 Glanford Avenue, Victoria, British Columbia, Canada. V8Z 4B9. Website: http://www.iti.northwestern.edu/tdr/tdr2001/reviewers/hardware/sun2/Sun2.pdf

Taghavifar, H. and Mardani, A. 2014. Effect of velocity, wheel load and multipass on soil compaction. Journal of the Saudi Society of Agricultural Sciences (2014) 13, 57–66.

Tarawally, M.A., Medina, H., Frómeta, M.E., Itza, C. A. 2004. Field compaction at different soil-water status: effects on pore size distribution and soil water characteristics of a Rhodic Ferralsol in Western Cuba. Soil & Tillage Research 76 (2004) 95–103.

Tekeste, M. Z., Raper, R. L., Tollner, E. R., Way, T. R. 2005. Effect of Soil Moisture, Soil Density, and Cone Penetrometer Material on Finite Element Prediction of Soil Hardpan Depth. ASAE. Paper Number: 051164 St. Joseph, Mich.: ASAE.

Tekin, Y.; Tumsavas, Z.; Mouazen, A.M., 2012. Effect of moisture content on prediction of organic carbon and pH using visible and near infrared spectroscopy. Soil Science Society of America Journal, 76(1): 188-198.

Terashima, E., Fujii, E., Mishima, K., 1999. Experimental studies on the effect of trampling on the root system of seedlings of Zelkova serrata Makino. Technical Bull. Faculty Horticult. Chiba Univ. 53, 85 –92.

Thomas, G.W., Haszler, G.R., Blevins, R.I., 1996. The effect of organic matter and tillage on maximum compactibility of soils using the proctor test. Soil Sci. 161, 502 –508.

Thompson, S. and Staley, J. 2014. Foundations of spectroscopy. Web-base document, visited on 20/02/2014, at: http://www.smallscalechemistry.colostate.edu/PowerfulPictures/FoundationsOfSpectroscopy.pdf .

Tolon-Becerra, A., Tourn, M., Botta, G.F., Lastra-Bravo, X. 2011. Effects of different tillage regimes on soil compaction, maize (Zea mays L.) seedling emergence and yields in the eastern Argentinean Pampas region. Soil & Tillage Research 117 (2011) 184–190.

Topp, G. C., and Reynolds, W. D. 1998. Time domain refectometry: a seminal technique for measuring mass and energy in soil. Soil & Tillage Research 47 (1998) 125-132.

Topp, G. C., Davies, J. L., Annan, A. P., 1980. Electromagnetic determination of soil water content: measurements in coaxial transmission lines. Water Res. Research 16, 574–582.

Tóth, G., Montanarella, L. and Rusco, E. 2008. Threats to Soil Quality in Europe. Institute for Environment and Sustainability, European Commission. Scientific and Technical Research series – ISSN 1018-5593.

Tranter, G., Holmes, J., Lindon, J. 2000. Encyclopedia of Spectroscopy and Spectrometry. Elsevier, ISBN: 0-12-226680-3.

Unillever, 2010. Soil Management, Good Practices for Soil Management. Website: http://www.growingforthefuture.com/unileverimpguid/content/3-3-3

Vaz, C.M.P., Bassoi, L. H. and Hopmans, J. W. 2001. Contribution of water and bulk density of field soil penetration resistance as measurement by a combined cone penetrometer-TDR probe. Soil and Tillage Research 60 (2001) 35-42.

Viacheslav I. Adamchuk, Abbas Hemmat, Abdul M. Mouazen. 2008. Soil Compaction Sensor Systems – Current Developments. Paper Number: 083994. St. Joseph, Michigan: ASABE.

Viscarra Rossel, R.A. and Behrens, T. 2010. Using data mining to model and interpret soil diffuse reflectance spectra. Geoderma 158 (2010) 46–54

Viscarra Rossel, R.A. and McBratney, A.B. 1998. Laboratory evaluation of a proximal sensing technique for simultaneous measurement of soil clay and water content. Geoderma 85 1998 19–39.

Viscarra Rossel, R.A. Cattle, S.R., Ortega, A. Fouad. Y. 2009. In situ measurements of soil colour, mineral composition and clay content by vis–NIR spectroscopy. Geoderma 150 (2009) 253–266.

Viscarra Rossel, R.A., Behrens, T. 2010. Using data mining to model and interpret soil diffuse reflectance spectra Original. Research Article Geoderma, Volume 158, Issues 1–2, 15 August 2010, Pages 46-54.

Viscarra Rossel, R.A., McBratney, A .B. 1998. Soil chemical analytical accuracy and costs: implications from Precision Agriculture. Australian Journal of Experimental Agriculture 38, 765 – 775.

Viscarra Rossel, R.A.; Walvoort, D. J. J.; McBratney, A. B.; Janik, L. J.; Skjemstad, J. O. (2006). Visible, near infrared, mid infrared or combined diffuse reflectance spectroscopy for simultaneous assessment of various soil properties. Geoderma 131, 59-75.

Waiser, T. H.; Morgan, C. L. S.; Brown, D. J.; Hallmark, C. T. (2007). In situ characterization of soil clay content with visible near-infrared diffuse reflectance spectroscopy. Soil Science Society of America Journal 71, 389-396.

Walker, J.P., Houser, P.R. 2002. Evaluation of the OhmMapper instrument for soil moisture measurement. Soil Sci. Soc. Am. J. 66:728–734.

Wang, X., Li, H., Gao, H., Du, B., He, J., Li, W., 2005. Controlled traffic conservation tillage using small to middle sized machinery in China, Proceedings of SPIE - The International Society for Optical Engineering, 5884, pp. 1-12.

Wijaya, K., NISHIMURA, T. and KATO, M. 2003. Estimation of Dry Bulk Density of Soils Using Amplitude Domain Reflectometry Probe. J. Jpn. Soc. Soil Phys. No. 95, p.63 – 73 (2003).

Wijaya, K., Nishimura, Y., Kato, M., Nakagawa, M., 2004. Field estimation of soil dry bulk density using amplitude domain reflectometry data. Journal of Japanese Society of Soil Physics 97, 3–12.

Wikipedia, 2014a. Porosity. The free encyclopedia, website: http://en.wikipedia.org/wiki/ Porosity. Website visited 20/04/2014.

Wikipedia. 2014b. Time-domain reflectometer. The free encyclopedia. Wikimedia Foundation, Inc. 2 December 2013. Web-based document accessed on 18th of January, 2014 at: http://en.wikipedia.org/wiki/Time-domain_reflectometer .

Willatt, S.T. and Pullar, D.M. (1983). Changes in soil physical properties under grazed pastures. Australian Journal of Soil Research 22: 343-348.

Wolkowski, R. and Lowery, B. 2008. Soil compaction, causes, concerns and cures. University of Wisconsin-Extension http://www.soils.wisc.edu/extension/pubs/A3367.pdf

Yang, H., Kuang, B., Mouazen, A. M. 2011. Prediction of soil TN and TC at a farm-scale using VIS-NIR spectroscopy. Advanced Materials Research, 2011, Volume 225-226, Issue 1-2, pp1258-1261.

Zhang, S., Grip, S. H. and Lövdahl, L. 2006. Effect of soil compaction on hydraulic properties of two loess soils in China. Soil & Tillage Research 90 (2006) 117–125.

Zhang, S., Grip, S. H. and Lövdahl, L. 2006. Effect of soil compaction on hydraulic properties of two loess soils in China. Soil & Tillage Research 90 (2006) 117–125.

Appendixes

Appendix 1 Different artificial neural networks (ANN) analyses for the measurement of volumetric (θv) and gravimetric (ω) moisture content for L1 (0.11 g g^{-1} and 0.15 cm^3 cm^{-3}), L2 (0.20 g g^{-1} and 0.23 cm^3 cm^{-3}) and L3 (0.28 g g^{-1} and 0.32 cm^3 cm^{-3}). Data used as input are output voltage (V) and visible and near infrared spectra (Spec).

MC Level	Network Structure	Training R^2	Cross-validation R^2	Training error	Cross-validation error	Training algorithm	Hidden activation	Output activation
L1	172-8-2	0.95	0.95	0.000104	0.000212	BFGS 38	Log.	Exp.
L2	172-8-2	0.99	0.98	0.000139	0.000125	BFGS 103	Log.	Exp.
L3	172-8-2	1.00	0.99	0.000056	0.000255	BFGS 162	Log.	Identity
Collective	172-18-2	0.99	0.96	0.000149	0.000276	BFGS 120	Log.	Exp.

BFGS: Broyden-Fletcher-Goldfarb-Shanno algorithm,

Log. Is logistic sigmoid function,

Exp. is negative exponential function,

MC: moisture content.

Appendix 2 Core sampling versus predicted soil volumetric moisture content (θv) with the artificial neural networks (ANN) calibration method, for the soil moisture levels effect experiment of level 1 (L1) (A), level 2 (L2) (B), level 3 (L3) (C), and the collective model (D). Dashed line = 1:1 line; bold red line = line of best fit; ⊕= error bars.

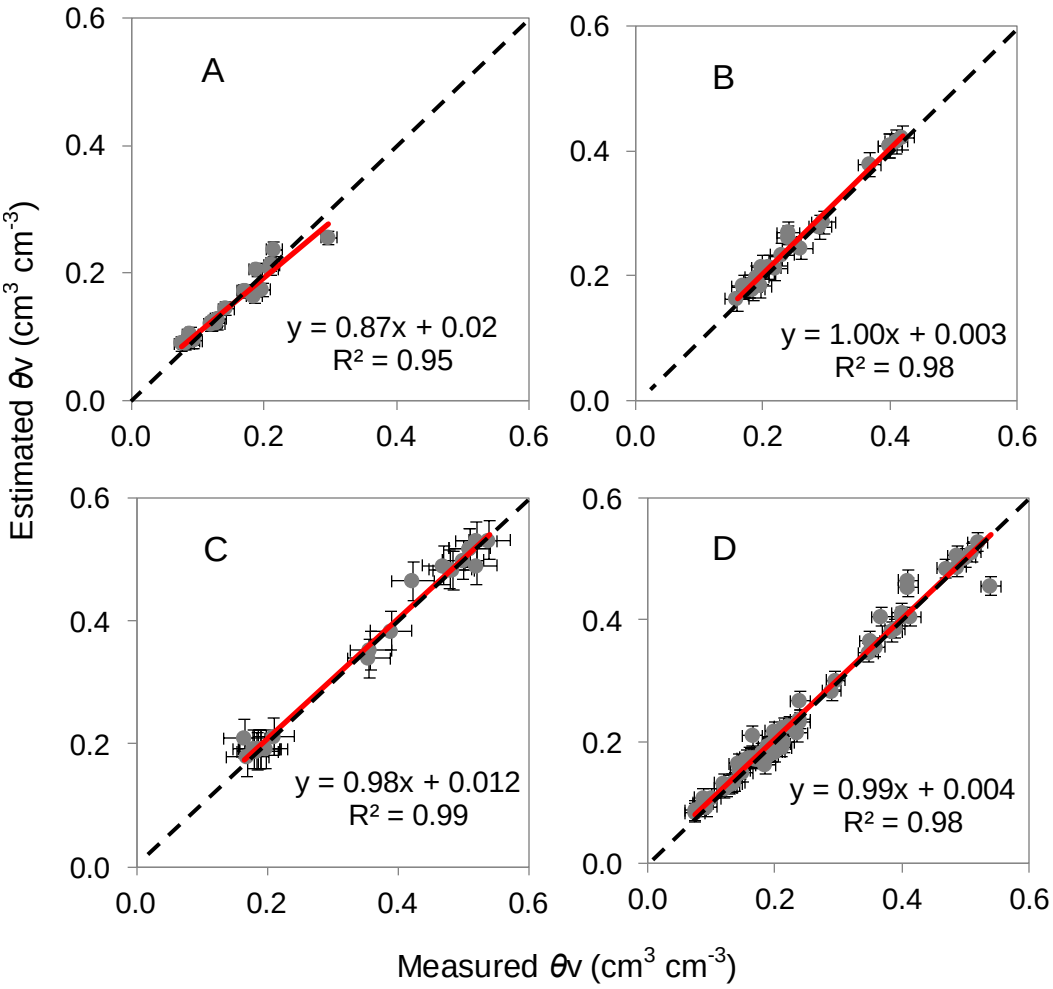

Appendix 3 Core sampling versus predicted soil gravimetric moisture content (ω) with the artificial neural networks (ANN) calibration method, for the soil moisture levels effect experiment of level 1 (L1) (A), level 2 (L2) (B), level 3 (L3) (C), and the collective model (D). Dashed line = 1:1 line; bold red line = line of best fit; ⊕= error bars.

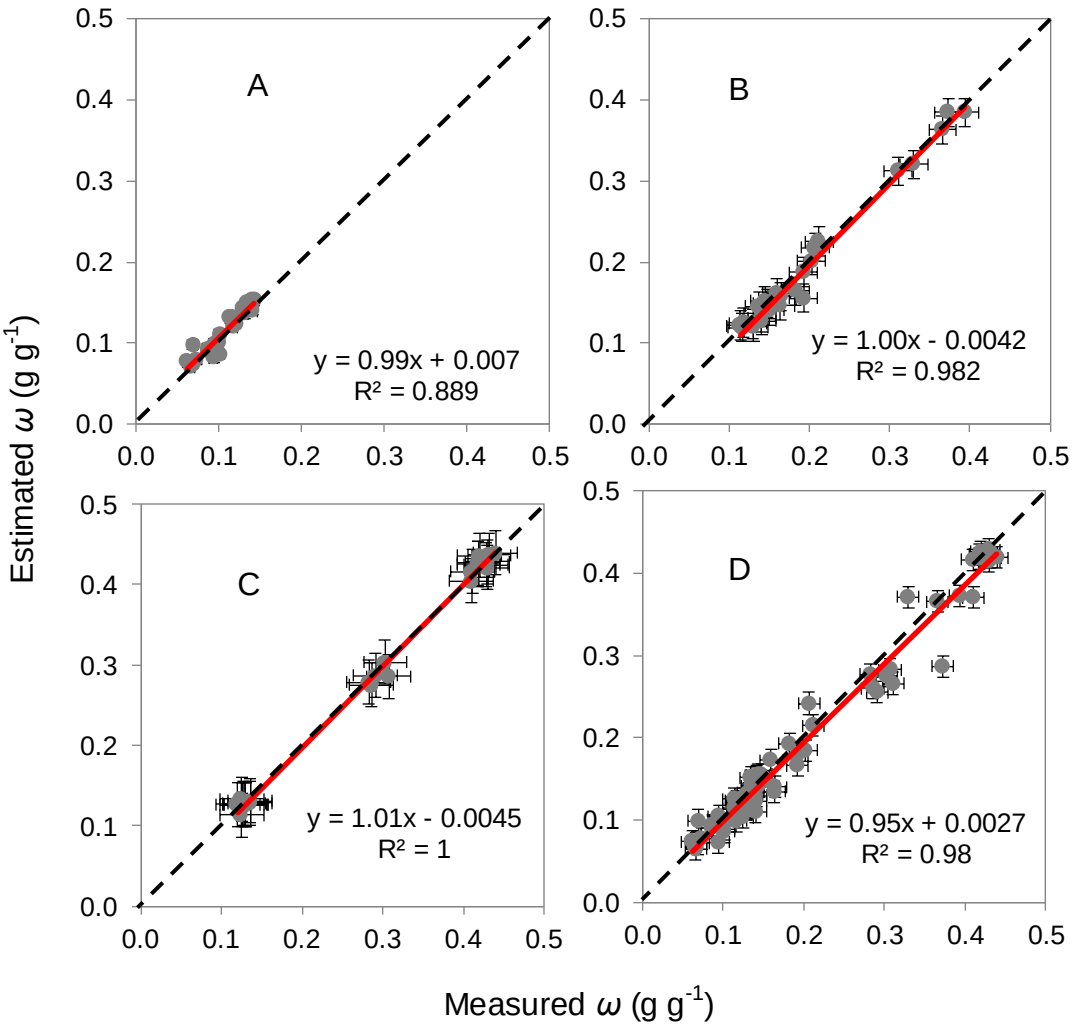

Appendix 4 Different artificial neural networks (ANN) analyses used for the measurement of volumetric (θv) and gravimetric (ω) moisture content for the soil texture effect. Data used as input are output voltage (V) and visible and near infrared spectra (Spec).

Texture classes	land use	Network structure	Training R^2	Validation R^2	Training error	Validation error	Training algorithm	Hidden activation	Output activation
Clay	Arable land	172-12-2	0.94	0.90	0.000235	0.000442	BFGS 81	Identity	Exp.
	Grassland	172-8-2	0.99	0.98	0.000122	0.000217	BFGS 87	Identity	Exp.
Clay Loam	Arable land	172-12-2	0.94	0.94	0.000423	0.000369	BFGS 58	Identity	Log.
	Grassland	172-24-2	1.00	1.00	0.000016	0.000043	BFGS 88	Exp.	Identity
Sandy loam	Arable land	172-8-2	0.96	0.94	0.000123	0.000353	BFGS 20	Exp.	Tanh
	Grassland	172-8-2	1.00	0.96	0.000024	0.000388	BFGS 98	Exp.	Tanh
Collective	Arable land	172-8-2	0.98	0.98	0.000332	0.000446	BFGS 54	Exp.	Tanh
	Grassland	172-8-2	0.99	0.99	0.000156	0.000162	BFGS 106	Tanh	Exp.

BFGS: Broyden-Fletcher-Goldfarb-Shanno algorithm.

Log.: logistic sigmoid function.

Exp.: negative exponential function.

Tanh: hyperbolic tangent function.

Appendix 5 Scatter plots of core sampling versus artificial neural networks (ANN) predicted soil volumetric moisture content (θv) for clay (A), clay loam (B), sandy loam (C) soils and the collective texture model (D), using samples collected from arable land fields. Dashed line = 1:1 line; bold red line = line of best fit; ⊢⊣ = error bars.

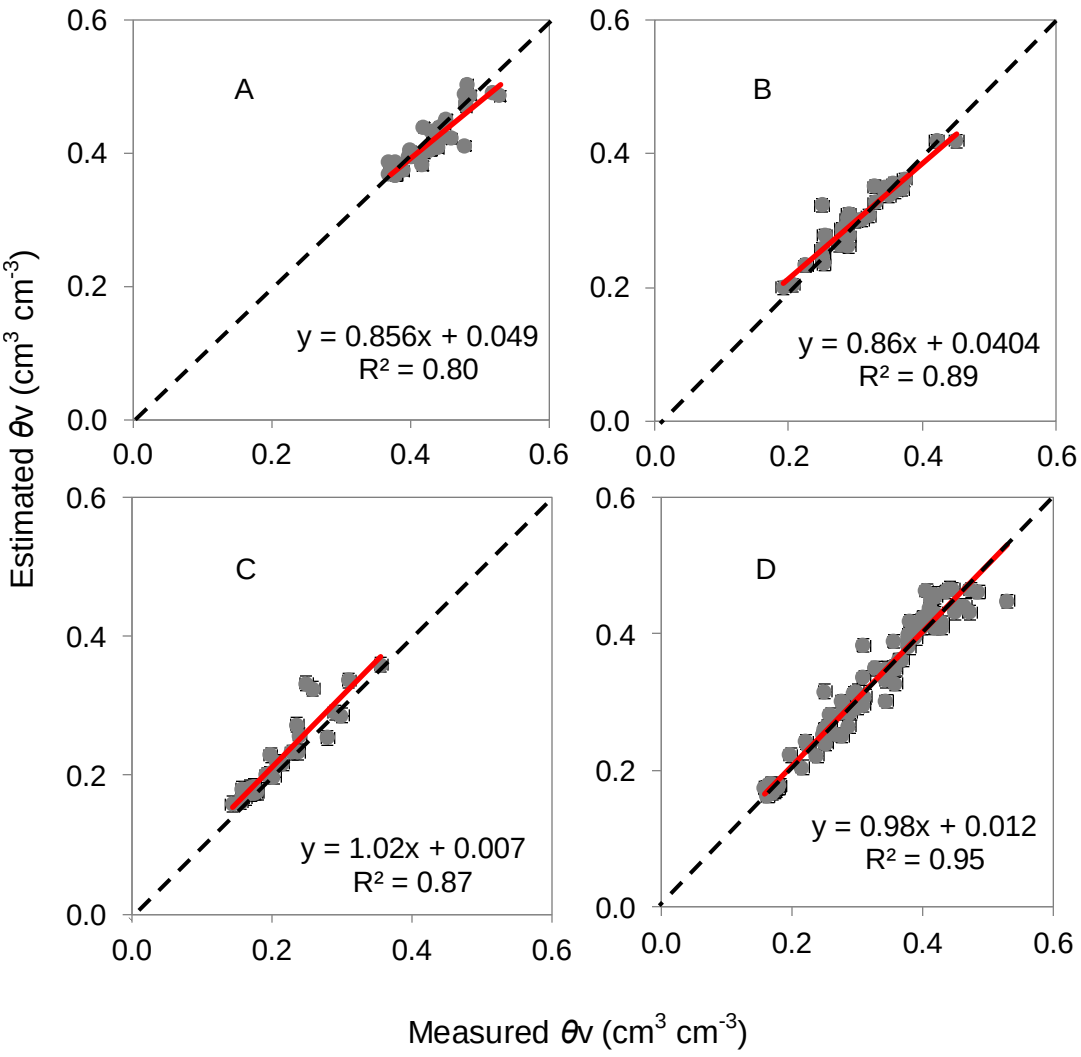

Appendix 6 Scatter plots of core sampling versus artificial neural networks (ANN) predicted soil volumetric moisture content (θv) for clay (A), clay loam (B), sandy loam (C) soils and the collective texture model (D), using samples collected from grassland fields. Dashed line = 1:1 line; bold red line = line of best fit; ⊢⊣ = error bars.

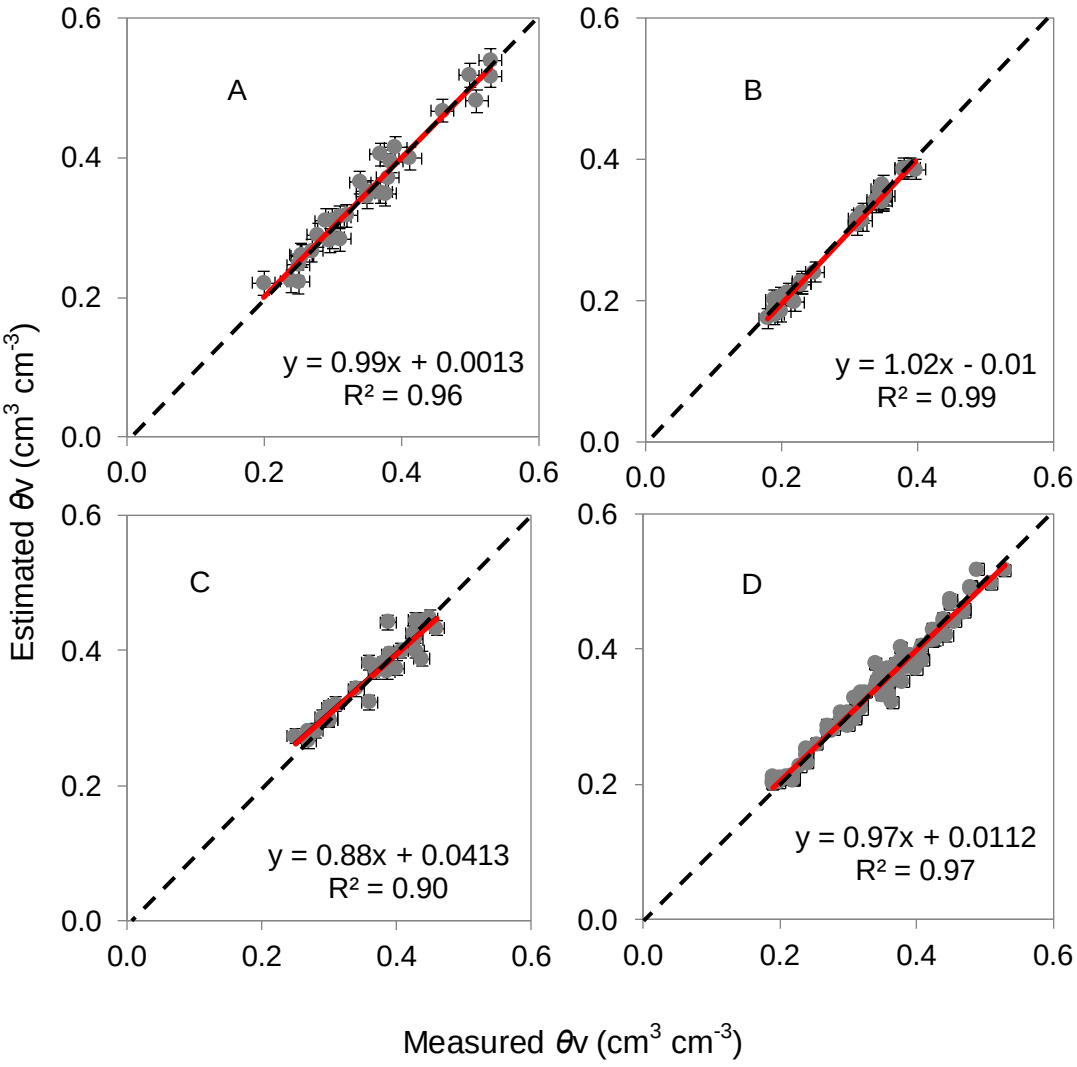

Appendix 7 Scatter plots of core sampling versus artificial neural networks (ANN) predicted soil gravimetric moisture content (ω) for clay (A), clay loam (B), sandy loam (C) textures and the collective texture model (D), for samples collected from arable land. Dashed line = 1:1 line; bold red line = line of best fit; ⊢⊣ = error bars.

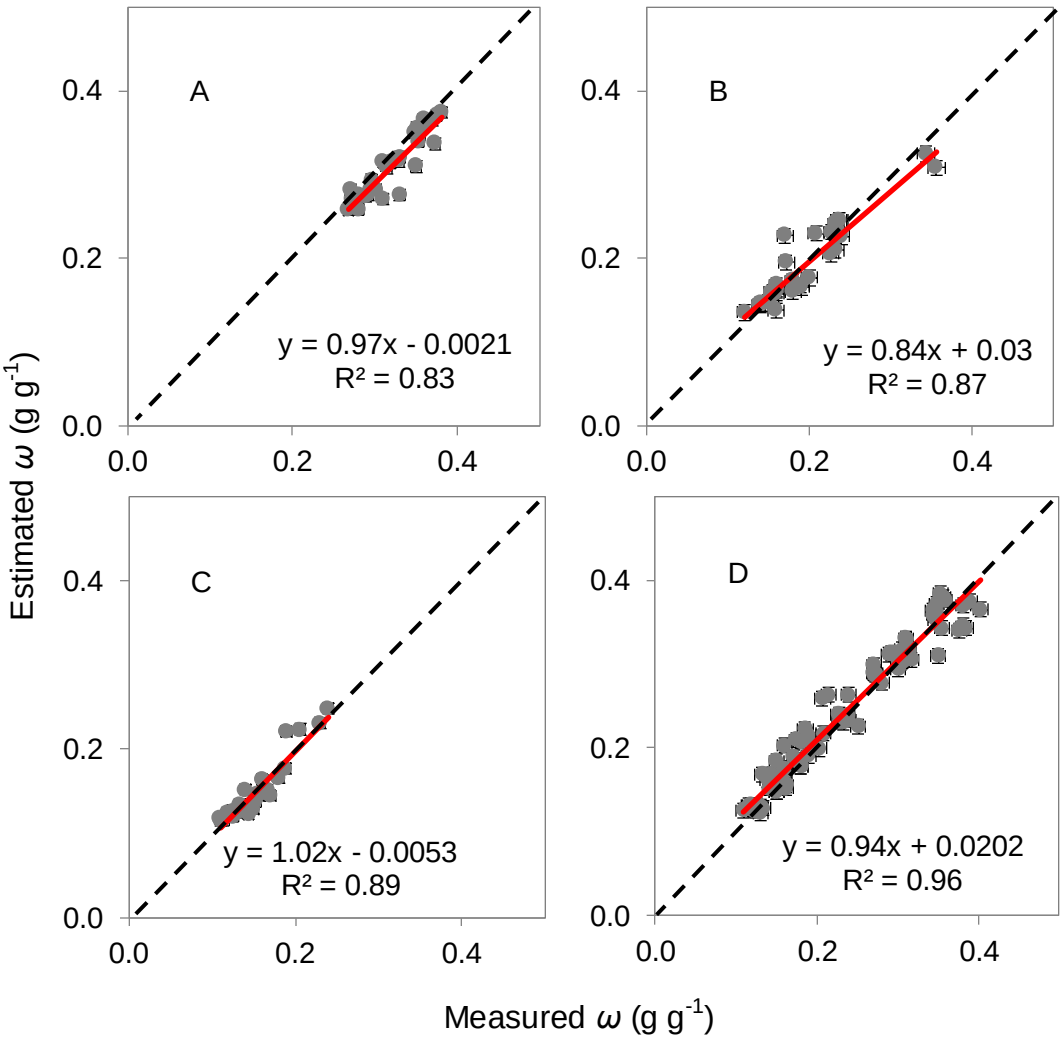

Appendix 8 Scatter plots of core sampling versus artificial neural networks (ANN) predicted soil gravimetric moisture content (ω) for clay (A), clay loam (B), sandy loam (C) textures and the collective texture model (D), for samples collected from grassland fields. Dashed line = 1:1 line; bold red line = line of best fit; ⊢⊣ = error bars.

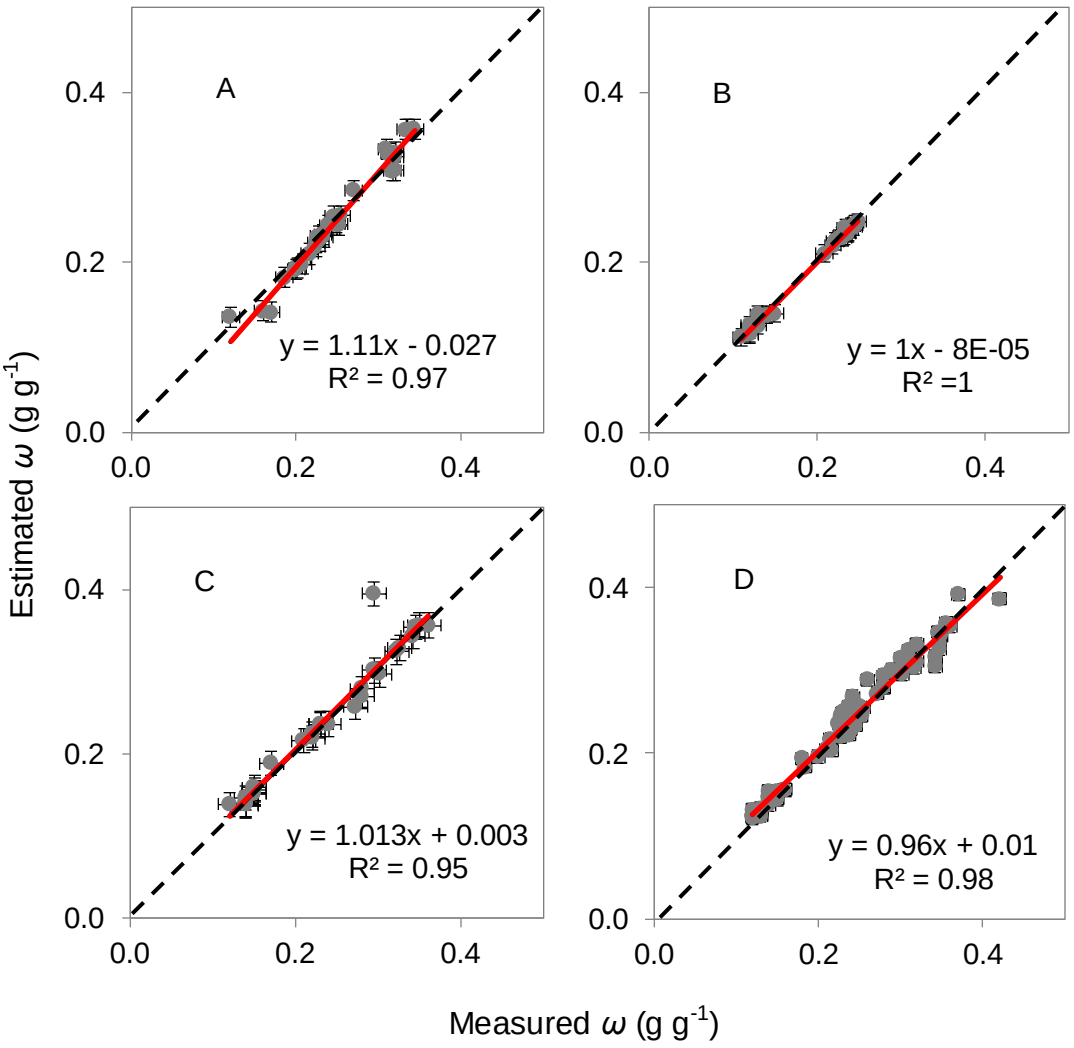

Appendix 9 Different artificial neural networks (ANN) analyses used for the measurement of volumetric (θv) and gravimetric (ω) moisture contents for light and heavy soils and for collective soil models. The data used as inputs are output voltage (V) and visible and near infrared spectra (Spec).

Index	Network structure	Training R^2	Validation R^2	Training error	Validation error	Training algorithm	Hidden activation	Output activation
Light	172-21-2	0.99	0.95	0.000086	0.000243	BFGS 96	Tanh	Exp.
Heavy	172-8-2	0.97	0.96	0.000275	0.000463	BFGS 138	Exp.	Identity
Collective	172-11-2	0.98	0.94	0.000375	0.000489	BFGS 59	Tanh	Identity

BFGS: Broyden-Fletcher-Goldfarb-Shanno algorithm.

Exp.: negative exponential function.

Tanh: hyperbolic tangent function

Appendix 10 Scatter plots of core sampling measured versus artificial neural networks (ANN) predicted soil volumetric moisture content (θv) for light soil textures (A), heavy soil textures (B) and the collective texture class model (C). Dashed line = 1:1 line; bold red line = line of best fit; ⊢⊣ = error bars.

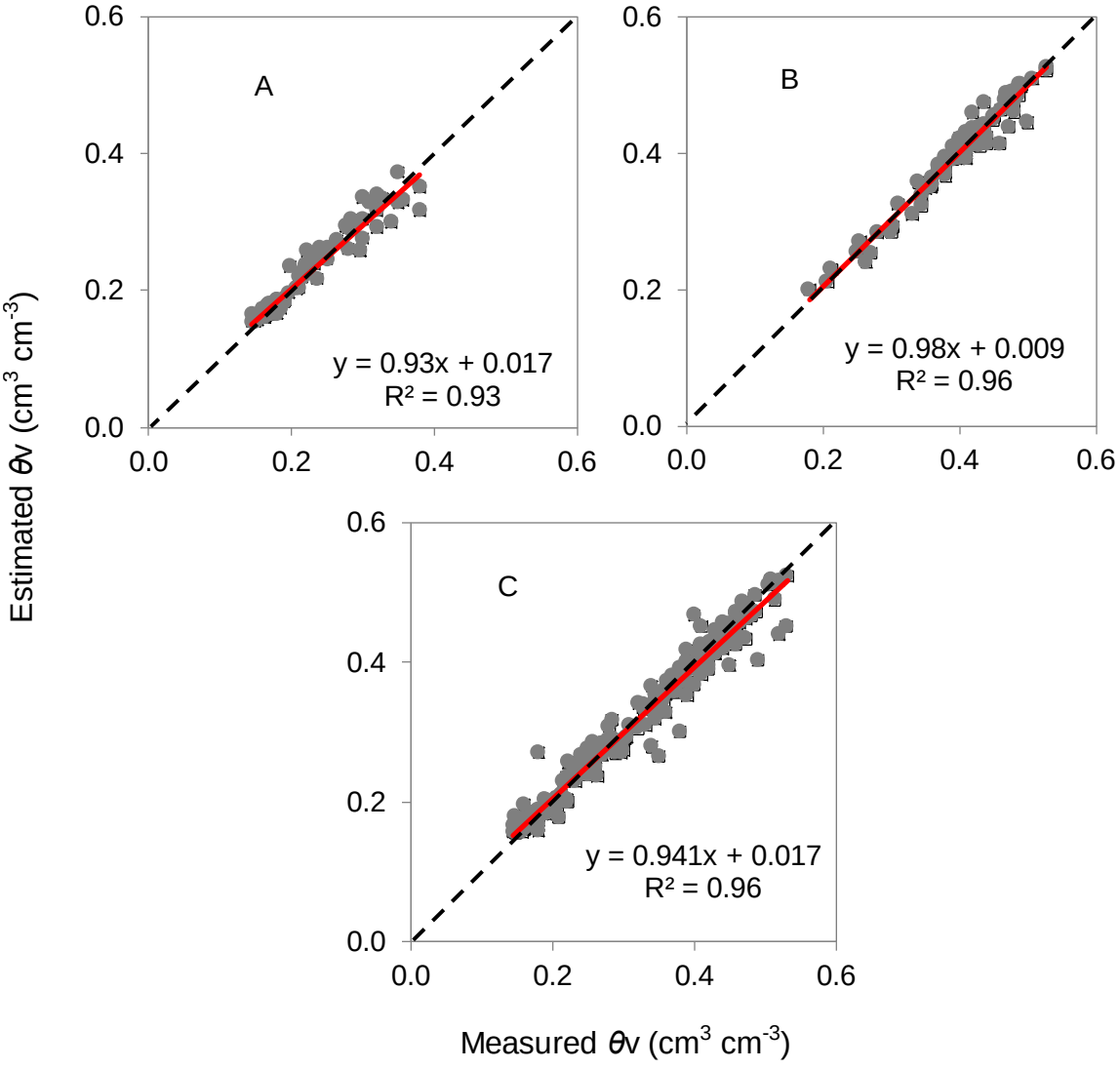

Appendix 11 Scatter plots of core sampling measured versus artificial neural networks (ANN) predicted soil gravimetric moisture content (ω) for the light soil textures (A), the heavy soil textures (B) and the collective texture model (C). Dashed line = 1:1 line; bold red line = line of best fit; ⊢⊣ = error bars.

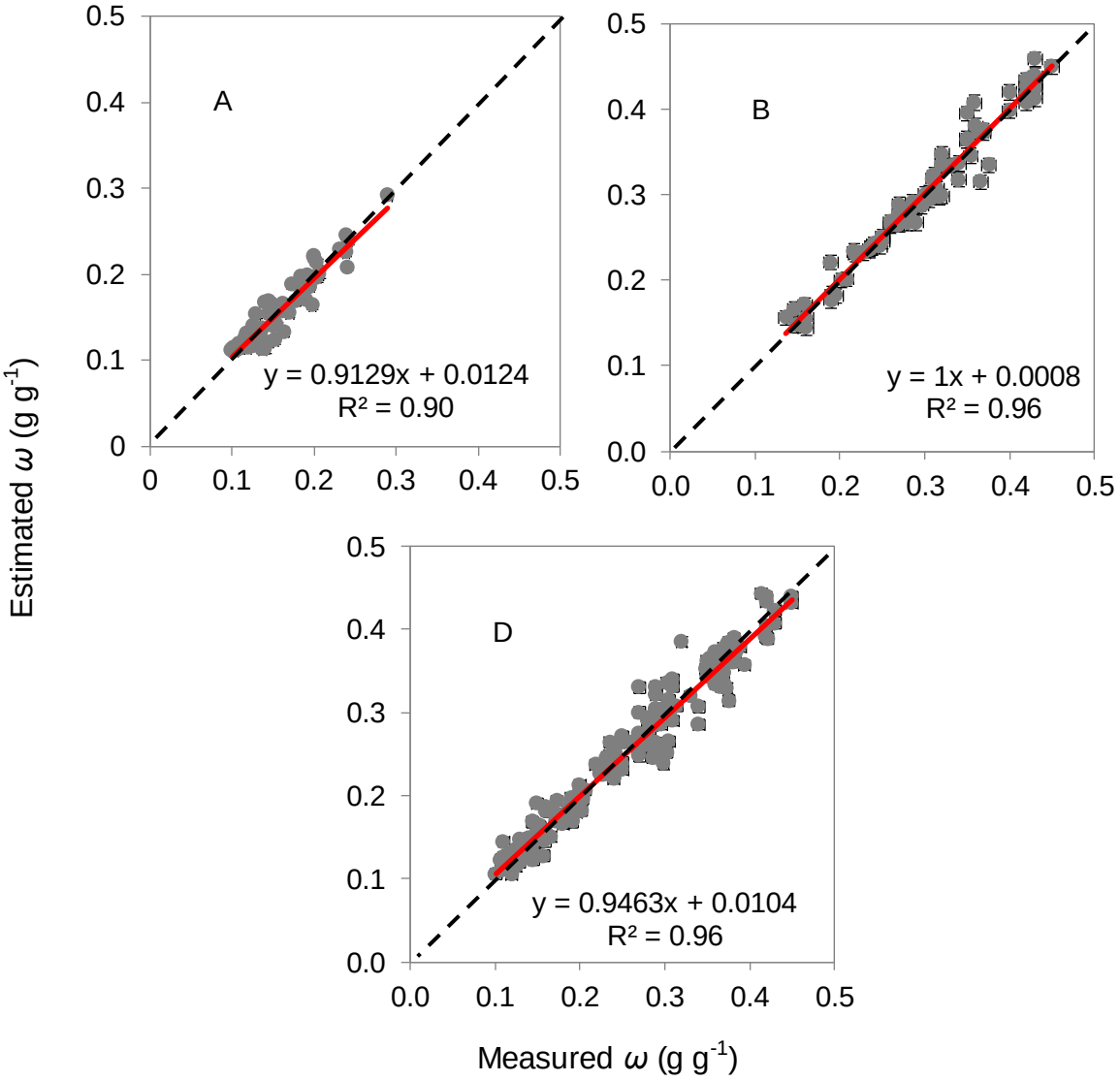

Appendix 12 Three different models obtained with artificial neural networks (ANN) analyses for the measurement of volumetric (θv) and gravimetric (ω) moisture contents using arable land, grassland and collective land use samples. Data used as inputs are output voltage (V) and visible and near infrared spectra (Spec).

Index	Network structure	Training R^2	Validation R^2	Training error	Validation error	Training algorithm	Hidden activation	Output activation
Arable land	172-24-2	0.992705	0.992676	0.000159	0.000147	BFGS 88	Exp.	Exp.
Grassland	172-21-2	0.996369	0.988902	0.000048	0.000182	BFGS 212	Log.	Identity
Collective	172-18-2	0.993149	0.987700	0.000127	0.000231	BFGS 180	Log.	Identity

BFGS: Broyden-Fletcher-Goldfarb-Shanno algorithm.

Log.: logistic sigmoid function.

Exp.: negative exponential function

Appendix 13 Scatter plots of core sampling measured versus artificial neural networks (ANN) predicted soil volumetric moisture content (θv) for arable land (A), grassland (B) and the collective sample model (C). Dashed line = 1:1 line; bold red line = line of best fit; ⊢⊣ = error bars.

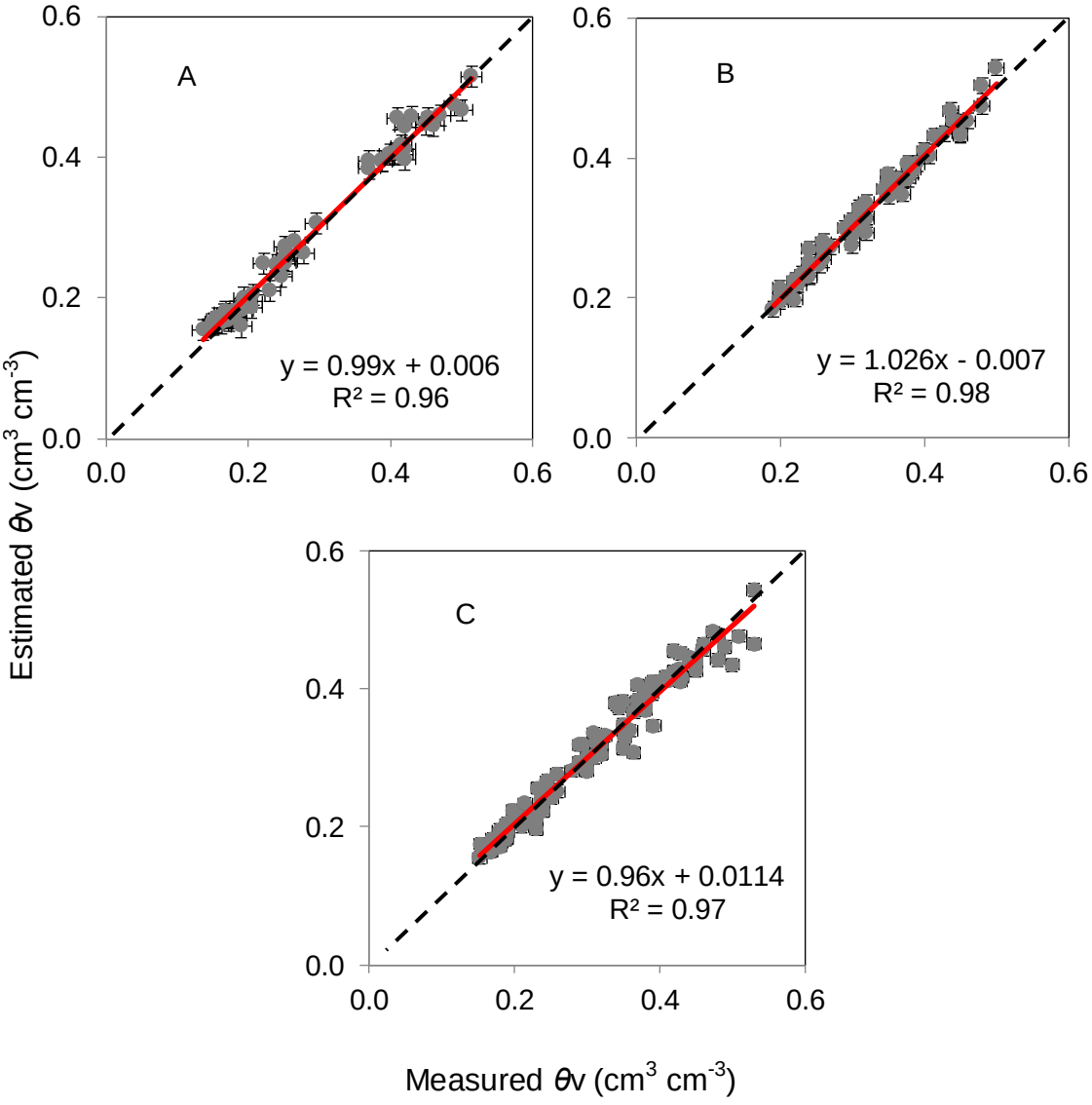

Appendix 14 Scatter plots of core sampling measured versus artificial neural networks (ANN) predicted soil gravimetric moisture content (ω) with arable land (A), grassland (B) and the collective sample (C) models. Dashed line = 1:1 line; bold red line = line of best fit; ⊢⊣ = error bars.

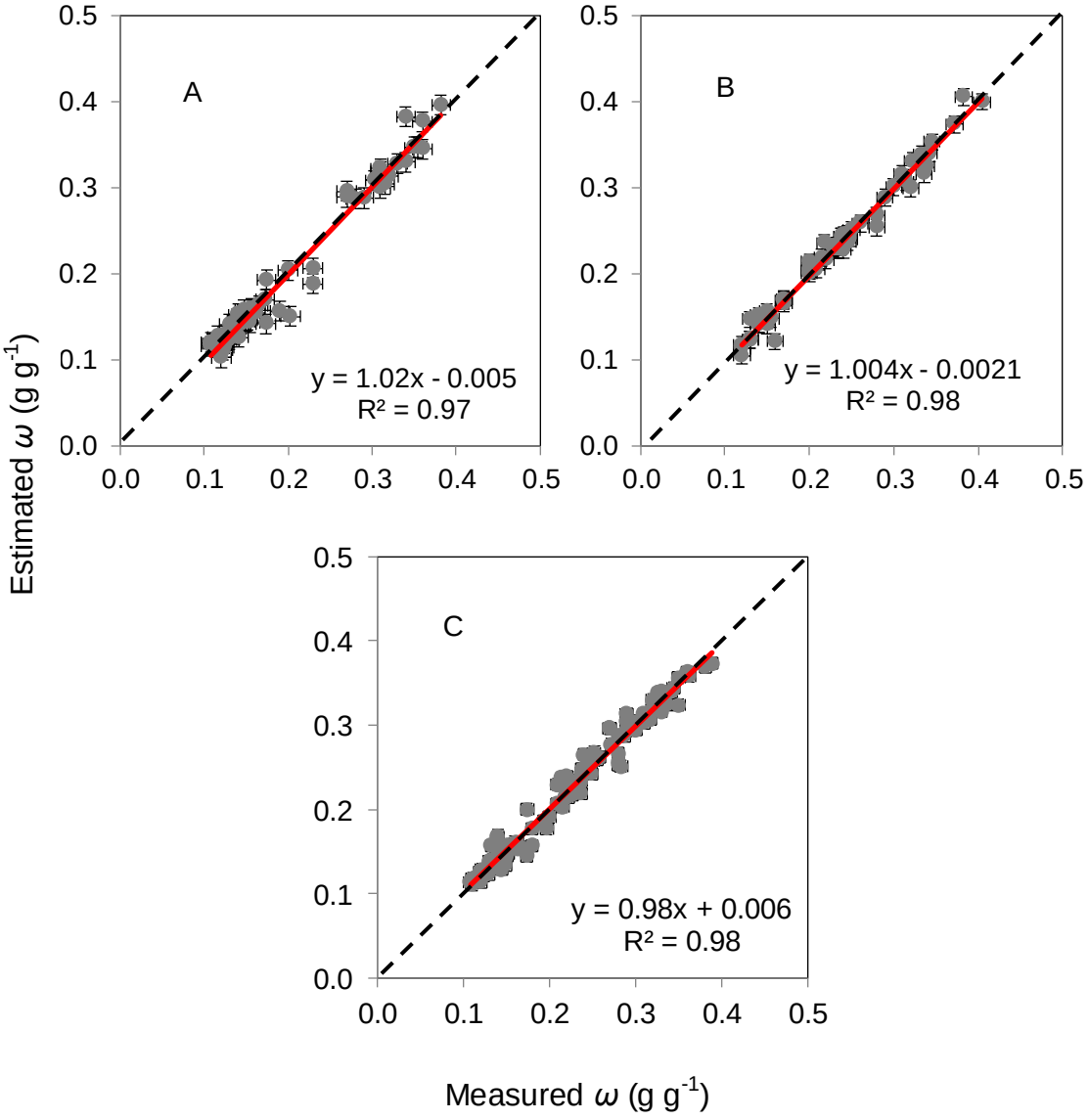

Appendix 15 The artificial neural networks (ANN) modelling results for the laboratory test of the prototype combined probe.

Index	Network structure	Training R^2	Validation R^2	Training error	Validation error	Training algorithm	Hidden activation	Output activation
Sandy loam	170-10-2	0.98	0.97	0.00028	0.000268	BFGS 14	Identity	Exp.
Clay loam	170-19-2	0.98	1.00	0.00033	5.55E-05	BFGS 56	Exp.	Logistic
Collective	170-8-2	0.996	0.99	9.03E-05	0.000202	BFGS 81	Tanh	Identity

BFGS: Broyden-Fletcher-Goldfarb-Shanno algorithm; Logistic: logistic sigmoid function; Exp.: negative exponential function; Tanh: hyperbolic tangent function.

Appendix 16 The artificial neural networks (ANN) modelling results of the field testing of the prototype combined probe.

Index	Network structure	Training R^2	Validation R^2	Training error	Validation error	Training algorithm	Hidden activation	Output activation
Arable land	170-17-2	1.00	0.98	0.000008	0.000458	BFGS 147	Exp.	Exp.
Grassland	170-8-2	0.99	0.99	0.000052	0.000065	BFGS 113	Log.	Exp.
Collective	170-15-2	0.97	0.95	0.000111	0.000652	BFGS 178	Exp.	Exp.

BFGS: Broyden-Fletcher-Goldfarb-Shanno algorithm.

Log.: logistic sigmoid function.

Exp.: negative exponential function.

Appendix 17 Artificial neural networks (ANN) modelling results of the individual field testing of the prototype combined probe.

Field	Network structure	Training R^2	Validation R^2	Training error	Validation error	Training algorithm	Hidden activation	Output activation
Avenue	173-1-2	0.99	0.98	0.000214	0.000353	BFGS 73	Identity	Exp.
Showground	173-2-2	1.00	0.99	0.000100	0.000282	BFGS 104	Exp.	Tanh
Orchard	173-5-2	0.98	0.98	0.00055	0.000501	BFGS 24	Tanh	Tanh
Clover Hill	173-1-2	0.99	0.97	0.000358	0.000720	BFGS 49	Log.	Exp.
Beechwood	173-2-2	1.00	0.99	0.000113	0.000351	BFGS 167	Exp.	Exp.
Avenue grass	173-1-2	0.99	0.99	0.000301	0.000337	BFGS 58	Exp.	Tanh
Onley grass	173-1-2	0.98	0.96	0.000456	0.001088	BFGS 88	Log.	Log.

BFGS: Broyden-Fletcher-Goldfarb-Shanno algorithm.

Logistic: logistic sigmoid function.

Exponential: negative exponential function.

Tanh: hyperbolic tangent function.